Synthese und Eigenschaften von Organozinnselenid- und Organosiliciumsulfid-Clustern

Kumulative Dissertationsschrift

zur Erlangung des akademischen Grades einer
Doktorin der Naturwissenschaften
(Dr. rer. nat.)

dem
Fachbereich Chemie der Philipps-Universität Marburg
(Hochschulkennziffer 1180)
vorgelegt von

Katharina Hanau, M.Sc.
aus Lennestadt

Marburg, 2020

Erstgutachterin: Prof. Dr. Stefanie Dehnen
Zweitgutachter: Prof. Dr. Sangam Chatterjee
Annahme der Dissertation: 14.12.2020
Tag der Disputation: 15.12.2020

„‚Was sind die drei wichtigsten Grundregeln des Chemikers?‘[...]
‚Eindeutige Beschriftungen. Immer zweimal messen. Nie dort essen, wo man arbeitet.‘“

— Patrick Rothfuss, *Der Name des Windes*

Lizenzierung

Erklärung

Ich erkläre, dass eine Promotion noch an keiner anderen Hochschule als an der Philipps-Universität Marburg, Fachbereich Chemie, versucht wurde. Hiermit versichere ich, dass ich meine vorgelegte Dissertation:
„Synthese und Eigenschaften von Organozinnselenid- und Organosiliciumsulfid-Clustern“
selbstständig, ohne unerlaubte Hilfe Dritter angefertigt und andere als die in der Dissertation angegebenen Hilfsmittel nicht benutzt habe. Alle Stellen, die wörtlich oder sinngemäß aus veröffentlichten oder unveröffentlichten Schriften entnommen sind, habe ich als solche kenntlich gemacht. Dritte waren an der inhaltlich-materiellen Erstellung der Dissertation nicht beteiligt; insbesondere habe ich hierfür nicht die Hilfe eines Promotionsberaters in Anspruch genommen. Kein Teil dieser Arbeit ist in einem anderen Promotions- oder Habilitationsverfahren verwendet worden. Mit dem Einsatz von Software zur Erkennung von Plagiaten bin ich einverstanden.

Marburg, 03. November 2020 Katharina Hanau

Die vorliegende Arbeit wurde im Zeitraum von Juni 2014 bis November 2020 unter der Leitung von Prof. Dr. Stefanie Dehnen am Fachbereich Chemie der Philipps-Universität Marburg angefertigt.

Inhaltsverzeichnis

Abbildungsverzeichnis

Tabellenverzeichnis

Verzeichnis der Schemata

Abkürzungsverzeichnis

Bn	Benzyl; $-CH_2C_6H_5$
bzw.	beziehungsweise
CIE	Internationale Beleuchtungskomission (*Commission internationale de l'éclairage*)
Cp	Cyclopentadienyl; $-C_5H_5$
cw	*continuous wave*
Cy	Cyclohexyl; $-C_6H_{11}$
DFT	Dichtefunktionaltheorie
Dipp	2,6-Di*iso*propylphenyl; $-C_6H_3(CH(CH_3)_2)_2$
E	Chalkogenatom
ESI	Elektrosprayionisation
Et	Ethyl, $-C_2H_5$
HOMO	*highest occupied molecular orbital*
***i*Pr**	*iso*-Propyl, $-CH(CH_3)_2$
LUMO	*lowest unoccupied molecular orbital*
Me	Methyl; $-CH_3$
MS	Massenspektrometrie
µ-RFA	Mikroröntgenfluoreszenzanalyse
***n*Bu**	*n*-Butyl; $-C_4H_9$
Np	1-Naphthyl; $-C_{10}H_7$
***n*Pr**	*n*-Propyl; $-C_3H_7$
Ph	Phenyl, $-C_6H_5$
py	Pyridinyl; $-C_5H_4N$
$\mathbf{R^1}$	CMe_2CH_2CMeO
$\mathbf{R^2}$	$CMe_2CH_2CMeNNH_2$
$\mathbf{R^f}$	organischer Substituent mit funktioneller Gruppe
SHG	*second harmonic generation*, Frequenzverdopplung
Sty	Styryl, 4-Vinylphenyl; $4-(CH_2{=}CH)-C_6H_5$
T	Tetrelatom

***t*Bu**	*tert*-Butyl; $-C(CH_3)_3$
Thex	1,1,2-Trimethylpropyl; $-CH_2CH(Me)CHMe_2$
THF	Tetrahydrofuran
UV	Ultraviolett
WLG	*white light generation*, Weißlichtemission

Vorbemerkung zu kristallographischen Abbildungen

Soweit nicht anders angegeben, sind die (Schwer)atome in allen Molekül- und Kristallstrukturen als Ellipsoide mit 50% Aufenthaltswahrscheinlichkeit dargestellt. Liganden mit C, N und O werden zudem nur als Bindungsskelett gezeigt. Nicht relevante Wasserstoffatome sind aus Übersichtlichkeitsgründen ausgeblendet.

1 Einleitung

1.1 Organotetrelchalkogenid-Cluster

Der erste Organotetrelchalkogenid-Cluster, $[(MeSn)_4S_6]$, ist seit 1903 bekannt.[1] Es dauerte jedoch bis zu den 50er bzw. 60er Jahren, bis analoge Silicium- oder Germaniumsulfid-Verbindungen synthetisiert wurden.[2,3] Ebenfalls in den 60er Jahren fanden erste kristallographische Untersuchungen statt, um die Molekülstrukturen der Verbindungen aufzuklären. Zuvor waren sowohl eine Heteroadamantan-Struktur als auch eine sogenannte Doppeldecker-Struktur, bei der zwei $\{T_2E_2\}$-Vierringe (T = Si, Ge, Sn; E = S, Se, Te) über zwei Chalkogenatome miteinander verbrückt sind, diskutiert worden (siehe Abbildung 1.1). Die Kristallstrukturanalysen

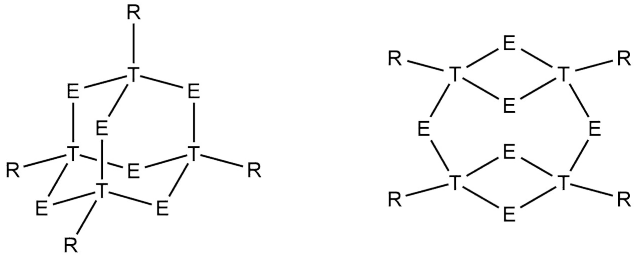

Abbildung 1.1: Für Organotetrelchalkogenid-Cluster der Zusammensetzung $[(RT)_4E_6]$ (T = Si, Ge, Sn, E = S, Se, Te) wurden sowohl der Adamantan-Strukturtyp (links) als auch der Doppeldecker-Strukturtyp (rechts) diskutiert.

bestätigten die Adamantanstruktur für die entsprechenden Methyl-substituierten Tetrelchalkogenid-Cluster.[4–8] Erst 1992 wurde der Doppeldecker-Strukturtyp für $[(t\text{BuGe})_4S_6]$ beobachtet und kristallographisch nachgewiesen.[9] Cluster mit Doppeldeckerstruktur folgten 1997 für T = Si ($[(\text{ThexSi})_4E_6$, E = S, Se, Thex = 1,1,2-Trimethylpropyl) bzw. 2007 für T = Sn ($[\{o\text{–}(Me_2NCH_2)C_6H_4\}Sn_4S_6]$).[10,11] Da-

bei handelt es sich um das kinetische Reaktionsprodukt, welches durch sterisch anspruchsvolle Reste oder, im Falle des Organozinnsulfid-Clusters, durch Rückkoordination eines σ-Donoratoms zum Zinnatom und damit verbundener Erhöhung der Koordinationszahl von vier auf fünf stabilisiert wird. Dies wird auch dadurch bestätigt, dass $[(ThexSi)_4E_6]$ und $[(t\text{BuGe})_4S_6]$ durch Erhitzen in die entsprechenden Adamantan-Cluster überführt werden konnten.[9,12]

Da ich mich während meiner Promotion mit Organozinn- und Organosiliciumchalkogenid-Clustern beschäftigt habe, möchte ich im Folgenden genauer auf diese Elementkombinationen eingehen.

1.2 Organisch funktionalisierte Zinnchalkogenid-Cluster und ihre Reaktivität

Die Arbeitsgruppe *Dehnen* beschäftigt sich seit mehreren Jahren mit organisch funktionalisierten Tetrelchalkogenid-Clustern. Dabei wurden unter anderem Reste mit Keto-, Carbonsäure- oder Aminosäure-Gruppen sowie Peptide oder Metallocene erfolgreich an die Cluster angebunden.[13–23] Dadurch sind oft Folgereaktionen sowohl an den organischen Gruppen als auch am Clusterkern möglich. So lassen sich beispielsweise ketofunktionalisierte Cluster in Kondensationsreaktionen mit Hydrazinderivaten in hydrazonfunktionalisierte Cluster überführen, welche dann wiederum zur Reaktion mit weiteren Aldehyden oder Ketonen und somit zur Erweiterung der organischen Reste zur Verfügung stehen.[13,24–26] Der Clusterkern steht vor allem für Umsetzungen mit Übergangsmetallverbindungen zur Verfügung, wobei sich dieser häufig umlagert und in Folge dessen ternäre Cluster mit organischen Resten entstehen.[13,25,27–36] Auf beide Reaktionstypen sowie mögliche Strukturmotive soll in den folgenden Abschnitten genauer eingegangen werden.

1.2.1 Strukturmotive

Die in Abschnitt 1.1 erwähnten Strukturmotive sind auch für organisch funktionalisierte Zinnchalkogenid-Cluster bekannt. Besteht die Möglichkeit zur Rückkoordination der Substituenten an die Zinnatome, so entstehen für die Zusammensetzung $[(R^fSn)_4E_6]$ (R^f = organischer Substituent mit funktioneller Gruppe) vorzugsweise

Cluster mit Doppeldeckerstruktur, wie beispielsweise $[(R^1Sn)_4E_6]$ oder $[(R^2Sn)_4E_6]$ (E = S, Se, Te; R^1 = CMe_2CH_2CMeO; R^2 = $CMe_2CH_2CMeNNH_2$).[13,25,37] Sind keine funktionellen Gruppen mit der Fähigkeit zur Rückbindung vorhanden oder befinden sich diese zu weit von den Zinnatomen entfernt, werden stattdessen Cluster mit Adamantanstruktur gebildet. Beispiele dafür sind $[(BnSn)_4S_6]$ (Bn = Benzyl) oder $[(CO_2Et(C_6H_4)CH_2CH_2Sn)_4E_6]$ (E = S, Se).[38,39] Weitere Strukturmotive können durch Variation des Chalkogenidanteils bei der Clustersynthese erhalten werden.[25,29] So führt die Umsetzung von R^1SnCl_3 mit $(SiMe_3)_2E$ im Verhältnis 2:1 zu einem V-förmigen Molekül, in dem zwei $\{R^1SnCl_2\}$-Einheiten durch ein Chalkogenatom verbunden sind. Eine Verdopplung des Chalkogenidanteils führt zu einem $[(R^1Sn)_2E_2Cl_2]$-Vierring, während bei einer 1:1,33-Stöchiometrie defektheterokubanartige Cluster der Zusammensetzung $[(RSn)_3E_4Cl]$ gebildet werden.[13,16,25] Eine weitere Erhöhung des Chalkogenidanteils bei einer Stöchiometrie von 1:1,5 führt zu dem bereits erwähnten Doppeldecker-Strukturmotiv. Für die Elementkombination Sn/S sind außerdem mehrere Cluster der Zusammensetzung $[R^f_4Sn_6S_{10}]$ mit Bisdefektheterokubanstruktur und einem noch höheren Chalkogenidanteil bekannt. Diese entstehen hauptsächlich bei der Verwendung von sterisch anspruchsvollen Substituenten, wie beispielsweise $CMe_2CH_2C(Me)Fc$ (Fc = Ferrocen), $(CMe_2CH_2CMeNNHCOCH_2)_2$–1,3–$C_{10}H_{14}$ oder $CMe_2CH_2CMeNNCMeC_{10}H_7$.[22,40,41] Es sind aber auch Bisdefektheterokuban-Cluster mit kleineren Substituenten bekannt.[13,16] Schema 1.1 gibt eine Übersicht über die verschiedenen Strukturmotive, die durch Variation des Chalkogenidanteils in einer Reihe von Kondensationsreaktionen einkristallin erhalten werden können, einschließlich mittels DFT-Methoden bestimmter Zwischenstufen.[16]

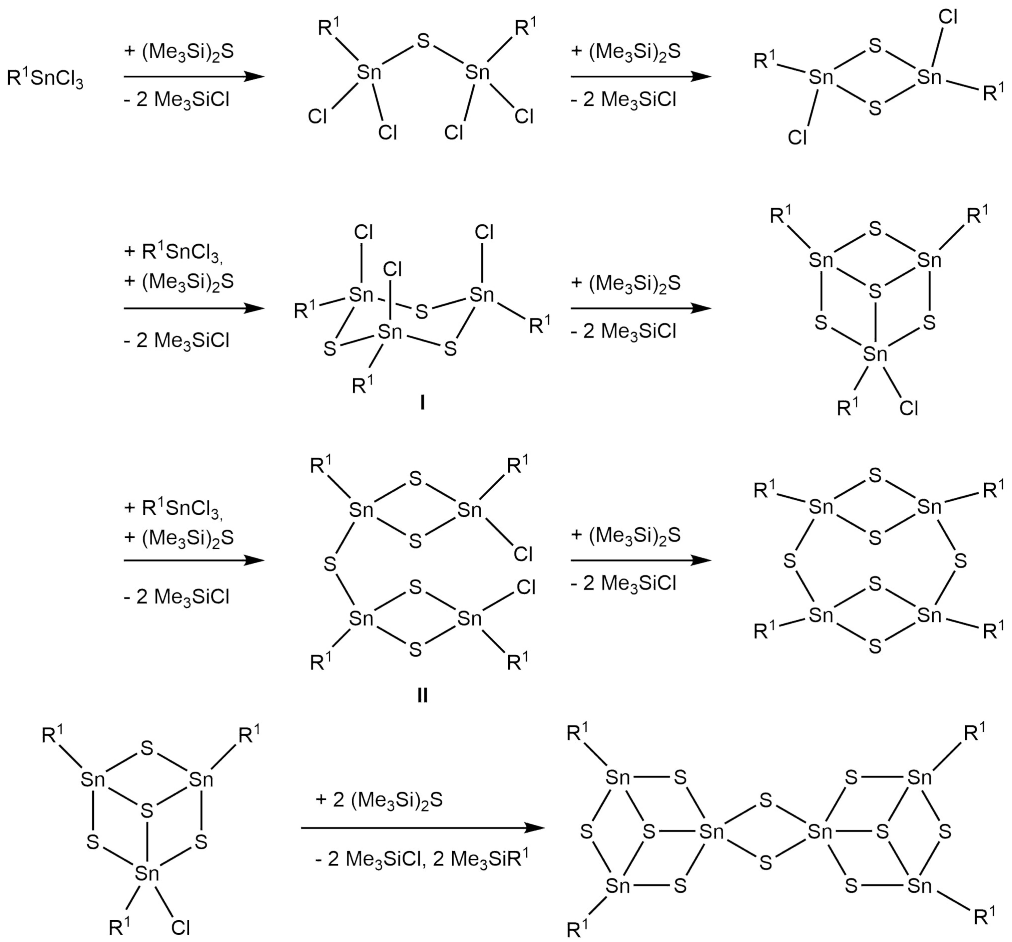

Schema 1.1: Strukturmotive, die durch die Variation des Chalkogenidanteils während der Synthese erhalten und kristallin isoliert werden können, sowie mittels DFT-Rechnungen bestimmte Zwischenstufen (**I** und **II**).

1.2.2 Reaktionen am organischen Substituenten

Wie eingangs erwähnt ermöglichen gerade die organischen Substituenten mit Ketofunktion die Anbindung verschiedener Reste durch Kondensationsreaktionen mit Hydrazinen oder Hydraziden. Die ersten Reaktionen dieser Art erfolgten zunächst mit Hydrazinhydrat und Phenylhydrazin, wodurch hydrazonfunktionalisierte Zinnselenid-Cluster mit Doppeldecker-Struktur entstanden (siehe Schema 1.2).[13] Analog wurden später auch hydrazonfunktionalisierte Zinnselenid-Cluster synthetisiert.[25] Diese Hydrazonfunktionen stehen nun für Reaktionen mit Aldehyden oder Ketonen zur Verfügung. Dadurch und durch die Reaktion der Ketogruppe mit weiteren Hydrazinderivaten ist eine Vielzahl an Verbindungen zugänglich. In der Vergangenheit wurden so beispielsweise Poly(hetero)aromaten,[28,41,42] Metallocene,[20–23] Diamantoide[40] oder Biomoleküle wie Aminosäuren[17] oder Dipeptide[18,19] an die Cluster angebunden.

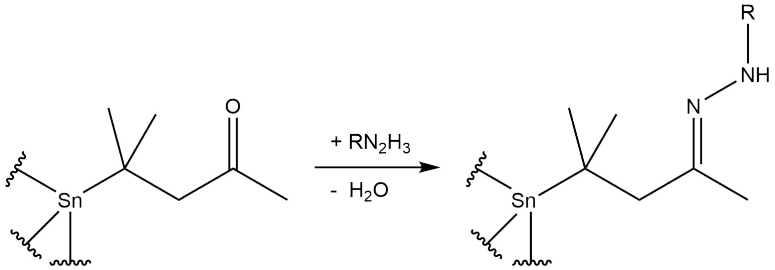

Schema 1.2: Durch Reaktion der Ketogruppe der Substituenten mit Hydrazinderivaten können neue Substituenten an den Cluster angebracht werden.

Des Weiteren wurde die Reaktivität des doppeldeckerartigen Clusters gegenüber verschiedenen bifunktionellen Molekülen untersucht.[21,24,27,40,43] Dabei kamen Moleküle mit verschiedenen Spacer-Längen, also Abständen zwischen den funktionellen Gruppen, zum Einsatz. Es zeigte sich, dass die verwendeten Substituenten einen großen Einfluss auf die Struktur des anorganischen Clusters haben. So führt die Umsetzung mit großen, starren Resten über eine Umlagerung des Clusterkerns zu Bisdefektheterokuban-Clustern, die entweder intramolekular (Kondensation zweier Reste an einem Clustermolekül) oder intermolekular (Kondensation zweier Reste an unterschiedlichen Clustermolekülen) miteinander verknüpft sind.[24,40,43]

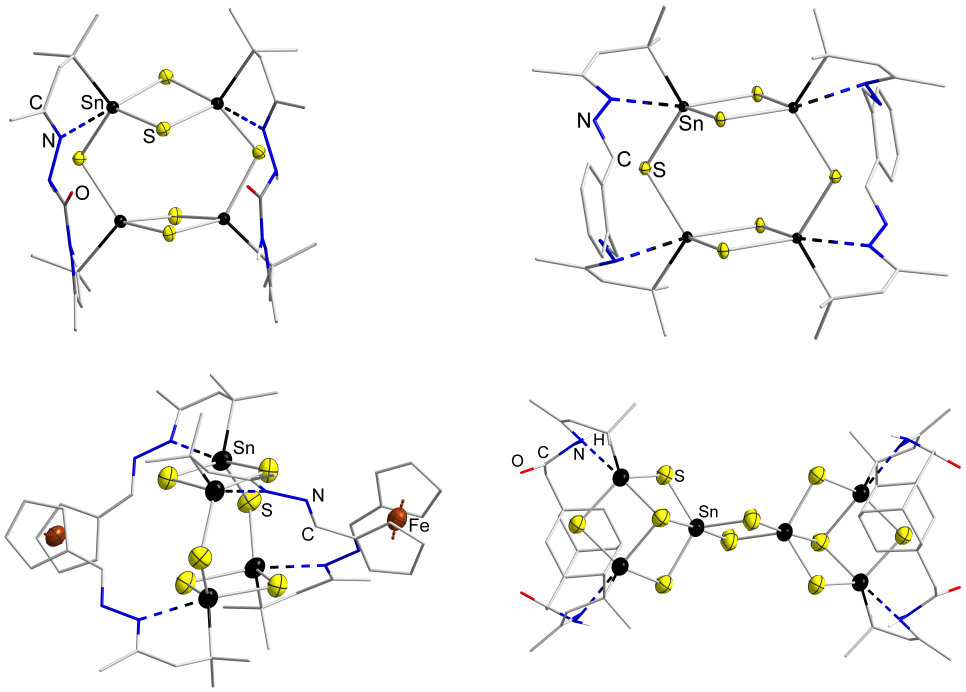

Abbildung 1.2: Verschiedene Möglichkeiten der intramolekularen Verbrückung nach Kondensation zweier Substituenten: *syn*-parallele (oben links), *anti*-parallele (oben rechts) und kreuzweise (unten links) Anordnung der kondensierten Substituenten am Doppeldecker-Cluster am Beispiel von $[\{(CMe_2CH_2CMeNNH)_2C(O)\}_2Sn_4S_6]$, $[\{(CMe_2CH_2CMeNNCH)_2C_6H_4\}_2Sn_4S_6]$ bzw. $[\{(CMe_2CH_2CMeCNNCHC_5H_5)_2Fe\}_2Sn_4S_6]$, sowie intramolekulare Verbrückung der Substituenten am Bisdefektheterokuban-Cluster $[\{(CMe_2CH_2CMeNNHCOCH_2)_2{-}1,3{-}C_{10}H_{14}\}_2Sn_6S_{10}]$ (unten rechts).

Bei kürzeren Spacer-Längen oder flexibleren Resten hingegen bleibt der Doppeldecker-Cluster intakt und jeweils zwei Reste sind miteinander verbunden, wobei hier verschiedene Anordnungen der Reste möglich sind: *syn*-parallel, überkreuzt und *anti*-parallel (siehe Abbildung 1.2).[21,24,27] Bei kurzen Spacer-Längen mit einem C=N···N=C-Abstand bis etwa 400 pm wird die *syn*-parallele Anordnung bevorzugt, zwischen 400 und 550 pm die *anti*-parallele Anordnung und über 600 pm die überkreuzweise Anordnung der Substituenten (siehe Abbildung 1.3). Noch größere Spacer-Längen ab etwa 850 pm führen zur Bildung von Kavitanden der Zusammensetzung $[R_4(Sn_6S_{10})_2]$ (R = $(CMe_2CH_2CMeNNCH)_2C_6H_4$,

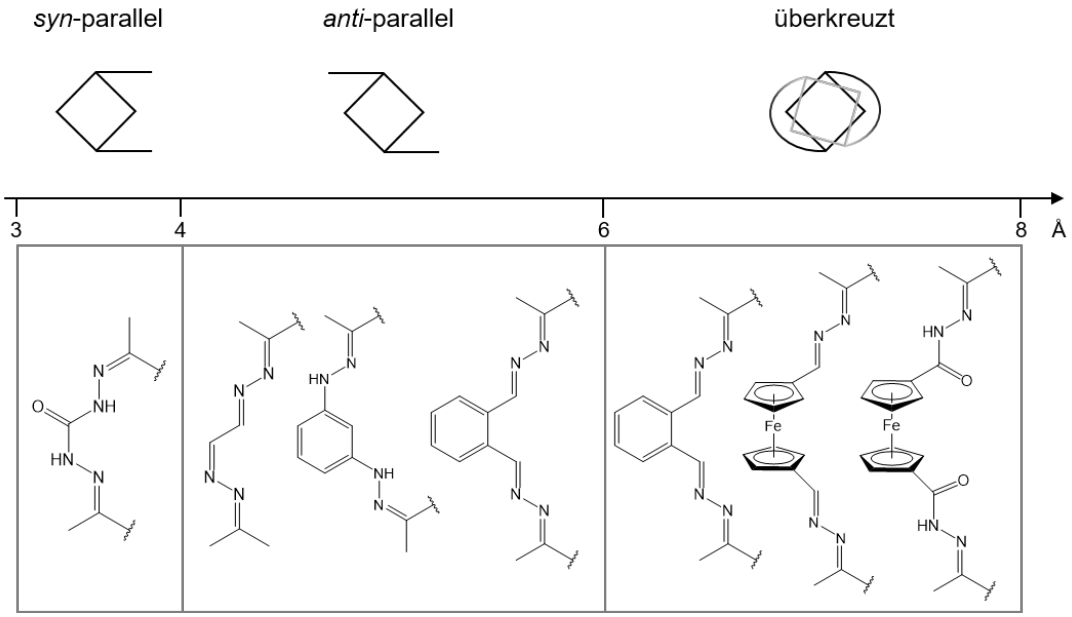

Abbildung 1.3: Übersicht über die verschiedene Anordnung der verbrückenden Substituenten an Doppeldecker-Clustern in Abhängigkeit von der Spacer-Länge. Die Doppeldecker-Cluster sind von oben als stilisierte Vierringe zu sehen, die die Vierringe verbrückenden S-Atome sind aus Übersichtlichkeitsgründen nicht dargestellt.

$(CMe_2CH_2CMeNNH)_2C_{10}H_6$), bestehend aus zwei Bisdefektheterokuban-Clustern, die über vier organische Substituenten miteinander verbunden sind (siehe Abbildung 1.4 links). Bei Spacer-Längen zwischen 600 und 800 pm ist außerdem die Flexibilität des Spacers entscheidend: Während die Verknüpfung über eine Ferrocenyl-Einheit zu einer kreuzweisen Anordnung der Substituenten führt und das Doppeldecker-Gerüst intakt bleibt, führt die starre Anordnung in *p*-Phthaldialdehyd dazu, dass kein Kondensationsprodukt isoliert werden kann. DFT-Rechnungen zeigten, dass dieser Substituent in der Tat zu starr ist, um den Doppeldecker-Cluster zu umschließen, aber auch zu kurz, um zwei Bisdefektheterokuban-Cluster miteinander zu verbinden und so einen Kavitanden zu bilden.[24] Die Umsetzung mit einem bifunktionellen Adamantanderivat führte hingegen zu einer Umlagerung des Clusters zu einem Bisdefektheterokuban-Cluster mit jeweils einem kondensierten Substituenten pro Defektheterokuban-Einheit (siehe Abbildung 1.2 unten rechts).[40] Hier scheint der Winkel der Reste am Adamantan eben diese Verbrückung zu ermög-

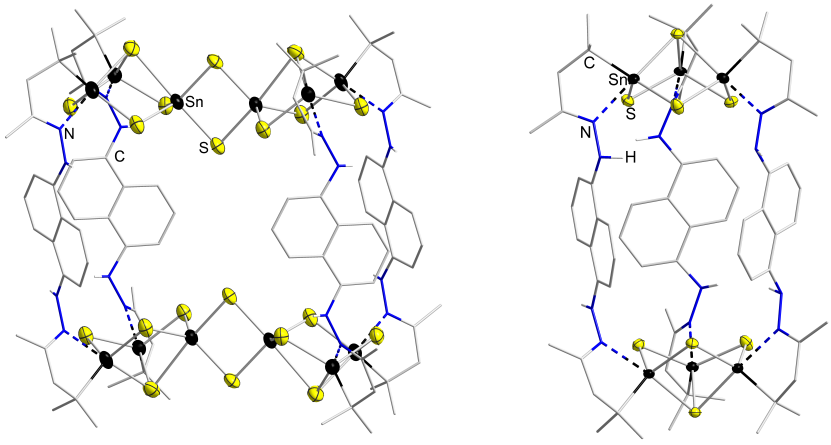

Abbildung 1.4: Molekülstrukturen von $[\{(CMe_2CH_2CMeNNH)_2C_{10}H_6\}_4\{Sn_6S_{10}\}_2]$ (links) und $[\{(CMe_2CH_2CMeNNH)_2C_{10}H_6\}_3\{Sn_3S_4\}]^{2+}$ (rechts) im Kristall.

lichen, wohingegen im Falle des *p*-Phthaldialdehyds der Winkel zu groß für eine Kondensation der Substituenten eines Moleküls ist.

Wird der Kavitand $[\{(CMe_2CH_2CMeNNH)_2C_{10}H_6\}_4\{Sn_6S_{10}\}_2]$ mit $HSnCl_3 \cdot 2\,Et_2O$ umgesetzt, führt dies zum teilweisen Abbau des Bisdefektheterokuban-Gerüsts und zur Bildung des rugbyballartigen Kapselmoleküls $[\{(CMe_2CH_2CMeNNH)_2C_{10}H_6\}_3\{Sn_3S_4\}]^{2+}$. Hier sind zwei Defektheterokuban-Cluster durch drei organische Substituenten miteinander verbunden (siehe Abbildung 1.4 rechts). Dieser Cluster konnte sowohl mit zwei $[SnCl_3]^-$-Anionen auskristallisiert als auch massenspektrometrisch nachgewiesen werden. Später konnte dieses Strukturmotiv auch mit drei Diadamantan-Substituenten nachgewiesen werden.[40] Alle Kavitanden und Kapsel-Moleküle haben gemeinsam, dass sie Lösunsgmittelmoleküle einschließen können, die unter ESI-MS-Bedingungen freigesetzt werden.

1.2.3 Reaktionen am Clusterkern – Ternäre Organozinn-Übergangsmetallchalkogenid-Cluster

Im Gegensatz zu Reaktionen an den organischen Substituenten der Zinnchalkogenid-Cluster, bei denen das anorganische Gerüst grundsätzlich intakt bleiben kann,

führen Umsetzungen mit Übergangsmetallverbindungen immer zu einer Reaktion am Clusterkern, wobei dieser unter Integration der Übergangsmetallatome umlagert und so ternäre Cluster mit organischen Substituenten entstehen.

Mittlerweile sind verschiedene Organozinn-Übergangsmetallchalkogenid-Cluster mit funktionellen Substituenten und zahlreichen Elementkombinationen bekannt.[26,36] Dabei wurde vor allem die Reaktivität gegenüber Münzmetallkomplexen (Kupfer, Silber, Gold) häufig untersucht, aber auch Platin-, Palladium-, Iridium-, Zink-, Molybdän- oder Wolframverbindungen kamen zum Einsatz.[13,25,27–33,35,44–46] Generell wurden dabei die entsprechenden Organotetrelchalkogenid-Cluster $[(RSn)_4E_6]$ oder $[(RSn)_3E_4Cl]$ mit einer Chalkogenidquelle (Na_2E oder $(SiMe_3)_2E$) und dem entsprechenden Übergangsmetallkomplex umgesetzt, wobei häufig Phosphin-Liganden zum Einsatz kamen. Des Weiteren wurden Bisdefektheterokuban-Cluster mit Chelatliganden mit Zinkhalogeniden umgesetzt, wobei in den resultierenden Clustern $[(RSn)_4(ZnX)_8S_{10}]$ (R = $CMe_2CH_2CMeNHNC(2\text{–}py)_2$ (py = Pyridinyl), X = Cl, Br, I) Zinkatome in den umgelagerten Clusterkern eingebunden und teilweise zusätzlich von Chelatliganden koordiniert werden.

Ternäre Cluster mit den Elementkombinationen Cu/Sn/E und Ag/Sn/E zeigen eine große Strukturvielfalt. Dabei bestehen sie häufig aus $\{(RSn)_2E_4\}$-Einheiten, welche andere Atome des Clusters koordinieren. Der kleinste Cluster mit einer $\{(RSn)_2E_4\}$-Einheit ist $[(R^1Sn)_2Se_4(CuPPh_3)_2]$, wobei die genannte Einheit hier zwei $\{CuPPh_3\}$-Einheiten so koordiniert, dass ein $\{Cu_2Se_2\}$-Vierring entsteht (siehe Abbildung 1.5 links).[25,33] $[(R^1Sn)_4(SnCl)_2(CuPPh_3)_2S_8]$ besteht aus zwei zentralen $\{Ph_3PCu\text{–}Sn\text{–}Cl\}$-Einheiten, die durch zwei $\{(R^1Sn)_2S_4\}$-Einheiten miteinander verbunden sind (siehe Abbildung 1.5 rechts).[29] Cluster der gleichen Topologie sind auch für die Elementkombinationen Ag/Sn/S, Ag/Sn/Se und Cu/Sn/Se bekannt, wobei bei letzterer durch Zugabe von Hydrazinhydrat bzw. Phenylhydrazin auch Cluster mit Hydrazonfunktion isoliert werden konnten.[29,31,33]

Ausgehend von dem defektheterokubanartigen Organozinnselenid-Cluster $[(R^1Sn)_3Se_4Cl]$ konnten drei weitere Cu/Sn/Se-Cluster synthetisiert werden.[33] Die Umsetzung mit $[Cu(PPh_3)_3Cl]$ und $(SiMe_3)_2Se$ führt zur Bildung von $[(CuPPh_3)_2(SnCu_2)\{(R^1Sn)_2Se_4\}_3]$ (siehe Abbildung 1.6 oben links). Bei Zugabe von Hydrazinhydrat zu Beginn der Reaktion kann stattdessen

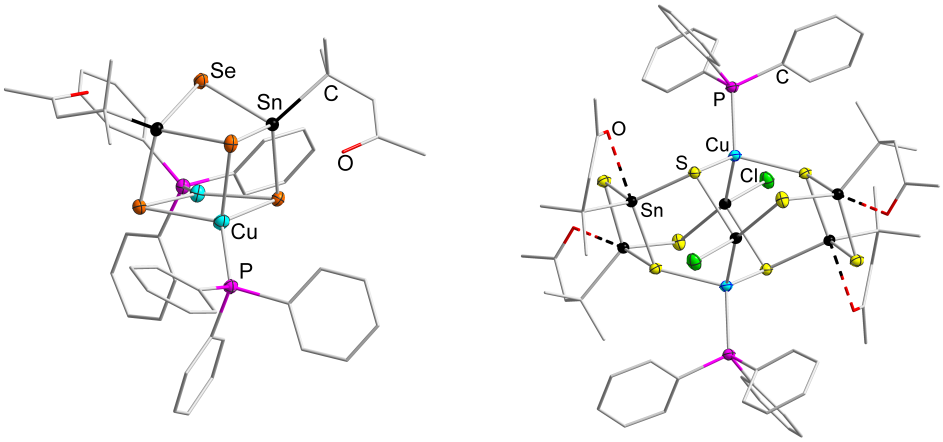

Abbildung 1.5: Links: Molekülstruktur von $[(R^1Sn)_2Se_4(CuPPh_3)_2]$. Rechts: Molekülstruktur von $[(R^1Sn)_4(SnCl)_2(CuPPh_3)_2S_8]$. Cluster der gleichen Topologie sind auch für die Elementkombinationen Cu/Sn/Se, Ag/Sn/S und Ag/Sn/Se bekannt.

$[(CuPPh_3)_2Sn\{(R^2Sn)_2Se_4\}_2]$ isoliert werden (siehe Abbildung 1.6 oben rechts). Alternativ kann auch ohne Zugabe von $(SiMe_3)_2Se$ ein Cluster mit ternärem Kern erhalten werden. Bei niedrigen Temperaturen entsteht so $[(CuPPh_3)_2(SnCl)_2(R^1SnClSe_2)_2]$, worin zwei $\{Ph_3PCu–Sn–Cl\}$-Einheiten von zwei $\{R^1SnClSe_2\}$-Einheiten koordiniert werden (siehe Abbildung 1.6 unten). Dies ist bisher der einzige Cluster der Elementkombination Cu/Sn/Se ohne $\{(RSn)_2Se_4\}$-Einheiten, was darauf schließen lässt, dass für die Entstehung dieser Einheiten die Zugabe von zusätzlichen Selenid-Ionen essentiell ist.

Teilweise konnten Zwischenstufen der Reaktionen von Organozinnsulfid-Clustern mit Sulfid-Ionen isoliert werden, bevor diese weiter mit Übergangsmetallkomplexen umgesetzt wurden. *Hauser* und *Merzweiler* zeigten bereits 2002, dass der Adamantan-Cluster $[(PhSn)_4S_6]$ mit Na_2S das Anion $[PhSnS_3]^{3-}$ bildet, welches mit $[PhPMe_2(bipy)CuCl]$ (bipy = 2,2'-Bipyridyl) weiter zu dem ternären Cu/Sn/S-Cluster $[(PhSnS_3)_2(CuPPhMe_2)_6]$ reagiert.[44] Dieser besteht aus zwei $\{PhSnS_3\}$- und sechs $\{Cu(PPhMe_2)\}$-Einheiten, wobei die sechs Kupferatome einen gewellten Cu_6-Ring bilden, der sandwichartig von den sechs Schwefelatomen koordiniert wird (siehe Abbildung 1.7 unten links).

Cluster mit ähnlicher Zusammensetzung und gleicher Topologie konnten auch ausgehend von $[(R^1Sn)_4S_6]$ mit PPh_2Me- oder PPh_3-Liganden an den Kupferatomen

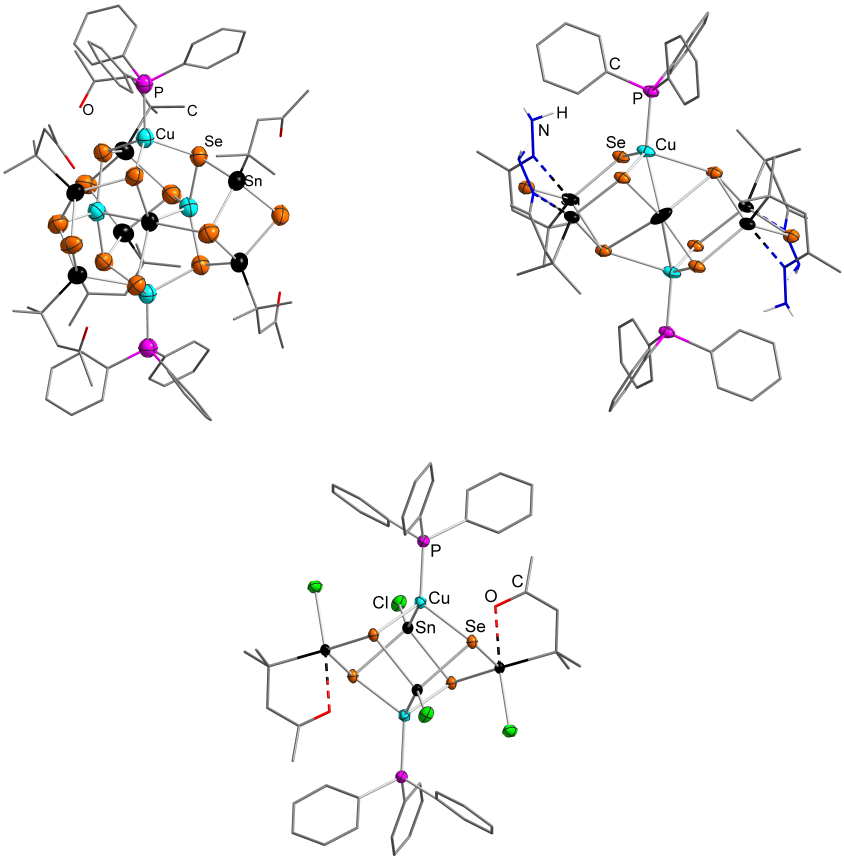

Abbildung 1.6: Oben links: Molekülstruktur von $[(CuPPh_3)_2(SnCu_2)\{(R^1Sn)_2Se_4\}_3]$. Oben rechts: Molekülstruktur von $[(CuPPh_3)_2Sn\{(R^2Sn)_2Se_4\}_2]$. Unten: Molekülstruktur von $[(CuPPh_3)_2(SnCl)_2(R^1SnClSe_2)_2]$.

synthetisiert werden.[13] Auch die Umsetzung des Carbyhydrazid-verbrückten Doppeldecker-Clusters $[R_2Sn_4S_6]$ (R = $(CMe_2CH_2CMeNNH)_2CO$) mit Na_2S führt zur teilweisen Zersetzung des Clusters und zur Bildung des anionischen Fragments $[RSn_2S_4]^{2-}$, welches als Dinatriumsalz isoliert werden konnte.[27] Die weitere Umsetzung mit $[(Ph_2MeP)_3CuCl]$ führt zur Bildung von $[R_2\{SnS_2Cu(Ph_2PMe)\}_4]$. Darin sind zwei $\{SnS_2Cu\}$-Vierringe über die beiden übrigen $\{SnS_2Cu\}$-Einheiten verbunden, welche wiederum SnS–Cu–S-Ketten bilden (siehe Abbildung 1.7 oben). Ein anderer Syntheseansatz wurde für $Na_4[(RSn)_6(OMe)_6Cu_2S_6]$ (R = $C_2H_4COO^-$) verwendet: Hier wurde das Natriumsalz des defektheterokubanartigen Clusters $[(RSn)_3S_4]^{2-}$ mit CuCl in flüssigem Ammoniak umgesetzt und anschließend mit

Methanol extrahiert.[13] Im resultierenden Cluster wird eine zentrale $\{Cu_2S_6\}$-Einheit von sechs {RSn}-Einheiten koordiniert, die wiederum durch sechs $(OMe)^-$-Liganden verbrückt werden (siehe Abbildung 1.7 unten rechts).

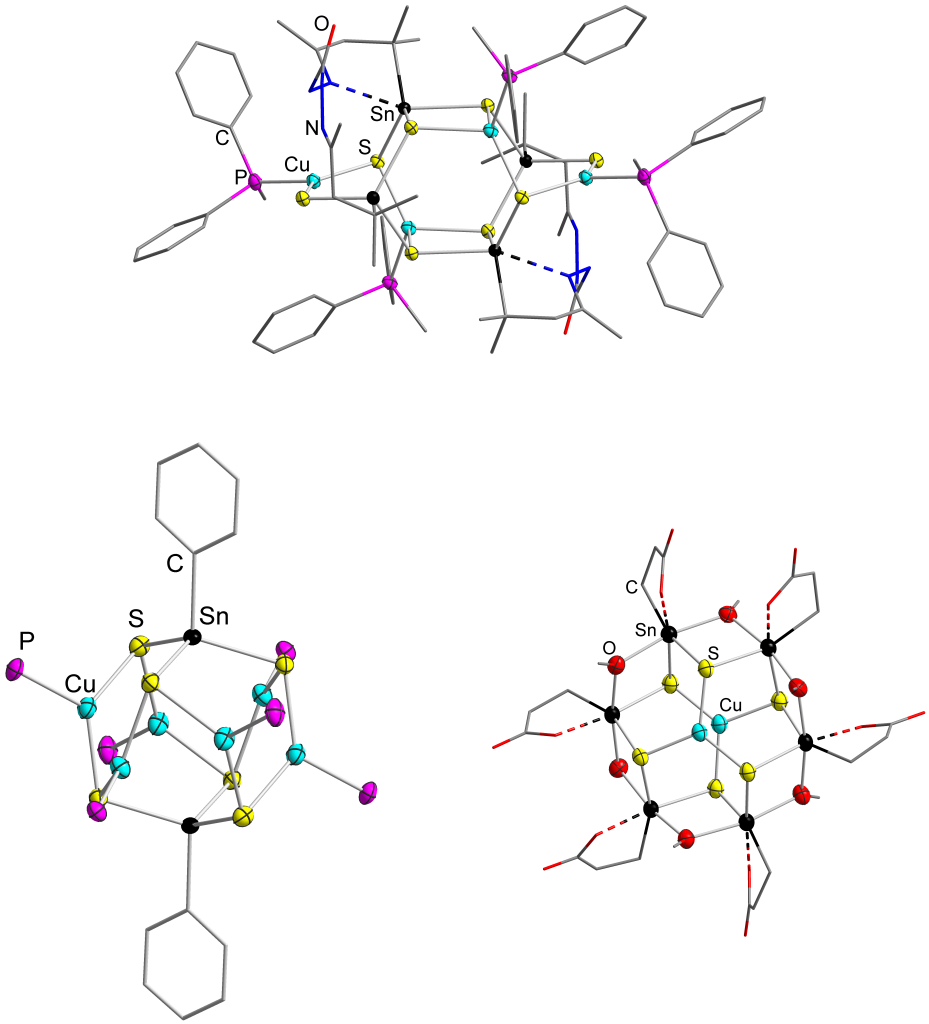

Abbildung 1.7: Oben: Molekülstruktur von $[R_2\{SnS_2Cu(Ph_2PMe)\}_4]$. Unten links: Molekülstruktur des ternären Clusters $[(PhSnS_3)_2(CuPPhMe_2)_6]$. Die organischen Reste an den Phosphoratomen sind aus Übersichtlichkeitsgründen nicht dargestellt. Unten rechts: Molekülstruktur des Anions in $Na_4[(RSn)_6(OMe)_6Cu_2S_6]$.

Die Umsetzung des adamantanartigen Clusters $[(PhSn)_4S_6]$ mit $[Cu(PPh_3)_3Cl]$

führt zu dem deutlich größeren Cluster $[(CuPPh_3)_4(PhSn)_{18}Cu_6S_{31}Cl_2]$.[34] Dessen $\{Sn_{18}Cu_{10}S_{31}\}$-Kern besteht aus zwei identischen Teilen, die über ein Schwefelatom miteinander verbunden sind (siehe Abbildung 1.8). Der Bildung des Clusters geht ein vollständiger Zerfall des binären Clusters in $[PhSn]^{3+}$- und S^{2-}-Fragmente voran. Bei kürzerer Reaktionsdauer konnte eine kleinere Vorstufe des Clusters isoliert werden, deren Molekülstruktur einem verzerrten Adamantan-Cluster ähnelt. In beiden Reaktionen wurde keine zusätzliche Sulfid-Quelle verwendet, was zeigt, dass $[(PhSn)_4S_6]$ nukleophil genug ist, um mit Kupferionen zu reagieren.

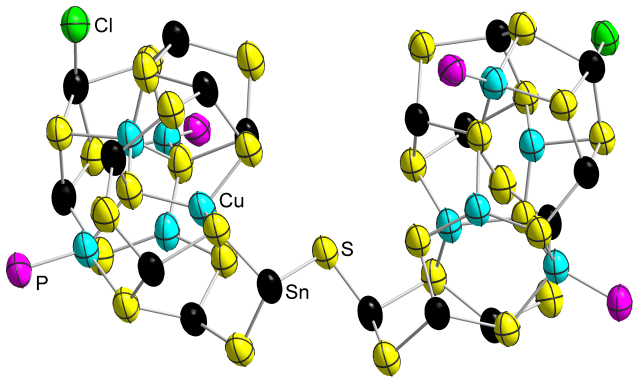

Abbildung 1.8: Molekülstruktur von $[(CuPPh_3)_4(PhSn)_{18}Cu_6S_{31}Cl_2]$. Zur besseren Übersicht sind die Phenylgruppen an den Zinn- und Phosphoratomen nicht dargestellt.

Organozinn-Silberchalkogenid-Cluster der Zusammensetzung $[(R^1Sn)_4(SnCl)_2(AgPPh_3)_2E_8]$ (E = S, Se) konnten auf ähnliche Weise wie die analogen Organozinn-Kupferchalkogenid-Cluster synthetisiert werden und zeigen dasselbe Strukturmotiv (siehe Abbildung 1.5).[29,31] Für E = Se konnte der Cluster nur unter Lichtausschluss erhalten werden.[31] Im Gegensatz zu den Organozinn-Kupferchalkogenid-Clustern reagiert der Organozinn-Silbersulfid-Cluster bei Zugabe von Hydrazinhydrat, zusätzlich zu der Veränderung des Substituenten, zu dem deutlich größeren Cluster $[(R^2Sn)_{10}Ag_{10}S_{20}]$, in dem fünf $\{(R^2Sn)_2S_4\}$-Einheiten über zehn Silberatome miteinander verbunden sind (siehe Abbildung 1.9 oben links). Für die Elementkombination Ag/Sn/Se sind zwei

weitere Cluster mit der Zusammensetzung $[(RSn)_{12}Ag_{14}Se_{25}]$ ($R = R^1$, R^2) bekannt, welche entstehen, wenn die Reaktion nicht unter Lichtausschluss durchgeführt wird. Beide unterscheiden sich in ihrer Struktur deutlich voneinander.[31] Der

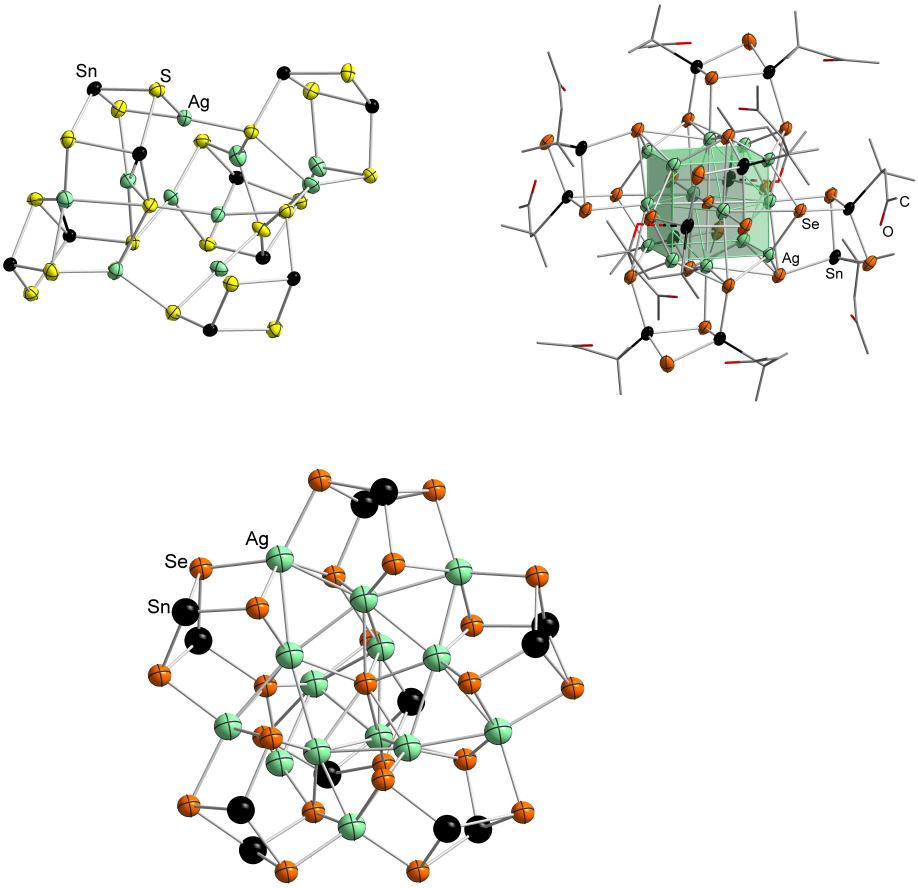

Abbildung 1.9: Oben links: Molekülstruktur von $[(R^2Sn)_{10}Ag_{10}S_{20}]$. Oben rechts: Molekülstruktur von $[(R^1Sn)_{12}Ag_{14}Se_{25}]$. Unten: Struktur des anorganischen Kerns von $[(R^2Sn)_{12}Ag_{14}Se_{25}]$.

mit dem ketofunktionalisierten Substituenten R^1 entstehende Cluster besteht aus einer oktaedrischen $\{Ag_6Se\}$-Einheit in einem $\{Ag_8\}$-Kubus, dessen Flächen von den $\{(R^1Sn)_2Se_4\}$-Einheiten überkappt werden (siehe Abbildung 1.9 oben rechts). Bei der Zugabe von Hydrazinhydrat zur Reaktionslösung entsteht ein deutlich unsymmetrischeres Isomer des Clusters. Dieses besitzt ein zentrales Selenatom, das sternförmig von zehn Silberatomen umgeben ist. Die Kanten

dieses fünfzackigen Sterns sind von fünf $\{(R^2Sn)_2Se_4\}$-Einheiten überkappt. Die fünfzählige Molekülsymmetrie wird durch eine zusätzliche $\{Ag_4(R^2Sn)_2Se_4\}$-Einheit gebrochen, die eine Seite des Moleküls überkappt.

Im Gegensatz zu den anderen Münzmetallen bevorzugt Gold eine lineare Koordination, sodass bei der Reaktion von Organozinnsulfid-Clustern mit $[Au(PR_3)Cl]$ (R = Me, Ph) kleinere Komplexe statt großer Cluster entstehen (siehe Abbildung 1.10).[29,36,45] Bisher sind vier Organozinn-Goldsulfid-Komplexe der Zusammensetzung $[(RSn)_2(AuPR_3)_2S_4]$ bekannt, zwei mit Keto- und zwei mit Hydrazonfunktion an den Zinnatomen. All diese Komplexe bestehen aus einem $\{(RSn)_2S_2\}$-Vierring,

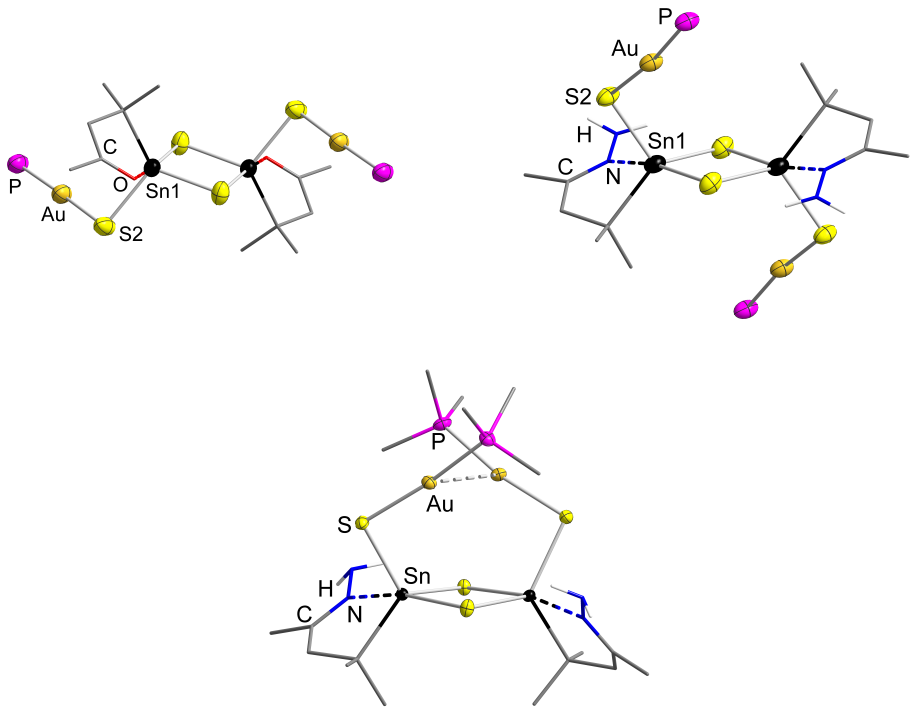

Abbildung 1.10: Molekülstrukturen von $[(R^1Sn)_2(AuPPh_3)_2S_4]$ (oben links), $[(R^2Sn)_2(AuPPh_3)_2S_4]$ (oben rechts) und $[(R^2Sn)_2(AuPMe_3)_2S_4]$ (unten). Die Phenylgruppen an den Phosphoratomen sind aus Übersichtlichkeitsgründen nicht dargestellt.

wobei die Zinnatome zusätzlich jeweils an eine $\{SAuPR_3\}$-Einheit gebunden sind. In den ketofunktionalisierten Komplexen sind die Gruppen an der Sn1–S2-Bindung dabei *cis*-ständig zueinander orientiert, wohingegen in den hydrazonfunktionaliserten

Komplexen eine *trans*-Anordnung bevorzugt wird. Aufgrund des geringeren sterischen Anspruchs der PMe_3-Gruppen kommt es in $[(R^2Sn)_2(AuPMe_3)_2S_4]$ zusätzlich zu aurophilen Wechselwirkungen zwischen den Goldatomen, wodurch sich die Molekülstruktur deutlich von der der analogen phenylsubstituierten Verbindung unterscheidet.[45]

1.3 Organisch substituierte Siliciumchalkogenid-Cluster

Im Vergleich zu Zinnchalkogenid-Clustern mit organischen Substituenten sind bisher deutlich weniger organisch substituierte Siliciumchalkogenid-Cluster bekannt. Die folgenden Abschnitte sollen einen Überblick über die bisher beschriebenen Strukturmotive dieser Cluster sowie die Möglichkeiten ihrer Synthese geben.

1.3.1 Strukturmotive

Organosiliciumsulfid-Verbindungen der generellen Zusammensetzung $[(RSi)_4S_6]$ (R = Me, *n*Pr) wurden erstmals 1952 beschrieben,[2] wobei zunächst über die genaue Molekülstruktur spekuliert wurde.[47,48] Denkbar sind auch hier der sogenannte Doppeldecker-Strukturtyp sowie ein heteroadamantanartiger Cluster. Die erste röntgendiffraktometrische Untersuchung an Einkristallen von $[(MeSi)_4S_6]$ erfolgte 1968 und zeigte für diese Verbindung eine adamantanartige Struktur.[5] Mittlerweile sind mehrere Sulfide und Selenide mit diesem Strukturmotiv bekannt, welches das thermodynamisch stabilste zu sein scheint.[12] Erst seit letztem Jahr ist ein Organosiliciumtellurid-Cluster mit Adamantanstruktur, $[\{Dipp(SiMe_3)NSi\}_4Te_6]$ (Dipp = 2,6-Di*iso*propylphenyl), bekannt.[49] Wird der sterisch anspruchsvolle Thex-Substituent verwendet, so ist auch der Doppeldecker-Strukturtyp zugänglich.[10] Des Weiteren ist ein Defektheterokuban-Cluster, $[(Dipp(SiMe_3)NSi)_4Se_3]$, bekannt, welcher sich von den bekannten Organozinnchalkogenid-Defektheterokuban-Clustern dahingehend unterscheidet, dass eine im Fall der Organozinnchalkogenid-Cluster von einem Chalkogenatom besetzte Ecke hier von einer {RSi}-Einheit besetzt ist und so drei Si–Si-Bindungen innerhalb des Clusters vorliegen.[49] Somit ist der Cluster neutral und benötigt im Gegensatz zu den bekannten Organozinnchalkogenid-Clustern

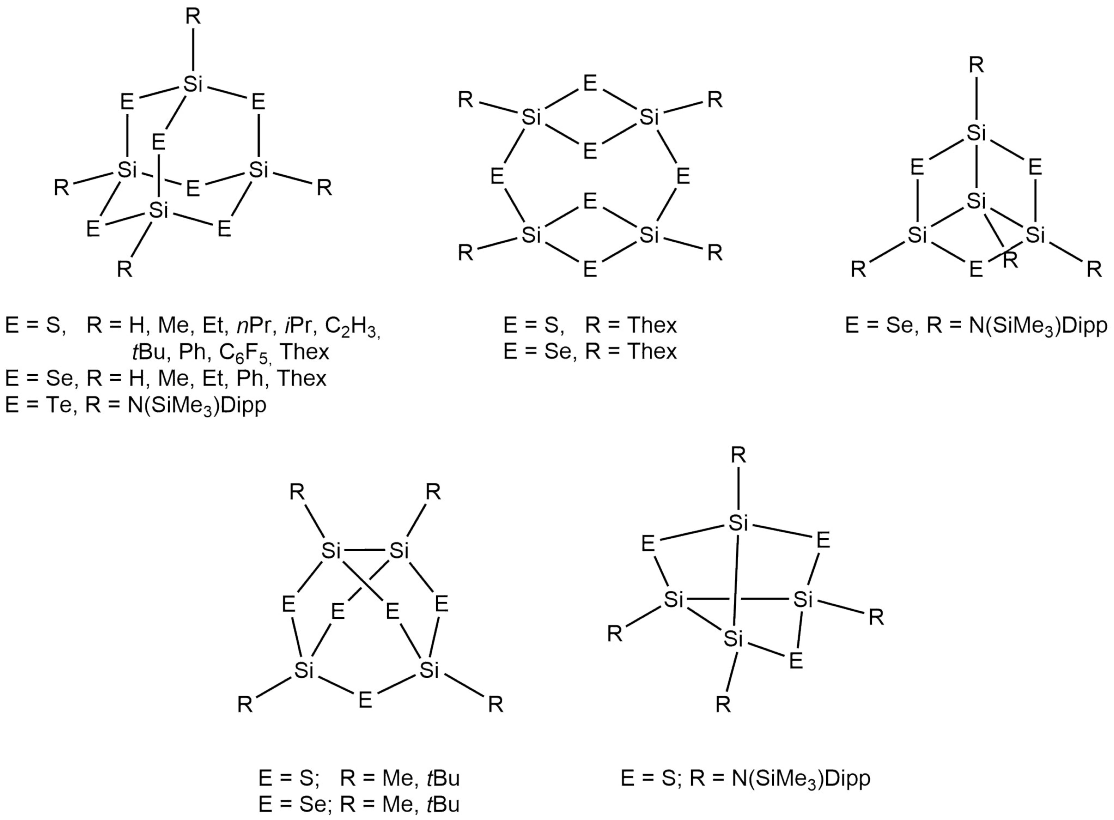

Abbildung 1.11: Übersicht über die verschiedenen Strukturmotive, die für organisch substituierte Siliciumchalkogenid-Cluster bisher bekannt sind.[5,10,48–57]

mit Defektheterokuban-Struktur keine Cl^--Anionen zum Ladungsausgleich. Für Methyl- und *tert*Butyl-Reste sind Sulfid- und Selenid-Cluster mit Noradamantanstruktur bekannt.[50,51] Eine Übersicht der bisher bekannten Strukturmotive von Organisiliciumchalkogenid-Cluster ist in Abb. 1.11 gezeigt.

Bei der Untersuchung der Isomerisierung der Verbindungen $[(ThexSi)_4E_6]$ (E = S, Se) mit Doppeldecker-Struktur wurde festgestellt, dass in Lösung ein Gleichgewicht zwischen Doppeldecker- und Adamantan-Strukturtyp vorliegt, welches für E = S auf der Seite des Adamantan-Strukturtyps und für E = Se auf der Seite des Doppeldecker-Strukturtyps liegt.[12] Dies ist sehr ungewöhnlich: Aufgrund von Ringspannungen sollte der Adamantan-Strukturtyp der stabilere sein, was auch dadurch gestützt wird, dass keine weiteren Organosiliciumchalkogenid-Cluster mit

Doppeldecker-Struktur bekannt sind. Warum das Gleichgewicht für $[(ThexSi)_4Se_6]$ auf der Seite des Doppeldecker-Strukturtyps liegt, konnte nicht geklärt werden. Jedoch wurde angenommen, dass aufgrund der größeren Si–Se-Bindungslängen (im Vergleich zu Si–S) die Ringspannung erniedrigt und so die Reaktivität gesenkt wird.[10]

1.3.2 Präparativer Zugang

In der Literatur sind verschiedene Synthesewege beschrieben, um Cluster des Typs $[(RSi)_4E_6]$ zu erhalten, wobei die meisten von den entsprechenden Organosiliciumtrichloriden $RSiCl_3$ ausgehen. Als Chalkogenidquelle kommen verschiedene Verbindungen zum Einsatz, auf deren Vor- und Nachteile im Folgenden genauer eingegangen werden soll.

Die erste beschriebene Syntheseroute verwendet Schwefelwasserstoff oder Selenwasserstoff als Chalkogenidquelle und ist für R = Me, Et, *n*Pr, *i*Pr, CH_2=CH und Ph erprobt.[2,48,53] Dabei wird entweder lösungsmittelfrei bei hohen Temperaturen gearbeitet,[48] oder es werden Benzol als Lösungsmittel und Pyridin oder Triethylamin als HCl-Akzeptor verwendet.[2,8,53] Die Ausbeuten liegen hierbei um 50%. Ein großer Nachteil dieser Reaktionsführung ist der apparative Aufwand bei der Verwendung von Gasen, welche außerdem schwierig zu dosieren sind. Des Weiteren spricht die hohe Toxizität der Chalkogenwasserstoffe gegen diesen Syntheseweg.

Eine weitere Synthesemöglichkeit besteht in der Verwendung von $(SiMe_3)_2S$ als Sulfidquelle. Erhitzen der Reaktanden auf 80-90 °C ohne Lösungsmittel führt hierbei zu Ausbeuten von über 80%.[58] Als Nebenprodukt entsteht Trimethylsilylchlorid, welches im Vakuum entfernt werden kann und so eine einfache Aufarbeitung des gewünschten Produkts ermöglicht. Während bei der Synthese von vergleichbaren Organozinnsulfid-Clustern die Bildung einer starken Si–Cl-Bindung in Trimethylsilylchlorid als zusätzliche Triebkraft fungiert, ist dies hier nicht der Fall, da in Organosiliciumtrichloriden bereits Si–Cl-Bindungen vorhanden sind. Die Triebkraft der Reaktion ist also nur die Bildung des flüchtigen Nebenprodukts, was die relativ hohen Reaktionstemperaturen bedingt. Da *Horn* und *Hemeke* keine Angaben zur eingesetzten Menge der Edukte machen, ist nicht klar, ob sich auf diese Weise auch größere Mengen der Organosiliciumchalkogenid-Cluster herstellen lassen.

Seit den 90er Jahren werden hauptsächlich Alkalimetallchalkogenide als Chalkogenidquellen eingesetzt.[50,51,54,56,59] Dabei erfolgt die Reaktion in THF, indem das Organosiliciumtrichlorid und das entsprechende Alkalimetallchalkogenid bei 0 °C zusammen gegeben und über mehrere Stunden langsam auf Raumtemperatur gebracht werden. Aufgrund der heterogenen Reaktionsführung ist die Aufarbeitung etwas aufwendiger als bei der Synthese von beispielsweise Organozinnsulfiden aus Organozinntrichlorid und Natriumsulfid. Dadurch, dass im Falle der Organozinnsulfid-Cluster kurzzeitig in wässrigen Lösungen gearbeitet wird, geht das Natriumsulfid vollständig in Lösung und der gewünschte Organozinnsulfid-Cluster fällt aus und kann abfiltriert werden. Aufgrund der Hydrolyseempfindlichkeit der verwendeten Siliciumtrichloride muss hier allerdings wasserfrei gearbeitet werden, sodass die Reaktionsmischung schon zu Beginn der Reaktion eine Suspension ist, aus der dann der gewünschte Cluster ausfällt. Dieser kann dann mit einem unpolaren Lösungsmittel (Benzol oder Toluol) extrahiert werden, und nach Abtrennung des entstehenden Alkalimetallchlorids wird der entsprechende Organosiliciumchalkogenid-Cluster erhalten. Diese Syntheseroute ist bisher für R = Me, Et, *t*Bu, Ph und Thex beschrieben worden,[10,50,54,59] wobei für Adamantan- oder doppeldeckerartige Cluster hauptsächlich Natriumchalkogenide verwendet werden, während die Reaktion von Lithiumchalkogeniden mit Tetrachlordisilanen zu Noradamantan-Clustern (R = Me, *t*Bu) führt.[50,51]

Der bisher einzige Organosilicumtellurid-Cluster $[\{Dipp(SiMe_3)NSi\}_4Te_6]$ wurde synthetisiert, indem die Ringverbindung $[Si_4\{N(SiMe_3)Dipp\}_4]$ mit $TeP(nBu)_3$ umgesetzt wurde. Wird die Ringverbindung stattdessen mit elementarem Selen umgesetzt, so entstehen Organosiliciumselenid-Cluster mit Tricycloheptan- oder Nortricyclan-Struktur, welche nach Erhitzen im Ofen in den Defektheterokuban-Cluster $[(Dipp(SiMe_3)NSi)_4Se_3]$ überführt werden konnten.[49]

1.4 Organotetrelchalkogenid-Cluster mit nichtlinearen optischen Eigenschaften

In den letzten Jahren zeigte sich, dass einige der in unserer Arbeitsgruppe untersuchten Organotetrelchalkogenid-Cluster teilweise extreme nichtlineare optische

Eigenschaften besitzen.[38,39,56,60] Im folgenden Abschnitt werden zunächst die physikalischen Grundlagen von nichtlinearer Optik am Beispiel der Frequenzverdopplung erklärt, woraufhin anschließend genauer auf die untersuchten Cluster eingegangen wird.

1.4.1 Nichtlineare Optik – Frequenzverdopplung

Bei der Wechselwirkung eines elektrischen Felds $\vec{E}$ mit einem Medium wird in diesem eine Polarisation $\vec{P}$ induziert. Dabei besteht zunächst ein linearer Zusammenhang zwischen Feldstärke und Polarisation, der folgendermaßen beschrieben werden kann:

$$\vec{P} = \varepsilon_0 \chi \vec{E} \tag{1.1}$$

Bei χ handelt es sich um die elektrische Suszeptibilität, ε_0 bezeichnet die elektrische Feldkonstante im Vakuum. Bei sehr großen Feldstärken kann $\vec{P}$ nicht beliebig weiterwachsen. So können beispielsweise bei der Orientierung von molekularen Dipolen maximal alle Dipole längs der Feldlinien ausgerichtet sein – es findet also ein Sättigungsvorgang statt. Somit muss die Suszeptibilität selbst eine Funktion der Feldstärke sein. Dies lässt sich über einen Potenzreihenansatz beschreiben. Für isotrope Substanzen gilt:

$$\begin{aligned} P &= \varepsilon_0(\chi_1 E + \chi_2 E^2 + \chi_3 E^3 + ...) \\ &= P_{lin} + \varepsilon_0(\chi_2 E^2 + \chi_3 E^3 + ...) \\ &= P_{lin} + P_{NL} \end{aligned} \tag{1.2}$$

Die höheren Terme χ_2, χ_3,... und damit der nichtlineare Anteil der Polarisation P_{NL} sind dabei so klein, dass ihr Beitrag erst bei sehr hohen Feldstärken, wie sie zum Beispiel durch leistungsfähige Laser erreicht werden können, wichtig wird. Um die Auswirkung der Nichtlineritäten zu diskutieren, kann man vereinfacht den Ansatz ebener Wellen $E = \frac{1}{2}E_0\,e^{i\omega t} + \frac{1}{2}E_0\,e^{-i\omega t} = E_0\cos(\omega t)$ verwenden:

$$\begin{aligned} P = \varepsilon_0\chi_1 E_0 \cos(\omega t) + \frac{1}{2}\varepsilon_0\chi_2 E_0^2[1 + \cos(2\omega t)] \\ + \frac{1}{4}\varepsilon_0\chi_3 E_0^3[3\cos(\omega t) + \cos(3\omega t)] + ... \end{aligned} \tag{1.3}$$

Wie aus Formel 1.3 ersichtlich wird, führt der nichtlineare Anteil dazu, dass die Polarisation mit verschiedenen Frequenzen schwingen kann: So verursacht χ_2 einen zeitlich konstanten Anteil der Polarisation sowie einen Term, der mit der doppelten Frequenz 2ω schwingt. χ_3 ergibt unter anderem eine mit dreifacher Frequenz schwingende Polarisation. Für die Nichtlinearität zweiter Ordnung χ_2 bedeutet dies, dass jedes Atom bzw. Molekül, das von der einfallenden Welle mit der Frequenz ω getroffen wird, eine Streuwelle auf der Frequenz ω sowie eine Oberwelle auf der Frequenz 2ω abstrahlt (Frequenzverdopplung, *second harmonic generation*, SHG).[61,62]

Die neu erzeugten Oberwellen sind nur über eine kurze Strecke innerhalb des Mediums in Phase und löschen sich durch destruktive Interferenz weitgehend aus. Das liegt daran, dass die Phasengeschwindigkeiten der Grundwelle ($c_n = \frac{c}{n(\omega)}$) und der Oberwelle ($c_n = \frac{c}{n(2\omega)}$) unterschiedlich sind, da sich die Brechungsindizes $n(2\omega)$ und $n(\omega)$ aufgrund der Dispersion unterscheiden. Um dieses Problem zu lösen, werden doppelbrechende Materialien verwendet, in denen der Brechungsindex abhängig von der Richtung und der Polarisation des eingestrahlten Lichts ist – häufig in Form von Einkristallen. Dabei wird der einfallende Strahl in zwei Teilstrahlen aufgespalten: einen ordentlichen Strahl (o-Strahl), der das Snellius'sche Brechungsgesetz befolgt, und einen außerordentlichen Strahl (ao-Strahl), der dies nicht tut. Beide Strahlen sind senkrecht zueinander polarisiert. Für den ao-Strahl gilt, dass der Brechungsindex n_{ao} von dem Winkel ϑ zwischen einfallendem Strahl und optischer Achse des Mediums abhängt. Es gibt also einen Winkel ϑ, bei dem die Phasenanpassungsbedingung $n_o = n_{ao}(\vartheta, 2\omega)$ exakt erfüllt ist. Wird dieser Winkel durch Drehen des Kristalls eingehalten, so werden die Oberwellen im Kristall kohärent erzeugt und die Frequenzverdopplung hat einen hohen Wirkungsgrad. Auf diese Weise sind Ausbeuten von nahezu 100% möglich. Dies ist zum Beispiel für Laser von Bedeutung, die sich vor allem im langwelligen Spektralbereich realisieren lassen. Durch Frequenzverdopplung ist die Erzeugung von Laserstrahlen bis in den UV-Bereich mit geringem Aufwand möglich.[61,63]

Voraussetzung für Frequenzverdopplung ist, dass der Kristall der eingesetzten Verbindung kein Inversionszentrum besitzt, da sonst nichtlineare Suszeptibilitäten mit gerader Ordnung gleich null werden (das Vorzeichen der Polarisation kehrt sich bei Umkehr des $\vec{E}$-Feldes ebenfalls um). Technisch gebräuchliche Materialien

mit hohen χ_2-Werten sind beispielsweise Kaliumdihydrogenphosphat, Lithiumiodat oder β-Bariumborat.[61]

1.4.2 Nichtlineare optische Eigenschaften bei Organotetrelchalkogenid-Clustern

Bei der Untersuchung von $[(StySn)_4S_6]$ zeigte sich, dass dieser Cluster extreme nichtlineare optische Eigenschaften besitzt. Die Anregung mit einer cw-Infrarotlaserdiode führte zu gerichteter Weißlichtemission (*white light generation*, WLG) über das gesamte sichtbare Spektrum.[38] Bei $[(StySn)_4S_6]$ handelt es sich um ein amorphes Pulver, dessen Molekülstruktur dementsprechend nicht röntgendiffraktometrisch bestimmt werden konnte. Mittels Dichtefunktionaltheorie (DFT)-Rechnungen konnte jedoch gezeigt werden, dass der Adamantantyp gegenüber dem Doppeldeckertyp für diesen Cluster energetisch bevorzugt wird. Der Farbeindruck der Weißlichtemission bei hohen Pumpleistungen (dunkelster Punkt) ähnelt dem einer Glühlampe (graues Viereck), wie in der in Abbildung 1.12 gezeigten CIE-Normfarbtafel zu sehen ist.

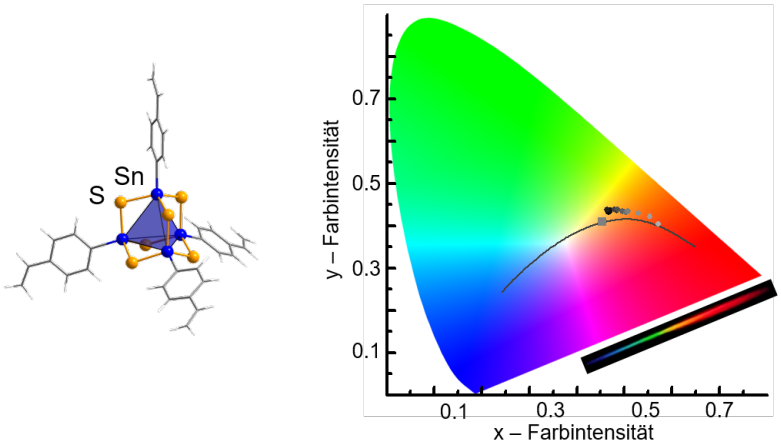

Abbildung 1.12: Links: DFT-optimierte Molekülstruktur von $[(StySn)_4S_6]$. Rechts: Farbtemperatur des emittierten Lichts in einer CIE-Normfarbtafel dargestellt durch Punkte. Die graue Linie zeigt zum Vergleich die Emission eines schwarzen Körpers. Das graue Quadrat stellt den Farbeindruck einer warmweißen Lichtquelle bei 2856 K dar.

Um den zugrundeliegenden Mechanismus sowie die Voraussetzungen für die Weißlichterzeugung zu verstehen, wurden weitere Studien durchgeführt.[39,56,60,64] Dabei wurden sowohl die Substituenten an den Zinnatomen als auch die verwendeten Tetrel- und Chalkogenatome variiert. Die untersuchten Varianten können Tabelle 1.1 entnommen werden. Es zeigte sich schnell, dass Weißlichtemission nur bei amorphen Verbindungen auftritt, wohingegen kristalline Adamantan-Cluster normalerweise SHG zeigen. Ausnahmen sind $[(MeSn)_4S_6]$ und $[(NpSn)_4S_6]$ (Np = 1-Naphthyl), welche zwar amorph sind, aber trotzdem nur SHG zeigen. Der Grund dafür ist bei $[(MeSn)_4S_6]$ das Fehlen ausreichender Elektronendichte und bei $[(NpSn)_4S_6]$ die beginnende Ausordnung der Moleküle im Pulver, welche durch π-π-Wechselwirkungen zwischen den Naphthyl-Substituenten verursacht wird und zur Erfüllung der Phasenanpassungsbedingung führt.[56] Auch die Weiß-

Tabelle 1.1: Übersicht über die bisher auf WLG untersuchten Organotetrelchalkogenid-Cluster.

Sn/S	Sn/Se	Ge/S	Si/S
$[(MeSn)_4S_6]$ ○, ◊,[1]			
$[(PhSn)_4S_6]$ ○	$[(PhSn)_4Se_6]$ ○	$[(PhGe)_4S_6]$ ○	$[(PhSi)_4S_6]$ ◊
$[(StySn)_4S_6]$ ○			
$[(BnSn)_4S_6]$ ◊	$[(BnSn)_4Se_6]$ ◊,[3]		
$[(NpSn)_4S_6]$ ○,[2]			
$[(R^{COO}Sn)_4S_6]$ ○	$[(R^{COO}Sn)_4Se_6]$ ○		
$[(\eta^1\text{–}CpSn)_4S_6]$ ○	$[(\eta^1\text{–}CpSn)_4Se_6]$ ○		
$[(CySn)_4S_6]$ ○	$[(CySn)_4Se_6]$ ○		
$[\{(Me_3P)_3AuSn\}\{PhSn\}_3S_6]$ ◊,[3]			
$[\{(Et_3P)_3AgSn\}\{PhSn\}_3S_6]$ ◊,[3]			
$[\{(Me_3P)_3CuSn\}\{PhSn\}_3S_6]$ ◊,[4]			

◊: kristallin, SHG ○: amorph
[1]: geringe Elektronendichte am Substituenten, SHG
[2]: (beginnende) Fernordnung im Feststoff, SHG
[3]: Amorphisierung oder Schmelzen bei Bestrahlung, WLG
[4]: Lumineszenzmaximum bei 1.45 eV, keine WLG
$R^{COO} = CO_2Et(C_6H_4)CH_2CH_2$

lichtemission von $[(BnSn)_4Se_6]$ (Bn = Benzyl), $[\{(Me_3P)_3AuSn\}\{PhSn\}_3S_6]$ und $[\{(Et_3P)_3AgSn\}\{PhSn\}_3S_6]$ scheint dieser Regel zunächst zu widersprechen. Allerdings stellte sich heraus, dass Kristalle dieser Verbindungen bei Laserbestrahlung schmolzen bzw. amorphisiert wurden, sodass das Weißlicht hier letztendlich auch von ungeordneten Medien generiert wurde.[39,60] Die Voraussetzung der Amorphizität wurde durch die Untersuchung von 1,3,5,7-Tetraphenyladamantan bestätigt. Dieses kann sowohl in kristalliner als auch in amorpher Form synthetisiert werden. Auch hier zeigte die amorphe Form Weißlichtemission, wohingegen die kristalline Form Frequenzverdopplung zeigte.[64]

Bei der Variation der im Cluster vorliegenden Atomsorten zeigte das Emissionsspektrum von $[(PhGe)_4S_6]$ eine geringfügige Blauverschiebung im Vergleich zu $[(PhSn)_4S_6]$.[56] Außerdem kam es bei einigen Organozinnselenid-Clustern zu einer leichten Rotverschiebung im Vergleich zu den entspechenden Sulfid-Clustern.[39] Dies kann darauf zurückgeführt werden, dass die Weißlichtemission auf der Anregung von Elektronen in extrem kurzlebige virtuelle Zustände innerhalb des HOMO-LUMO-Gaps basiert, aus denen die Moleküle in verschiedene schwingungsangeregte Zustände relaxieren.[65] Da die Bandlücke von GeS_2 mit 3.4 eV größer ist als die von SnS_2 mit 2.18-2.44 eV, ist das gemessene Spektrum also blauverschoben.[66–69] Analog sollte der Farbeindruck für entsprechende Organosiliciumsulfid-Cluster noch weiter in den blauen Bereich verschoben sein (Bandlücke von SiS_2: 2.44-5.0 eV).[70,71] Der bisher einzige auf nichtlineare optische Eigenschaften untersuchte Organosiliciumsulfid-Cluster ist allerdings kristallin und zeigt deswegen nur Frequenzverdopplung.[56] Eine weitere Voraussetzung für Weißlichtemission ist also ein hinreichend großes HOMO-LUMO-Gap, da sonst die Anregungen in elektronisch angeregte Zustände mit größerer Lebensdauer dominieren und zu anderen Relaxationswegen, zum Beispiel Photolumineszenz, führen würden.

Die bisher bekannten Voraussetzungen für Weißlichtemission sind also:

- Amorphizität
- hohe Elektronendichte am Substituenten (cyclische oder aromatische Substituenten)

Die Emissionsspektren werden dabei am unteren Ende von der Anregungsenergie und am oberen Ende durch das HOMO-LUMO-Gap der Verbindung begrenzt.

Ob die Abwesenheit von Inversionssymmetrie in den Verbindungen eine weitere Voraussetzung für WLG ist, ist bisher noch unklar. Zwar besitzen die untersuchten adamantanartigen Cluster selbst kein Inversionszentrum, die Raumgruppen der kristallinen Cluster jedoch sehr wohl. Dass diese trotzdem SHG zeigen, wird auf Oberflächeneffekte oder Defekte im Kristall zurückgeführt.

2 Motivation und Zielsetzung

Wie aus dem vorangegangenen Kapitel ersichtlich ist, sind bisher vor allem Organozinnsulfid-Cluster auf ihre Reaktivität sowohl an ihren Substituenten als auch am Clusterkern untersucht worden, wohingegen Organozinnselenid-Cluster weit weniger gut untersucht wurden. In ersten Studien waren sie mit Übergangsmetallkomplexen umgesetzt worden. Vor allem bei den daraus entstandenen ternären Clustern mit der Elementkombination Cu/Sn/Se zeigte sich dabei eine große Strukturvielfalt auch bei geringen Veränderungen der Reaktionsbedingungen. Ein Ziel meiner Arbeit war es, die Bildung ternärer Cluster mit dieser Elementkombination genauer zu untersuchen und dabei verschiedene Paramater zu variieren, beispielsweise die Reaktionszeit oder den Zeitpunkt der Zugabe von weiteren Reaktanden, wie etwa Hydrazinhydrat. Dies sollte die Bildung neuer Cluster ermöglichen und zu einem besseren Verständnis dieser Reaktionen führen.

Obwohl eine Vielzahl an Derivatisierungsreaktionen an den Substituenten der Organozinnsulfid-Cluster duchgeführt worden sind, sind die entsprechenden ketofunktionalisierten Organozinnselenid-Cluster bisher nur in *proof-of-principle*-Reaktionen mit Hydrazinhydrat bzw. Phenylhydrazin umgesetzt worden, wobei die entsprechenden hydrazonfunktionalisierten Cluster entstanden. Bisher war allerdings nicht bekannt, ob sich auch andere Reaktionen an den Substituenten auf Organozinnselenid-Cluster übertragen lassen. Deswegen sollte deren Reaktivität gegenüber bifunktionellen Verbindungen untersucht werden. Dabei sollte zunächst vom Doppeldecker-Cluster ausgegangen werden, um so intramolekular verbrückte Cluster zu erhalten. Die Reaktionsführung hin zu größeren Kavtitanden oder kapselartigen Molekülen kann nicht direkt von Organozinnsulfid- auf Organozinnselenid-Cluster übertragen werden, da Organozinnselenid-Cluster deutlich empfindlicher gegenüber Säuren sind. Deshalb sollte zur Bildung von kapselartigen Molekülen mit intermolekularer Verbrückung stattdessen vom Defektheterokuban-Cluster

ausgegangen werden. Ein erster rugbyballartiger Cluster mit Substituenten auf Adipinsäuredihydrazid-Basis konnte bereits von *Mario Argentari* im Rahmen seiner Masterarbeit erhalten werden.[72] Mein Ziel war es, den Einfluss der Länge und Flexibilität der Substituenten auf die Form des Clusters zu untersuchen. Dazu sollte neben dem flexiblen Adipinsäuredihydrazid auch das deutlich starrere 1,1'-(1,5-Naphthalindiyl)bishydrazin als Substituent verwendet werden. Gleichzeitig sollte es so möglich sein, den Einfluss der größeren Selenatome auf die Clusterstruktur zu untersuchen, da bereits ein Organozinnsulfid-Cluster mit 1,1'-(1,5-Naphthalindiyl)bishydrazin-basierendem Substituenten existiert. Die Syntheseplanung für die Untersuchung der Reaktivität von Organozinnselenid-Clustern an ihrem Clusterkern sowie an ihren organischen Substituenten ist in Schema 2.1 dargestellt.

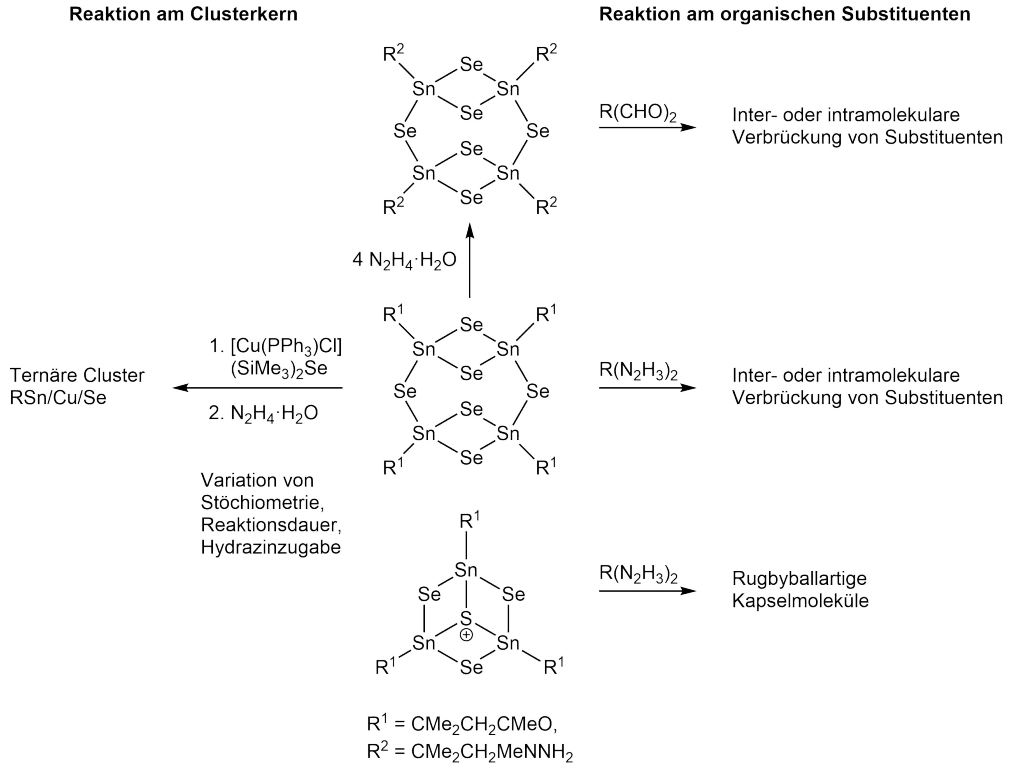

Schema 2.1: Syntheseplan für die Untersuchung der Reaktivität von Organozinnselenid-Clustern gegenüber $[Cu(PPh_3)_3Cl]$ unter Variation der Reaktionsbedingungen sowie gegenüber bifunktionellen organischen Verbindungen.

Im Gegensatz zu Organozinnchalkogenid-Clustern ist die Reaktivität von

Organosiliciumchalkogenid-Clustern bislang nicht untersucht worden. Gleichzeitig könnten Organosiliciumchalkogenid-Adamantan-Cluster mit elektronenreichen Substituenten für Weißlichtemission (WLG) interessant sein. Da die Bandlücke von SiS_2 mit 2.44-5.0 eV größer ist als die von SnS_2 mit 2.18-2.44 eV, sollte der Farbeindruck im Vergleich zu den bisher auf WLG untersuchten Organozinnchalkogenid-Clustern blauverschoben sein. Im letzten Teil meiner Arbeit habe ich mich deshalb mit der Synthese neuer Organosiliciumsulfid-Cluster beschäftigt. Als Ausgangsverbindungen sollten dazu Organotrichlorsilane mit elektronenreichen, cyclischen Substituenten, beispielsweise Naphthyl- oder Styrylsubstituenten, verwendet werden. Die deutlich größere Hydrolyseempfindlichkeit dieser Ausgangsverbindungen im Vergleich zu Organotrichlorstannanen sowie die Si–Cl-Bindungen darin erforderte einen anderen Syntheseansatz als bei den analogen Organozinnsulfid-Clustern. So war auf vollständigen Feuchtigkeitsausschluss zu achten und statt $(SiMe_3)_2S$ sollte Na_2S als Sulfidquelle verwendet werden, was zu einer heterogenen Reaktion und komplizierterer Aufarbeitung führen würde. Sämtliche so neu synthetisierten Cluster sollten in Kooperation mit der Arbeitsgruppe *Chatterjee* auf ihre optischen Eigenschaften untersucht werden. Des Weiteren sollten die Cluster mit Übergangsmetallkomplexen umgesetzt werden, um zu erkunden, ob sich ihre Reaktivität von der der Organozinnchalkogenid-Cluster unterscheidet. Der in diesem Absatz genannte Syntheseplan ist in Schema 2.2 zusammengefasst.

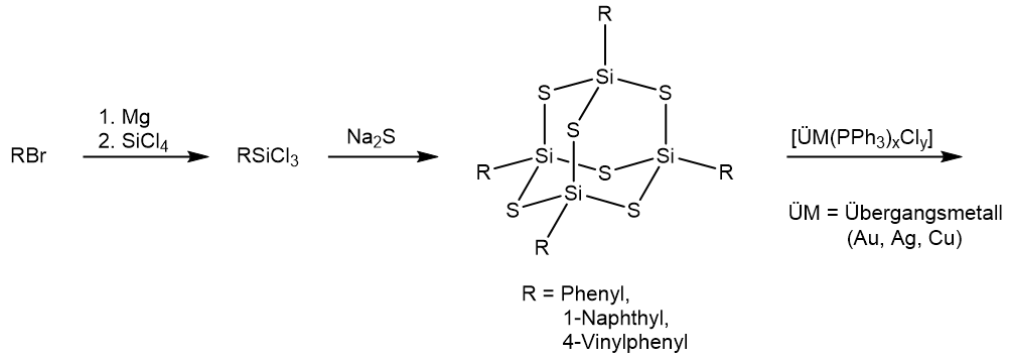

Schema 2.2: Plan für die Synthese von adamantanartigen Organosiliciumsulfid-Clustern sowie die Untersuchung deren Reaktivität gegenüber Übergangsmetallkomplexen.

3 Übersicht über die im kumulativen Teil enthaltenen Publikationen

Im Rahmen meines Promotionsprojekts sind bisher drei veröffentlichte Publikationen entstanden. Des Weiteren bin ich Co-Autorin dreier weiterer Artikel, die entweder auf Ergebnissen eines Vertiefungspraktikums während meines Masterstudiums basieren oder nicht in thematischem Zusammenhang zu meinem Promotionsprojekt stehen (siehe vollständige Publikationsliste in Abschnitt **C**). Zum kumulativen Teil der vorliegenden Dissertation zählen die im Folgenden genannten und beschriebenen drei Publikationen.

Die Bilder und Benennungen der Verbindungen in den folgenden Abschnitten werden so verwendet, wie es in der entsprechenden Publikation der Fall war.

3.1 *Organotin Selenide Clusters and Hybrid Capsules*
Katharina Hanau, Niklas Rinn, Mario Argentari, Stefanie Dehnen, *Chem. Eur. J.* **2018**, *24*, 11711–11716.

3.2 *Variations in the Interplay of Intermetallic and Metal Chalcogenide Units in Organotin-Copper Selenide Clusters*
Katharina Hanau, Niklas Rinn, Stefanie Dehnen, *Inorg. Chem.* **2020**, *59*, 198–202.

3.3 *Towards Understanding the Reactivity and Optical Properties of Organosilicon Sulfide Clusters*
Katharina Hanau, Sebastian Schwan, Moritz R. Schäfer, Marius J. Müller, Christof Dues, Niklas Rinn, Simone Sanna, Sangam Chatterjee, Doreen Mollenhauer, Stefanie Dehnen, *Angew. Chem.* **2021**, *133*, 1196–1206; *Angew. Chem. Int. Ed.* **2021**, *60*, 1176–1186.

3.1 Organotin Selenide Clusters and Hybrid Capsules

In dieser Publikation wurden Strukturmotive, die für die organisch funktionalisierten Zinnsulfid-Cluster schon länger bekannt waren, erstmals auch für organisch funktionalisierte Zinnselenid-Cluster beobachtet und beschrieben. Die beschriebenen Reaktionen erfolgten ausgehend von $[(R^1Sn)_4Se_6]$ oder $[(R^1Sn)_3Se_4Cl]$ als Edukt (R^1 = CMe_2CH_2CMeO). Sämtliche Verbindungen wurden mittels Einkristallstrukturanalyse, NMR-spektroskopisch und massenspektrometrisch sowie mittels µ-RFA untersucht. Das erste beschriebene Strukturmotiv ist das des Bis-Defektheterokubans in $[\{(RSn)_2SnSe_4\}_2(\mu\text{–}Se)_2]$ (R = R^2 ($CMe_2CH_2CMeNNH_2$, **1**), R^3 ($CMe_2CH_2CMeNNPhH$, **2**)). Diese Verbindungen kristallisieren in mehreren Raumgruppen bzw. mit unterschiedlicher Anzahl an Lösungsmittelmolekülen (**1** als **1**·2 CH_2Cl_2 in $P2_1/n$, $P2_1$ und $P\bar{1}$ und als **1**·3 CH_2Cl_2 in $P2_1/n$; **2** als **2**·CH_2Cl_2 in $C2/c$, als **2**·4 CH_2Cl_2 in $P2_1/c$ und als **2**·4 CH_2Cl_2 in $P\bar{1}$). Der Hauptunterschied zwischen den Solvaten besteht in den Abständen der Zinnatome des zentralen $\{Sn_2Se_2\}$-Rings (Sn1, Sn4) zu den dreifach koordinierten Selenatomen (Se3, Se9). So beträgt der Sn4–Se9-Abstand in **1**·2CH_2Cl_2 2.9125(11) Å, während der Sn1–Se3-Abstand in **2**·CH_2Cl_2 mit 3.6279(11) Å deutlich größer ist.

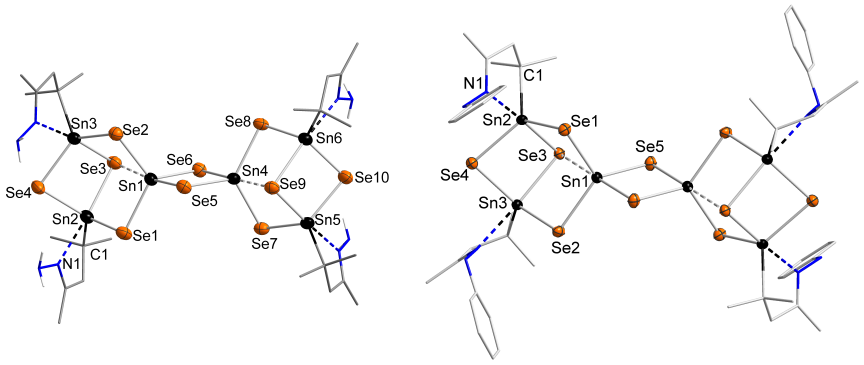

Abbildung 3.1: Molekülstrukturen von **1** (links) und **2** (rechts) im Kristall.

Ebenfalls ausgehend vom Doppeldecker-Strukturmotiv wurde $[(R^4Sn_2)_2Se_6]$ (R^4 = $(CMe_2CH_2CMeNNCH)_2C_6H_4$ (**3**)) synthetisiert. Diese Verbindung ist isostrukturell zu dem bereits bekannten Sulfid-Cluster, in dem jeweils

zwei organische Substituenten durch Reaktion der Hydrazon-Gruppen des doppeldeckerartigen Clusters mit dem Dialdehyd zu einem verbrückenden Substituenten kondensieren. Aufgrund der Spannung der verbrückenden Substituenten, die in gegenüberliegenden Richtungen angeordnet sind, ist der anorganische Clusterkern leicht verzerrt (siehe Abbildung 3.2). Das letzte

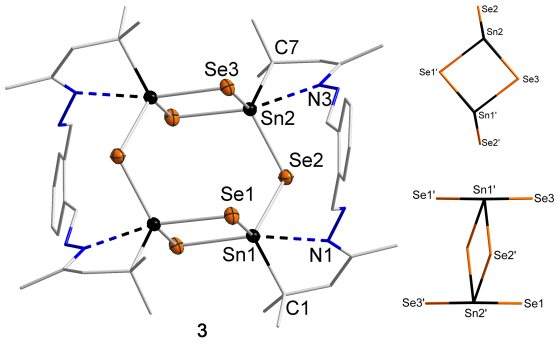

Abbildung 3.2: Molekülstruktur von **3** im Kristall (links) und Ansicht des anorganischen Gerüsts von oben (rechts oben) und von der Seite (rechts unten).

Strukturmotiv, das in der Publikation beschrieben wird, ist das einer molekularen rugbyballartigen Kapsel des Typs $[(\mu\text{–}R)_3(Sn_3Se_4)_2]X_2$ (X = Cl, $[SnCl_3]$). Dies war zuvor für Organozinnselenid-Cluster nicht bekannt. Die Verbindungen wurden durch Reaktionen des Defektheterokuban-Clusters $[(R^1Sn)_3Se_4Cl]$ mit Adipinsäuredihydrazid bzw. 1,1'-(1,5-Naphthalindiyl)bishydrazin erhalten. Bei der Reaktion mit Adipinsäuredihydrazid konnten zwei verschiedene Verbindungen isoliert werden: $[(\mu\text{–}R^5)_3(Sn_3Se_4)_2][SnCl_3]_2$ (**4a**; $R^5 = (CMe_2CH_2CMeNNHC(O))_2(CH_2)_4$) und $[(\mu\text{–}R^5)_3(Sn_3Se_4)_2]Cl_2$ (**4b**). Die Reaktion mit 1,1'-(1,5-Naphthalindiyl)bishydrazin führte zur Bildung von $[(\mu\text{–}R^6)_3(Sn_3Se_4)_2][SnCl_3]_2$ (**5**, $R^6 = (CMe_2CH_2CMe)NNH)_2C_{10}H_6$). Im Gegensatz zum bereits bekannten Sulfid-Cluster konnten hier erstmals auch Anionen innerhalb der „Kapsel“ nachgewiesen werden: In **4a** befindet sich hier ein fehlgeordnetes $[SnCl_3]^-$-Anion innerhalb der molekularen Kavität, während es in **4b** beide Chlorid-Anionen und zwei Wassermoleküle sind. In **5** hingegen befindet sich nur ein Lösungsmittelmolekül innerhalb der Kapsel. Dies wird mit dem in **4** deutlich größeren Innenvolumen erklärt (145.5 Å^3 in **4a** bzw. 162.0 Å^3 in **4b** gegenüber

134.0 Å^3 in **5**), welches auf die flexibleren Alkylketten in R^5 zurückgeführt wird (siehe Abbildung 3.3). Der Vergleich mit dem bereits bekannten Sulfid-Cluster $[(\mu\text{–}R^6)_3(Sn_3S_4)_2]^+$ (Innenvolumen: 129.0 Å^3) zeigt, dass die Substituenten den größten Einfluss auf das Innenvolumen der Cluster haben, wohingegen die eingesetzten Chalkogene keine große Rolle spielen.

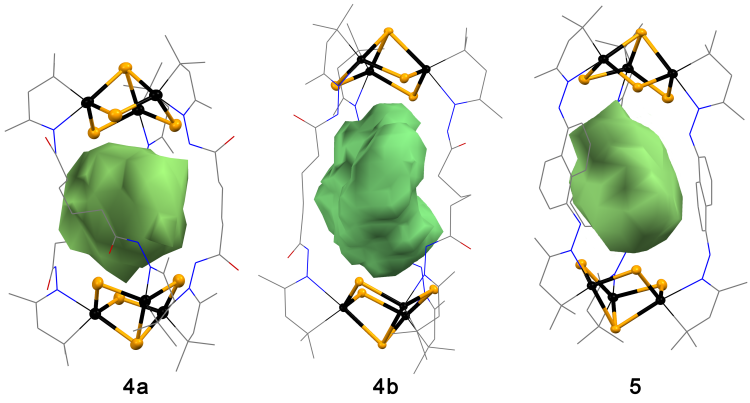

Abbildung 3.3: Vergleich der Innenvolumina der rugbyballartigen Kapseln in **4a** (145.5 Å^3), **4b** (162.0 Å^3) und **5** (134.0 Å^3).

3.2 Variations in the Interplay of Intermetallic and Metal Chalcogenide Units in Organotin-Copper Selenide Clusters

In dieser Publikation wird die Reaktion von $[(R^1Sn)_4Se_6]$ mit $[Cu(PPh_3)_3Cl]$ und $(SiMe_3)_2Se$ beschrieben, welche zunächst zum Ausfallen eines leuchtend orangefarbenen Pulvers (**I**) führt. Die Identität dieses Pulvers konnte nicht vollständig geklärt werden, aber es gibt Hinweise auf eine Vorstufe eines Clusters mit $\{Cu_xSn\}$-Kern. So zeigen µ-RFA-Messungen ein P:Cu:Sn:Se-Verhältnis von 1:3:4.8:9.2, was relativ ähnlich zu dem des bereits bekannten ternären Organozinn-Kupferselenid-Clusters $[(CuPPh_3)_2(SnCu_2)\{(R^1Sn)_2Se_4\}_3]$ (**B**) ist (1.5:3:5.25:9). **B** konnte mittels Röntgenpulverdiffraktometrie auch tatsächlich in dem Pulver nachgewiesen werden. Mittels ^{1}H- und ^{31}P-NMR-Spektroskopie konnte außerdem die Gegenwart von $Ph_3P{=}Se$, PPh_3 und des Edukts nachgewiesen werden, was zeigt, dass **I** eine Mischung verschiedener Substanzen ist, von denen nicht alle identifiziert werden konnten. **I** wurde anschließend mit $N_2H_4{\cdot}H_2O$ umgesetzt, wobei, abhängig von der Reaktionszeit und der anschließenden Aufarbeitung, zwei unterschiedliche Cu/Sn/Se-Cluster isoliert werden konnten. Eine Reaktionszeit von 16 Stunden gefolgt von Filtration und anschließender Überschichtung des Filtrats mit *n*-Hexan führt zu Bildung von gelben Nadeln der Zusammensetzung $[(Cu_3Sn)\{(R^2Sn)_2Se_4\}_2\{(R^2Sn_2)Se_3\}]{\cdot}1.87\,CH_2Cl_2{\cdot}2solv$ (**1**$\cdot1.87\,CH_2Cl_2\cdot$2solv; solv = CH_2Cl_2 und/oder C_6H_{14}). **1** kristallisiert mit zwei Molekülen in der asymmetrischen Einheit, die sich allerdings nur geringfügig voneinander unterscheiden (z.B. im $\{Cu_3Sn\}$-Faltungswinkel mit 106.5° gegenüber 107.1°). Das Clustermolekül besteht aus einer $\{Cu_3Sn\}$-butterflyartigen Einheit, die von verschiedenen $R_xSn_yE_z$-Einheiten umgeben ist: einer $\{(R^2Sn)_2Se_4\}$-Einheit, die die Spitzen des Butterflys (Cu1A und Cu3A) überkappt, und einer $\{(R^2Sn)_3SnSe_7\}$-Einheit auf der gegenüberliegenden Seite der Butterfly-Einheit, die auch verstanden werden kann als eine $\{(R^2Sn)SnSe_4\}$- und eine $\{(R^2Sn)_2Se_4\}$-Einheit, die sich ein Selenatom (Se3A) teilen (siehe Abbildung 3.4 links). Die bereits zuvor von *Rinn et al.* beschriebenen Organozinn-Kupferselenid-Cluster beinhalten ebenfalls größtenteils mindestens eine solche $\{(RSn)_2Se_4\}$-Einheiten, was zeigt, dass diese einen großen Einfluss auf die

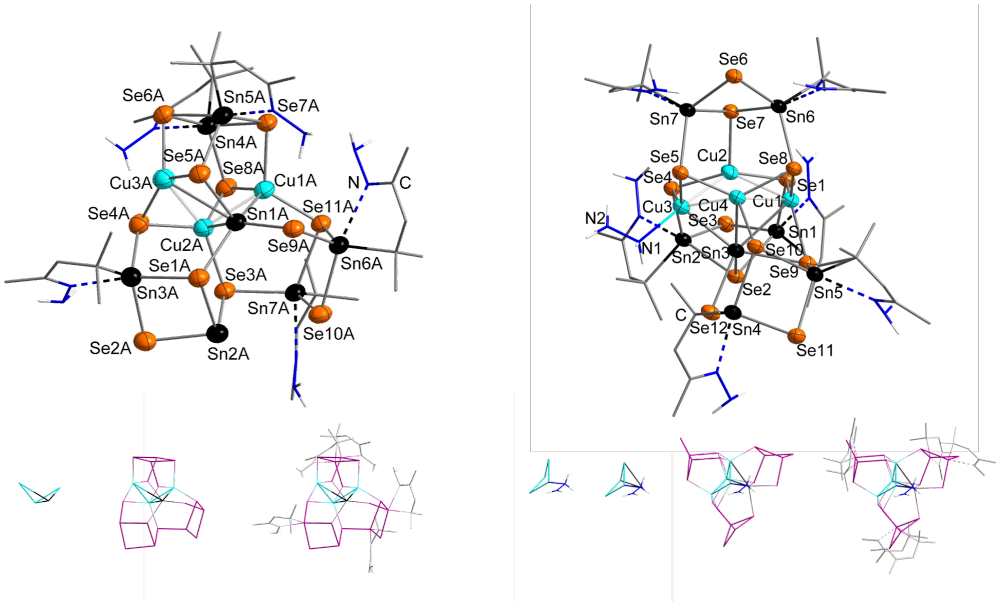

Abbildung 3.4: Oben: Molekülstrukturen von **1** (links) und **2** (rechts) im Kristall. Unten: Darstellung des Aufbaus des jeweiligen Clusters, wie im Text beschrieben.

Bildung der Cluster und die entstehenden Strukturen zu haben scheinen. Wird die Reaktionslösung von **I** nach der Zugabe von $N_2H_4{\cdot}H_2O$ sofort mit *n*-Hexan überschichtet, so bilden sich dunkelorangefarbene Blöcke einer Verbindung der Zusammensetzung $[(N_2H_4)(Cu_4Sn)\{(R^2Sn)_2Se_4\}_3]$ (**2**). Auch **2** basiert auf einer $\{Cu_3Sn\}$-butterflyartigen Einheit im Zentrum des Clusters, allerdings ist an diese noch ein viertes Kupferatom angebunden, welches zusammen mit den anderen drei Kupferatomen einen zweiten $\{Cu_4\}$-Butterfly bildet. Diese $\{Cu_4Sn\}$-Einheit ist umgeben von drei $\{(R^2Sn)_2Se_4\}$-Einheiten und einem N_2H_4-Liganden, der an ein Kupferatom bindet (siehe Abbildung 3.4 rechts). Im Vergleich zu den bereits bekannten Cu/Sn/Se-Clustern fällt in **1** und **2** vor allem die Abwesenheit von PPh_3- und Cl-Liganden auf. Dies kann auf die höhere Stoßzahl bei der Synthese von **I** zurückgeführt werden, welche entweder durch die verlängerte Reaktionszeit oder die erhöhte Reaktandenkonzentration zustande kommt. Die Abwesenheit der genannten Liganden scheint wichtig für die Bildung größerer $\{Cu_xSn\}$-Einheiten (x = 3, 4) zu sein.

3.3 Towards Understanding the Reactivity and Optical Properties of Organosilicon Sulfide Clusters

In dieser Publikation werden die Synthese und Reaktivität neuer Organisiliciumsulfid-Cluster sowie ihre optischen Eigenschaften anhand von Experimenten und DFT-Rechnungen beschrieben. Die Synthese der adamantanartigen Cluster $[(RSi)_4S_6]$ (R = Ph (**IV**), 1-Naphthyl (Np, **1**), 4-Vinylphenyl (Sty, **2**)) erfolgte durch Umsetzung der entsprechenden Organotrichlorsilane mit 1.5 eq Na_2S, wobei sowohl die Synthese als auch die Kristallstruktur von **IV** bereits literaturbekannt waren.[55,56] Die Molekülstruktur von **1** (siehe Abbildung 3.5) wurde mittels Einkristallstrukturröntgendiffraktometrie bestimmt und außerdem NMR-spektroskopisch und massenspektrometrisch bestätigt. Aufgrund der Neigung der Styryl-Reste zur Polymerisation konnte **2** nur als amorphes Rohprodukt isoliert werden. Der Nachweis der Verbindung erfolgte über ^{1}H-, ^{13}C- und ^{29}Si-NMR-Spektroskopie. Im ^{29}Si-NMR-Spektrum des Rohprodukts ist ein neues Signal zu beobachten, welches im Vergleich zum Signal des Edukts um 9.6 ppm tieffeldverschoben ist, was in der Literatur bereits für andere Edukt/Produkt-Kombinationen, wie beispielsweise $EtSiCl_3$/$[(EtSi)_4S_6]$, $PhSiCl_3$/$[(PhSi)_4S_6]$ oder CH_2=$CHSiCl_3$/$[(CH_2$=$CHSi)_4S_6]$, beschrieben worden ist.[53] Eine Tieffeldverschiebung der dem Siliciumatom am nächsten gelegenen Wasserstoff- und Kohlenstoffatome wird in den entsprechenden NMR-Spektren beobachtet. Des Weiteren ändern sich Aufspaltungsmuster aller Protonen sowie die chemische Verschiebung der vinylischen Protonen im ^{1}H-NMR-Spektrum nicht, sodass zunächst von der Bildung eines monomeren adamantanartigen Clusters ausgegangen werden kann, der bei längerer Reaktionsdauer oligo- oder polymerisiert.

Die weitere Umsetzung von **IV** und **1** mit Na_2S und $[AuCl(PPh_3)]$ führte zur Bildung von ternären Komplexen der Zusammensetzung $[\{RSi(\mu\text{-}S)\}_2\{AuPPh_3(\mu\text{-}S)\}_2]$ (**3**: R = Ph, **4**: R = Np). Diese bestehen aus einem zentralen $\{RSi(\mu\text{-}S)\}_2$-Ring mit nahezu linearen $\{Au(PPh_3)(\mu\text{-}S)\}$-Substituenten an den Siliciumatomen (siehe Abbildung 3.5). Die Orientierung

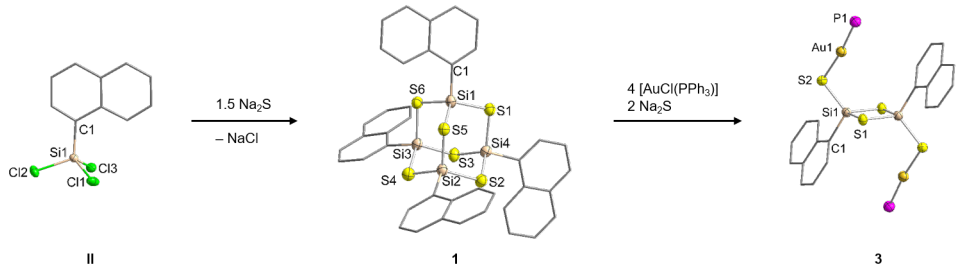

II 1 3

Abbildung 3.5: Schrittweise Synthese adamantanartiger Cluster $[(RSi)_4S_6]$ und ternärer Komplexe $[\{RSi(\mu\text{-}S)\}_2\{AuPPh_3(\mu\text{-}S)\}_2]$ ausgehend von $RSiCl_3$ am Beispiel von R = Np. Die Phenyl-Substituenten an den Phosphoratomen sind aus Gründen der Übersichtlichkeit ausgeblendet.

dieser Substituenten unterscheidet sich dabei deutlich: In **3** zeigen sie eine *cis*-Anordnung entlang C1–Si1–S2–Au1, wohingegen die entsprechenden Atome in **4** eine *trans*-Anordnung aufweisen. Homologe Sn/S-Verbindung mit diesem Strukturmotiv sowie einer *cis*- oder *trans*-Anordnung, abhängig vom organischen Substituenten am Tetrelatom, sind bereits beschrieben worden und zeigen dieselben Trends in den T–S–Au- und S–Au–P-Bindungswinkeln.[29,73]

Im Gegensatz zu den analogen Organozinnsulfid-Clustern, welche intrinsisch amorph sind, sind $[(PhSi)_4S_6]$ und $[(NpSi)_4S_6]$ kristallin. Mit Hilfe von quantenchemischen Rechnungen wurden in der Arbeitsgruppe *Mollenhauer* die Beiträge von Substituent-Substituent-, Clusterkern-Clusterkern- und Clusterkern-Substituent-Wechselwirkungen zu den Bindungsenergien der verschiedenen Cluster untersucht. Dabei wurde festgestellt, dass die relativ isotropen Kern-Kern-Wechselwirkungen in $[(PhSn)_4S_6]$ einen deutlich größeren Einfluss haben als die gerichteten Wechselwirkungen mit Substituentenbeteilung, was erklärt, warum $[(PhSn)_4S_6]$ eine geringere Neigung zur Ordnung hat als der analoge Organosiliciumsulfid-Cluster, in dem die Kern-Kern-Wechselwirkungen deutlich geringer sind (siehe Abbildung 3.6 links). Derselbe Trend konnte für die naphthylsubstituierten Cluster beobachtet werden, wobei die ähnlich starken Kern-Kern- und Substituent-Substituent-Wechselwirkungen in $[(NpSn)_4S_6]$ zu einem höheren Grad an intermolekularer Ordnung führen. Dies passt zu den experimentellen Beobachtungen: Obwohl $[(NpSn)_4S_6]$ röntgenamorph ist, zeigt es dennoch SHG, was ein Zeichen von Phasenanpassung und damit intermolekularer Ordnung ist. Für $[(PhSn)_4S_6]$ konnte hingegen WLG

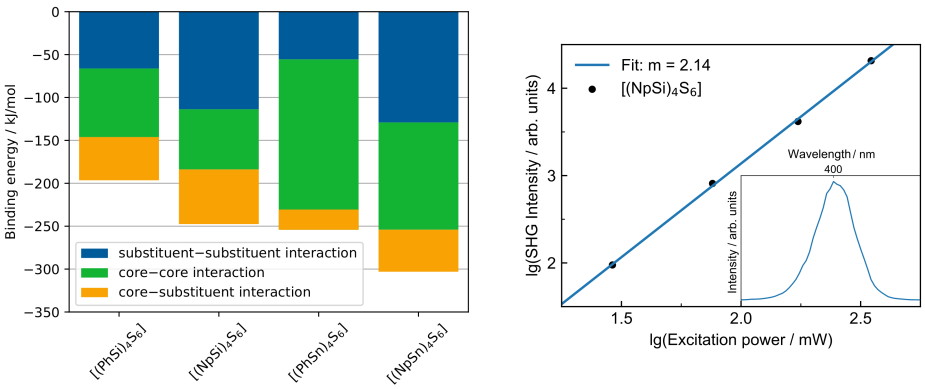

Abbildung 3.6: Links: Beiträge von Substituent-Substituent-, Kern-Kern- und Kern-Substituent-Wechselwirkungen zu den Bindungsenergien von $[(RT)_4S_6]$ (R = Ph, Np; T = Si, Sn). Rechts: Anregungsenergieabhängigkeit der SHG-Intensität von $[(NpSi)_4S_6]$ und SHG-Spektrum nach Anregung bei 800 nm (Bild im Bild).

beobachtet werden.[56]

Die photophysikalischen Eigenschaften der neuen Verbindungen wurden in der Arbeitsgruppe *Chatterjee* untersucht. **1** zeigt deutliche nichtlineare optische Eigenschaften: Trotz zentrosymmetrischer Raumgruppe kann, wie für $[(PhSi)_4S_6]$,[56] SHG beobachtet werden (siehe Abbildung 3.6 rechts), was auf Oberflächeneffekte oder strukturelle Defekte im Kristall zurückgeführt wird. Die anderen Verbindungen zeigen keine nichtlinearen optischen Eigenschaften, die sich eindeutig von Lumineszenzeffekten infolge von chemischen Umwandlungen, also der Zerstörung der Proben, unterscheiden lassen. Dementsprechend kann bisher keine eindeutige Aussage darüber getroffen werden, ob **2** WLG zeigt. Statische und zeitabhängige DFT-Rechnungen zu den Molekülen sowie den kristallinen Materialien, die in der Arbeitsgruppe *Sanna* durchgeführt wurden, bestätigen die experimentellen Befunde und zeigen die gute Eignung der verwendeten Methoden und Modelle.

4 Kumulativer Teil

4.1 Organotin Selenide Clusters and Hybrid Capsules

Katharina Hanau, Niklas Rinn, Mario Argentari, Stefanie Dehnen, *Chem. Eur. J.* **2018**, *24*, 11711–11716.

Abstract

Several compounds with unique structural motifs that have already been known from organotin sulfide chemistry, but remained unprecedented in organotin selenide chemistry so far, have been synthesized. The reaction of $[(R^1Sn)_4Se_6]$ (R^1 = $CMe_2CH_2C(O)Me$) with $N_2H_4{\cdot}H_2O/(SiMe_3)_2Se$ and $PhN_2H_3/(SiMe_3)_2Se$ led to the formation of $[\{(R^2Sn)_2SnSe_4\}_2(\mu\text{–}Se)_2]$ (**1**; R^2 = $CMe_2CH_2C(Me)NNH_2$) and $[\{(R^3Sn)_2SnSe_4\}_2(\mu\text{–}Se)_2]$ (**2**; R^3 = $CMe_2CH_2C(Me)NNPhH$). The addition of *ortho*-phthalaldehyde to $[(R^2Sn)_4Se_6]$ yielded a cluster with intramolecular bridging of the organic groups, namely, $[(R^4Sn_2)_2Se_6]$ (**3**; R^4 = $(CMe_2CH_2C(Me)NNCH)_2C_6H_4$). The introduction of organic ligands with longer chains finally allowed the isolation of inorganic-organic capsules of the type $[(\mu\text{–}R)_3(Sn_3Se_4)_2]X_2$, with R = $(CMe_2CH_2C(Me)NNHC(O))_2(CH_2)_4$ and X = $[SnCl_3]$, Cl (**4a**, **b**) or R = $(CMe_2CH_2C(Me)NNH)_2)C_{10}H_6$ and X = $[SnCl_3]$ (**5**). The capsules enclose solvent molecules and/or anions as guests. All compounds were characterized by means of single-crystal X-ray diffraction studies, NMR spectroscopy, and mass spectrometry.

Eigener Anteil

Die Verbindungen **1** und **2** wurden erstmals von Dr. Niklas Rinn synthetisiert und röntgenographisch untersucht und anschließend von mir als Polymorph reproduziert

und daher erneut röntgenographisch untersucht. Die Synthesen der Verbindungen **3**, **4a** und **5** wurden von mir geplant und durchgeführt. Verbindung **4b** wurde von Mario Argentari im Rahmen seiner Masterarbeit unter der Anleitung von Dr. Niklas Rinn synthetisiert. Die Einkristallstrukturanalysen wurden von Dr. Niklas Rinn (**1**, **2**·CH_2Cl_2, **2**·2CH_2Cl_2, **4b**), Dr. Carsten Donsbach (**5**·6.5CH_2Cl_2), Dr. Eike Dornsiepen (**5**·3CH_2Cl_2) und mir (**2**·4CH_2Cl_2, **3**, **4a**) durchgeführt und von Dr. Niklas Rinn (**1**, **2**·CH_2Cl_2, **2**·2CH_2Cl_2, **4b**) und mir (**2**·4CH_2Cl_2, **3**, **4a**, **5**·6.5CH_2Cl_2, **5**·3CH_2Cl_2) ausgewertet. ^{1}H- und ^{119}Sn-NMR-Experimente wurden von der zentralen NMR-Abteilung des Fachbereichs Chemie der Philipps-Universität Marburg unter der Leitung von Dr. Xiulan Xie durchgeführt und von mir ausgewertet. Die massenspektrometrischen Untersuchungen wurden von der zentralen Serviceabteilung für Massenspektrometrie und Elementaranalytik des Fachbereichs Chemie der Philipps-Universität Marburg unter der Leitung von Dr. Uwe Linne durchgeführt. Die µ-RFA-Messungen wurden von Dr. Carsten Donsbach durchgeführt und ausgewertet. Das Manuskript habe ich in Kooperation mit Prof. Dr. Stefanie Dehnen geschrieben, wobei sich alle Co-Autor_innen an der Be- und Überarbeitung beteiligten.

ChemPubSoc Europe

DOI: 10.1002/chem.201801652

CHEMISTRY A European Journal Full Paper

Cluster Compounds

Organotin Selenide Clusters and Hybrid Capsules

Katharina Hanau, Niklas Rinn, Mario Argentari, and Stefanie Dehnen*[a]

Dedicated to Professor Klaus Jurkschat on the occasion of his 65th birthday

Abstract: Several compounds with unique structural motifs that have already been known from organotin sulfide chemistry, but remained unprecedented in organotin selenide chemistry so far, have been synthesized. The reaction of $[(R^1Sn)_4Se_6]$ ($R^1 = CMe_2CH_2C(O)Me$) with $N_2H_4{\cdot}H_2O$/$(SiMe_3)_2Se$ and PhN_2H_3/$(SiMe_3)_2Se$ led to the formation of $[\{(R^2Sn)_2SnSe_4\}_2(\mu\text{-}Se)_2]$ (**1**; $R^2 = CMe_2CH_2C(Me)NNH_2$) and $[\{(R^3Sn)_2SnSe_4\}_2(\mu\text{-}Se)_2]$ (**2**; $R^3 = CMe_2CH_2C(Me)NNPhH$)). The addition of *ortho*-phthalaldehyde to $[(R^2Sn)_4Se_6]$ yielded a cluster with intramolecular bridging of the organic groups, namely, $[(R^4Sn_2)_2Se_6]$ (**3**; $R^4 = (CMe_2CH_2C(Me)NNCH)_2C_6H_4$). The introduction of organic ligands with longer chains finally allowed the isolation of inorganic–organic capsules of the type $[(\mu\text{-}R)_3(Sn_3Se_4)_2]X_2$, with $R = (CMe_2CH_2C(Me)\text{-}NNHC(O))_2(CH_2)_4$ and $X = [SnC_3]$, Cl (**4a**,**b**) or $R = CMe_2CH_2C(Me)NNH)_2$ and $X = [SnCl_3]$ (**5**). The capsules enclose solvent molecules and/or anions as guests. All compounds were characterized by means of single-crystal X-ray diffraction studies, NMR spectroscopy, and mass spectrometry.

Introduction

The formation of inorganic–organic hybrid compounds that are based on inorganic chalcogenide substructures has been very actively pursued in the recent past.[1] One aspect in this regard is the variation of the elemental combination within related structure types, thus resulting in a change in the optical absorption properties and chemical stability versus reactivity, for example, within a homologous series. Such systematic studies allow for detailed insight into the structure–property relationships of corresponding families of compounds and eventually their targeted development for potential use as building blocks in hybrid materials, for example, in optoelectronic applications or catalysis.

Although organotin selenide clusters with inert ligands were synthesized and fully characterized as early as 1981,[2] the first examples of organotin selenide clusters with functional ligands have only been reported recently,[3–6] which represent heavy homologues of known organotin sulfide clusters in most cases.[3,7,8] With these studies, we were able to demonstrate that the reaction conditions, which eventually allow for the isolation of the selenium compounds, require significant adaption and that both physical and chemical properties of the heavier homologues are notably different from the sulfide analogues.

However, three structural motifs have so far been resistant to a transfer to the heavier homologue: 1) a doubly μ-Se-bridged dimer of two defect-heterocubanes, according to the general formula $[(RSn)_4Sn_2E_{10}]$, which is a very common motif for E = S;[3,8–11] 2) a rugby-ball-shaped cluster capsule, previously reported for E = S as $[R_3(Sn_3S_4)_2]$ ($R = (CMe_2CH_2C(Me)NNH)_2C_{10}H_6$ and $(CMe_2CH_2C(Me)NNHC(O)CH_2)_2\text{-}C_{14}H_{20}$));[10–12] and 3) a macrocyclic cavitand that results from the linkage of two of the latter clusters by a bridging ligand R, previously reported for E = S as $[R_4(Sn_6S_{10})_2]$ ($R = (CMe_2CH_2C(Me)NNH)_2C_{10}H_6$ and $(CMe_2CH_2C(Me)NNH)_2C_6H_4$).[11,12]

Herein, we report the continuation of the search for suitable organic linkers and reaction conditions to afford these uncommon molecular clusters. In addition to one smaller organotin selenide complex, which is also included in this report, this approach led us to the isolation of two of the three mentioned target architectures, whereas the third cluster type, the quoted macrocycle, remains elusive in organotin selenide chemistry. Schemes 1 and 2 summarize the reactions reported herein.

Results and Discussion

The reaction of $[(R^1Sn)_4Se_6]$ ($R^1 = CMe_2CH_2C(O)Me$) with four equivalents of $N_2H_4{\cdot}H_2O$ and four equivalents of $(SiMe_3)_2Se$ led to the replacement of the keto groups by hydrazone groups upon condensation, but also came along with a rearrangement of the inorganic cluster core to yield $[\{(R^2Sn)_2SnSe_4\}_2(\mu\text{-}Se)_2]$ (**1**; $R^2 = CMe_2CH_2C(Me)NNH_2$). Compound **1** crystallizes as $\mathbf{1}{\cdot}2\,CH_2Cl_2$ in three different space groups ($P2_1/n$, $P2_1$, and $P\bar{1}$) and as $\mathbf{1}{\cdot}3\,CH_2Cl_2$ in the monoclinic space group $P2_1/n$. Likewise, the reaction of $[(R^1Sn)_4Se_6]$ with four equivalents of PhN_2H_3 and $(SiMe_3)_2Se$ led to the formation of $[\{(R^3Sn)_2SnSe_4\}_2(\mu\text{-}Se)_2]$ (**2**; $R^3 = CMe_2CH_2C(Me)NNPhH$), which

[a] K. Hanau, Dr. N. Rinn, M. Argentari, Prof. Dr. S. Dehnen
Fachbereich Chemie und Wissenschaftliches Zentrum für Materialwissenschaften (WZMW)
Philipps-Universität Marburg
Hans-Meerwein-Str. 4, 35043 Marburg (Germany)
E-mail: dehnen@chemie.uni-marburg.de

Supporting information and the ORCID identification number(s) for the author(s) of this article can be found under: https://doi.org/10.1002/chem.201801652.

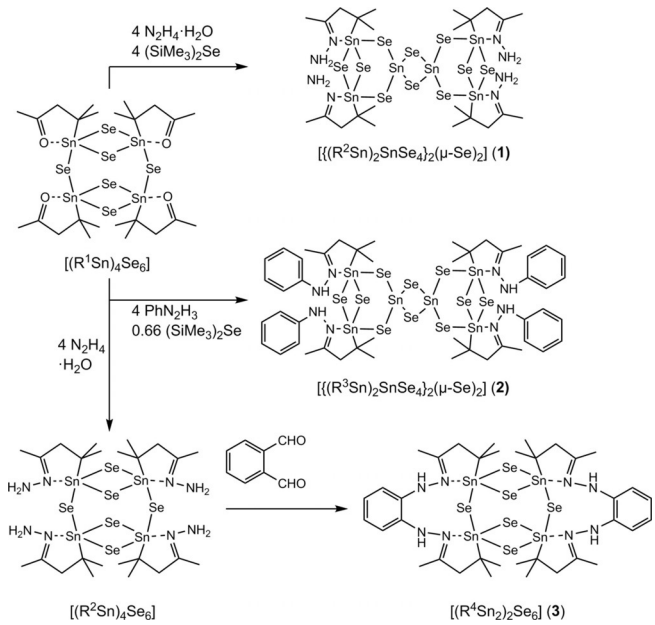

Scheme 1. Non-stoichiometric reaction schemes for the synthesis of **1**–**3**. $R^1 = CMe_2CH_2C(O)Me$, $R^2 = CMe_2CH_2C(Me)NNH_2$, $R^3 = CMe_2CH_2C(Me)NNPhH$, and $R^4 = (CMe_2CH_2C(Me)NNCH)_2C_6H_4$.

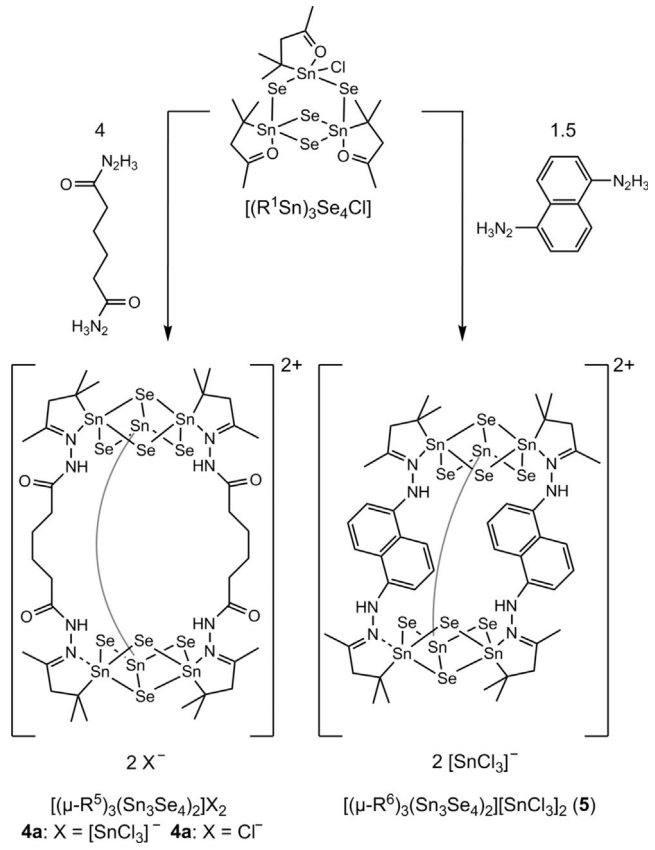

Scheme 2. Non-stoichiometric reaction schemes for the synthesis of **4** and **5**. $R^5 = (CMe_2CH_2C(Me)NNHC(O))_2(CH_2)_4$ and $R^6 = CMe_2CH_2C(Me)NNH)_2C_{10}H_6$. One of the three organic ligands was replaced in both molecules by a simplified representation (gray line) for clarity.

contains phyenylhydrazone groups at the organic periphery. Three different crystalline solvates of **2** could be obtained with one, two, or four molecules of CH_2Cl_2, respectively. Clusters **2**·CH_2Cl_2 and **2**·2 CH_2Cl_2 crystallize in the monoclinic space groups *C*2/*c* and $P2_1/c$, respectively, whereas **2**·4 CH_2Cl_2 crystallizes in the triclinic space group $P\bar{1}$.

Both **1** and **2** consist of the long-sought-for structural motif of the dimer of two $[(RSn)_2SnSe_4]$ defect-heterocubane units that are bridged by two Se atoms. The latter contribute to a central planar $\{Sn_2Se_2\}$ four-membered ring that encloses an inversion center. The two defect-heterocubane units are twisted by 180° against each other, such that the defect positions are at opposite sides of the molecule. Apart from the number of solvent molecules, the main difference between the molecular cluster structures in the different solvates is the Sn1–Se3/Sn4–Se9 distances, which range from 2.9125(11) Å in **1**·2 CH_2Cl_2 to 3.6279(11) Å in **2**·CH_2Cl_2. All of these distances are considerably longer than in the parent defect-heterocubane-type cluster $[(R^1Sn)_3Se_4Cl]$,[3,4] and these distances also exceed the sum of the covalent radii (i.e., 2.56 Å).[13] However, these values are well within the range of the sum of the van der Waals radii (i.e., 4.07 Å),[14] thus indicating an existing interaction. Figure 1 illustrates the cluster structures in **1** and **2**.

Based on this first success with regard to the transfer of the larger organotin sulfide cluster chemistry to the homologous selenides, we intended to explore the behavior of bridging ligands to form macrocyclic or capsulelike clusters.

First, we performed a reaction analogous to the reaction of $[(R^2Sn)_4S_6]$ with *ortho*-phthalaldehyde, which previously afforded a $[Sn_4S_6]$ cluster with intramolecular bridging by organic

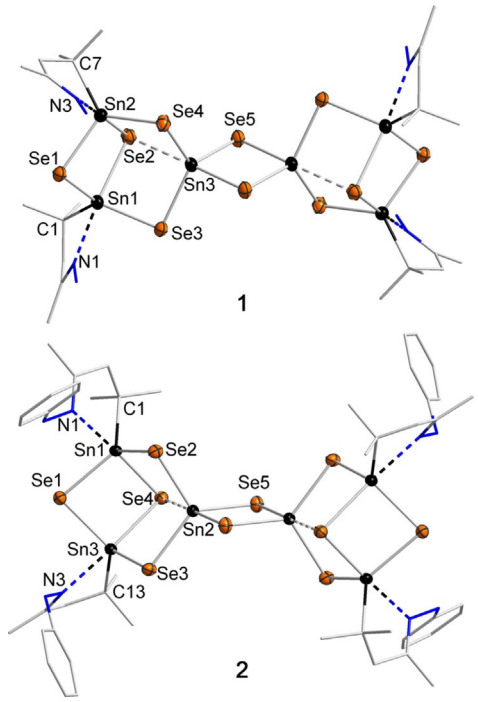

Figure 1. Molecular structures of **1** (top) and **2** (bottom), drawn from the crystal structure of **1**·2 CH_2Cl_2 in the space group $P\bar{1}$ and **2**·4 CH_2Cl_2, respectively. The hydrogen atoms have been omitted for clarity. Thermal ellipsoids were drawn at 50% probability.

linker groups. Indeed, the reaction of $[(R^2Sn)_4Se_6]$[3,4] with four equivalents of *ortho*-phthalaldehyde yielded the new compound $[(R^4Sn_2)_2Se_6]\cdot CH_2Cl_2$ (**3**·CH_2Cl_2; $R^4 = (CMe_2CH_2CMeNNCH)_2C_6H_4$; Figure 2, left). Compound **3** is isostructural to the reported sulfide cluster, hence it is based on an inorganic $[Sn_4Se_6]$ "double-decker" motif, in which two organic ligands are linked with each other upon condensation of the hydrazone groups on the parent cluster with the aldehyde groups of the bisaldehyde. As in the lighter homologue, the molecule contains an inversion center. Hence, the phenyl groups are oriented in opposite directions, which forces the μ-Se atoms away from each other, thus causing a slight distortion of the inorganic cluster core (Figure 2, right). The distortion is further illustrated by the three Se-Sn-Se angles at each of the Sn atoms, although Se1′-Sn2-Se3 and Se1′-Sn1′-Se3 are practically identical (92.608(16) vs. 93.970(16)°, respectively), Se1′-Sn2-Se2 and Se1′-Sn1′-Se2′ differ significantly (104.689(16) vs. 115.313(18)°, respectively) as well as Se2-Sn2-Se3 and Se2-Sn1-Se3′ (127.917(17) and 107.746(16)°, respectively).

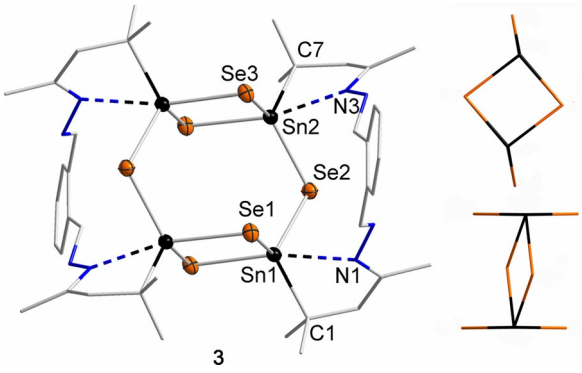

Figure 2. Left: Molecular structure of **3**. The hydrogen atoms have been omitted for clarity. Thermal ellipsoids were drawn at 50% probability. Right: Two simplified, perpendicular views of the inorganic cluster core of **3** in wire-frame representation that disregards the organic ligands (top and bottom).

In organotin sulfide chemistry, the formation of molecular capsules required larger spacer molecules to connect the two hydrazine groups of the parent cluster, with a maximum spacer length found with the 1,4-bis(diazomethyl)benzene and 1,5-bisnaphthalene-functionalized groups, which led to the formation of macrocycles.[12] However, in contrast to the reactions of organotin sulfide clusters, the cagelike compounds could not be obtained upon reaction of the "double-decker"-shaped $[(R^2Sn)_4Se_6]$ precursor. Hence, we directly used a precursor cluster that exhibits the envisaged structural motif of the defect-heterocubane unit $[(R^1Sn)_3Se_4Cl]$.[3,4] Reactions of the latter structure with dihydrazides or dihydrazines result in condensation reactions, as desired.

Upon reaction with adipic acid dihydrazide and layering with *n*-hexane, single crystals of $[(\mu\text{-}R^5)_3(Sn_3Se_4)_2][SnCl_3]_2\cdot 4CH_2Cl_2$ (**4a**·$4CH_2Cl_2$, $R^5 = (CMe_2CH_2C(Me)NNHC(O))_2(CH_2)_4$) and **4b**·$3H_2O\cdot 4CH_2Cl_2$, $[(\mu\text{-}R^5)_3(Sn_3Se_4)_2]Cl_2\cdot 3H_2O\cdot 4CH_2Cl_2$) could be isolated. The molecular structures of the cluster cations are shown in Figure 3. Each cationic molecule consists of two defect-heterocubane units that are bridged by three organic ligands, thus forming a rugby-ball-like capsule molecule, as described for the sulfide analogues, albeit with other bridging ligands. However, a notable contrast to the sulfide analogues is found upon comparison of the content of the capsules. Although only solvent molecules were included in the sulfide clusters, the selenide-based cations with adipinic acid-derived ligands may also contain anions. We ascribe this finding to the larger cross section of the capsules for E = Se and $R = R^4$ (9.33 Å on average) than for E = S, Se and $R = R^5$ (6.68 Å on average), which is due to the higher flexibility of the alkyl chains in the R^4 group.

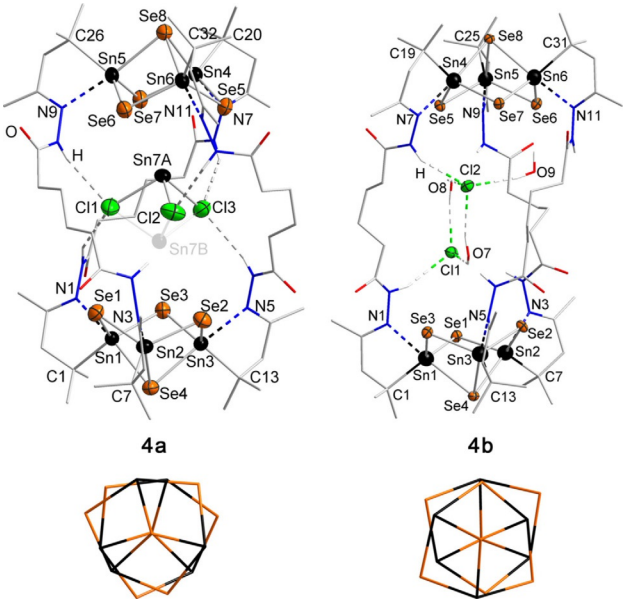

Figure 3. Top: Molecular structure of the cations in **4a** and **4b**, with the 80:20 (%) disorder of the inner Sn atom in **4a** reflected by black and gray spheres, respectively. The hydrogen atoms (except those involved in hydrogen bonding) have been omitted for clarity. External solvent molecules and counterions are not shown. Thermal ellipsoids were drawn at 50% probability. Bottom: Simplified view of the inorganic cluster core of **4a** and **4b** along the Se4···Se8 axis.

As a consequence, one $[SnCl_3]^-$ ion is found inside of the capsule of **4a**. The second anion is located outside the capsule, along with solvent molecules. The Sn atom of the anion inside the capsule is disordered over two positions (80:20 (%)). One of the positions is closer to one of the defect-heterocubane moieties (distance of Sn7A to the mean plane through Se5-Se6-Se7: 2.7869(18) Å), whereas the other position is further apart from the adjacent $\{Sn_3Se_4\}$ unit (distance of Sn7B to the mean plane through Se1-Se2-Se3: 2.8761(83) Å). The Sn7A atom has the higher occupancy, thus suggesting that distinct interactions exist that favor this site, as rationalized in the following: The positions of the three Cl atoms are staggered with respect to the closer defect-heterocubane unit, whereas these atoms are eclipsed with regard to the other, more distant $\{Sn_3Se_4\}$ unit, which is rotated against the other defect-heterocubane by about 30°. Five N-H···Cl hydrogen bonds hold the

internal anion in place, thereby causing the organic ligands to twist considerably. All three organic ligands show a *cisoid* arrangement.

In contrast, the counterions of **4b** are Cl^- ions, both of which are situated inside the capsule, along with three water molecules. The defect-heterocubane units are rotated against each other by only about 5°, so that the ligands do not to twist as much as in **4a** and show a *transoid* arrangement in two of the units. This effect is accompanied by less pronounced N-H···Cl hydrogen interactions than in **4a**, and no significant interactions between the capsule and the counterions are present at all. This way, the ligands are sterically much more relaxed, thus resulting in a longer Se4—Se8 distance and a more elongated capsule.

Hence, we summarize that the nature of the counterions largely controls the structural details in the two cations with relatively flexible organic linkers. Both $[SnCl_3]^-$ and Cl^- counterions are commonly observed in organotin chalcogenide chemistry with functional ligands. The appearance of these counterions was previously explained by partial (reductive) decomposition of the precursor clusters $[(R^1Sn)_3Se_4Cl]$ precursor (besides oxidized organic molecules).[3,6,15]

A third rugby-ball-like capsule was synthesized by treating $[(R^1Sn)_3Se_4Cl]$ with 1,1′-(1,5-naphthalenediyl)bishydrazine and crystallized as the salts $[(\mu\text{-}R^6)_3(Sn_3Se_4)_2][SnCl_3]_2\cdot 3\,CH_2Cl_2$ and $[(\mu\text{-}R^6)_3(Sn_3Se_4)_2][SnCl_3]_2\cdot 6.75\,CH_2Cl_2$ (**5**·3 CH_2Cl_2 and **5**·6.75 CH_2Cl_2; $R^6 = (CMe_2CH_2C(Me)NNH)_2C_{10}H_6$). In the cation of **5** (see Figure 4), the defect-heterocubane units are eclipsed, with the relatively rigid ligands (as opposed to those in **4a** and **4b**), thus forming straight connections from the top to the bottom unit. Also, there is only one solvent molecule inside the capsule, whereas the counterions and the other solvent molecules are outside of the capsule. This molecule is an exact homologue of the reported organotin sulfide cluster referred to above.

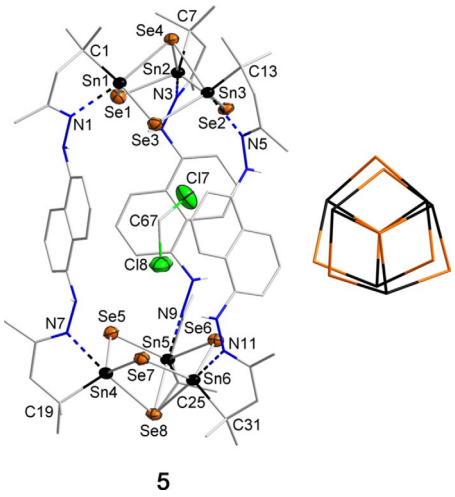

5

Figure 4. Left: Molecular structure of the cation in **5**. The hydrogen atoms have been omitted for clarity. Thermal ellipsoids were drawn at 50% probability. Right: Simplified view of the inorganic cluster core along the Se4···Se8 axis.

The inner volume of the capsule molecules was determined with PLATON software[16] and by deleting the crystallographically determined contents of the capsule and subsequent calculation of solvent-accessible volume using the CALC SOLV routine. As can be seen in Figure 5, the inner volume in **5** is the smallest, followed by **4a**, and then **4b** (134.0, 145.5, and 162.0 Å^3, respectively). This finding again reflects the rigidity of the naphthyl ligand, relative to the adipic acid hydrazide ligand, and also indicates the strain of the ligand system in **4a**. Due to the lack of ligand twisting in **4b**, the ligands can arch outward more, thus providing a larger volume for counterions and/or solvent molecules. Notably, the accessible volume of **4a** is calculated to be smaller than for **4b**, although this volume does accommodate the $[SnCl_3]^-$ ion. We assume that the intense N-H···Cl hydrogen interactions pull the ligands closer to the inside of the cluster, whereas there are no such intermolecular forces in **4b**.

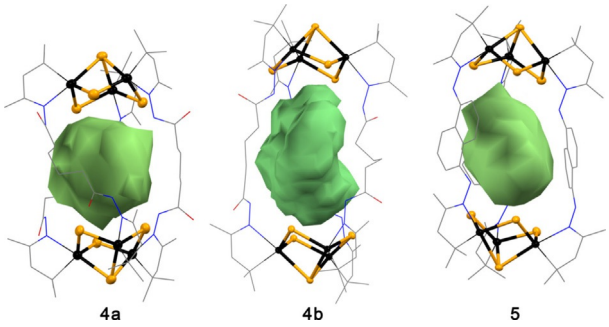

Figure 5. Illustration of the inner volumes of **4a**, **4b**, and **5** as determined by PLATON/CALC SOLV. Numbers are given in the main text.

Relative to the known capsule with tin sulfide moieties, the inner volumes do not differ much. Because the inner volume of the tin sulfide capsule had been determined differently, we applied the CALC SOLV routine for comparison with the newly synthesized capsules as well. These calculations show that the inner volume of the tin sulfide capsule is smaller than the respective tin selenide capsule by only 5 Å^3, thus suggesting that the organic ligand has the greatest impact in this regard.

The structures of the cations in **3**–**5** also conform to the explanation for the ligand arrangement and structural rearrangement of the cluster core in terms of spacer lengths (C=N···N=C).[12] While the spacer length in **3** (4.33 Å) lies within the range for an *anti*-parallel arrangement of the ligands (4–6 Å), the spacer lengths in **4a**, **4b**, and **5** (9.44, 9.71, and 8.52 Å, respectively) are well above the lower limit for bigger capsules or cavitands (8 Å). As indicated above, no cavitand molecules were obtained yet, supposedly because we started directly from the defect-heterocubane unit instead of the "double-decker" unit.

The ^{119}Sn NMR spectrum of the reaction solution that yielded **2** shows three singlets at $\delta = -274.3$, -264.3, and -243.5 ppm. The signal at $\delta = -274.3$ ppm can be attributed to the defect-heterocubane-type cluster with phenylhydrazone termination, thus confirming that the formation of this cluster is the first step in the formation of **2**. The ratio of the signals at

$\delta = -264.3$ and -243.5 ppm is approximately 2:1, thus suggesting that these signals can be assigned to the Sn atoms in **2**. However, this assignment could not be confirmed due to the poor solubility of the crystals. The ^{119}Sn NMR spectrum of the reaction solution of **3** shows two singlets at $\delta = -219.3$ and -235.9 ppm. The latter can be assigned to **3**, whereas the former seems to belong to an unknown intermediate. The ^{119}Sn NMR spectra of the reaction solution of **5** were recorded after 16 hours and 3 days. Only the "double-decker"-type cluster $[(R^1Sn)_4Se_6]$ could be detected after 16 hours, whereas there were four new signals after 3 days in addition to the one signal that indicates the defect-heterocubane $[(R^1Sn)_3Se_4Cl]$ ($\delta = -185.2$ ppm); that is, one singlet at $\delta = -39.5$ ppm and three singlets at $\delta = -297.7$, -300.8, and -305.9 ppm. While these three singlets were also detected upon the dissolution of crystals of **5**, the singlet at $\delta = -39.5$ ppm can be unambiguously assigned to the $[SnCl_3]^-$ ion.[17] The three singlets around $\delta = -300$ ppm suggest the formation of three slightly different species in solution that only form the rugby-ball-like capsule upon crystallization. The ^{1}H NMR spectrum supports this assumption by showing several signals (even for methyl groups that usually cause singlets only).

Analysis of **5** by means of positive-ion electrospray ionization mass spectrometry (ESI-MS) showed a signal that corresponds to the $[C_{66}H_{90}N_{12}Se_8Sn_6]^{2+}$ ion, thus confirming that the capsule stays intact, even upon release of the solvent molecule. Another intense signal arises from the capsule cation with one Cl^- ion (i.e., $[C_{66}H_{90}N_{12}Se_8Sn_6Cl]^+$) and one $[SnCl_3]^-$ ion (i.e., $[C_{66}H_{90}N_{12}Se_8Sn_7Cl_3]^+$), thus suggesting that the capsule can hold on to anions even under conditions for ESI-MS.

Conclusions

In summary, we have presented a way to synthesize new organotin selenide clusters with structural motifs that were exclusive to organotin sulfide clusters until now. These clusters include rugby-ball-like capsules of the general formula $[(\mu\text{-}R)_3(Sn_3Se_4)_2]X_2$ ($X = Cl/1.5\,H_2O$, $SnCl_3$), which can hold solvent or anionic molecules in their cavities, the volumes of which depend mostly on the organic ligands. Notably, the inclusion of host molecules was not observed in related compounds with spacer-bridged tetraorganodistannoxane double-ladder structures or a molecular diorganotin oxide, which we ascribe to the presence of polar groups in the backbone of the spacer ligands present in **4** and **5**, which the reported compounds lacked,[18] but served to stabilize the guest molecules by means of noncovalent interactions. The presented synthetic approach possibly allows for the design and formation of capsules with accurately tunable inner volumes that could be used for anion exchange.

Experimental Section

General: All syntheses were performed under exclusion of air and moisture by using standard Schlenk techniques. All solvents were dried and freshly distilled prior to use. $[(R^1Sn)_4Se_6]$, $[(R^1Sn)_3Se_4]Cl$, and $(SiMe_3)_2Se$ were prepared according to reported procedures.[4,19] Further chemicals were purchased from Sigma Aldrich.

Spectroscopy and spectrometry: ^{1}H, ^{13}C, and ^{119}Sn NMR measurements were carried out on a Bruker AV 500 spectrometer. ^{77}Se NMR spectra could not be obtained in a satisfying quality, most likely due to the low overall solubility of the compounds. The ^{1}H NMR chemical shifts are quoted in ppm relative to the residual protons of deuterated solvents. Me_4Sn was used as an internal standard for ^{119}Sn NMR spectroscopic measurements. High-resolution mass spectra (ESI) were acquired with an LTQ-FT Ultra mass spectrometer (Thermo Fischer Scientific; resolution set to 100 000). Micro X-ray fluorescence spectroscopy (μ-XRF) was carried out by using a Bruker M4 Tornado spectrometer with a Rh target X-ray tube, polycapillary optics, and a Si drift detector. Further details on the spectroscopic and spectrometric results are provided in the Supporting Information.

Synthesis of $[\{(R^2Sn)_2SnSe_4\}_2(\mu\text{-}Se)_2]$ (1): $[(R^1Sn)_4Se_6]$ (100 mg, 0.074 mmol) was dissolved in CH_2Cl_2 (20 mL). $N_2H_4{\cdot}H_2O$ (15 mg, 0.297 mmol) and $(SiMe_3)_2Se$ (67 mg, 0.297 mmol) were subsequently added. The reaction mixture was stirred at room temperature for 16 h. After filtering and layering with *n*-hexane (20 mL) at room temperature, yellow crystals of **1** were isolated in approximately 10% yield (as a mixture of $\mathbf{1}{\cdot}2CH_2Cl_2$ and $\mathbf{1}{\cdot}3CH_2Cl_2$). ^{1}H NMR (300 MHz, $CDCl_3$, 25 °C): $\delta = 1.22$ (s, 6H; CMe_2), 1.87 (s, 3H; C(N)Me), 2.52 (s, 2H; CH_2), 5.49 ppm (br s, 2H; NNH_2); the low solubility of the crystals inhibited the collection of ^{119}Sn NMR spectroscopic data.

Synthesis of $[\{(R^3Sn)_2SnSe_4\}_2(\mu\text{-}Se)_2]$ (2): PhN_2H_3 (100 mg, 0.922 mmol) was added to $[(R^1Sn)_4Se_6]$ (310 mg, 0.23 mmol) dissolved in CH_2Cl_2 (20 mL). After stirring for 15 min, $(SiMe_3)_2Se$ (35 mg, 0.154 mmol) was added to the reaction mixture, which was stirred at room temperature for three days. The resulting dark-red solution was filtered and layered with *n*-hexane (20 mL) at room temperature to give yellow crystals of **2** in approximately 15% yield (as a mixture of $\mathbf{2}{\cdot}CH_2Cl_2$, $\mathbf{2}{\cdot}2CH_2Cl_2$, and $\mathbf{2}{\cdot}4CH_2Cl_2$). ^{1}H NMR (300 MHz, $CDCl_3$, 25 °C): $\delta = 1.28$ (s, 6H; $C(CH_3)_2$), 1.91 (s, 3H; $C(CH_3)N$), 2.68 (s, 2H; CMe_2CH_2), 5.35 (br s, 1H; NNH), 6.61 (m, 2H; *o*-Ph), 6.88 (m, 2H; *m*-Ph), 7.07 ppm (s, 1H; *p*-Ph); ^{119}Sn NMR (186.5 MHz, $CDCl_3$, 25 °C): $\delta = -243.5$ (s, Sn(μ-Se)), -264.3 ppm (s, SnR^3).

Synthesis of $[(R^4Sn_2)_2Se_6]$ (3): $[(R^2Sn)_4Se_6]$ (100 mg, 0.071 mmol) and *ortho*-phthalaldehyde (38 mg, 0.285 mmol) were dissolved in CH_2Cl_2 (14 ml), and stirred at room temperature for 16 h. The reaction mixture was filtered, and the filtrate was layered with *n*-hexane to give colorless crystals of $\mathbf{3}{\cdot}CH_2Cl_2$ (58 mg, 0.036 mmol, 51% based on $[(R^2Sn)_4Se_6]$). ^{1}H NMR (300 MHz, $CDCl_3$, 25 °C): $\delta = 1.29$ (s, 24H; CMe_2), 2.19 (s, 12H; C(Me)N), 2.70 (s, 8H; CH_2), 7.78 (m, 4H; Ar), 7.98 (m, 4H; Ar), 10.55 ppm (s, 4H; HC=N); ^{119}Sn NMR (186.5 MHz, CD_2Cl_2, 25 °C): $\delta = -237.3$ ppm. μ-XRF: calcd for Sn/Se/Cl: 4:6:2; found: 4.1:6.1:1.8.

Synthesis of $[(Sn_3Se_4)_2(\mu\text{-}R^5)_3][X]_2$ (4): $[(R^1Sn)_3Se_4Cl]$ (100 mg, 0.100 mmol) and adipic acid dihydrazide (100 mg, 0.574 mmol) were dissolved in CH_2Cl_2 (20 mL) and stirred at room temperature for 16 h. A brown precipitate was removed by filtration, and the yellow solution was layered with *n*-hexane (20 mL) at room temperature to yield yellow crystals of $\mathbf{4a}{\cdot}4CH_2Cl_2$ ($X = SnCl_3$) and $\mathbf{4b}{\cdot}3H_2O{\cdot}4CH_2Cl_2$ ($X = Cl$) in approximately 10% total yield. ^{1}H NMR (300 MHz, $CDCl_3$, 25 °C): $\delta = 1.22$ (s, 36H; CMe_2), 1.26 (s, 12H; $C(O)CH_2CH_2$), 1.48 (s, 12H; $C(O)CH_2CH_2$), 2.08 (s, 18H; $C(N)CH_3$), 2.72 (s, 12H; $CMe_2CH_2C(Me)N$), 9.57 ppm (s, 6H; NNH); ^{119}Sn NMR (186.5 MHz, $CDCl_3$, 25 °C): $\delta = -308.7$ ppm; μ-RFA: calcd for Sn/Se/Cl: 8:8:6; found: 7.8:8.5:5.7; HRMS (ESI): *m/z* calcd for $[C_{54}H_{96}N_{12}O_6Se_8Sn_3]^{2+}$ ($\mathbf{4a}{\cdot}2SnCl_3$): 1176.7545, found: 1176.7592.

Synthesis of $[(Sn_3Se_4)_2(\mu\text{-}R^6)_3][SnCl_3]_2$ (5): $[(R^1Sn)_3Se_4Cl]$ (105 mg, 0.104 mmol) and 1,1′-(1,5-naphthalenediyl)bishydrazine (30 mg, 0.157 mmol) were dissolved in CH_2Cl_2 (20 mL) and stirred at room temperature for 16 h. After filtering, the brownish solution was layered with *n*-hexane at room temperature to give colorless needles of **5**·3 CH_2Cl_2 and **5**·6.75 CH_2Cl_2 (together 29 mg, approximately 20% based on $[(R^1Sn)_3Se_4Cl]$). ^{1}H NMR (500 MHz, CD_2Cl_2, 25 °C): $\delta =$ 1.33 (m, 36H; CMe_2), 1.87 (s, 6H; C(N)CH_3), 1.97 (s, 6H; C(N)CH_3), 2.05 (s, 6H; C(N)CH_3), 2.64 (m, 6H; CMe_2CH_2C(Me)N), 3.14 (m, 6H; CMe_2CH_2C(Me)N), 6.36 (m, 6H; NH), 7.42 ppm (m, 18H; naph); ^{119}Sn NMR (186.5 MHz, CD_2Cl_2, 25 °C): $\delta = -297.4$, -300.4, -305.2 ppm (and in the reaction solution: $\delta = -39$ ppm ($[SnCl_3]^-$)); due to the low solubility of the compound, the signal of the $[SnCl_3]^-$ ion could not be detected upon dissolution of the crystals; HRMS (ESI): *m/z* calcd for $C_{66}H_{90}N_{12}Se_8Sn_6^{2+}$ (**5**–2 $SnCl_3^-$): 1197.7464, found: 1197.7431; *m/z* calcd for $C_{66}H_{90}N_{12}Se_8Sn_7Cl_3^+$ (**5**–$SnCl_3^-$): 2620.2994, found: 2620.3051; calcd *m/z* for $C_{66}H_{90}N_{12}Sn_6Se_8Cl^+$ (**5**–2 $SnCl_3^- + Cl^-$):2430.4627, found: 2430.4617; *m/z* calcd for $C_{66}H_{89}N_{12}Se_8Sn_6$ (**5**–2 $SnCl_3^- - H^+$): 2394.4854; found: 2394.4899; compound **5** was also crystallized (**5**·6.5 CH_2Cl_2).

Single-crystal X-ray diffraction: Crystals suitable for X-ray diffraction analyses were investigated with a STOE IPDS-2T diffractometer (**1**·2 CH_2Cl_2 ($P2_1/n$), **2**·4 CH_2Cl_2, and **5**·3 CH_2Cl_2), a STOE IPDS-2 diffractometer (**1**·2 CH_2Cl_2 ($P2_1$), **1**·2 CH_2Cl_2 ($P\bar{1}$), **1**·3 CH_2Cl_2, **2**·1 CH_2Cl_2, **2**·2 CH_2Cl_2, **3**, **4a**, and **4b**) at 100 K using $Mo_{K\alpha}$ radiation and a graphite monochromator ($\lambda = 0.71073$ Å), or a STOE StadiVari diffractometer (**5**·6.75 CH_2Cl_2) at 100 K using $Cu_{K\alpha}$ radiation ($\lambda =$ 1.54186) from an X-ray microsource with X-ray optics and a Pilatus 300 K Si hybrid pixel-array detector. Upon numerical absorption correction (STOE X-AREA), the structure solution was performed by using direct methods, followed by full-matrix-least-squares refinement against F^2 with using SHELXT15, SHELXL15, and OLEX2 software.[20]

Crystallographic data (excluding structure factors) for the structures reported herein have been deposited with the Cambridge Crystallographic Data Centre as supplementary publication. CCDC 1834602, 1834603, 1834604, 1834605, 1834606, 1834607, 1834608, 1834609, 1834610, 1834611, 1834612, and 1834613 contain the supplementary crystallographic data for this paper. These data can be obtained free of charge from The Cambridge Crystallographic Data Centre.

Acknowledgements

This work was supported by the Deutsche Forschungsgemeinschaft (DFG) within the framework of GRK 1782 "Functionalization of Semiconductors".

Conflict of interest

The authors declare no conflict of interest.

Keywords: cluster compounds · molecular trapping · organic–inorganic hybrid composites · organotin · X-ray diffraction

[1] a) O. Fuhr, S. Dehnen, D. Fenske, *Chem. Soc. Rev.* **2013**, *42*, 1871 – 1906; b) S. Santner, J. Heine, S. Dehnen, *Angew. Chem. Int. Ed.* **2016**, *55*, 876 – 893; *Angew. Chem.* **2016**, *128*, 886 – 904; c) P. Feng, X. Bu, N. Zheng, *Acc. Chem. Res.* **2005**, *38*, 293 – 303.

[2] a) D. Dakternieks, K. Jurkschat, H. Wu, E. R. T. Tiekink, *Organometallics* **1993**, *12*, 2788 – 2793; b) K. Wraage, T. Pape, R. Herbst-Irmer, M. Noltemeyer, H.-G. Schmidt, H. W. Roesky, *Eur. J. Inorg. Chem.* **1999**, 869 – 872; c) A. Blecher, M. Dräger, B. Mathiasch, *Z. Naturforsch. B* **1981**, *36*, 1361 – 1367; d) K. Merzweiler, L. Weisse, *Z. Naturforsch. B* **1990**, *45*, 971 – 978.

[3] J. P. Eußner, B. E. K. Barth, E. Leusmann, Z. You, N. Rinn, S. Dehnen, *Chem. Eur. J.* **2013**, *19*, 13792 – 13802.

[4] N. Rinn, J. P. Eußner, W. Kaschuba, X. Xie, S. Dehnen, *Chem. Eur. J.* **2016**, *22*, 3094 – 3104.

[5] N. Rinn, L. Guggolz, K. Gries, K. Volz, J. Senker, S. Dehnen, *Chem. Eur. J.* **2017**, *23*, 15607 – 15611.

[6] N. Rinn, K. Hanau, L. Guggolz, A. Rinn, S. Chatterjee, S. Dehnen, *Z. Anorg. Allg. Chem.* **2017**, *643*, 1508 – 1512.

[7] a) J. P. Eußner, S. Dehnen, *Chem. Commun.* **2014**, *50*, 11385 – 11388; b) Z. Hassanzadeh Fard, C. Müller, T. Harmening, R. Pöttgen, S. Dehnen, *Angew. Chem. Int. Ed.* **2009**, *48*, 4441 – 4444; *Angew. Chem.* **2009**, *121*, 4507 – 4511.

[8] Z. H. Fard, L. Xiong, C. Müller, M. Holyńska, S. Dehnen, *Chem. Eur. J.* **2009**, *15*, 6595 – 6604.

[9] a) B. E. K. Barth, E. Leusmann, K. Harms, S. Dehnen, *Chem. Commun.* **2013**, *49*, 6590 – 6592; b) E. Leusmann, E. Geringer, B. Weinert, S. Dehnen, *Dalton Trans.* **2016**, *45*, 15298 – 15302; c) E. Leusmann, N. W. Rosemann, B. Weinert, S. Chatterjee, S. Dehnen, *Eur. J. Inorg. Chem.* **2016**, 5300 – 5304; d) E. Leusmann, F. Schneck, S. Dehnen, *Organometallics* **2015**, *34*, 3264 – 3271; e) E. Leusmann, M. Wagner, N. W. Rosemann, S. Chatterjee, S. Dehnen, *Inorg. Chem.* **2014**, *53*, 4228 – 4233; f) Z. You, S. Dehnen, *Inorg. Chem.* **2013**, *52*, 12332 – 12334.

[10] B. E. K. Barth, B. A. Tkachenko, J. P. Eußner, P. R. Schreiner, S. Dehnen, *Organometallics* **2014**, *33*, 1678 – 1688.

[11] Z. H. Fard, M. R. Halvagar, S. Dehnen, *J. Am. Chem. Soc.* **2010**, *132*, 2848 – 2849.

[12] M. R. Halvagar, Z. H. Fard, S. Dehnen, *Chem. Eur. J.* **2011**, *17*, 4371 – 4374.

[13] P. Pyykkö, M. Atsumi, *Chem. Eur. J.* **2009**, *15*, 12770 – 12779.

[14] A. Bondi, *J. Phys. Chem.* **1964**, *68*, 441 – 451.

[15] S. Heimann, M. Hołyńska, S. Dehnen, *Z. Anorg. Allg. Chem.* **2012**, *638*, 1663 – 1666.

[16] A. L. Spek, *Acta Crystallogr. Sect. D* **2009**, *65*, 148 – 155.

[17] M. I. García-Seijo, A. Castiñeiras, B. Mahieu, L. Jánosi, Z. Berente, L. Kollár, M. E. García-Fernández, *Polyhedron* **2001**, *20*, 855 – 868.

[18] a) D. Dakternieks, A. Duthie, B. Zobel, K. Jurkschat, M. Schürmann, E. R. T. Tiekink, *Organometallics* **2002**, *21*, 647 – 652; b) D. Dakternieks, B. Zobel, K. Jurkschat, M. Schürmann, E. R. T. Tiekink, *Organometallics* **2003**, *22*, 1343 – 1345; c) J. Beckmann, D. Dakternieks, A. Duthie, F. S. Kuan, K. Jurkschat, M. Schürmann, E. R. T. Tiekink, *New J. Chem.* **2004**, *28*, 1268 – 1276.

[19] M. R. Detty, M. D. Seidler, *J. Org. Chem.* **1982**, *47*, 1354 – 1356.

[20] a) G. M. Sheldrick, *Acta Crystallogr. Sect. C* **2015**, *71*, 3 – 8; b) G. M. Sheldrick, *Acta Crystallogr. Sect. A* **2015**, *71*, 3 – 8; c) O. V. Dolomanov, L. J. Bourhis, R. J. Gildea, J. A. K. Howard, H. Puschmann, *J. Appl. Crystallogr.* **2009**, *42*, 339 – 341.

Manuscript received: April 4, 2018
Accepted manuscript online: May 22, 2018
Version of record online: July 15, 2018

CHEMISTRY
A European Journal

Supporting Information

Organotin Selenide Clusters and Hybrid Capsules

Katharina Hanau, Niklas Rinn, Mario Argentari, and Stefanie Dehnen*[a]

chem_201801652_sm_miscellaneous_information.pdf

1. Details of the X-ray diffraction measurements and refinements

Table S1. Crystallographic data and refinement results of **1**–**5**.

Compound (CCDC number)	**1**·2CH_2Cl_2 (1834603)	**1**·2CH_2Cl_2 (1834609)	**1**·2CH_2Cl_2 (1834602)
Empirical Formula	$C_{26}H_{56}Cl_4N_8Se_{10}Sn_6$	$C_{24}H_{52}N_8Se_{10}Sn_6$	$C_{26}H_{56}Cl_4N_8Se_{10}Sn_6$
Formula weight /g·mol^{-1}	2124.32	1954.47	2124.32
Crystal color and shape	yellow block	yellow plate	yellow
Crystal size /mm³	0.1 x 0.09 x 0.05	0.17 x 0.08 x 0.02	needle
Crystal system	triclinic	Monoclinic	monoclinic
Space group [Flack parameter]	$P\bar{1}$	$P2_1/n$	$P2_1$ [0.237(16)]
a /Å	11.2464(6)	12.7438(5)	11.0494(4)
b / Å	11.3589(7)	14.2960(4)	12.8429(4)
c / Å	12.00.63(7)	29.1752(11)	20.2126(7)
α /°	97.240(5)	90	90
β /°	108.188(4)	96.721(3)	95.689(3)
γ /°	101.265(5)	90	90
V / Å³	1399.98(15)	5278.8(3)	2854.17(17)
Z	1	4	2
ρ_{calcd} / g·cm^{-3}	2.520	2.459	2.472
$\mu_{(Mo\ K\alpha)}$ / mm^{-1}	9.355	9.716	9.177
$\mu_{(Cu\ K\alpha)}$ / mm^{-1}	–	–	–
Absorption correction type	numerical	numerical	numerical
Min./max. transmission	0.379 / 0.697	0.207 / 0.847	0.139 / 0.807
2*θ* range / deg	3.644 – 53.51	2.812 – 53.572	3.704 – 50
No. of measured reflections	21559	37416	26596
R(int)	0.0663	0.1040	0.0938
Independent Reflections	5917	11139	9017
Independent Reflections ($I>2\sigma(I)$)	4731	7282	7614
No. of parameters	252	449	504
R_1 ($I>2\sigma(I)$) / wR_2 (all data)	0.0392 / 0.0951	0.0480 / 0.0994	0.0410 / 0.0997
S (all data)	0.969	0.918	0.952
Max. peak / hole / e$^-$ Å³	2.17 / −1.55	0.98 / −1.09	0.84 / −0.96

Table S1. Crystallographic data and refinement results of **1**–**5** (continued).

1·3CH_2Cl_2 (1834608)	**2**·1CH_2Cl_2 (1834606)	**2**·2CH_2Cl_2 (1834605)	**2**·4CH_2Cl_2 (1834604)
$C_{24}H_{53}N_8Se_{10}Sn_6$	$C_{49}H_{70}Cl_2N_8Se_{10}Sn_6$	$C_{50}H_{72}Cl_4N_8Se_{10}Sn_6$	$C_{52}H_{76}Cl_8N_8Se_{10}Sn_6$
1955.48	2343.77	2428.69	2598.54
yellow plate	yellow plank	yellow block	yellow plank
0.08 x 0.07 x 0.02	0.32 x 0.11 x 0.03	0.29 x 0.1 x 0.03	0.394 x 0.119 x 0.107
monoclinic	monoclinic	Monoclinic	Triclinic
$P2_1/n$	C2/*c*	$P2_1/c$	$P\bar{1}$
12.2857(8)	28.1861(12)	11.2069(3)	11.0524(5)
15.6893(14)	10.7978(4)	21.9501(6)	11.0937(5)
28.2007(19)	24.1374(10)	15.0578(4)	16.5906(7)
90	90	90	76.399(3)
101.493(5)	104.597(3)	104.255(2)	87.667(3)
90	90	90	83.906(3)
5326.8(7)	7109.0(5)	3590.05(17)	1965.73(15)
4	4	2	1
2.438	2.190	2.247	2.195
9.629	7.308	7.312	6.816
–	–	–	–
Numerical	numerical	Numerical	numerical
0.356 / 0.802	0.144 / 0.797	0.336 / 0.611	0.231 / 0.683
3.41 – 50	2.986 – 50	3.352 – 58.378	5.026 – 53
25396	25875	38804	16940
0.2053	0.0763	0.0831	0.0728
9309	6262	9610	8067
2597	3348	8015	6178
449	346	358	389
0.0605 / 0.1203	0.0390 / 0.0853	0.0350 / 0.0769	0.0393 / 0.0980
0.706	0.782	1.051	0.960
0.89 / −0.69	1.02 / −0.82	1.01 / −1.02	1.97 / −1.99

Table S1. Crystallographic data and refinement results of **1**–**5** (continued).

3·2CH_2Cl_2 (1834607)	**4a**·4CH_2Cl_2 (1834611)	**4b**·3H_2O·4CH_2Cl_2 (1834610)	**5**·3CH_2Cl_2 (1834612)	**5**·6.75CH_2Cl_2 (1834613)
$C_{42}H_{60}Cl_4N_8Se_6Sn_4$	$C_{58}H_{104}Cl_{14}N_{12}O_6Se_8Sn_8$	$C_{54}H_{102}Cl_2N_{12}O_9Se_8Sn_6$	$C_{69}H_{94}Cl_{12}N_{12}Se_8Sn_8$	$C_{72.75}H_{103.5}Cl_{19.5}N_{12}Se_8Sn_8$
1767.30	3143.03	2478.19	3098.16	3418.64
colorless block	yellow plate	colorless block	colorless block	colorless block
0.173 x 0.125 x 0.118	0.05 x 0.04 x 0.01	0.1 x 0.04 x 0.04	0.23 x 0.21 x 0.14	0.30 x 0.23 x 0.23
monoclinic	triclinic	Triclinic	triclinic	triclinic
$P2_1/n$	$P\bar{1}$	$P\bar{1}$	$P\bar{1}$	$P\bar{1}$
11.4931(3)	15.7877(10)	15.7971(6)	16.5953(17)	15.0889(12)
16.7792(5)	16.2409(12)	16.4005(7)	17.1055(12)	19.4689(14)
15.7971(5)	22.3787(12)	19.4670(7)	20.5195(13)	21.8628(14)
90	104.481(5)	92.723(3)	97.651(5)	99.095(6)
111.190(2)	105.872(5)	97.846(3)	108.885(6)	105.759(6)
90	101.187(6)	113.349(3)	101.438(7)	106.879(6)
2840.42(15)	5127.4(6)	4558.4(3)	5278.2(8)	5715.7(8)
2	2	2	2	2
2.066	2.036	1.806	1.949	1.986
5.808	5.165	4.919	4.963	–
–	–	–	–	21.105
numerical	numerical	numerical	numerical	numerical
0.479 / 0.596	0.338 / 0.516	0.373 / 0.630	0.342 / 0.533	0.1438 / 0.3429
4.51 – 53.668	2.7 – 50	3.036 – 53.572	2.684 – 53.57	4.346 – 144.992
27340	38608	42727	47007	112818
0.0546	0.0845	0.0994	0.0718	0.0782
6019	17993	19175	22250	22351
4643	10425	10275	16019	18780
295	1024	854	1019	1108
0.0254 / 0.0557	0.0989 / 0.2843	0.0418 / 0.0623	0.0471 / 0.1162	0.0536 / 0.1427
0.940	0.985	0.690	0.963	1.012
1.00 / −0.45	5.12 / −1.86	0.98 / −1.02	4.05 / −3.10	3.25 / −2.58

Crystal structure of 1·2CH_2Cl_2 (*P*2_1/*n*)

The highest peak of residual electron density on the difference Fourier map (0.98 Å) is found 1.199 Å away from Se5 on the Sn4–Se5 bond.

A cut-out of the crystal structure is shown in Figure S1.

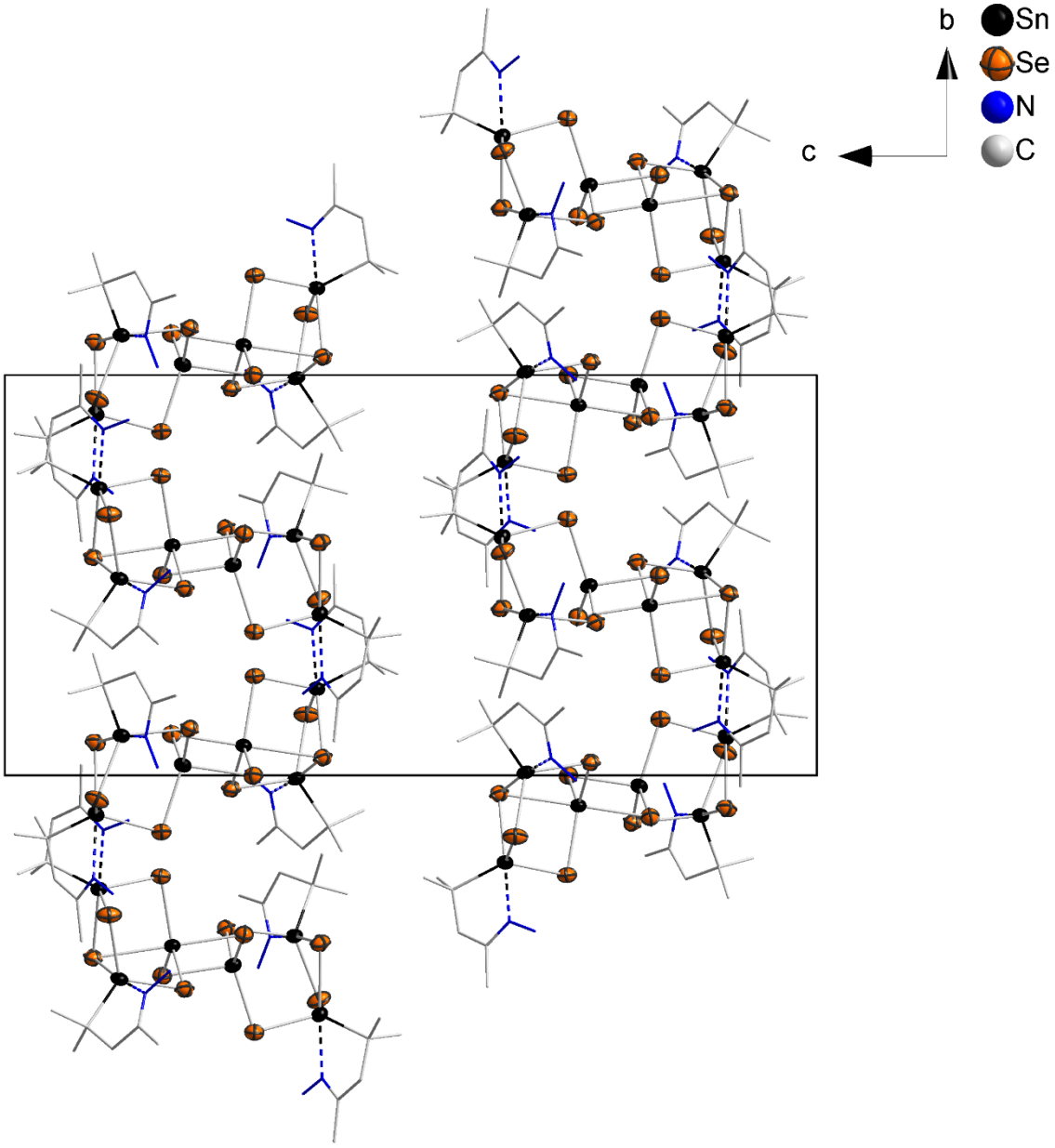

Figure S1: Cut-out of the crystal structure of **1**·2CH_2Cl_2 ($P2_1/n$) viewed along the *a* axis.

Crystal structure of 1·2CH_2Cl_2 (*P*2_1)

The highest peak of residual electron density on the difference Fourier map (0.84 Å) is found 0.735 Å away from the Sn3–Se4 bond.

A cut-out of the crystal structure is shown in Figure S2.

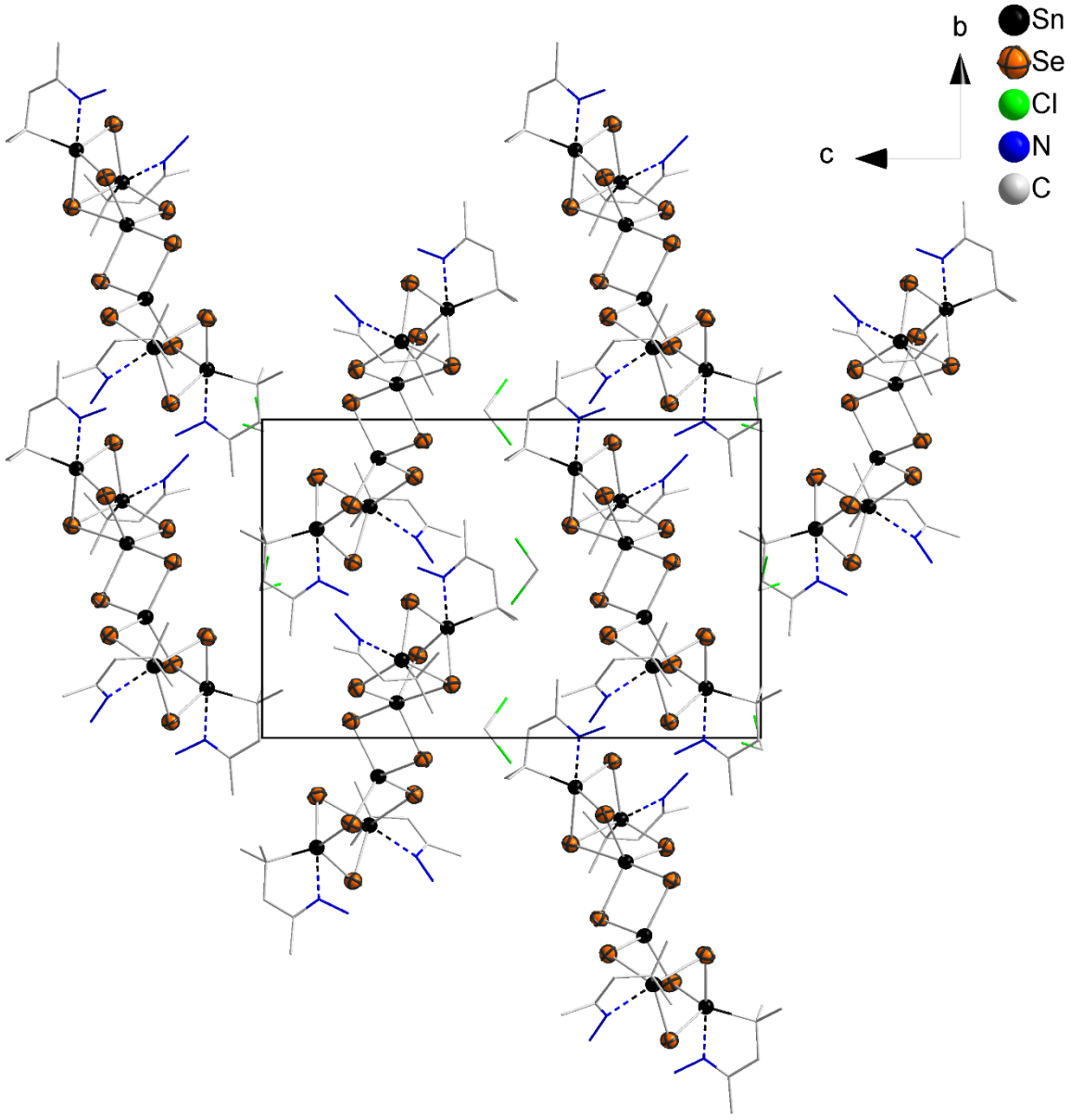

Figure S2: Cut-out of the crystal structure of **1**·2CH_2Cl_2 ($P2_1$) viewed along the *a* axis.

Crystal structure of 1·2CH_2Cl_2 (*P*$\bar{1}$)

The highest peak of residual electron density on the difference Fourier map (2.17 Å) is found 0.992 Å away from Sn3/0.456 Å away from the Sn3–C7 bond.

A cut-out of the crystal structure is shown in Figure S3.

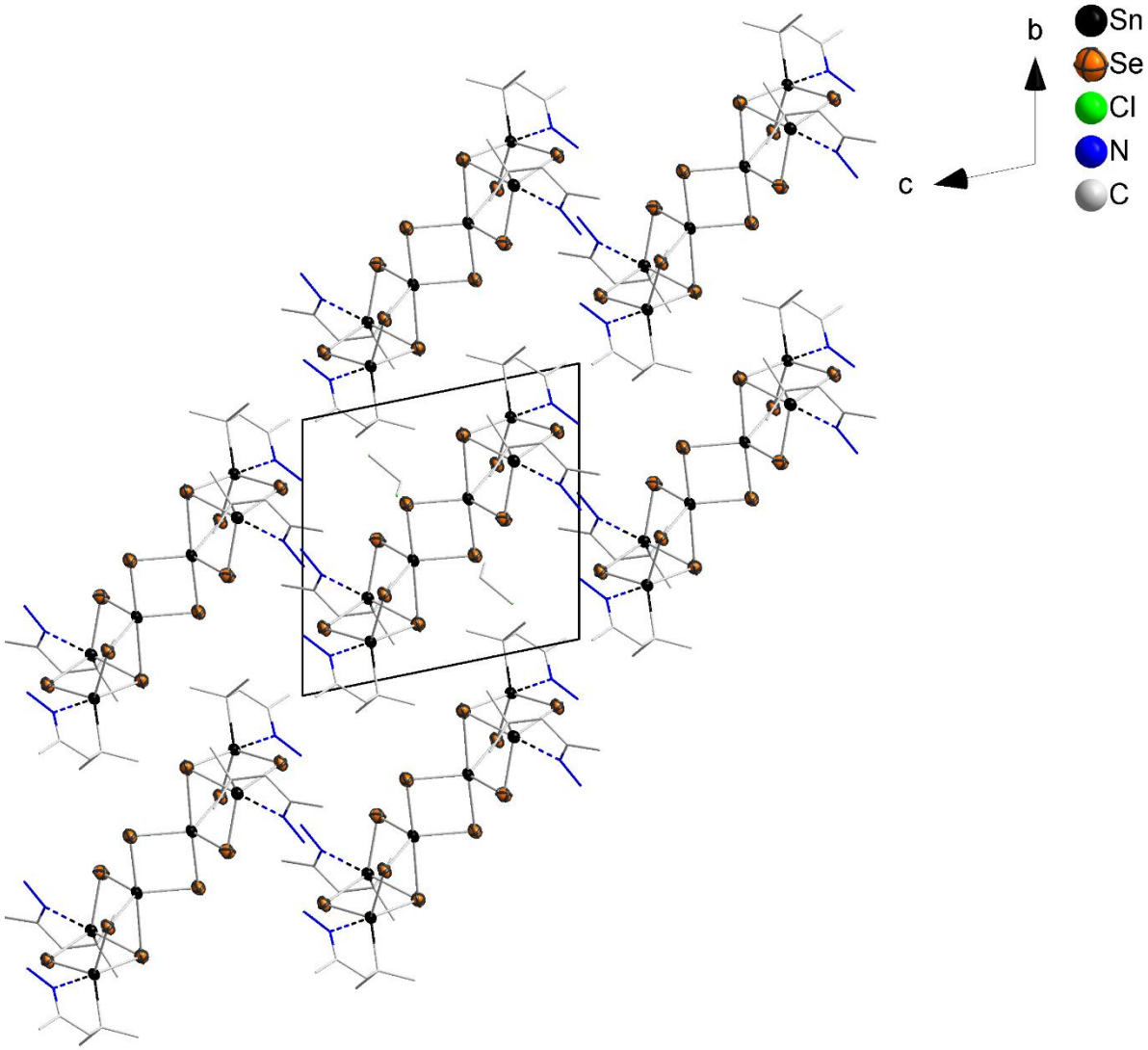

Figure S3: Cut-out of the crystal structure of 1·2CH_2Cl_2 (P$\bar{1}$) viewed along the *a* axis.

Crystal structure of 1·3CH_2Cl_2 (*P*2_1/*n*)

The highest peak of residual electron density on the difference Fourier map (0.84 Å) is found 3.599 Å away from C18.

A cut-out of the crystal structure is shown in Figure S4.

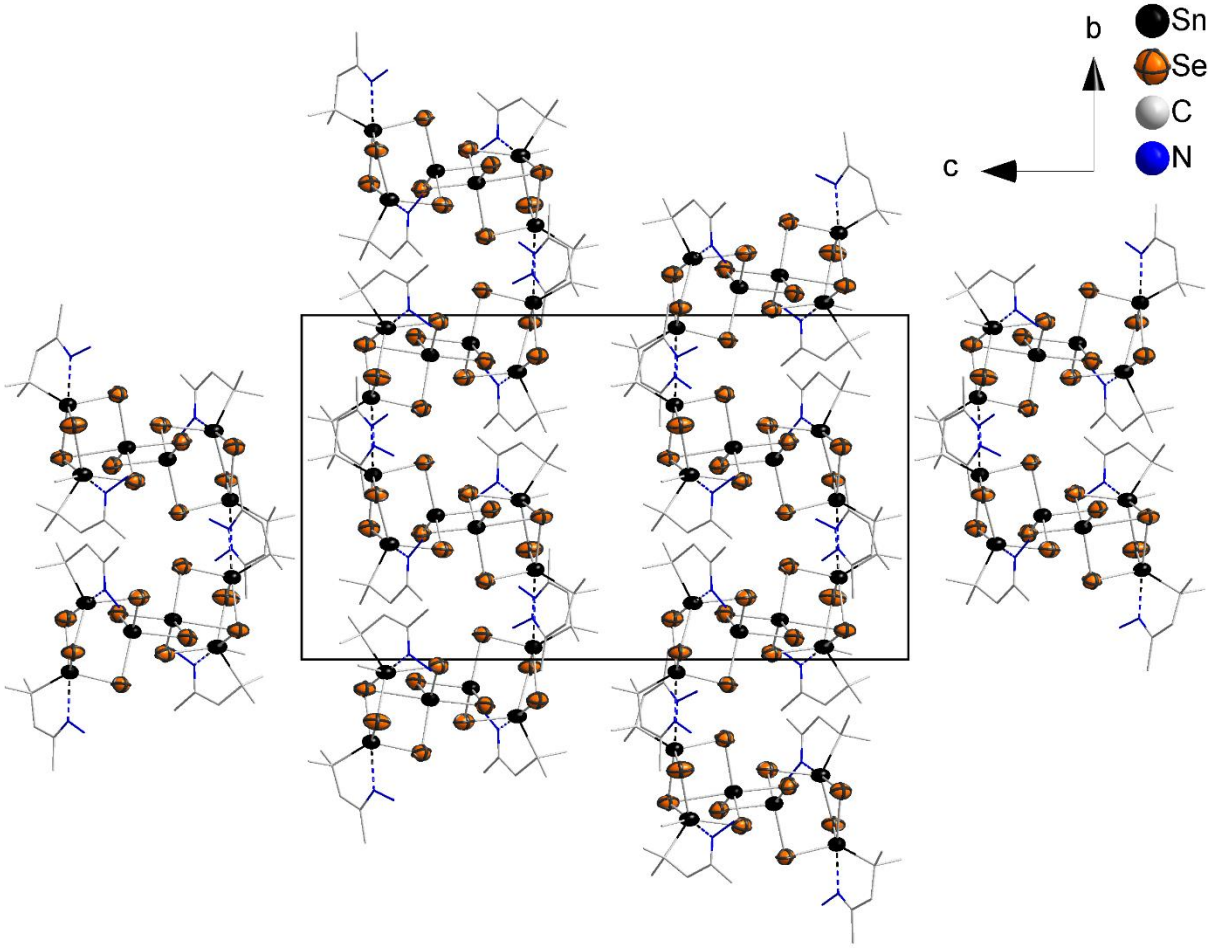

Figure S4: Cut-out of the crystal structure of 1·3CH_2Cl_2 viewed along the *a* axis.

Crystal structure of 2·1CH_2Cl_2

The highest peak of residual electron density on the difference Fourier map (1.02 Å) is found 1.383 Å away from Cl2.

A cut-out of the crystal structure is shown in Figure S5.

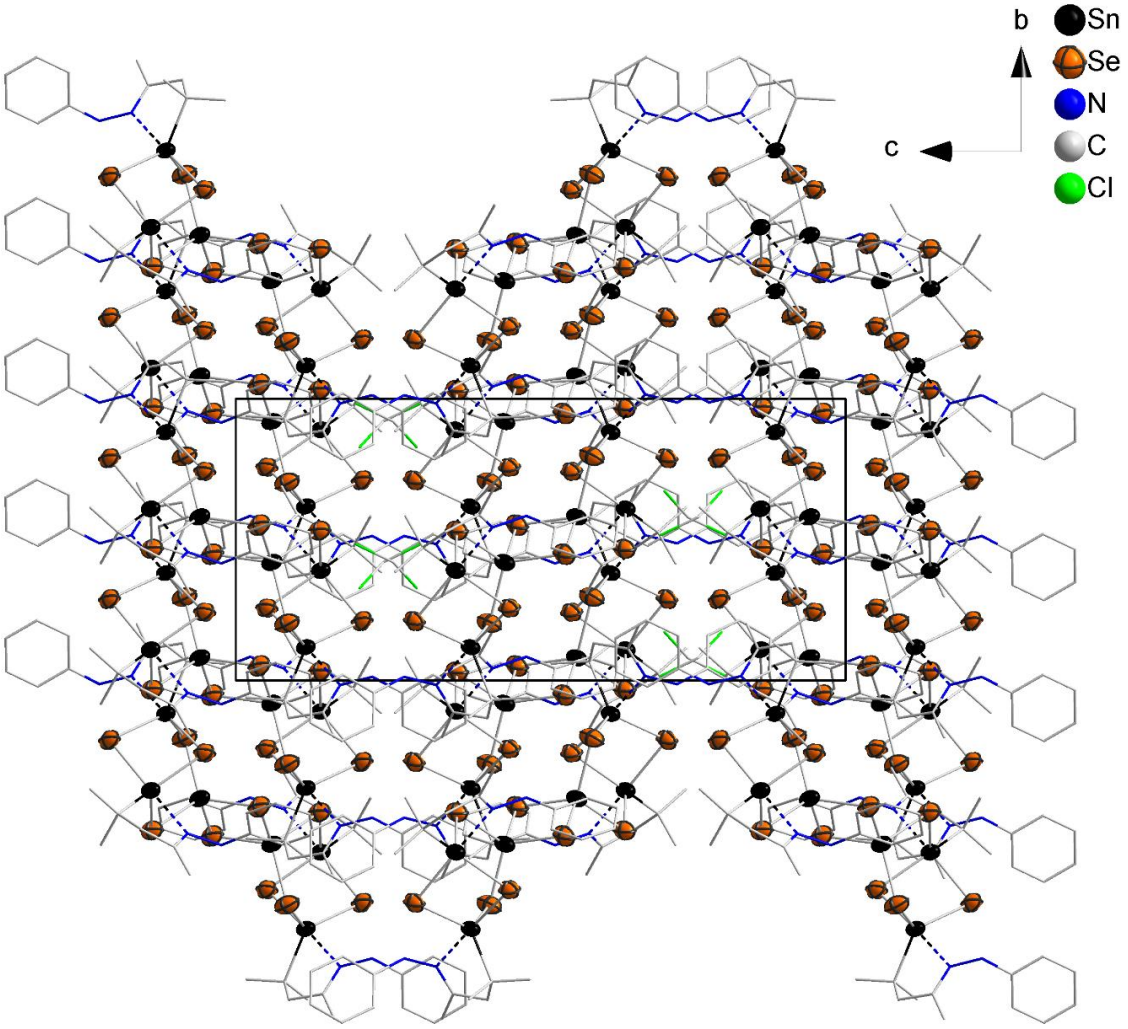

Figure S5: Cut-out of the crystal structure of **2**·1CH_2Cl_2 viewed along the *a* axis.

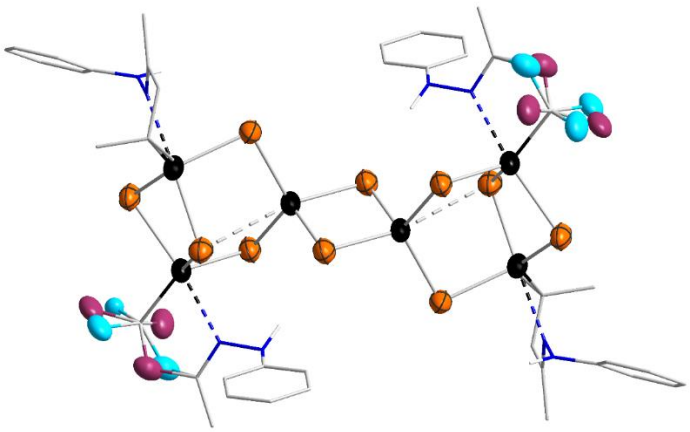

Figure S6: Disorder of C14, C15, and C16 in **2**·1CH_2Cl_2.

Crystal structure of 2·2CH_2Cl_2

The highest peak of residual electron density on the difference Fourier map (1.01 Å) is found 0.820 Å away from Sn1.

A cut-out of the crystal structure is shown in Figure S7.

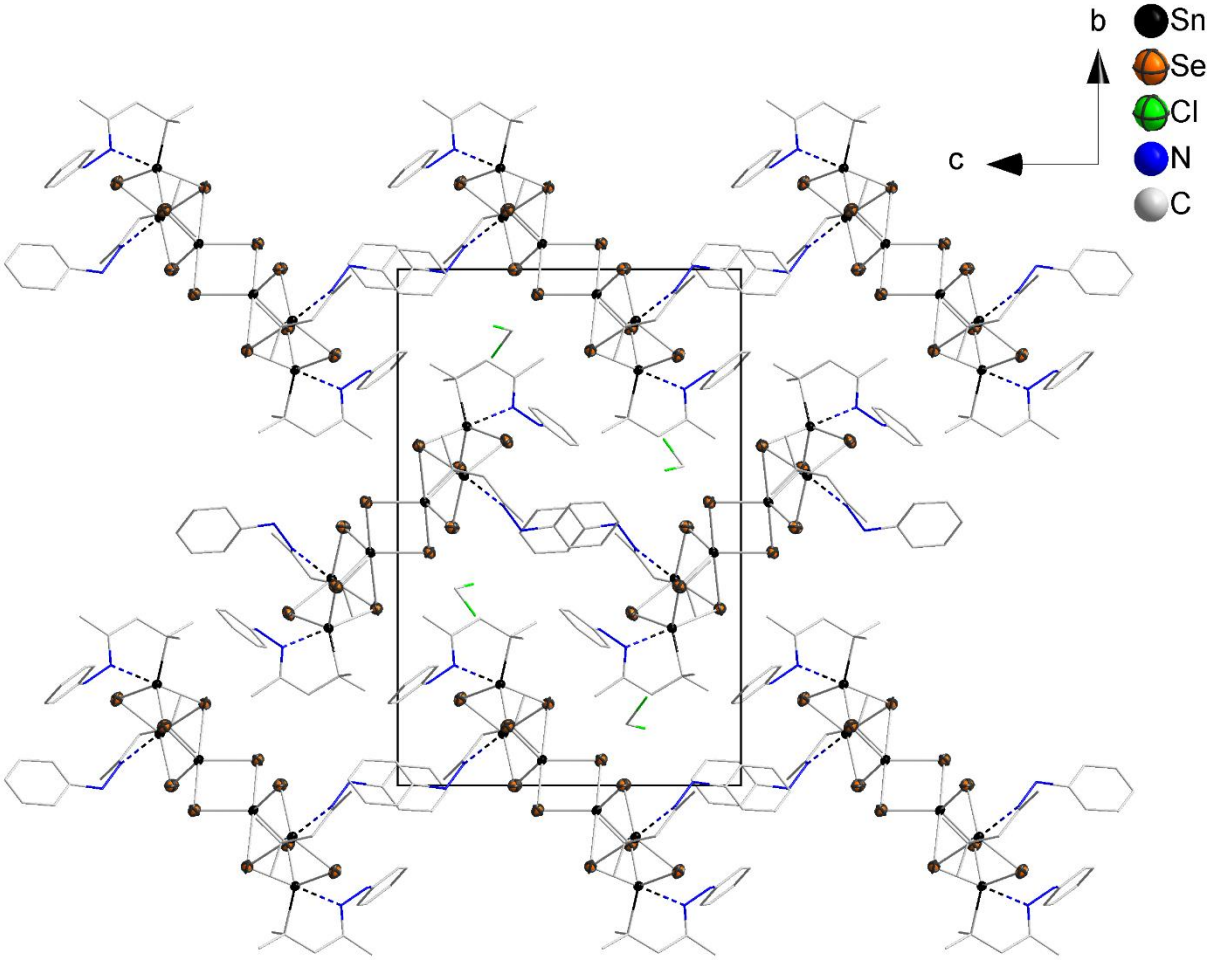

Figure S7: Cut-out of the crystal structure of **2**·2CH_2Cl_2 viewed along the *a* axis.

Crystal structure of 2·4CH_2Cl_2

The highest peak of residual electron density on the difference Fourier map (1.97 $e^-/Å^3$) is found 0.717 Å apart from Se3.

A cut-out of the crystal structure is shown in Figure S8.

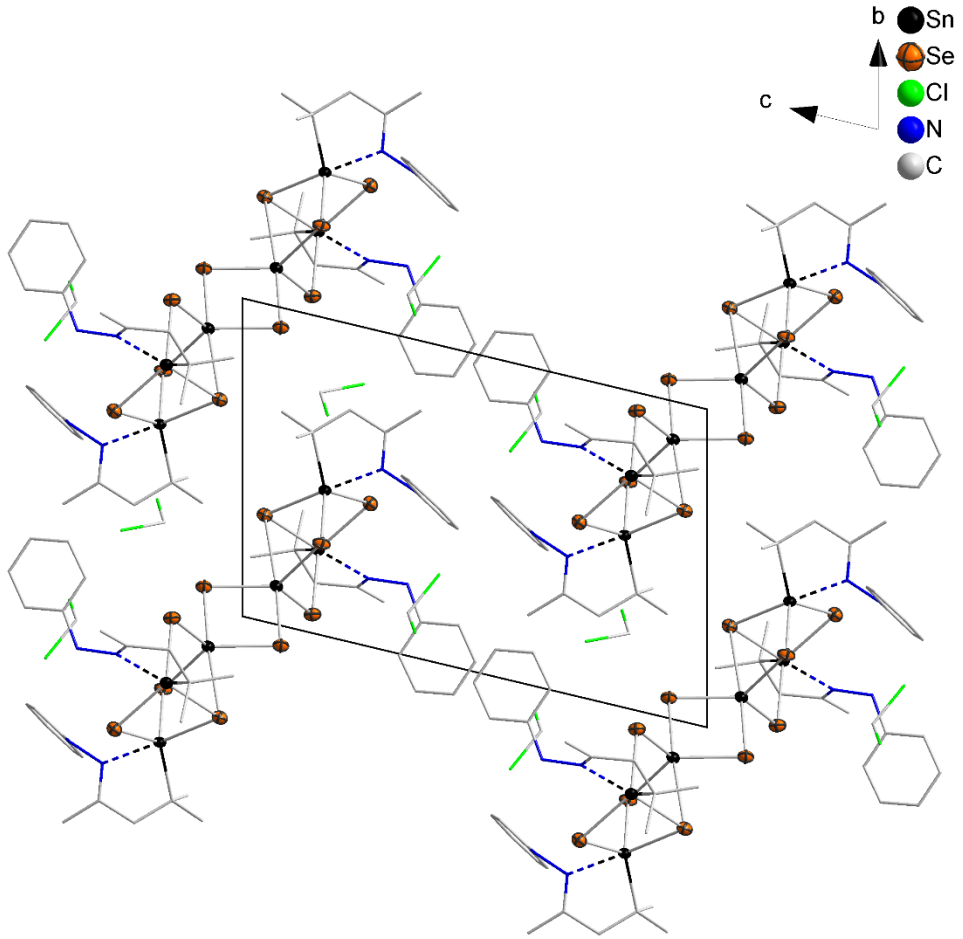

Figure S8: Cut-out of the crystal structure of **2**·4CH_2Cl_2 viewed along the *a* axis.

Crystal structure of 3

The highest peak of residual electron density on the difference Fourier map (1.00 $e^-/Å^3$) is found 0.944 Å apart from Cl1

A cut-out of the crystal structure is shown in Figure S9.

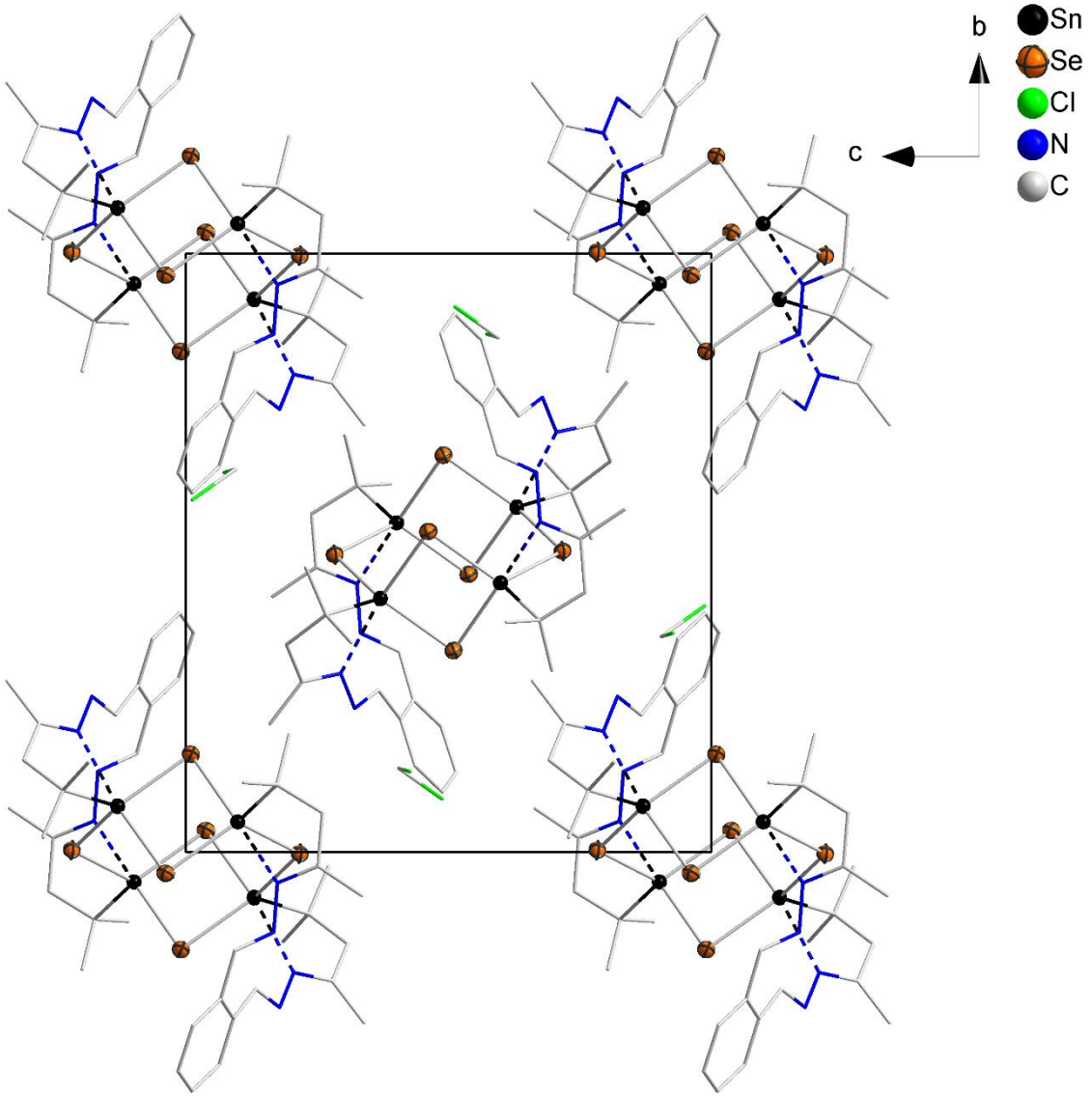

Figure S9: Cut-out of the crystal structure of **3**·CH_2Cl_2 viewed along the *a* axis.

Crystal structure of 4a·4CH_2Cl_2

The highest peak of residual electron density on the difference Fourier map (5.12 e^-/ $Å^3$) is found near the Sn5–Se8 bond 1.058 Å apart from Sn5.

A cut-out of the crystal structure is shown in Figure S10.

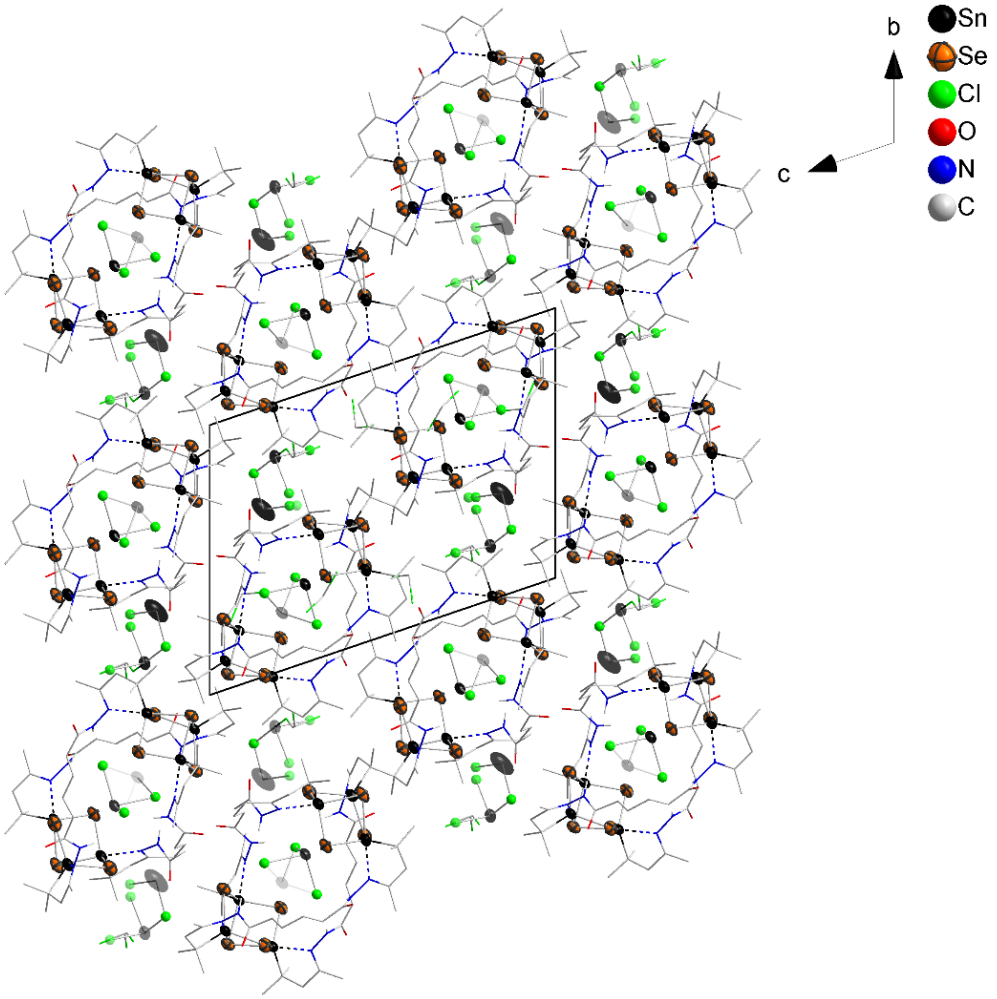

Figure S10: Cut-out of the crystal structure of **4a**·4CH_2Cl_2 viewed along the *a* axis.

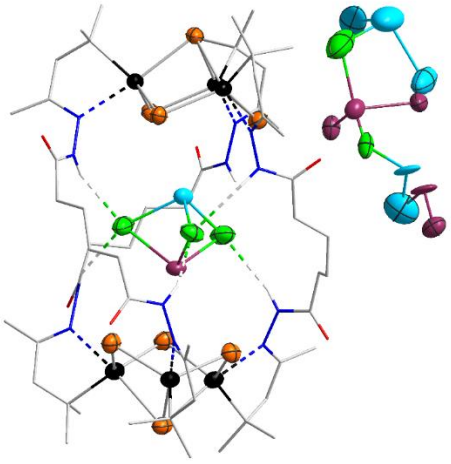

Figure S11: Disorder of Sn7, Sn8, Cl5, Cl6, Cl14, Cl15, and C57 in **4a**·4CH_2Cl_2.

Crystal structure of 4b·3H₂O·4CH₂Cl₂

The highest peak of residual electron density on the difference Fourier map (0.98 e⁻/ Å³) is found 3.467 Å apart from C6.

A cut-out of the crystal structure is shown in Figure S12.

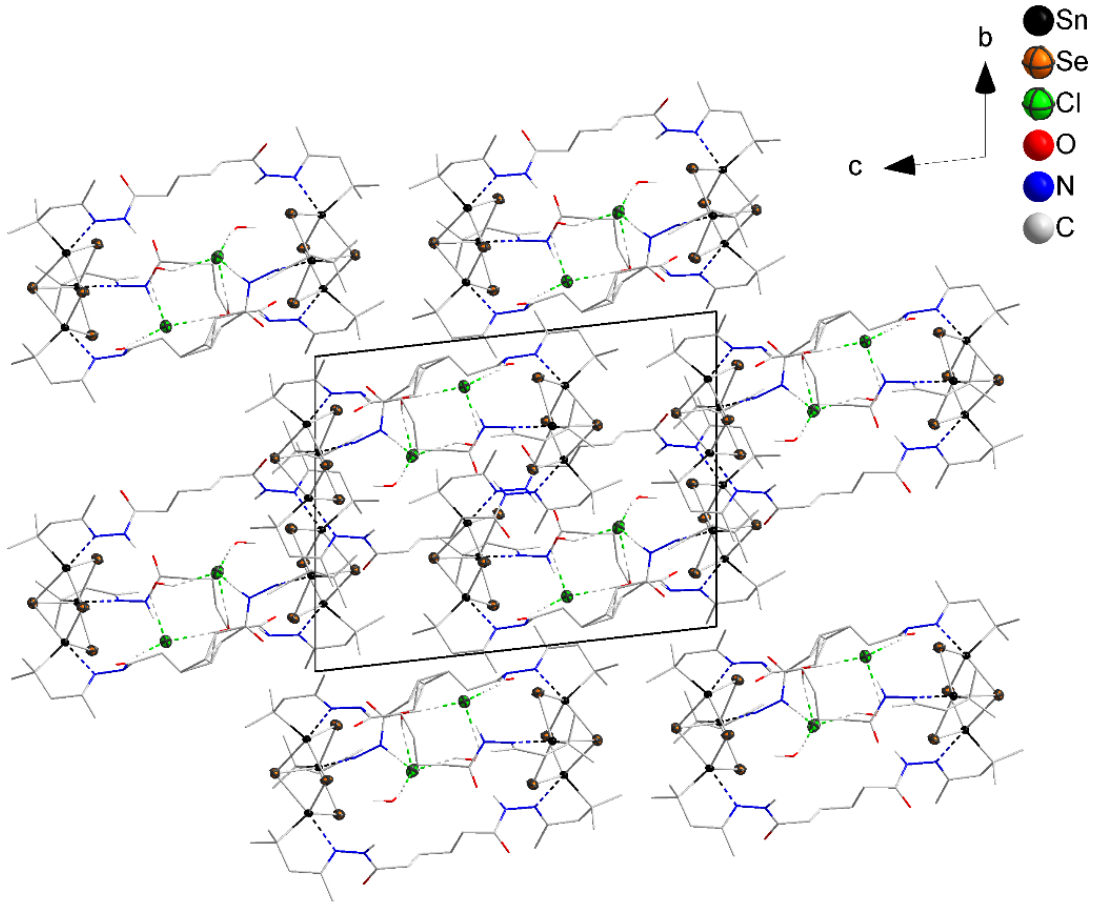

Figure S12: Cut-out of the crystal structure of **4b**·3H₂O·4CH₂Cl₂ viewed along the *a* axis.

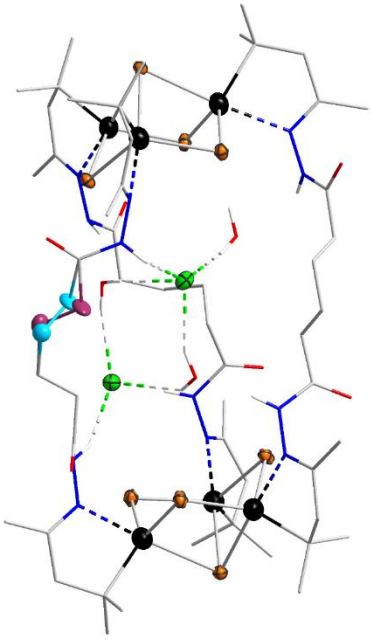

Figure S13: Disorder of C41 and C42 in **4b**·3H₂O·4CH₂Cl₂.

Crystal structure of 5·3CH_2Cl_2

The highest peak of residual electron density on the difference Fourier map (4.05 e^-/ $Å^3$) is found 0.922 Å apart from Sn7.

A cut-out of the crystal structure is shown in Figure S14.

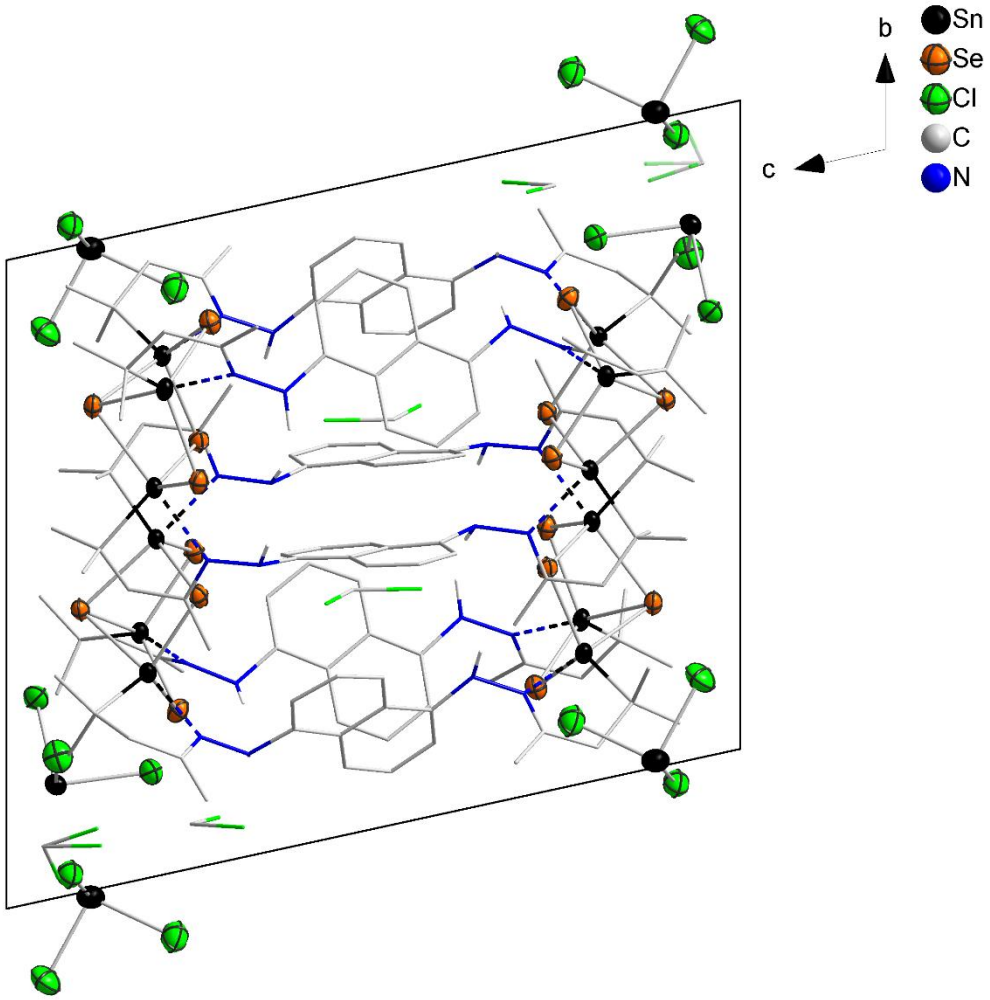

Figure S14: Cut-out of the crystal structure of **5**·3CH_2Cl_2 viewed along the *a* axis.

Crystal structure of 5·6.75CH_2Cl_2

The highest peak of residual electron density on the difference Fourier map (3.25 Å) is found 0.991 Å away from Cl17.

A cut-out of the crystal structure is shown in Figure S15.

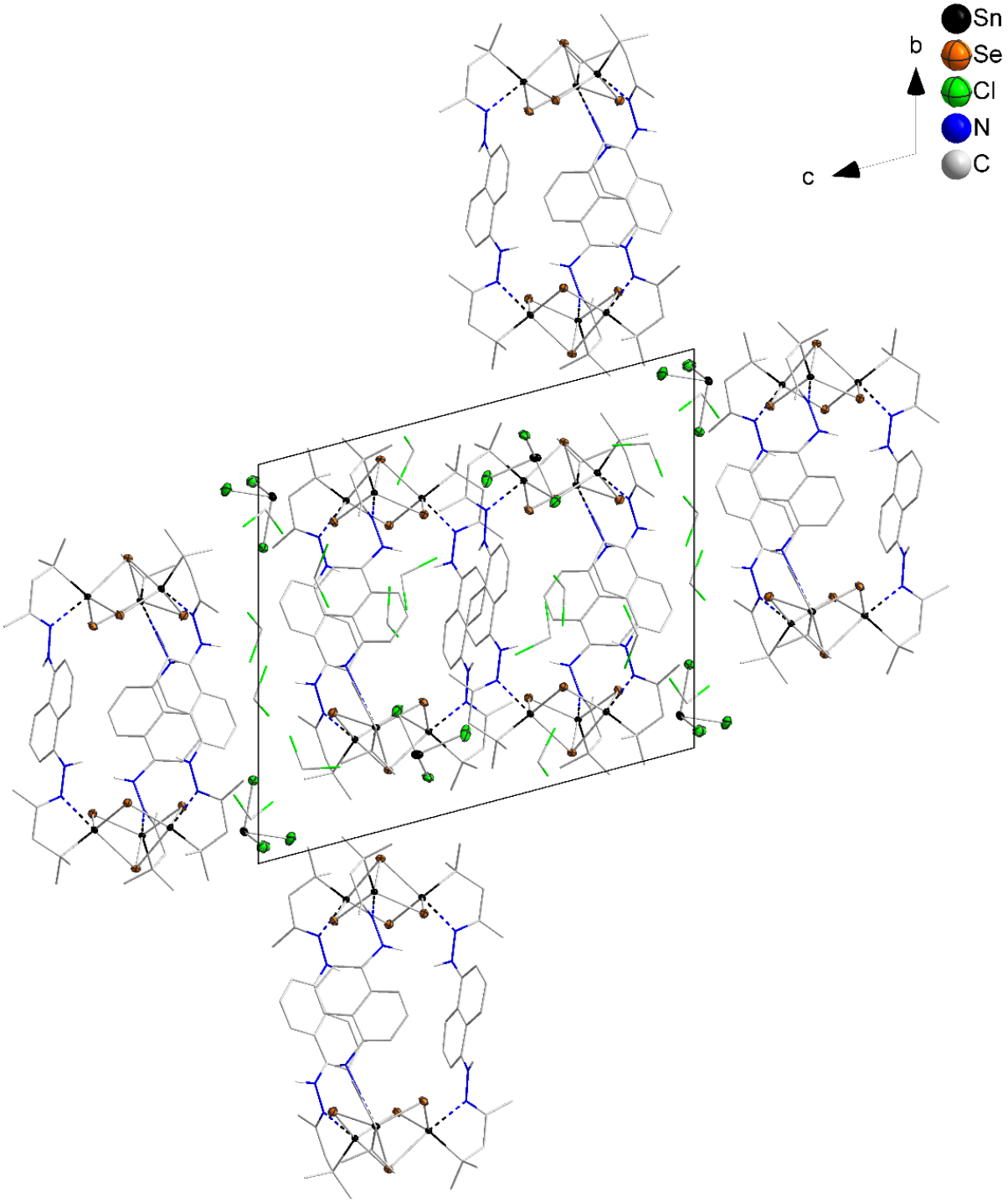

Figure S15: Cut-out of the crystal structure of **5**·6.75CH_2Cl_2 viewed along the *a* axis.

Table S2. Selected atom distances in **1** – **3**.

Distance	**1**·2CH_2Cl_2 ($P\bar{1}$)	**1**·2CH_2Cl_2 ($P2_1/n$)	**1c**·2CH_2Cl_2 ($P2_1$)	**1**·3CH_2Cl_2	**2**·1CH_2Cl_2	**2**·2CH_2Cl_2	**2**·4CH_2Cl_2	**3**
Sn1−Se1	2.5388(8)	2.5215(10)	2.5189(19)	5.530(3)	2.5057(9)	2.5470(5)	2.5396(8)	2.5031(5)
Sn1−Se2	2.5446(8)	2.5281(11)	2.522(2)	2.535(3)	2.5168(10)	2.5352(5)	2.5481(7)	2.5544(4)
Sn1−Se3	2.9769(8)	3.2478(10)	3.4059(22)	3.056(3)	3.6279(11)	2.9739(5)	3.0154(7)	
Sn1-Se3^{i}								2.5963(5)
Sn1−Se5	2.5014(7)	2.5861(11)	2.576(2)	2.598(4)	2.5316(13)	2.5091(5)	2.5170(8)	
Sn1−Se5$^{i/ii/iii/iv}$	2.6426(8)				2.5550(10)	2.6308(5)	2.6127(7)	
Sn1−Se6		2.5020(12)	2.494(2)	2.531(3)				
Sn1-C1								2.2053(49)
Sn1-N1								2.6219(36)
Sn2−Se1	2.5357(8)	2.5427(11)	2.553(2)	2.553(4)	2.5765(11)	2.5305(5)	2.5445(7)	
Sn2-Se1^{i}								2.6259(5)
Sn2-Se2								2.5529(5)
Sn2−Se3	2.6452(7)	2.6288(10)	2.615(2)	2.617(3)	2.6520(11)	2.6410(5)	2.6470(8)	2.5310(5)
Sn2−Se4	2.5503(8)	2.5403(12)	2.546(2)	2.535(3)	2.5144(11)	2.5515(5)	2.5526(7)	
Sn2−C1	2.193(7)	2.164(10)	2.180(16)	2.18(2)	2.200(8)	2.184(4)	2.178(6)	
Sn2-C7								2.194(4)
Sn2−N1	2.384(5)	2.397(7)	2.396(13)	2.44(2)	2.397(7)	2.420(4)	2.376(5)	
Sn2-N3								2.55(3)
Sn3−Se2	2.5404(7)	2.5529(11)	2.552(2)	2.539(4)	2.5608(10)	2.5443(5)	2.5399(7)	
Sn3−Se3	2.6631(8)	2.6310(12)	2.602(2)	2.643(3)	2.5185(11)	2.6498(5)	2.6210(7)	
Sn3−Se4	2.5478(7)	2.5316(10)	2.529(2)	2.556(3)	2.6517(11)	2.5450(5)	2.5523(8)	
Sn3−C7	2.188(6)	2.170(8)	2.188(17)	2.16(2)	2.199(8)	2.184(4)	2.183(6)	
Sn3−N3	2.395(6)	2.422(8)	2.536(14)	2.367(18)	2.429(7)	2.407(4)	2.394(5)	
Sn4−Se5		2.5320(12)	2.524(2)	2.598(4)				
Sn4−Se6		2.6391(11)	2.640(2)	2.598(4)				
Sn4−Se7		2.5443(11)	2.546(2)	2.550(3)				
Sn4−Se8		2.5509(10)	2.5325(19)	2.536(3)				
Sn4−Se9		2.9125(11)	2.934(2)	3.1177(33)				
Sn5−Se7		2.5339(11)	2.539(2)	2.538(4)				
Sn5−Se9		2.6551(12)	2.630(2)	2.637(3)				
Sn5−Se10		2.5295(11)	2.5565(19)	2.551(3)				
Sn5−C13		2.181(9)	2.198(16)	2.15(2)				
Sn5−N5		2.355(9)	2.398(14)	2.46(2)				
Sn6−Se8		2.5353(11)	2.6775(19)	2.551(4)				
Sn6−Se9		2.6757(10)	2.534(2)	2.630(3)				
Sn6−Se10		2.5450(12)	2.552(2)	2.547(3)				
Sn6−C19		2.165(10)	2.173(17)	2.14(3)				
Sn6−N7		2.365(8)	2.378(12)	2.37(2)				

i = 1−X, 1−Y, 1−Z, ii = 1−X, −Y, 1−Z; iii = 1-X, 1-Y, 2-Z; iv = 1-X, -Y, 2-Z

Table S3. Selected distances in **4** – **5**.

Distance	**4a**	**4b**	**5**·3CH_2Cl_2	**5**·6.75CH_2Cl_2
Sn1−Se1	2.523(2)	2.5166(9)	2.5339(8)	2.5423(8)
Sn1−Se3	2.530(2)	2.5374(9)	2.5375(8)	2.5341(8)
Sn1−Se4	2.692(2)	2.7318(9)	2.6999(8)	2.6994(7)
Sn1−N1	2.395(14)	2.324(6)	2.344(5)	2.335(5)
Sn1−C1	2.182(18)	2.175(7)	2.171(6)	2.177(6)
Sn2−Se1	2.544(2)	2.5391(9)	2.5433(9)	2.5478(8)
Sn2−Se2	2.532(2)	2.5300(8)	2.5486(8)	2.5449(8)
Sn2−Se4	2.705(2)	2.7225(9)	2.7020(7)	2.7021(8)
Sn2−N3	2.307(16)	2.295(6)	2.348(5)	2.328(6)
Sn2−C7	2.161(18)	2.178(7)	2.183(6)	2.167(6)
Sn3−Se2	2.544(2)	2.5197(9)	2.5543(7)	2.5470(8)
Sn3−Se3	2.540(2)	2.5223(9)	2.5422(8)	2.5281(7)
Sn3−Se4	2.698(2)	2.7206(8)	2.7093(8)	2.7374(8)
Sn3−N5	2.345(15)	2.362(5)	2.333(5)	2.343(6)
Sn3−C13	2.15(2)	2.174(8)	2.178(6)	2.169(7)
Sn4−Se5	2.531(2)	2.5434(8)	2.5450(8)	2.5360(7)
Sn4−Se7	2.541(2)	2.5438(9)	2.5515(9)	2.5367(9)
Sn4−Se8	2.685(2)	2.6983(9)	2.6736(8)	2.6961(8)
Sn4−N7	2.379(16)	2.386(6)	2.356(5)	2.374(6)
Sn4−C19	2.139(19)	2.184(8)	2.186(6)	2.166(6)
Sn5−Se5	2.542(2)	2.5337(9)	2.5309(9)	2.5364(8)
Sn5−Se6	2.544(3)	2.5388(9)	2.5498(9)	2.5504(9)
Sn5−Se8	2.710(2)	2.7016(8)	2.7281(8)	2.7411(7)
Sn5−N9	2.366(17)	2.382(8)	2.357(6)	2.344(5)
Sn5−C25	2.19(2)	2.183(7)	2.179(6)	2.177(6)
Sn6−Se6	2.541(2)	2.5582(8)	2.5413(8)	2.5523(7)
Sn6−Se7	2.553(2)	2.5380(9)	2.5484(8)	2.5484(8)
Sn6−Se8	2.700(2)	2.7088(9)	2.6990(8)	2.6898(8)
Sn6−N11	2.336(15)	2.354(6)	2.347(5)	2.364(6)
Sn6−C31	2.183(19)	2.195(7)	2.176(6)	2.168(7)
Se8···Se4	14.0032(35)	15.6548(12)	14.9139(15)	14.9176(15)

Table S4. Selected angles in **1** – **3**.

Angle	**1**·2CH_2Cl_2 (*P*1)	**1**·2CH_2Cl_2 ($P2_1/n$)	**1**·2CH_2Cl_2 ($P2_1$)	**1**·3CH_2Cl_2	**2**·1CH_2Cl_2	**2**·2CH_2Cl_2	**2**·4CH_2Cl_2	**3**
Se1-Sn1-Se2	116.58(3)	115.31(4)	114.36(7)	115.22(11)	114.83(4)	116.295(17)	93.09(2)	115.309(16)
Se1-Sn1-Se2^{iv}								104.691(15)
Se1-Sn1-Se3	86.22(2)	85.91(3)	81.74(6)	84.85(9)	79.42(3)	86.328(14)	86.96(2)	
Se1-Sn1-Se3^{iv}								93.968(15)
Se1-Sn2-Se3^{iv}								92.607(15)
Se1-Sn1-Se5	120.96(3)	100.02(4)	99.96(7)	96.72(11)	116.39(4)	123.460(17)	120.22(3)	
Se1-Sn1-Se5$^{i/ii/iii}$	92.17(2)				109.29(4)	94.480(15)	97.86(2)	
Se1-Sn1-Se6		117.74(4)	119.13(7)	123.57(11)				
Se1-Sn2-Se3	93.77(2)	92.09(4)	99.17(7)	94.22(11)	100.23(3)	94.218(15)	95.33(2)	
Se1-Sn2-Se4	111.08(3)	110.38(4)	114.18(7)	113.70(12)	112.74(4)	114.067(16)	117.16(3)	
Se2-Sn1-Se3	84.83(2)	81.45(3)	80.63(6)	87.44(10)	81.27(3)	85.563(15)	85.11(2)	127.918(16)
Se2-Sn1-Se3^{iv}								107.749(15)
Se2-Sn1-Se5	121.54(3)	97.23(4)	100.39(7)	96.72(11)	113.49(4)	118.800(18)	127.51(3)	
Se2-Sn1-Se5$^{i/ii/iii}$	94.47(3)				104.64(4)	94.480(15)	95.25(2)	
Se2-Sn1-Se6		122.56(4)	120.03(7)	118.59(11)				
Se2-Sn2-Se3								127.918(16)
Se2-Sn3-Se3	91.80(2)	94.53(4)	98.13(7)	96.92(11)	107.24(3)	92.594(15)	94.11(2)	
Se2-Sn3-Se4	113.62(2)	119.80(4)	93.13(6)	109.99(11)	93.42(3)	117.376(18)	115.03(3)	
Se3-Sn2-Se4	94.12(2)	92.09(4)	92.46(6)	93.79(10)	93.51(3)	92.620(16)	91.73(2)	
Se3-Sn3-Se4	93.75(2)	92.23(4)	93.13(6)	92.67(10)	93.42(3)	92.558(15)	92.35(2)	
Se3-Sn1-Se5	89.32(2)	173.87(3)	177.37(7)	174.92(11)	69.73(3)	86.101(14)	83.41(2)	
Se5-Sn1-Se5$^{i/i/ii/}$	92.90(2)				95.56(4)	92.941(15)	92.20(2)	
Se5-Sn1-Se6		93.94(4)	95.36(7)	93.29(12)				
Se5-Sn4-Se6		91.95(3)	93.09(7)	93.83(12)				
Se5-Sn4-Se7		117.44(4)	123.46(7)	118.10(11)				
Se5-Sn4-Se8		122.90(4)	117.93(7)	123.27(11)				
Se5-Sn4-Se9		88.42(3)	83.76(6)	78.99(4)				
Se5^{i}-Sn1-Se3	177.72(2)				165.25(3)	178.924(16)	174.69(3)	
Se6-Sn4-Se7		93.98(4)	94.09(7)	98.62(10)				
Se6-Sn4-Se8		91.95(3)	95.43(6)	98.08(11)				
Se6-Sn4-Se9		179.47(4)	175.24(7)	172.51(10)				
Se7-Sn4-Se9		86.15(3)	84.73(6)	86.77(9)				
Se7-Sn5-Se9		92.09(4)	91.56(6)	98.28(11)				
Se7-Sn5-Se10		114.35(4)	115.92(7)	109.18(10)				
Se8-Sn4-Se9		87.53(3)	89.21(6)	84.29(9)				
Se8-Sn6-Se9		93.23(3)	95.20(6)	94.91(11)				
Se8-Sn6-Se10		111.14(4)	107.85(7)	115.68(11)				
Se9-Sn5-Se10		92.86(4)	93.44(6)	92.45(10)				
Se9-Sn6-Se10		92.03(3)	92.40(6)	92.70(10)				
Sn1-Se1-Sn2	93.47(2)	94.21(3)	96.62(7)	93.45(10)	98.11(3)	93.260(16)	93.09(2)	
Sn1-Se2-Sn2								106.705(16)
Sn1-Se1-Sn2^{iv}								86.670(14)
Sn1-Se2^{iv}-Sn3^{iv}								86.733(14)
Sn1-Se2-Sn3	94.25(3)	95.74(4)	98.58(7)	92.60(11)	96.33(3)	93.440(15)	94.57(2)	
Sn1-Se5-Sn1$^{i/ii/iii}$	87.10(2)				84.44(4)	87.057(15)	87.80(2)	
Sn1-Se5-Sn4		87.30(4)	86.15(6)	86.67(10)				
Sn1-Se6-Sn4		86.78(4)	85.39(6)	86.20(10)				
Sn1-Se3-Sn2	81.95(2)	77.50(3)	76.71(5)	81.03(9)	73.52(2)	81.967(14)	81.07(2)	
Sn1-Se3-Sn3	82.51(2)	78.96(3)	78.36(6)	79.71(8)	73.49(3)	82.011(13)	82.78(2)	
Sn2-Se3-Sn3	82.50(2)	82.19(3)	82.63(6)	82.92(9)	83.39(4)	82.911(14)	82.62(2)	
Sn2-Se4-Sn3	86.72(2)	85.95(3)	85.46(6)	86.33(10)	83.48(3)	86.829(15)	85.88(2)	
Sn4-Se7-Sn5		92.42(4)	92.52(6)	93.03(10)				
Sn4-Se8-Sn6		92.41(3)	92.10(6)	93.80(10)				
Sn4-Se9-Sn5		82.22(3)	82.45(6)	79.32(9)				
Sn4-Se9-Sn6		82.02(3)	80.94(5)	80.03(9)				
Sn5-Se9-Sn6		83.48(3)	83.46(6)	83.07(9)				
Sn5-Se10-Sn6		88.76(4)	87.50(6)	86.48(10)				

i = 1−X, 1−Y, 1−Z, ii = 1−X, −Y, 1−Z; iii = 1-X, 1-Y, 2-Z; iv = 1-X, -Y, 2-Z

Table S5. Selected angles in **4** – **5**.

Angle	**4a**·3CH_2Cl_2	**4b**·3H_2O·4CH_2Cl_2	**5**·3CH_2Cl_2	**5**·6.75CH_2Cl_2
Se1-Sn1-Se3	114.12(8)	119.37(3)	113.86(3)	112.32(3)
Se1-Sn1-Se4	93.86(7)	90.64(3)	91.52(2)	91.20(2)
Se3-Sn1-Se4	92.50(7)	92.10(3)	93.67(3)	94.46(2)
Se1-Sn2-Se4	93.07(7)	90.38(3)	91.27(2)	91.02(2)
Se2-Sn2-Se1	113.28(8)	120.39(3)	116.77(3)	118.05(3)
Se2-Sn2-Se4	92.47(7)	92.11(3)	91.90(2)	92.45(3)
Se2-Sn3-Se4	92.40(7)	92.38(3)	91.60(2)	91.59(2)
Se3-Sn3-Se2	114.13(7)	114.49(3)	113.22(3)	114.18(3)
Se3-Sn3-Se4	92.14(7)	92.70(3)	93.34(3)	93.68(2)
Se5-Sn4-Se7	116.47(8)	116.42(3)	116.22(3)	113.62(3)
Se5-Sn4-Se8	93.59(7)	91.87(3)	92.02(3)	94.31(2)
Se7-Sn4-Se8	92.56(8)	92.35(3)	92.30(3)	91.26(3)
Se5-Sn5-Se6	113.43(8)	113.73(3)	113.46(3)	112.18(3)
Se5-Sn5-Se8	92.75(7)	92.01(3)	91.07(3)	93.23(2)
Se6-Sn5-Se8	92.08(8)	92.88(3)	92.11(3)	91.61(2)
Se6-Sn6-Se7	111.85(8)	113.84(3)	115.77(3)	118.11(3)
Se6-Sn6-Se8	92.40(7)	92.28(3)	92.98(2)	92.76(3)
Se7-Sn6-Se8	91.96(7)	92.23(3)	91.78(3)	91.15(3)
Sn1-Se1-Sn2	87.79(7)	89.11(3)	89.04(3)	89.02(3)
Sn2-Se2-Sn3	88.55(7)	89.08(3)	88.69(2)	88.28(2)
Sn1-Se3-Sn3	88.37(7)	89.24(3)	88.21(2)	88.29(2)
Sn1-Se4-Sn2	81.22(6)	81.13(3)	82.45(2)	82.69(2)
Sn1-Se4-Sn3	81.95(6)	81.35(2)	81.62(2)	80.85(2)
Sn3-Se4-Sn2	81.98(6)	81.19(2)	82.48(2)	81.37(2)
Sn4-Se5-Sn5	87.49(8)	88.72(3)	89.46(3)	88.57(2)
Sn6-Se6-Sn5	89.30(7)	88.68(3)	88.88(3)	88.40(2)
Sn4-Se7-Sn6	88.20(7)	88.41(3)	87.81(3)	88.45(3)
Sn4-Se8-Sn5	81.08(6)	82.20(2)	82.79(2)	81.28(2)
Sn4-Se8-Sn6	82.33(6)	81.89(3)	82.34(2)	82.37(2)
Sn6-Se8-Sn5	82.70(7)	82.36(2)	82.11(2)	81.84(2)

2. NMR Spectroscopy

^{119}Sn NMR spectra of the reaction solution of the synthesis of **5** were recorded on a Bruker AV 500 spectrometer after stirring for 16 h, 2 days, and 7 days. The recorded spectra are shown in Figure S16.

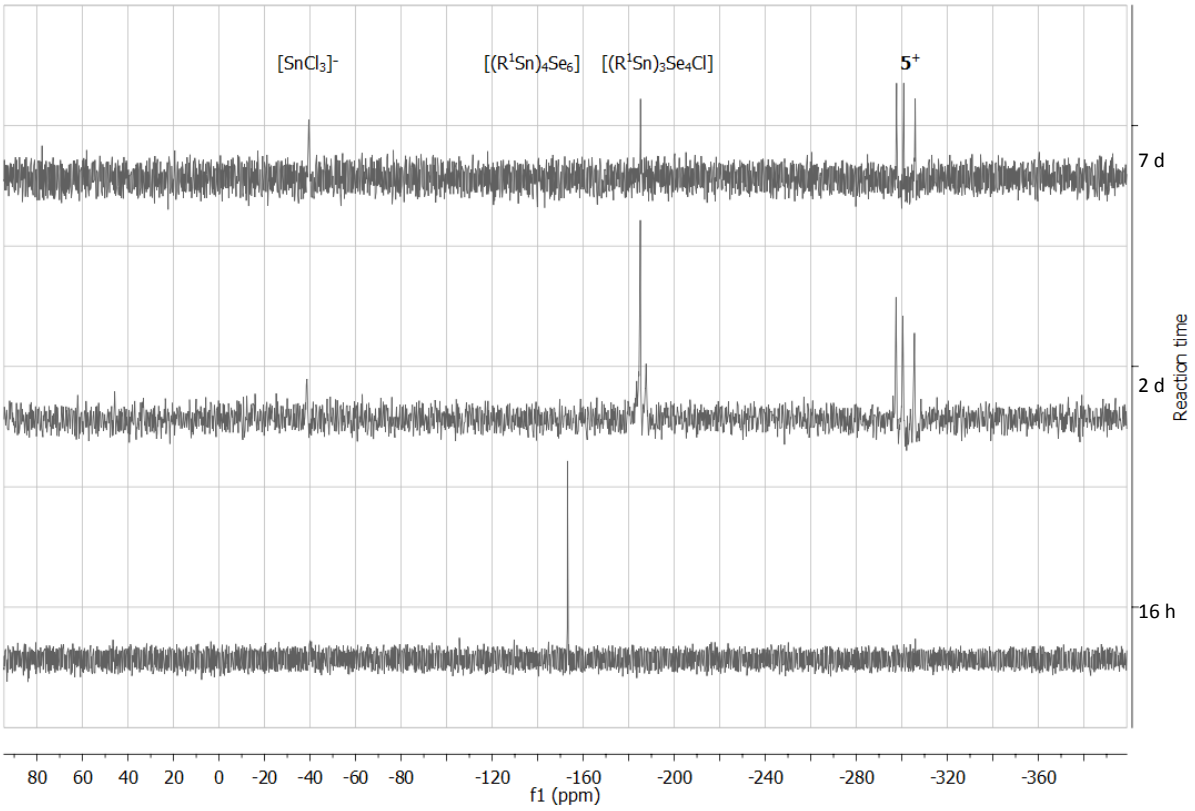

Figure S16: ^{119}Sn NMR spectra of the reaction solution of the synthesis of **5** after 16 h, 2d, and 7 d.

The ^{1}H NMR spectrum of **5** in Figure S17 was recorded on a Bruker AV 500 spectrometer after dissolution of the crystals.

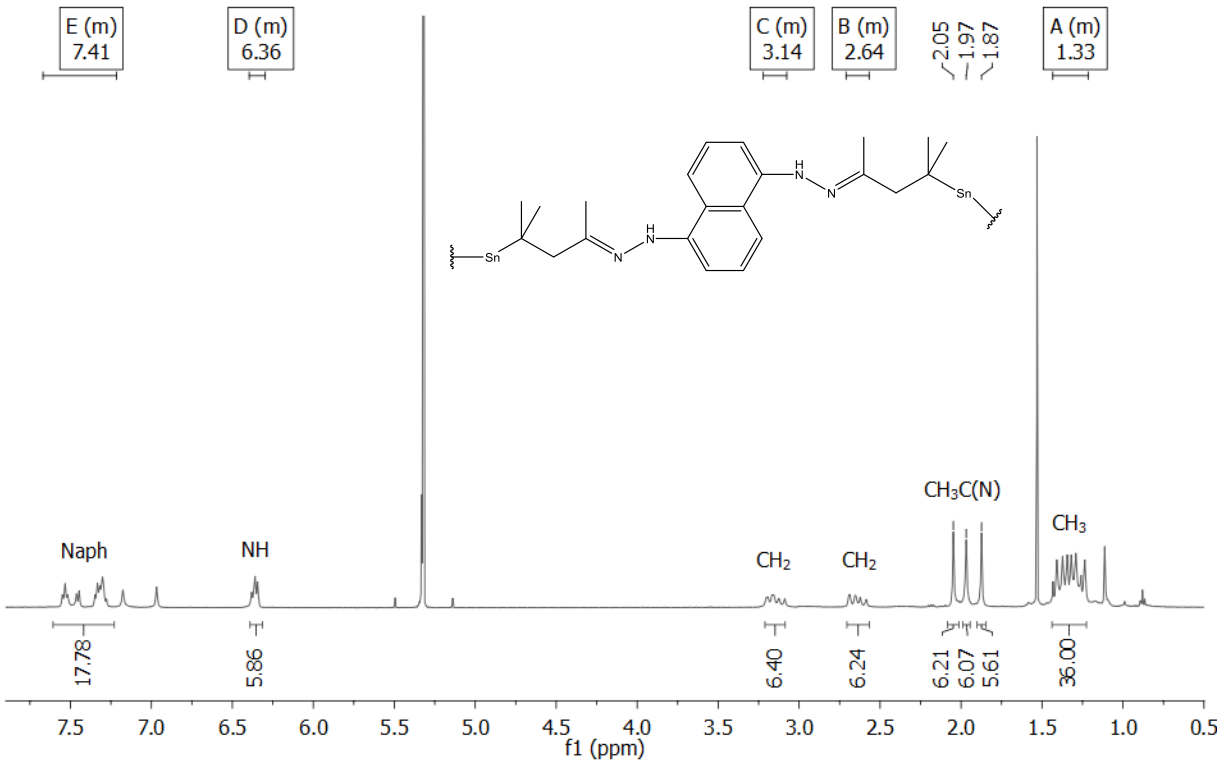

Figure S17: ^{1}H NMR spectrum of the re-dissolved crystals of **5**.

3. Electrospray-Ionization (ESI) Mass Spectrometry

HR-ESI mass spectra were acquired with a LTQ-FT Ultra mass spectrometer (Thermo Fischer Scientific). The resolution was set to 100.000.

The ESI$^+$ mass spectrum of crystals of **5** is shown in Figure S17. Figures S18 – S23 show the measured and calculated isotope patterns of certain peaks and their assigned molecules.

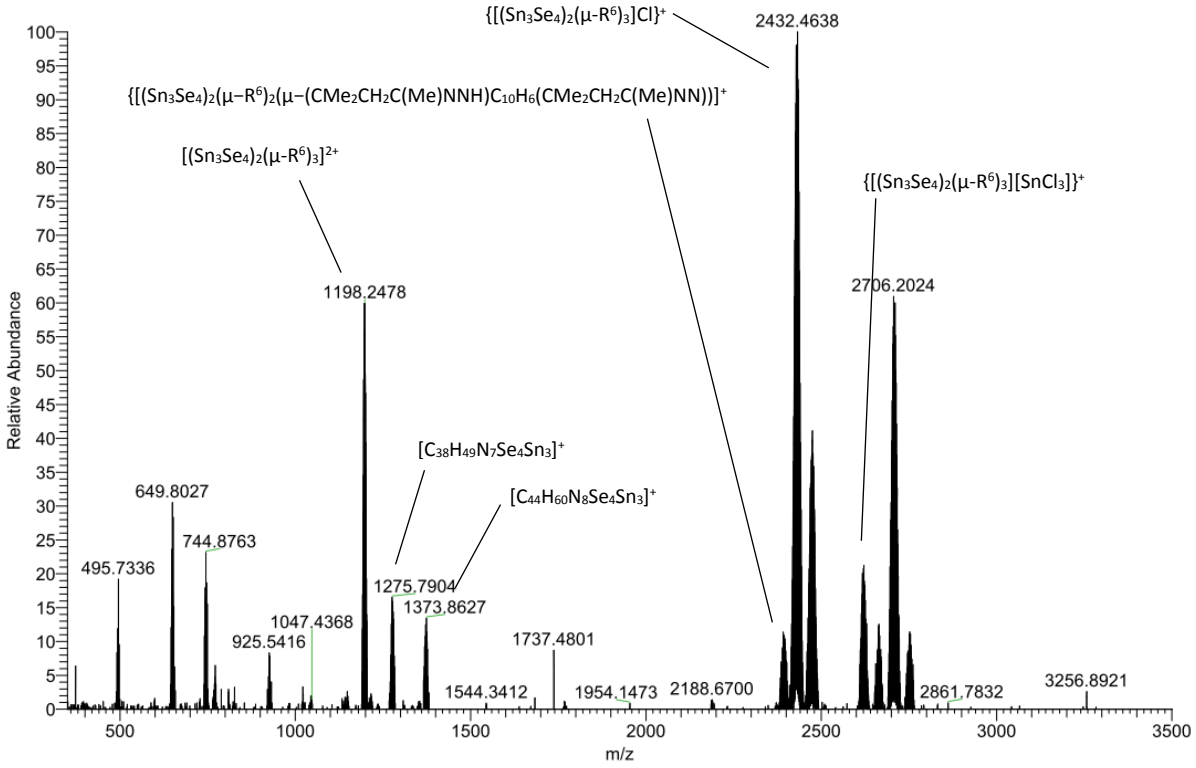

Figure S18: Overview of the ESI$^+$ mass spectrum of **5**.

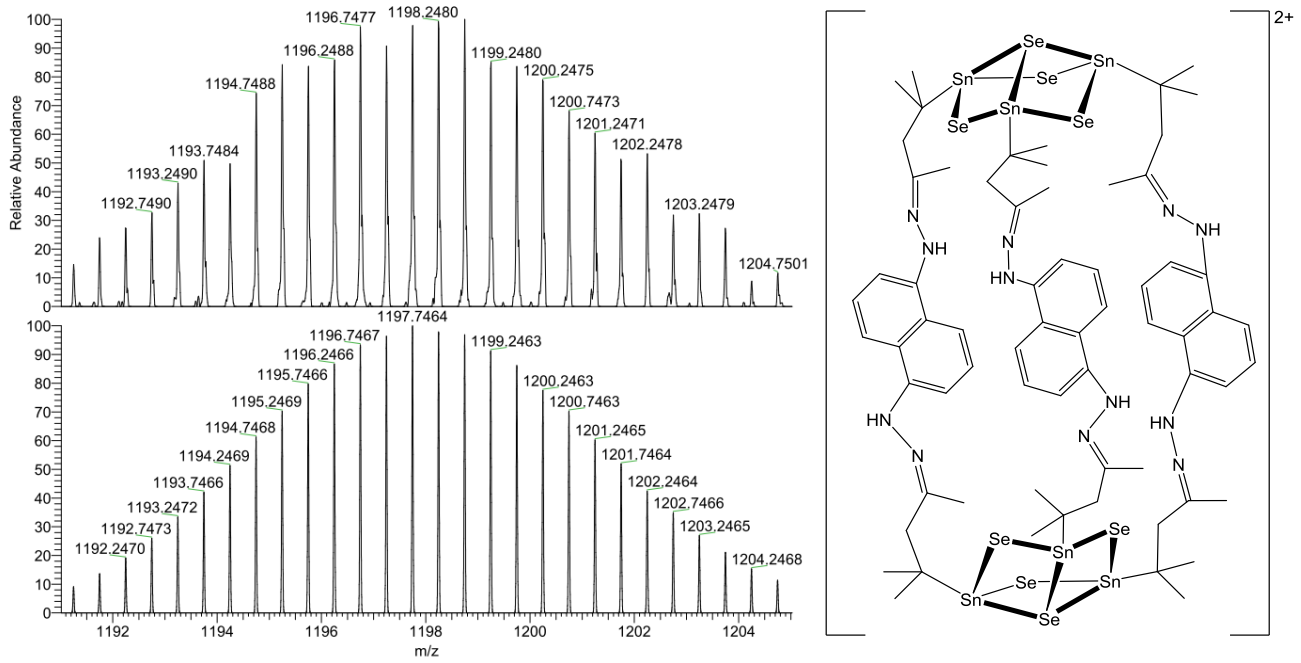

Figure S19: Measured (top) and calculated (bottom) ESI$^+$ mass spectrum of $[(Sn_3Se_4)_2(\mu\text{-}R^6)_3]^{2+}$.

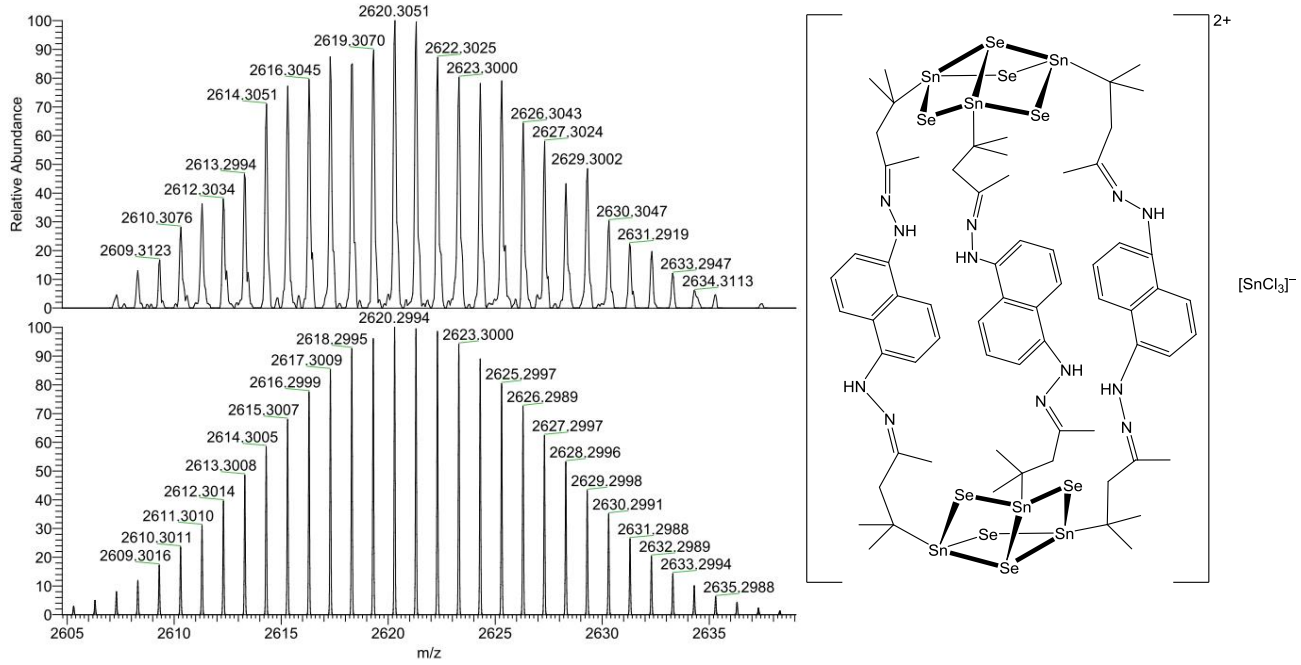

Figure S20: Measured (top) and calculated (bottom) spectrum of $\{[(Sn_3Se_4)_2(\mu\text{-}R^6)_3][SnCl_3]\}^+$.

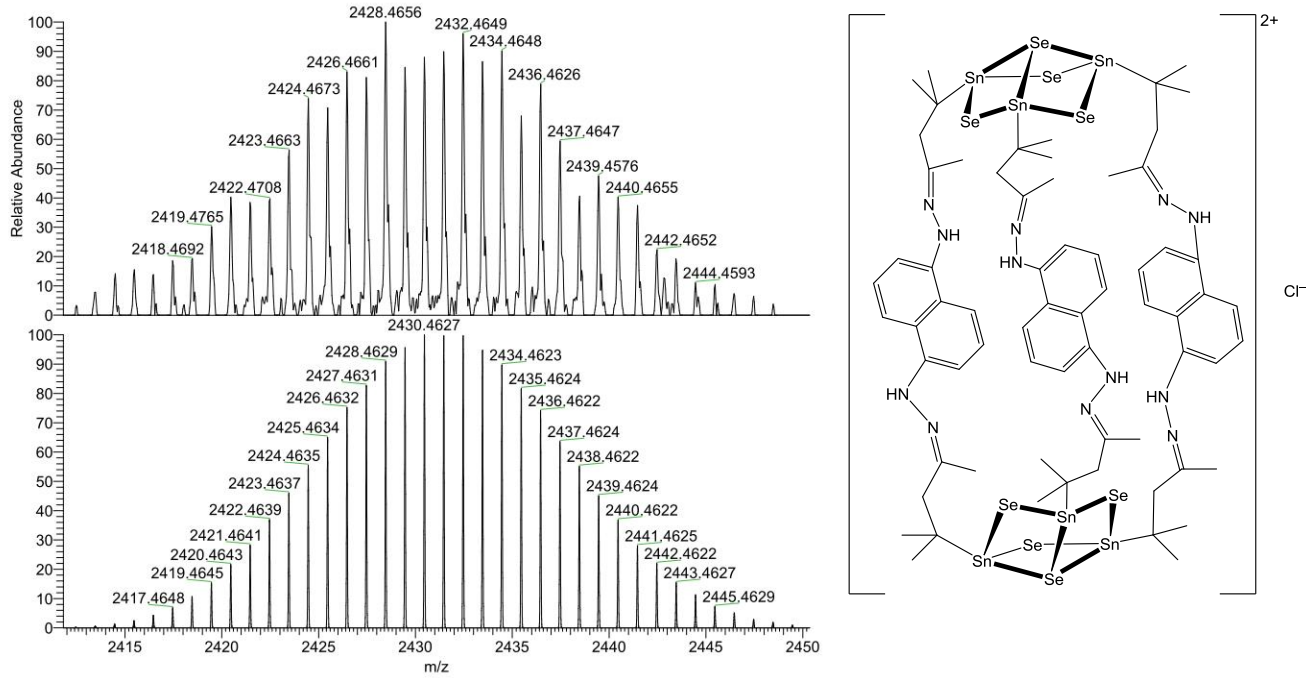

Figure S21: Measured (top) and calculated (bottom) ESI$^+$ mass spectrum of {[$(Sn_3Se_4)_2(\mu\text{-}R^6)_3$]Cl}$^+$.

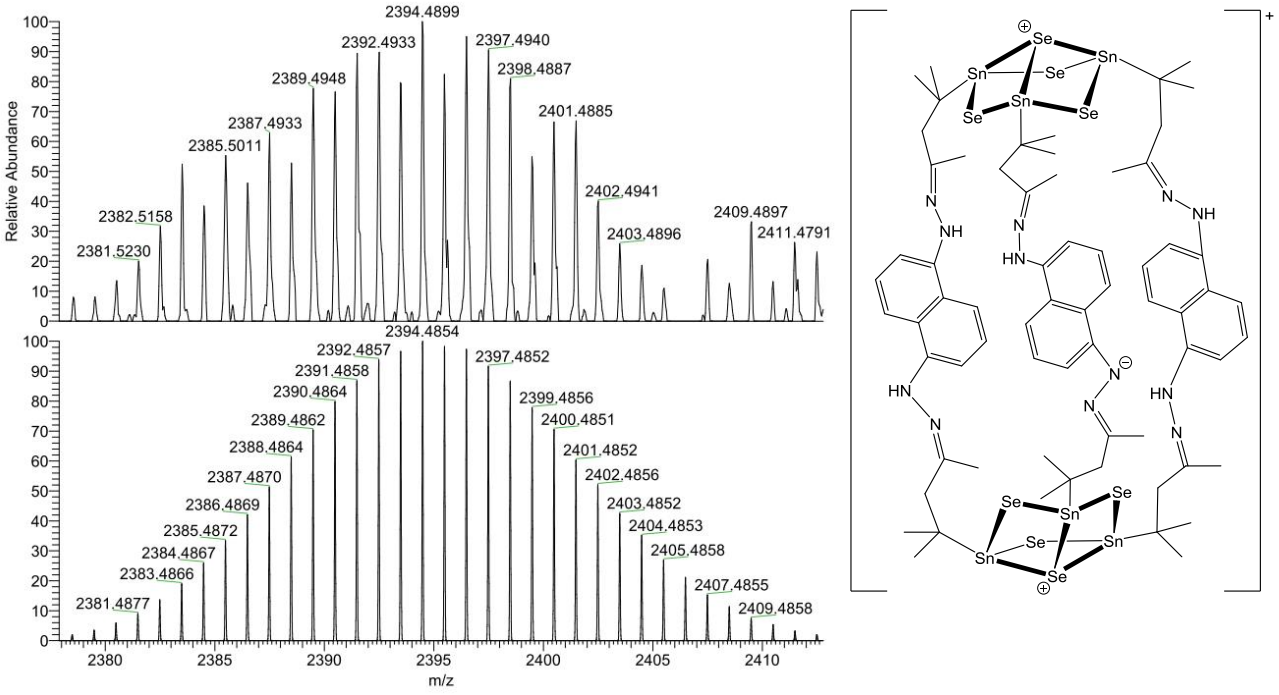

Figure S22: Measured (top) and calculated (bottom) ESI$^+$ mass spectrum of {[$(Sn_3Se_4)_2(\mu\text{-}R^6)_2(\mu\text{-}(CMe_2CH_2C(Me)NNH)C_{10}H_6(CMe_2CH_2C(Me)NN))$]}$^+$.

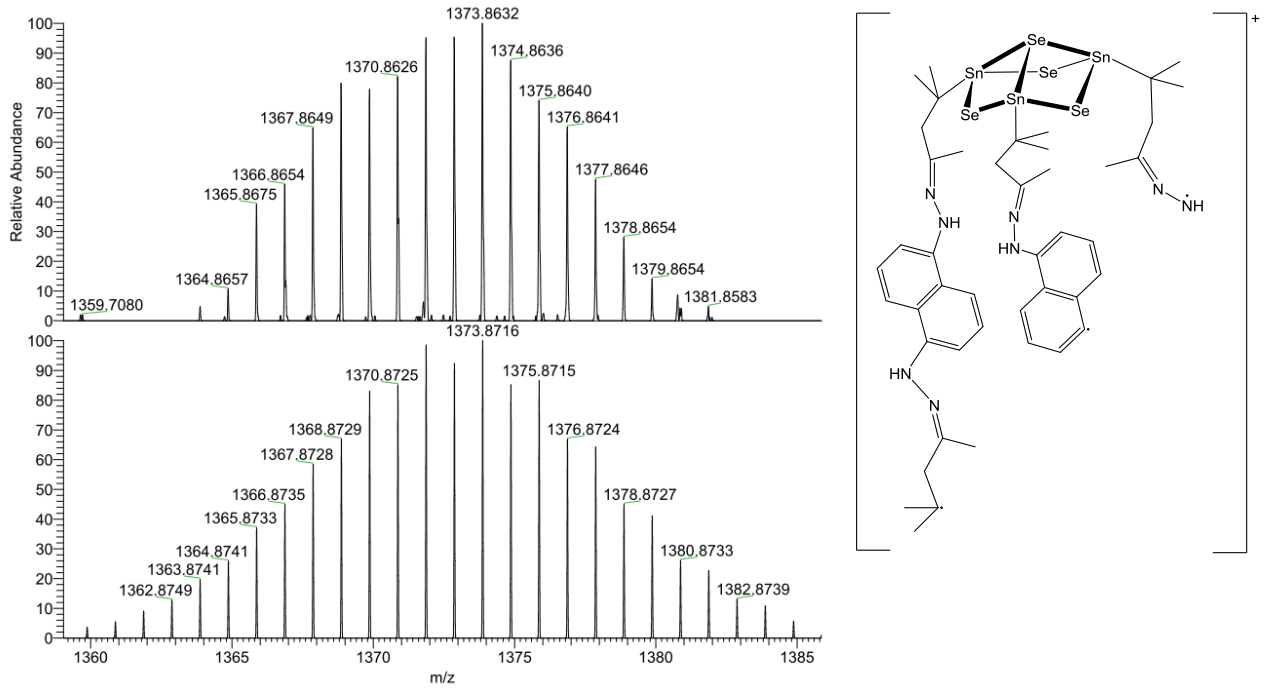

Figure S23: Measured (top) and calculated (bottom) ESI$^+$ mass spectrum of $[C_{44}H_{60}N_8Se_4Sn_3]^+$.

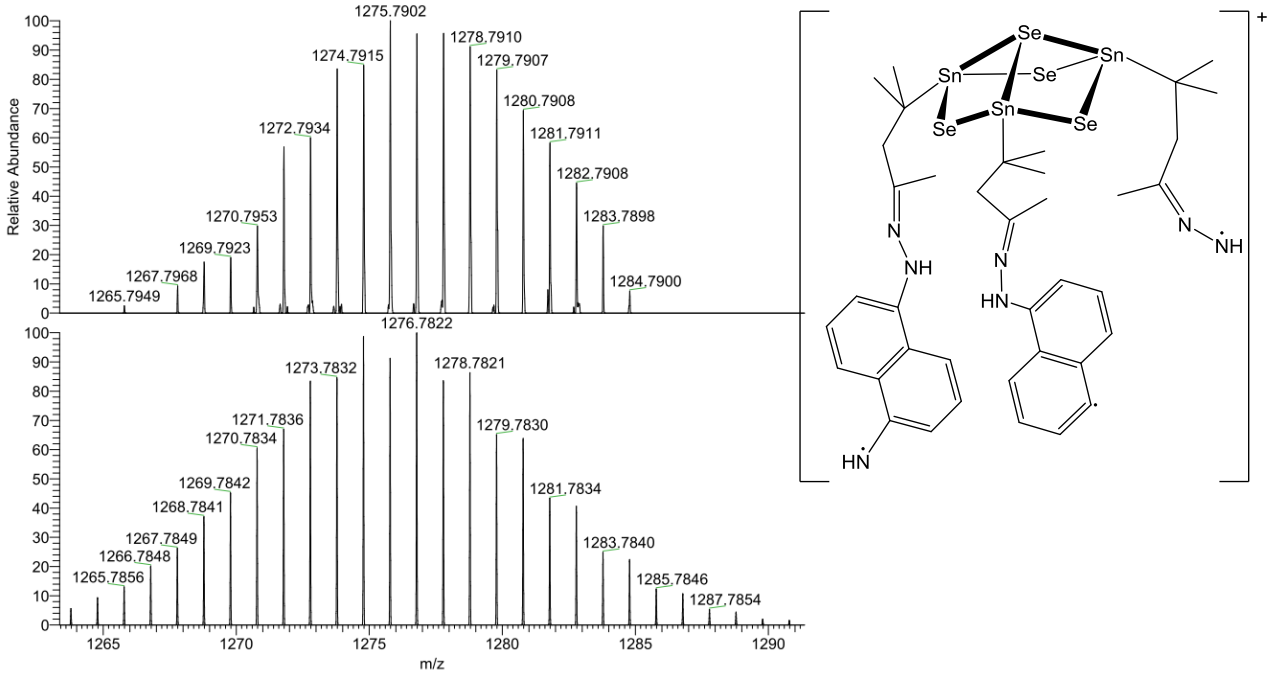

Figure S24: Measured (top) and calculated (bottom) ESI$^+$ mass spectrum of $[C_{38}H_{49}N_7Se_4Sn_3]^+$.

4.2 Variations in the Interplay of Intermetallic and Metal Chalcogenide Units in Organotin-Copper Selenide Clusters

Katharina Hanau, Niklas Rinn, Stefanie Dehnen, *Inorg. Chem.* **2020**, *59*, 198–202.

Abstract

We report the formation and structures of two new organotin-copper selenide clusters that were obtained in a two-step procedure. First, $[(R^1Sn)_4S_6]$ [$R^1 = CMe_2CH_2C(O)Me$] is reacted with $[Cu(PPh_3)_3Cl]$ and $(SiMe_3)_2Se$ to form a bright-orange powder, the nature of which could not be identified in detail, yet a suspension of it in CH_2Cl_2 reacts with $N_2H_4{\cdot}H_2O$ to afford single crystals of two cluster compounds, either $[(Cu_3Sn)\{(R^2Sn)_2Se_4\}_2\{(R^2Sn_2)Se_3\}]$ (**1**) or $[(N_2H_4)(Cu_4Sn)\{(R^2Sn)_2Se_4\}_3]$ [**2**; $R^2 = CMe_2CH_2C(NNH_2)Me$]. Both are based on an intermetallic Cu_xSn cluster core (x = 3, 4), which is surrounded by organotin selenide units in different fashions. The results foster the assumption of a complex equilibrium to be present in according reaction mixtures.

Eigener Anteil

Die Verbindungen wurden erstmals von Zhong Zheng im Rahmen ihres Vertiefungspraktikums unter der Anleitung von Dr. Niklas Rinn und mir synthetisiert. Die Reproduktion und Optimierung der Synthesen erfolgte durch mich, wobei Dr. Niklas Rinn eine verbesserte Reproduktion von Verbindung **2** erzielte. Die Einkristallsytrukturanalysen wurden von Eugenie Geringer (**1**) und mir (**2**) durchgeführt und von mir ausgewertet. ^{1}H- und ^{31}P-NMR-Experimente wurden von der zentralen NMR-Abteilung des Fachbereichs Chemie der Philipps-Universität Marburg unter der Leitung von Dr. Xiulan Xie durchgeführt und von mir ausgewertet. Das Röntgenpulverdiffraktogramm von **I** wurde von Bertram Peters aufgenommen und von mir ausgewertet. Die µ-RFA-Messung von **I** wurde von Bertram Peters durchgeführt und ausgewertet. Das Manuskript wurde von mir und Prof. Dr. Stefanie Dehnen verfasst, wobei Dr. Niklas Rinn an dessen Überarbeitung beteiligt war.

Inorganic Chemistry
Cite This: Inorg. Chem. 2020, 59, 198−202
Communication
pubs.acs.org/IC

Variations in the Interplay of Intermetallic and Metal Chalcogenide Units in Organotin−Copper Selenide Clusters

Katharina Hanau, Niklas Rinn, and Stefanie Dehnen*

Fachbereich Chemie and Wissenschaftliches Zentrum für Materialwissenschaften, Philipps-Universität Marburg, Hans-Meerwein-Strasse 4, 35039 Marburg, Germany

Supporting Information

ABSTRACT: We report the formation and structures of two new organotin−copper selenide clusters that were obtained in a two-step procedure. First, $[(R^1Sn)_4Se_6]$ [R^1 = $CMe_2CH_2C(O)Me$] is reacted with $[Cu(PPh_3)_3Cl]$ and $(SiMe_3)_2Se$ to form a bright-orange powder, the nature of which could not be identified in detail, yet a suspension of it in CH_2Cl_2 reacts with $N_2H_4{\cdot}H_2O$ to afford single crystals of two cluster compounds, either $[(Cu_3Sn)\{(R^2Sn)_2Se_4\}_2\{(R^2Sn_2)Se_3\}]$ (**1**) or $[(N_2H_4)(Cu_4Sn)\{(R^2Sn)_2Se_4\}_3]$ [**2**; R^2 = $CMe_2CH_2C(NNH_2)Me$]. Both are based on an intermetallic Cu_xSn cluster core (x = 3, 4), which is surrounded by organotin selenide units in different fashions. The results foster the assumption of a complex equilibrium to be present in according reaction mixtures.

In the last decades, a large variety of ternary metal chalcogenide clusters have been studied, ranging from small, ligand-stabilized heterocubanes to huge anionic supertetrahedra or spherical molecules, featuring different transition or main-group metals, respectively, or combining both.[1−5] Because of their (photo)conductive properties, the elemental combinations Cu/Sn/S and Cu/Sn/Se, in particular, have been of interest; hence, corresponding clusters were addressed as potential precursor materials for thin-film solar cells, based on $Cu_2ZnSnSe_4$ (CZTSe) or $Cu_2ZnSn(S_{1-x}Se_x)_4$, or as thermoelectric materials like Cu_2SnSe_3 or Cu_2SnSe_4.[6−10] Another reason for studying metal chalcogenide clusters, especially with electron-rich organic ligands, is the recent finding of an extreme nonlinear optical behavior of this class of compounds[11−14] or their use as molecular models of the attachment of clusters to transition-metal dichalcogenide surfaces.[15]

Different synthetic approaches have been followed in order to gain access to new compositions and structures. We showed, in the past years, that an efficient strategy toward such clusters is the reaction of organo-functionalized binary precursors of the type $[(RSn)_4E_6]$ or $[(RSn)_3E_4Cl]$ (R = organic ligand with a keto or a hydrazine group; E = S, Se) with transition-metal complexes, which yield organo-functionalized metal chalcogenide clusters with ternary inorganic cores.[5,16−26]

In this context, we have recently reported a series of first examples of organo-functionalized copper−tin selenide clusters, such as $[(CuPPh_3)_2(Sn^{II}Cl)_2\{(RSn)_2Se_4\}_2]$ [**A1** with R = R^1 = $CMe_2CH_2C(O)Me$ and **A2** with R = R^2 = $CMe_2CH_2(NNH_2)Me$] or $[(CuPPh_3)_2(SnCu_2)\{(R^1Sn)_2Se_4\}_3]$ (**B**).[27,28] We could show that these species are involved in complex equilibria in solution, from which they eventually crystallize. Thus, we observed close structural relationships and recognized that many of the clusters may be viewed as snapshots during the formation of larger units. As a common feature in most of these clusters, $\{(RSn)_2Se_4\}$ units coordinate to copper complex fragments and heteroatomic Cu_xSn units within the cluster.

In order to gain more insight into the formation and nature of these compounds and to explore whether further examples of these structurally related compounds exist and can be isolated, we studied the reaction leading to **A** at various reaction times and concentrations. The results of these experiments are presented and discussed herein (Scheme 1). If the reaction mixture of $[(R^1Sn)_4Se_6]$ with 2 equiv of $[Cu(PPh_3)_3Cl]$ and 4 equiv of $(SiMe_3)_2Se$ is left to stir for 24 h instead of 18 h, as reported previously, a bright-orange powder (**I**) precipitates. Alternatively, this process can be sped up by doubling the concentration of the reaction mixture, resulting in precipitation of this powder after 5 h. Micro X-ray fluorescence (μ-XRF) spectroscopy shows the powder to contain the four elements P, Cu, Sn, and Se in a ratio of 1:3:4.8:9.2 (see the Supporting Information). The ^{1}H NMR spectrum exhibits signals that can be assigned to the starting material, $Ph_3P{=}Se$, and free PPh_3, alongside a variety of minor signals that could not be assigned to specific compounds. ^{31}P NMR spectroscopy confirms the formation of $Ph_3P{=}Se$ during the reaction. Powder X-ray diffraction suggests the presence of **B**, while other compounds cannot be identified. The P:Cu:Sn:Se composition of **I** observed by means of μ-RFA (1:3:4.8:9.2) is relatively close to that of compound **B** (1.5:3:5.25:9); hence, **I** might comprise **B** besides further unknown minor components. However, because no further analytical data could be obtained as a result of the powder's very poor solubility, we refrain from further speculating on its identity. Suspending **I** in dichloromethane, adding 1.8 equiv of $N_2H_4{\cdot}H_2O$, stirring for 16 h, and layering with n-hexane affords $[(Cu_3Sn)\{(R^2Sn)_2Se_4\}_2\{(R^2Sn_2)Se_3\}]{\cdot}1.87CH_2Cl_2{\cdot}2solv$ (**1**·$1.87CH_2Cl_2{\cdot}2solv$; solv = CH_2Cl_2 and/or C_6H_{14}) as single crystals. On the basis of the atomic ratio of **1** (P:Cu:Sn:Se = 0:3:7:11), the formation of a hydrazine derivative might be viewed as a "reactive recrystallization" from the related keto-

Received: October 29, 2019
Published: December 26, 2019

DOI: 10.1021/acs.inorgchem.9b03173
Inorg. Chem. 2020, 59, 198−202

Scheme 1. Overview of the Reactions Starting from $[(R^1Sn)_4Se_6]$ and Yielding the New Ternary (RSn)/Cu/Se Clusters 1 and 2, as Well as the Previously Reported Clusters A1, A2, and B under Slightly Different Reaction Conditions (Two of the Three $\{(R^1Sn)_2Se_4\}$ Units Are Given in a Simplified Manner in the Structural Diagram of B for the Sake of Clarity)[a]

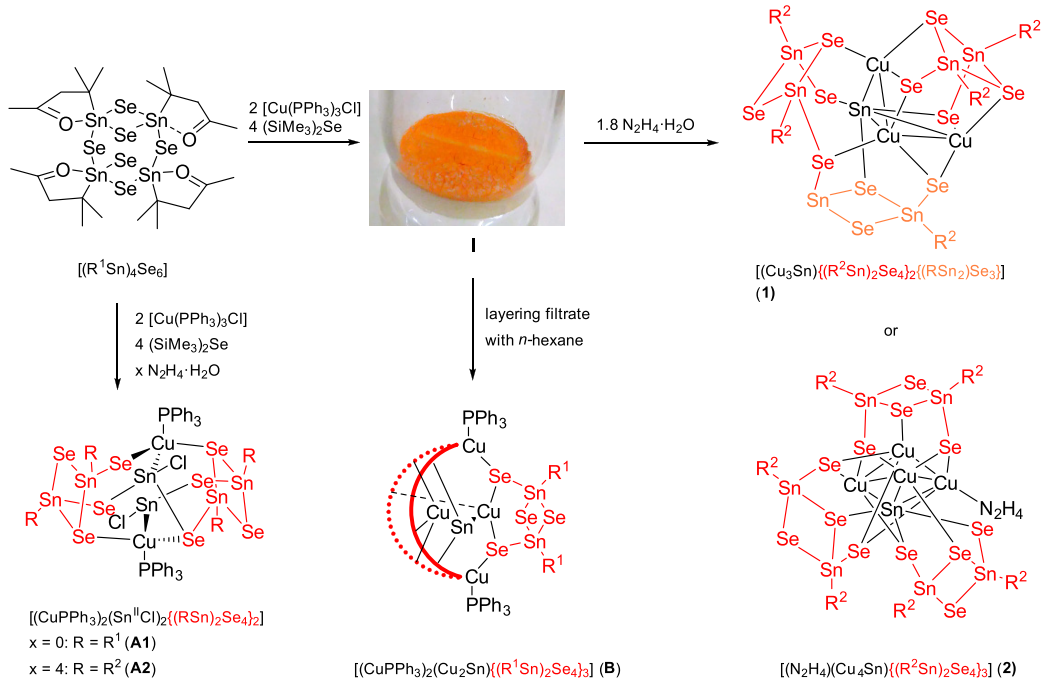

[a]For details of the synthesis of **A1**, **A2**, and **B**, see refs 27 and 28. $R^1 = CMe_2CH_2C(O)Me$; $R^2 = CMe_2CH_2(Me)NNH_2$. The $\{(RSn)_2Se_4\}$ building units are highlighted in red; the related $\{(RSn)_2Se_3\}$ unit, which is one Se atom and one organic group short, is drawn in orange.

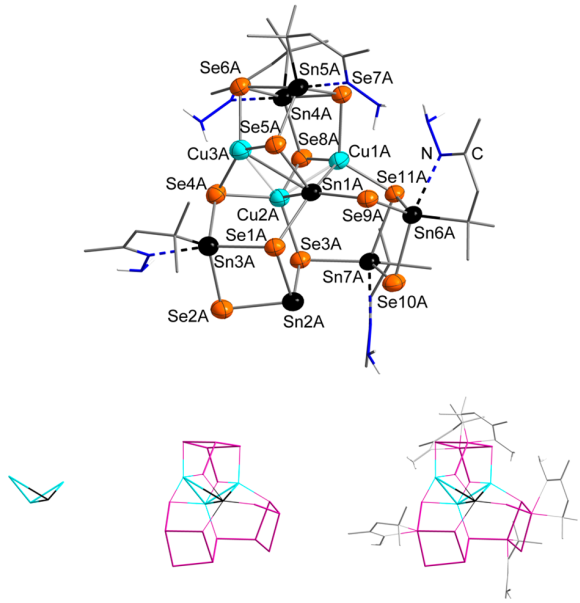

Figure 1. Molecular structure of one of the two individual molecules in **1** (top) and illustration of its architecture (bottom, from left to right). A Cu_3Sn butterfly-shaped ring (turquoise/black) is connected to three $\{Sn_2Se_4\}$ moieties (pink), two of which share a Se atom to form an $\{Sn_4Se_7\}$ unit. All Sn atoms, except one of those in the $\{Sn_4Se_7\}$ unit, carry one $CMe_2CH_2C(Me)NNH_2$ substituent each (gray). Displacement ellipsoids are drawn at 50% probability. C-bound H atoms are omitted for clarity.

functionalized compound, but we cannot exclude that other processes have taken place.

1 crystallizes in the monoclinic space group $P2_1/n$, with two molecules per asymmetric unit, one of which is shown in Figure 1 (for the other one, see the Supporting Information). The two crystallographically independent clusters differ only slightly in their geometric arrangement (e.g., $\{Cu_3Sn\}$ folding angle: 106.5° vs 107.1°). Each of the cluster molecules consists of a $\{Cu_3Sn\}$ butterfly-shaped moiety, which is surrounded by different (R)Sn/Se moieties: one $\{(R^2Sn)_2Se_4\}$ unit bridges rather symmetrically above the atoms Cu1A and Cu3A, which form the tips of the butterfly. In this way, a distorted heterocubane-like unit $[Cu_2\{(R^2Sn)_2Se_4\}]$ is formed, which was also found in other clusters, e.g., $[(CuPPh_3)_2\{(R^1Sn)_2Se_4\}]$.[28] However, two of the Se atoms additionally bind to the other two atoms of the butterfly (Cu2A and Sn1A); hence, the overall topology of this part of the cluster is better described as a pentagonal prism slightly distorted toward an antiprism. Another $\{(R^2Sn)_2Se_4\}$ unit and one $\{(R^2Sn)SnSe_4\}$ moiety are linked by sharing Se3A to form an $\{(R^2Sn)_3SnSe_7\}$ unit altogether. Five of the selenide ligands coordinate to the $\{Cu_3Sn\}$ butterfly from beneath, such that four of them possess μ^3-bridging character, while one is a μ-selenide ligand. In this way, all Sn−Cu bonds and one of the two Cu−Cu contacts are part of five-membered rings, together with two more Se atoms and one Sn atom. The Cu1A−Cu2A contact is only bridged by one μ-selenide ligand (Se8A). As mentioned above, the previously reported organotin−copper selenide clusters also comprised $\{(RSn)_2Se_4\}$ moieties, which thus seem to play an important role in the formation of these clusters and their resulting architectures.

DOI: 10.1021/acs.inorgchem.9b03173
Inorg. Chem. 2020, 59, 198−202

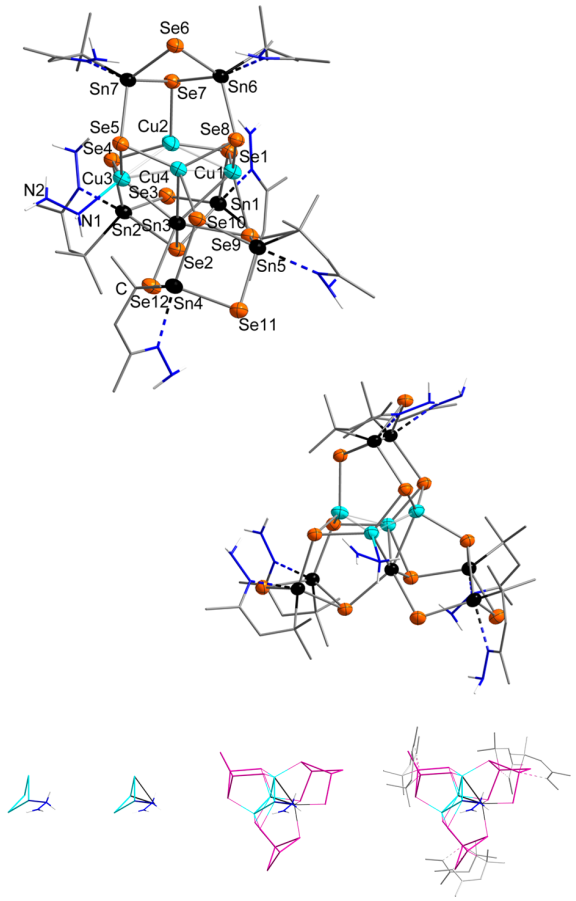

Figure 2. Molecular structure of **2** (top and center) and illustration of its architecture (bottom, from left to right). A slightly inclined Cu_4 diamond (turquoise) with an N_2H_4 moiety (blue) connects to a Sn atom to form a Cu_3Sn ring (Sn = black). This cluster core is connected to three Sn_2Se_4 moieties (pink) carrying organic ligands (gray). Displacement ellipsoids are drawn at 50% probability. C-bound H atoms are omitted for clarity.

Scheme 2. Three-Component Diagram of Known Organo-Functionalized Clusters Comprising Cu, Sn, and Se Atoms[a]

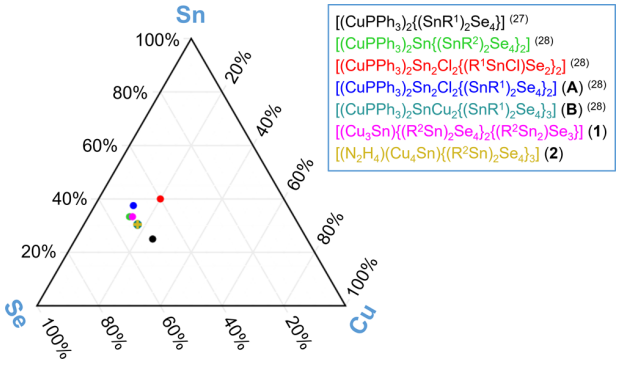

[a]Note that terminal ligands Cl and PPh_3 are not taken into consideration because these mainly serve to compensate for charges and provide kinetic stabilization of the molecules.

Upon a slight change in the reaction procedure, namely, by immediate layering of the reaction solution with *n*-hexane upon the addition of $N_2H_4{\cdot}H_2O$, and filtration, yet another organotin–copper selenide cluster could be isolated, although the physical reaction conditions were not altered otherwise. Compound $[(N_2H_4)(Cu_4Sn)\{(R^2Sn)_2Se_4\}_3]$ (**2**) crystallizes in the triclinic space group $P\bar{1}$ with one molecule per asymmetric unit. Similar to **1**, the structure of **2** (Figure 2) is based on a butterfly-shaped central unit comprising three of the Cu atoms and one Sn atom. However, this unit is extended by another Cu atom, which together with the other three Cu atoms also forms a butterfly-type structure [folding angles: 128.4(1)° for $\{Cu_3Sn\}$ and 132.5(2)° for Cu_4].

The surrounding units are both different and differently arranged with respect to the structure of **1**. The Cu_4 substructure is capped by an $\{(R^2Sn)_2Se_4\}$ moiety, but different from the coordination of the $\{Cu_3Sn\}$ unit in **1**, only one of the two "in-ring" Se atoms coordinates additionally to one of the Cu atoms at the unit's "knee". As another slight difference from **1**, two complete $\{(R^2Sn)_2Se_4\}$ units coordinate to the inner Cu_4Sn core, but the Se atoms are again μ^3- or μ-bridging. The most striking deviation from the structure of **1**, however, is the presence of an N_2H_4 group that is bound to one of the Cu atoms. Only six Cu-bound hydrazine derivatives have been reported to date, two of which are inorganic polymers.[29−33] The Cu–N distance in **2** [2.126(19) Å] is within the range of those reported in the literature (ranging from 1.95(2) Å in $[\{Cu(CN)\}_2(\mu\text{-}N_2H_4)]_n$[31] to 2.2526(17) Å in $[N_2H_5Cu(HEDTA)]H_2O$[33]), and the N1–N2 distance of 1.42(3) Å is within the normal range for a N–N single bond. The Cu3 atom is surrounded by four atoms in a distorted tetrahedral manner (average bond angle: 108.85°). The Cu3–N1–N2 angle of 108.1(12)° is at the lower end for terminally coordinated hydrazine derivatives. In order to obtain an overall electronically neutral molecule, the ligand is assigned as N_2H_4, although the H atoms were not detected by means of X-ray diffraction. The results have shown that small alterations to the reaction conditions have a big influence on which compound is formed.[28]

When both **1** and **2** are compared with the previously reported Cu/Sn/Se clusters, the most obvious difference is the complete absence of any PPh_3 or Cl ligands. This might be due to the higher number of collisions of the reactants before the precursor solid **I** precipitated; although P atoms were still present in **I** according to microanalysis, the P:Cu ratio was considerably smaller than that in **A** and **B** (1:3 in **I** vs 1:1 in **A** and **B**), whereas Cl could not be detected at all. The absence of PPh_3 and Cl groups seems critical to the assembly of Cu–Cu and Cu–Sn units and the growth of larger inner moieties $\{Cu_3Sn\}$ and $\{Cu_4Sn\}$ in **1** and **2**, respectively, than those in the reported clusters.

In conclusion, we reported the formation of two new organotin–copper selenide clusters that exhibit new variations of core–shell clusters with an inner intermetallic $\{Cu_xSn\}$ unit (x = 3, 4), surrounded by organotin selenide units $\{(RSn)_2Se_4\}$, $\{(RSn)SnSe_3\}$, or the new $\{(RSn)SnSe_4\}$. The two clusters are structurally related to a series of known clusters that were obtained under similar reaction conditions yet from lower concentrations of reactants. Compositionwise, they are also related to two sulfides that comprise anionic networks $[CuSnS_3]^-$ and $[Cu_2SnS_4]^{2-}$.[34] The results demonstrate the subtle influence of all parameters in the reaction space of such cluster systems, which apparently features a very flat energy hypersurface. Remarkably, all organo-functionalized clusters that were obtained in this system to date possess relatively Sn-rich Cu:Sn:Se ratios of (approximately) 1:1:2,

DOI: 10.1021/acs.inorgchem.9b03173
Inorg. Chem. 2020, 59, 198−202

1:2:1, 1:2:2, 1:2:3, 1:2:4, or 1:3:4 compared with Cu_2SnSe_3 or Cu_2SnSe_4 (Scheme 2). However, works on complementary zinc−tin selenide clusters with compositions that also deviated from those in CZTSe have shown that the desired CZTSe phases are formed upon the addition of the missing fourth component.[35]

■ ASSOCIATED CONTENT

Supporting Information

The Supporting Information is available free of charge at https://pubs.acs.org/doi/10.1021/acs.inorgchem.9b03173.

Details on the synthesis, single-crystal and powder X-ray diffraction data, NMR spectroscopic data, X-ray fluorescence spectroscopy, and thermogravimetric analysis data (PDF)

Accession Codes

CCDC 1964152 and 1964153 contain the supplementary crystallographic data for this paper. These data can be obtained free of charge via www.ccdc.cam.ac.uk/data_request/cif, or by emailing data_request@ccdc.cam.ac.uk, or by contacting The Cambridge Crystallographic Data Centre, 12 Union Road, Cambridge CB2 1EZ, UK; fax: +44 1223 336033.

■ AUTHOR INFORMATION

Corresponding Author

*Email: dehnen@chemie.uni-marburg.de.

ORCID

Stefanie Dehnen: 0000-0002-1325-9228

Author Contributions

The manuscript was written through contributions of all authors. All authors have given approval to the final version of the manuscript.

Notes

The authors declare no competing financial interest.

■ ACKNOWLEDGMENTS

This work was supported by the Deutsche Forschungsgemeinschaft within the frameworks of SFB 1083 and GRK 1782. We thank Bertram Peters for powder X-ray diffraction and μ-XRF measurements.

■ REFERENCES

(1) Bechlars, B.; Issac, I.; Feuerhake, R.; Clérac, R.; Fuhr, O.; Fenske, D. Syntheses, Structures and Magnetic Properties of New Chalcogen-Bridged Heterodimetallic Cluster Compounds with Heterocubane Structure. *Eur. J. Inorg. Chem.* **2008**, *2008*, 1632−1644.

(2) Koutmos, M.; Georgakaki, I. P.; Tsiolis, P.; Coucouvanis, D. Synthesis and Characterization of $MoFe_3S_4$ and $Mo_2Fe_2S_4$ Single Cubanes. *Z. Anorg. Allg. Chem.* **2008**, *634*, 255−261.

(3) Zimmermann, C.; Melullis, M.; Dehnen, S. Reactivity of Chalcogenostannate Salts: Unusual Synthesis and Structure of a Compound Containing Ternary Cluster Anions $[Co_4(\mu_4\text{-Se})(SnSe_4)_4]^{10-}$. *Angew. Chem., Int. Ed.* **2002**, *41*, 4269−4272; *Angew. Chem.* **2002**, *114*, 4444−4447.

(4) Wu, T.; Wang, L.; Bu, X.; Chau, V.; Feng, P. Largest molecular clusters in the supertetrahedral T*n* series. *J. Am. Chem. Soc.* **2010**, *132*, 10823−10831.

(5) Lin, Y.; Massa, W.; Dehnen, S. "Zeoball" $[Sn_{36}Ge_{24}Se_{132}]^{24-}$: A molecular anion with zeolite-related composition and spherical shape. *J. Am. Chem. Soc.* **2012**, *134*, 4497−4500.

(6) Wang, W.; Winkler, M. T.; Gunawan, O.; Gokmen, T.; Todorov, T. K.; Zhu, Y.; Mitzi, D. B. Device Characteristics of CZTSSe Thin-Film Solar Cells with 12.6% Efficiency. *Adv. Energy Mater.* **2014**, *4*, 1301465.

(7) Taskesen, T.; Steininger, V.; Chen, W.; Ohland, J.; Mikolajczak, U.; Pareek, D.; Parisi, J.; Gütay, L. Resilient and reproducible processing for CZTSe solar cells in the range of 10%. *Prog. Photovoltaics* **2018**, *26*, 1003−1006.

(8) Ge, Z.-H.; Salvador, J. R.; Nolas, G. S. Selective Synthesis of Cu_2SnSe_3 and Cu_2SnSe_4 Nanocrystals. *Inorg. Chem.* **2014**, *53*, 4445−4449.

(9) Marcano, G.; Rincón, C.; Marín, G.; Tovar, R.; Delgado, G. Crystal growth and characterization of the cubic semiconductor Cu_2SnSe_4. *J. Appl. Phys.* **2002**, *92*, 1811−1815.

(10) Li, W.; Lin, S.; Zhang, X.; Chen, Z.; Xu, X.; Pei, Y. Thermoelectric Properties of Cu_2SnSe_4 with Intrinsic Vacancy. *Chem. Mater.* **2016**, *28*, 6227−6232.

(11) Rosemann, N. W.; Eußner, J. P.; Dornsiepen, E.; Chatterjee, S.; Dehnen, S. Organotetrel Chalcogenide Clusters: Between Strong Second-Harmonic and White-Light Continuum Generation. *J. Am. Chem. Soc.* **2016**, *138*, 16224−16227.

(12) Rosemann, N. W.; Eußner, J. P.; Beyer, A.; Koch, S. W.; Volz, K.; Dehnen, S.; Chatterjee, S. A highly efficient directional molecular white-light emitter driven by a continuous-wave laser diode. *Science* **2016**, *352*, 1301−1304.

(13) Dornsiepen, E.; Dobener, F.; Mengel, N.; Lenchuk, O.; Dues, C.; Sanna, S.; Mollenhauer, D.; Chatterjee, S.; Dehnen, S. White-Light Generation Upon In-Situ Amorphization of Single Crystals of $[\{(Me_3P)_3AuSn\}(PhSn)_3S_6]$ and $[\{(Et_3P)_3AgSn\}(PhSn)_3S_6]$. *Adv. Opt. Mater.* **2019**, *7*, 1801793.

(14) Dornsiepen, E.; Dobener, F.; Chatterjee, S.; Dehnen, S. Controlling the White-Light Generation of $[(RSn)_4E_6]$: Effects of Substituent and Chalcogenide Variation. *Angew. Chem., Int. Ed.* **2019**, *58*, 17041.

(15) Dornsiepen, E.; Pieck, F.; Tonner, R.; Dehnen, S. $[\{(PhSn)_3SnS_6\}\{(MCp)_3S_4\}]$ (M = W, Mo): Minimal Molecular Models of the Covalent Attachment of Metal Chalcogenide Clusters on Doped Transition Metal Dichalcogenide Layers. *J. Am. Chem. Soc.* **2019**, *141*, 16494−16500.

(16) Barth, B. E. K.; Leusmann, E.; Harms, K.; Dehnen, S. Towards the installation of transition metal ions on donor ligand decorated tin sulfide clusters. *Chem. Commun.* **2013**, *49*, 6590−6592.

(17) Dornsiepen, E.; Weigend, F.; Dehnen, S. Transition-Metal-Induced Rearrangement of $[(PhSn)_4S_6]$ Towards Ternary CuI /Sn/S or CuII /Sn/S Clusters. *Chem. - Eur. J.* **2019**, *25*, 2486−2490.

(18) Eußner, J. P.; Dehnen, S. Bronze, silver and gold: Functionalized group 11 organotin sulfide clusters. *Chem. Commun.* **2014**, *50*, 11385−11388.

(19) Fard, Z. H.; Xiong, L.; Müller, C.; Hołyńska, M.; Dehnen, S. Synthesis and reactivity of functionalized binary and ternary thiometallate complexes $[(RT)_4S_6]$, $[(RSn)_3S_4]^{2-}$, $[(RT)_2(CuPPh_3)_6S_6]$, and $[(RSn)_6(OMe)_6Cu_2S_6]^{4-}$ (R = C_2H_4COOH, CMe_2CH_2COMe; T = Ge, Sn). *Chem. - Eur. J.* **2009**, *15*, 6595−6604.

(20) Geringer, E.; Dehnen, S. $[(PPh_3)_4Pt_2S_2(SnCl)]^+$: A Pt-Sn-S Cluster with a Ternary Trigonal Bipyramidal Cluster Core. *Z. Anorg. Allg. Chem.* **2018**, *644*, 920−924.

(21) Halvagar, M. R.; Fard, Z. H.; Dehnen, S. Directed derivatization of organotin sulfide compounds: Synthesis and self-assembly of an SnS backpack-like cage and a CuSnS ternary cluster. *Chem. Commun.* **2010**, *46*, 4716−4718.

(22) Halvagar, M. R.; Hassanzadeh Fard, Z.; Xiong, L.; Dehnen, S. Facile access to the hydrazone functionalized PdGeS cluster $[\{R^NGe(\mu\text{-}S)_3\}_4Pd_6]$ from the thiogermanate anion $[\{R^NGe\}_2(\mu\text{-}S)_2S_2]^{2-}$. *Inorg. Chem.* **2009**, *48*, 7373−7377.

(23) Leusmann, E.; Geringer, E.; Weinert, B.; Dehnen, S. $\{Ir_3(cod)_3(\mu_3\text{-}S)_2(\mu_3\text{-}S)SnCl\}_2$ − a ternary Ir−Sn−S cluster with the iridium atoms in three different chemical environments. *Dalton Trans* **2016**, *45*, 15298−15302.

DOI: 10.1021/acs.inorgchem.9b03173
Inorg. Chem. 2020, 59, 198−202

(24) Rinn, N.; Guggolz, L.; Gries, K.; Volz, K.; Senker, J.; Dehnen, S. Formation and Structural Diversity of Organo-Functionalized Tin-Silver Selenide Clusters. *Chem. - Eur. J.* **2017**, *23*, 15607−15611.
(25) Rinn, N.; Hanau, K.; Guggolz, L.; Rinn, A.; Chatterjee, S.; Dehnen, S. Trigonal Bipyramidal Metalselenide Clusters with Palladium and Tin Atoms in Various Positions. *Z. Anorg. Allg. Chem.* **2017**, *643*, 1508−1512.
(26) Dornsiepen, E.; Geringer, E.; Rinn, N.; Dehnen, S. Coordination chemistry of organometallic or inorganic binary group 14/16 units towards transition metal atoms. *Coord. Chem. Rev.* **2019**, *380*, 136−169.
(27) Rinn, N.; Eußner, J. P.; Kaschuba, W.; Xie, X.; Dehnen, S. Formation and Reactivity of Organo-Functionalized Tin Selenide Clusters. *Chem. - Eur. J.* **2016**, *22*, 3094−3104.
(28) Rinn, N.; Guggolz, L.; Lange, J.; Chatterjee, S.; Block, T.; Pöttgen, R.; Dehnen, S. Ternary Mixed-Valence Organotin Copper Selenide Clusters. *Chem. - Eur. J.* **2018**, *24*, 5840−5848.
(29) Cheng, D.; Feng, C.; Xia, S. The directional reaction of hydrazine with silver complexes. Part 3. Synthesis and characterization of a copper(I)-hydrazine intermediate complex, $Na(N_2H_4)CuCl_2$. *Transition Met. Chem.* **2000**, *25*, 635−638.
(30) Bushuyev, O. S.; Arguelles, F. A.; Brown, P.; Weeks, B. L.; Hope-Weeks, L. J. New Energetic Complexes of Copper(II) and the Acetone Carbohydrazide Schiff Base as Potential Flame Colorants for Pyrotechnic Mixtures. *Eur. J. Inorg. Chem.* **2011**, *2011*, 4622−4625.
(31) Cromer, D. T.; Larson, A. C.; Roof, R. B. The crystal structure of copper(I) cyanide hydrazine complex. *Acta Crystallogr.* **1966**, *20*, 279−282.
(32) Paulat, F.; Lehnert, N.; Ishikawa, Y.; Okamoto, K.-I.; Fujisawa, K. Mononuclear and binuclear copper(I)−diazene complexes: A new chapter of copper coordination chemistry. *Inorg. Chim. Acta* **2008**, *361*, 901−915.
(33) Ragunath, L.; Sivasankar, B. N. Preparation, Characterisation and Crystal and Molecular Structure of $[N_2H_5Cu(HEDTA)]H_2O$. *J. Chem. Crystallogr.* **2010**, *40*, 1170−1174.
(34) Pienack, N.; Näther, C.; Bensch, W. Two new copper thiostannates synthesised under solvothermal conditions: Crystal structures, spectroscopic and thermal properties of (DBUH)$CuSnS_3$ and (1,4-dabH2)Cu_2SnS_4. *Solid State Sci.* **2007**, *9*, 100−107.
(35) Fuhrmann, D.; Dietrich, S.; Krautscheid, H. Zinc Tin Chalcogenide Complexes and Their Evaluation as Molecular Precursors for Cu_2ZnSnS_4 (CZTS) and $Cu_2ZnSnSe_4$ (CZTSe). *Inorg. Chem.* **2017**, *56*, 13123−13131.

DOI: 10.1021/acs.inorgchem.9b03173
Inorg. Chem. 2020, 59, 198−202

Variations in the Interplay of Intermetallic and Metal Chalcogenide Units in Organotin-Copper Selenide Clusters

Katharina Hanau,[a] Niklas Rinn,[a] and Stefanie Dehnen*[a]

[a] K. Hanau, Dr. N. Rinn, Prof. Dr. S. Dehnen
Fachbereich Chemie und Wissenschaftliches Zentrum für Materialwissenschaften (WZMW)
Philipps−Universität Marburg
Hans−Meerwein−Str. 4, 35043 Marburg (Germany)
E−mail: dehnen@chemie.uni−marburg.de

Supporting Information

1 Experimental Details

General: All syntheses were performed under exclusion of air and moisture using standard Schlenk techniques. All solvents were dried and freshly distilled prior to use. $[(R^1Sn)_4Se_6]$,[1] $(SiMe_3)_2Se$,[2] and $[CuCl(PPh_3)_3]$[3] were prepared according to literature procedures. Further chemicals were purchased from Sigma Aldrich.

Preparation of I: $[(R^1Sn)_4Se_6]$ (235 mg, 0.175 mmol) and $[CuCl(PPh_3)_3]$ (310 mg, 0.350 mmol) were suspended in 40 mL of dichloromethane and $(SiMe_3)_2Se$ (157 mg, 0.699 mmol) was added. After stirring at room temperature for 24 h, a orange powder precipitated. Alternatively, only 20 mL of dichloromethane can be used, which speeds up the reaction as follows: After stirring for 30 min, the reaction mixture changed from a yellow suspension to a clear, orange solution, and an orange powder started precipitating after 5 h. The reaction mixture was stirred at room temperature for additional 14.5 h (18 h reaction time altogether). The bright orange powder (**I**) was filtered off and dried *in vacuo*. Layering the filtrate with 10 mL of *n*-hexane yielded single crystals of $[(CuPPh_3)_2(SnCu_2)\{(R^1Sn)_2Se_4\}_3]$ (**B**). **I** is metastable when stored in a dry argon atmosphere, yet turning (dark) red after ~5 d.

Preparation of 1: All of the powder that was isolated in the preparation step described above was suspended in 31 mL of dichloromethane and $N_2H_4{\cdot}H_2O$ (80% in H_2O, 20 mg, 0.320 mmol) was added. After 10 min, the powder had dissolved completely. The clear, orange solution was stirred for 16 h, filtered, and layered with 10 mL of *n*-hexane. After 1 d, yellow needles of **1** could be isolated (28 mg, 19.5% compared to $[(R^1Sn)_4Se_6]$). Due to the low solubility of **1**, no NMR data could be obtained.
Alternative Preparation Method of 1: Alternatively, compound **1** can be prepared by extraction of the powder **I** with 10 mL of dichloromethane, filtration, addition of $N_2H_4{\cdot}H_2O$ (80% in H_2O, 20 mg, 0.320 mmol), stirring for 16 hours, and layering with 10 mL of *n*-hexane.

Preparation of 2: Compound **2** was prepared following the alternative preparation method for the synthesis of compound **1**, yet with the difference of layering with 10 mL of *n*-hexane *immediately* upon addition of $N_2H_4{\cdot}H_2O$ (80% in H_2O, 20 mg, 0.320 mmol). Single crystals of **2** were obtained in small yields as dark orange blocks, besides orange powder. Owing to the poor solubility of **2**, sufficient amounts for NMR spectroscopy could not be obtained. Notably, the same batch affords compound **1** if following the other reaction procedure.

All our materials, including the products, were handled under Argon atmosphere. These compounds and our reported similar selenium clusters are especially sensitive to water. The single crystals themselves do also lose solvent molecules when handled in a solvent free atmosphere, and thereupon lose their crystallinity.

2 NMR Spectroscopy

^{1}H NMR spectra of the reaction mixture producing powder **I**, or solutions of **I**, respectively, were recorded with a Bruker AV 500 spectrometer, and ^{31}P NMR spectra were recorded with a Bruker AV III HD 300 spectrometer.

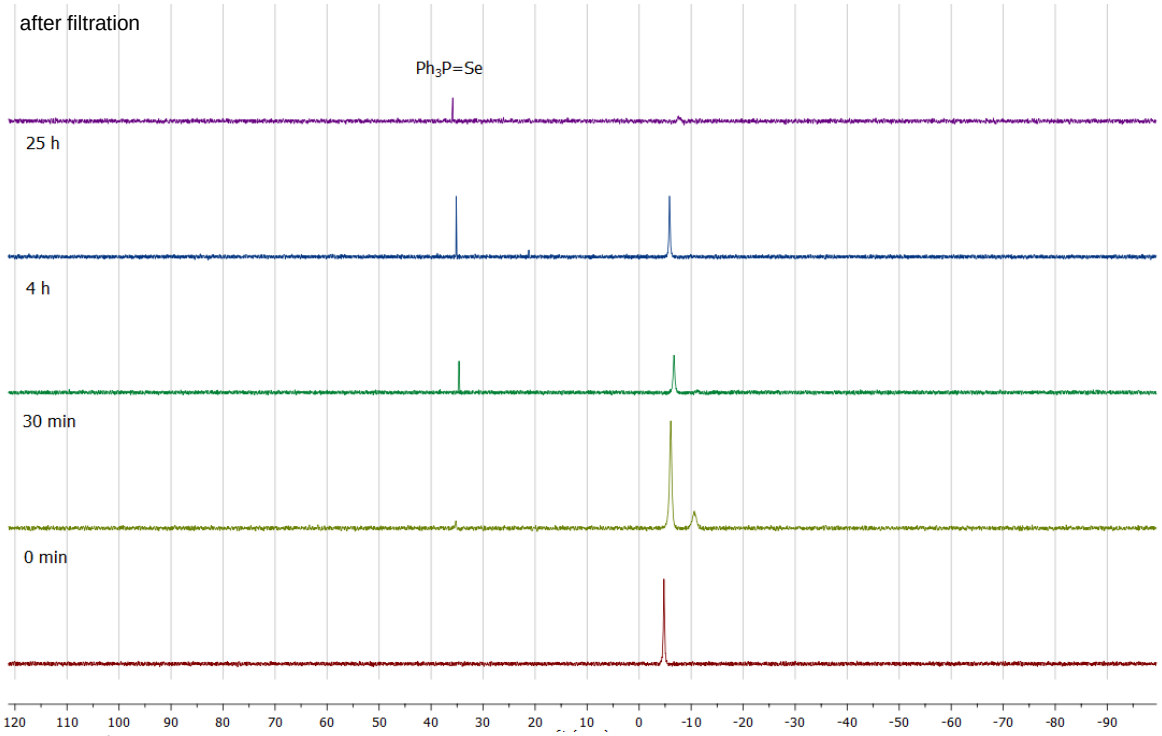

Figure S1. ^{31}P NMR spectra of the reaction yielding **I** at the beginning of the reaction, after 30 min, 4 h, 25 h, and after work-up, respectively.

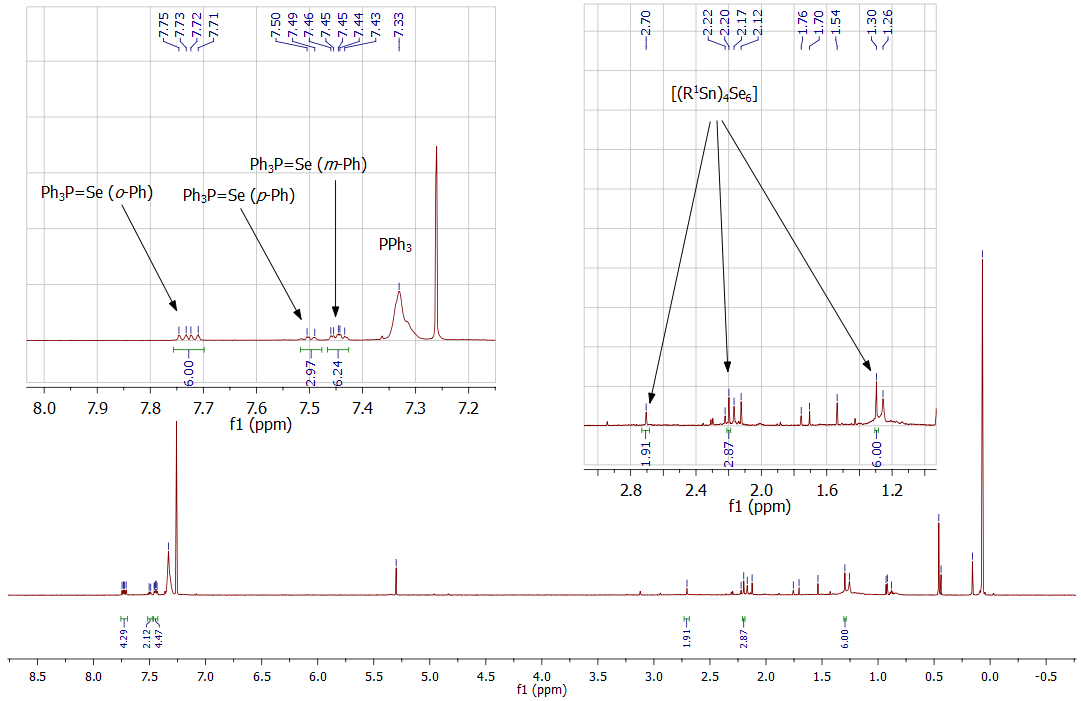

Figure S2. ^{1}H NMR spectrum of a solution of **I** in $CDCl_3$.

3 X-ray Powder Diffraction

In order to gain further insight into the composition of **I**, the powder was examined via X-ray powder diffraction and compared to the calculated powder diffractograms of **B** and **1**. The diffractograms are shown in Figure S3. Powder X-ray diffraction patterns were measured on a StadiMP diffractometer by Stoe equipped with a Mythen 1K silicon strip detector and a Cu-K_α (λ = 1.54056 Å) x-ray source. Samples were measured in transmission in a capillary.

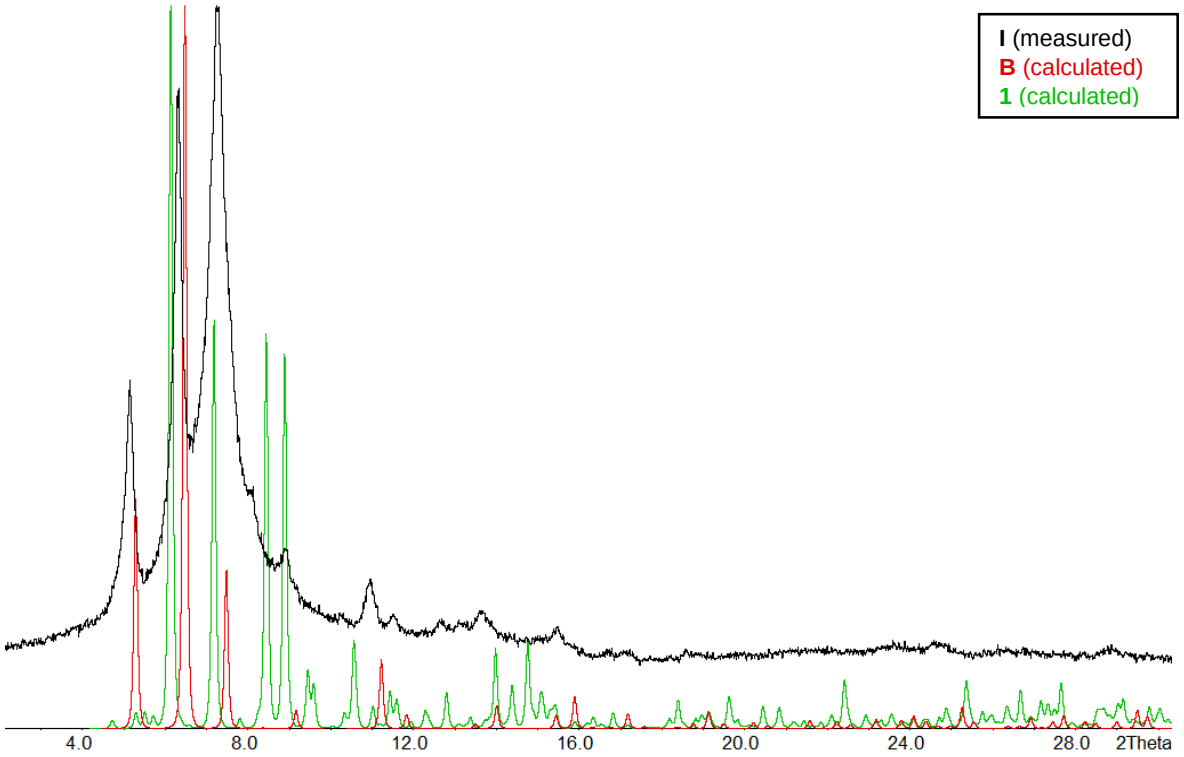

Figure S3. Comparison of the X-ray powder diffractograms of **I**, **1**, and **B**. The slight angular shift between the measured diffractogram of **I** and the calculated diffractogram of **B** is due to the single-crystal measurement of **B** being carried out at 100 K while the powder diffractogram was measured at 293 K.

4 Micro X-ray Fluorescence Spectroscopy

Micro X-ray fluorescence spectroscopy (µ-XRF) was carried out using a Bruker M4 Tornado spectrometer with an Rh target X-ray tube, poly-capillary optics and a Si drift detector.

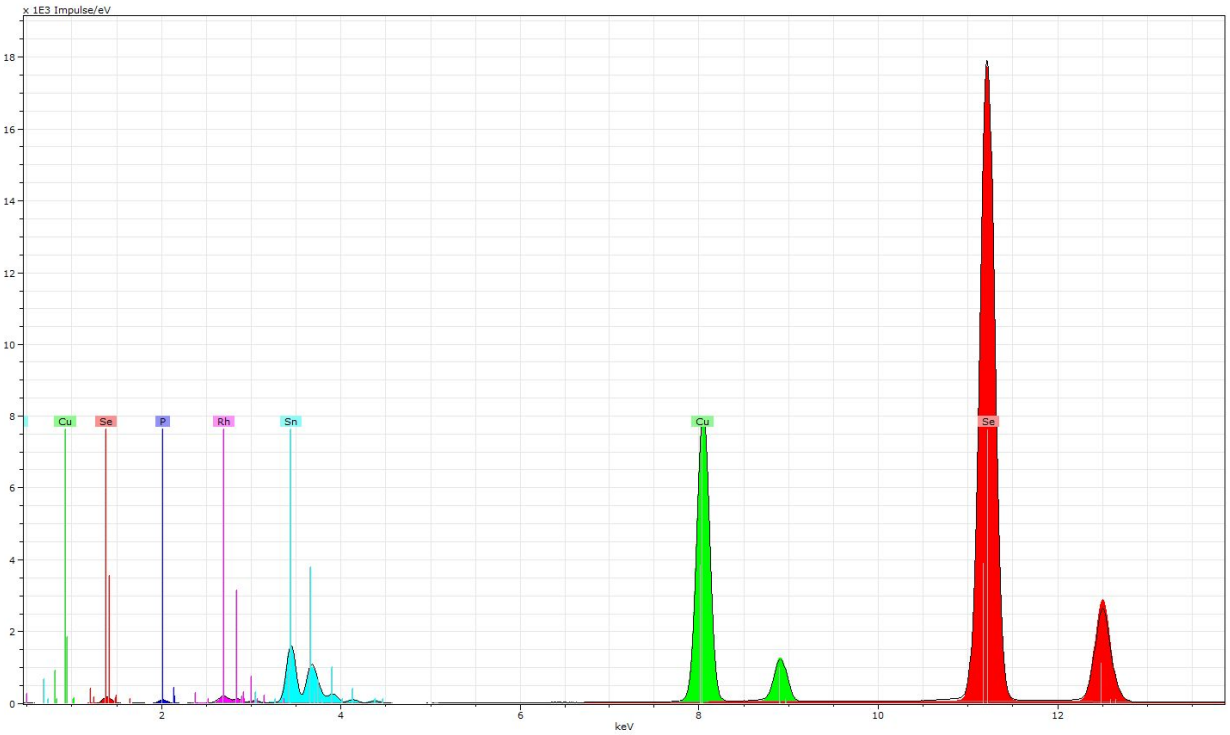

Figure S4. µ-XRF spectrum of **I**. Values (% found) for the elemental composition of P:Cu:Sn:Se was detected as follows: P: 5.57, Cu: 16.84, Sn: 26.57, Se: 51.03, corresponding to atomic ratios of: 1:3:4.8:9.2.

5 Details of the X-ray Diffraction Measurements and Refinements

Crystal Structure of 1

Crystals suitable for X-ray diffraction analyses were investigated with a STOE STADIVARI (**1**) diffractometer at 100 K using Cu-K_α radiation (λ = 1.54186) from an X-ray micro source with X-ray optics and a Pilatus 300K Si hybrid pixel array detector. Upon spherical absorption correction and scaling (STOE LANA), the structure solution was performed by direct methods, followed by full-matrix-least-squares refinement against F^2, using SHELXT15, SHELXL15, and OLEX2 software.[4–6]

Hydrogen atom positions were calculated. Some of the co-crystallized solvent molecules could not be found/refined due to their disorder. They were thus detracted from the data by the back-Fourier-transform method.[7] The voids are located at (-0.071, 0.293, -0.004), (0.071, 0.707 0.004), (0.429, 0.207, 0.496), and (0.571, 0.793, 0.504), have a volume of 182.2 each and contain 41.5, 38.4, 41.3, and 38.4 electrons, respectively, which amounts to 2 molecules of either disordered dichloromethane or partially occupied *n*-hexane per formula unit.

The highest peak of residual electron density on the difference Fourier map (4.437 e⁻/Å³) is found 1.030 Å away from Sn5A.

A photograph of single crystals of 1 is shown in Figure S5 and excerpts of the crystal structure are shown in Figure S6.

Figure S5. Photograph of single crystals of **1** picked for X-ray diffraction.

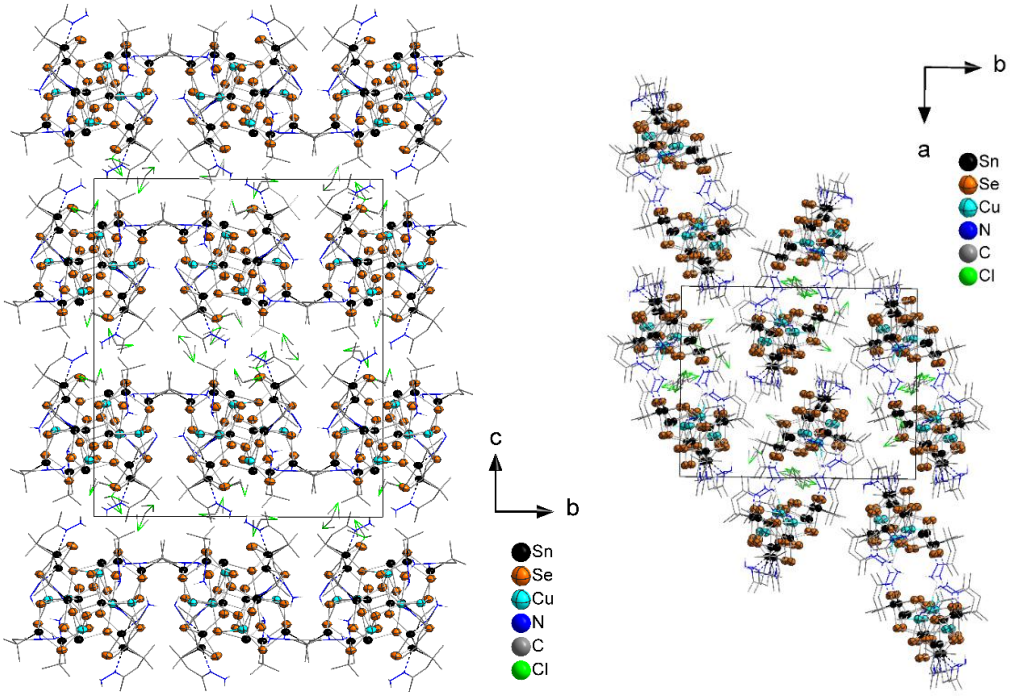

Figure S6. Excerpt of the crystal structure of **1** viewed along the *a* axis (left) and along the *c* axis (right).

Table S1. Crystallographic data and refinement results of **1**.

Compound	**1**·1.87CH_2Cl_2·2solv
Empirical Formula	$C_{30}H_{65}Cu_3N_{10}Se_{11}Sn_7$, 1.87$CH_2Cl_2$
Formula weight /g·mol^{-1}	2615.16
Crystal color and shape	yellow needle
Crystal size /mm³	0.032 x 0.039 x 0.191
Crystal system	monoclinic
Space group	$P2_1/n$
a /Å	19.9060(5)
b / Å	24.6240(4)
c / Å	28.8354(6)
α /°	90
β /°	92.446(2)
γ /°	90
V / Å³	14121.2(5)
Z	8
Measurement Temperature /K	100
ρ_{calcd} / g·cm^{-3}	2.460
$\mu_{(Cu\ K\alpha)}$ / mm^{-1}	28.335
Absorption correction type	sphere
Min./max. transmission	0.074 / 0.464
2*θ* range / deg	5.71 – 144.22
No. of measured reflections	216363
R(int)	0.1780
Independent Reflections	22493
Independent Reflections ($I>2\sigma(I)$)	11006
No. of parameters	1271
R_1 ($I>2\sigma(I)$) / wR_2 (all data)	0.0868 / 0.2390
S (all data)	0.889
Max. peak / hole / e$^-$ Å³	4.437 / –1.432

Table S2. Fractional Atomic Coordinates ($\times 10^4$) and Equivalent Isotropic Displacement Parameters ($Å^2 \times 10^3$) for EG062y. U(eq) is defined as 1/3 of the trace of the orthogonalised U_{IJ} tensor.

Atom	*x*	*y*	*z*	U(eq)	Atom	*x*	*y*	*z*	U(eq)
Sn1A	6833.1(7)	5276.6(6)	7554.3(4)	56.0(4)	C17A	4776(12)	5801(9)	6118(8)	74(7)
Sn2A	7843.5(8)	4491.8(7)	8644.5(5)	67.4(4)	C18A	4012(13)	5724(11)	6131(8)	92(8)
Sn3A	8415.8(7)	4106.0(6)	7468.8(5)	60.3(4)	C19A	4915(12)	6175(10)	8853(7)	74(7)
Sn4A	7878.2(8)	6652.0(6)	6594.1(4)	59.5(4)	C20A	5065(11)	6670(10)	9150(7)	77(7)
Sn5A	6324.8(8)	5846.1(6)	6323.3(4)	61.8(4)	C21A	4789(12)	5650(9)	9189(6)	71(7)
Sn6A	5809.9(7)	5970.4(6)	8467.2(4)	57.6(4)	C22A	4331(10)	6247(9)	8528(7)	63(6)
Sn7A	7568.0(7)	6036.0(6)	8881.3(4)	58.9(4)	C23A	4497(10)	6568(8)	8084(6)	52(5)
Se1A	7155.7(12)	4278.9(9)	7821.5(7)	59.4(6)	C24A	3945(11)	6790(10)	7777(7)	75(7)
Se2A	8880.6(13)	3978.1(11)	8289.0(8)	71.5(7)	C25A	8072(11)	6740(9)	9182(8)	68(6)
Se3A	8361.1(12)	5476.7(9)	8407.2(7)	59.6(6)	C26A	7620(13)	7043(11)	9502(8)	90(8)
Se4A	8650.9(11)	4998.9(9)	7082.9(7)	59.8(6)	C27A	8270(12)	7106(8)	8802(7)	66(6)
Se5A	6459.7(12)	4919.5(10)	6701.4(7)	60.7(6)	C28A	8715(12)	6529(11)	9464(7)	81(7)
Se6A	7628.7(12)	5852.1(10)	6057.5(7)	60.8(6)	C29A	8587(13)	6055(11)	9744(7)	74(7)
Se7A	6546.9(12)	6677.3(10)	6822.3(7)	60.5(6)	C30A	9056(11)	5928(10)	10159(7)	78(7)
Se8A	8290.4(12)	6589.1(10)	7425.8(7)	59.6(6)	Sn1B	3130.8(7)	4477.4(6)	7452.2(4)	57.5(4)
Se9A	5599.7(12)	5235.4(9)	7873.5(7)	59.3(6)	Sn2B	2115.3(8)	5280.2(6)	6376.2(5)	67.1(4)
Se10A	6579.9(13)	5473.8(11)	9110.9(8)	68.7(7)	Sn3B	1546.0(8)	5651.3(6)	7553.8(5)	61.7(4)
Se11A	6756.9(11)	6621.5(9)	8293.1(7)	56.4(6)	Sn4B	2090.0(8)	3105.2(6)	8421.1(4)	58.7(4)
Cu1A	7125.6(15)	6325.9(12)	7549.8(9)	58.4(8)	Sn5B	3643.9(8)	3902.5(6)	8679.2(4)	60.5(4)
Cu2A	8126.1(15)	5643.5(12)	7577.0(9)	58.0(8)	Sn6B	4141.4(7)	3774.0(6)	6529.1(4)	57.2(4)
Cu3A	7649.0(16)	5158.5(13)	6674.0(10)	66.6(8)	Sn7B	2381.7(7)	3733.3(6)	6124.9(4)	57.0(4)
N1A	9452(8)	3772(7)	7232(6)	66(5)	Se1B	2810.8(12)	5480.1(10)	7196.0(7)	60.5(6)
N2A	10076(10)	3936(10)	7438(8)	106(9)	Se2B	1078.9(13)	5784.6(11)	6739.8(8)	71.1(7)
N3A	9014(9)	6588(7)	6379(5)	60(5)	Se3B	1599.1(12)	4297.3(9)	6606.2(7)	59.3(6)
N4A	9390(9)	6113(6)	6395(6)	65(5)	Se4B	1324.1(12)	4755.6(10)	7933.1(7)	61.3(6)
N5A	5161(8)	5868(7)	6485(5)	62(5)	Se5B	1672.6(12)	3170.4(9)	7589.2(7)	57.8(6)
N6A	4868(9)	5927(7)	6923(6)	70(5)	Se7B	2345.7(12)	3904.5(10)	8955.8(7)	63.6(6)
N7A	5120(9)	6608(8)	8006(6)	68(5)	Se6B	3414.8(12)	3073.8(9)	8180.1(7)	58.7(6)
N8A	5306(10)	6904(9)	7606(6)	81(6)	Se8B	3514.6(12)	4832.4(10)	8304.2(7)	61.8(6)
N9A	8094(10)	5748(8)	9602(6)	69(5)	Se9B	4354.7(12)	4508.1(10)	7122.0(7)	60.6(6)
N10A	7962(10)	5268(9)	9848(7)	91(7)	Se10B	3387.1(12)	4254.2(11)	5871.2(8)	67.9(7)
C1A	8130(11)	3437(9)	7010(7)	62(6)	Se11B	3184.8(11)	3136.6(9)	6712.5(7)	55.6(5)
C2A	7528(10)	3593(9)	6700(6)	61(6)	Cu1B	2835.1(16)	3427.7(12)	7461.3(9)	59.9(8)
C3A	7950(11)	2938(10)	7342(7)	78(7)	Cu2B	1842.4(16)	4113.9(13)	7433.9(9)	61.4(8)
C4A	8714(12)	3271(10)	6740(8)	77(7)	Cu3B	2330.7(17)	4595.6(14)	8342.7(11)	70.7(9)
C5A	9431(12)	3421(9)	6924(7)	66(6)	N1B	517(9)	5975(8)	7797(7)	73(5)
C6A	10006(13)	3153(10)	6733(8)	84(7)	N2B	-125(11)	5709(12)	7671(9)	127(10)
C7A	8081(13)	7409(9)	6232(7)	72(6)	N3B	963(9)	3164(8)	8634(5)	63(5)
C8A	7656(12)	7871(9)	6397(8)	73(6)	N4B	569(10)	3635(9)	8631(6)	82(6)
C9A	7957(12)	7326(9)	5715(6)	69(6)	N5B	4812(9)	3871(6)	8513(5)	56(4)
C10A	8811(13)	7545(10)	6356(9)	82(7)	N6B	5095(8)	3816(8)	8088(5)	66(5)
C11A	9274(14)	7060(13)	6353(8)	85(8)	N7B	4834(9)	3109(7)	6987(5)	62(5)
C12A	10052(13)	7115(11)	6351(10)	100(9)	N8B	4644(10)	2811(7)	7383(5)	66(5)
C13A	5853(13)	5872(11)	5639(8)	81(7)	N9B	1841(10)	4056(9)	5407(6)	76(6)
C14A	6143(15)	5443(13)	5343(8)	107(10)	N10B	1968(10)	4547(7)	5194(6)	72(5)
C15A	5921(17)	6411(13)	5433(10)	123(12)	C1B	1823(11)	6345(7)	7980(7)	60(6)
C16A	5076(15)	5723(15)	5674(8)	119(12)	C2B	2028(13)	6787(8)	7643(8)	73(7)

Atom	*x*	*y*	*z*	U(eq)	Atom	*x*	*y*	*z*	U(eq)
C3B	2431(12)	6196(9)	8316(8)	80(7)	C25B	1886(11)	3024(8)	5808(7)	61(6)
C4B	1228(12)	6523(9)	8271(7)	70(6)	C26B	1647(12)	2641(9)	6173(7)	73(7)
C5B	533(10)	6354(8)	8088(7)	55(5)	C27B	2398(14)	2747(9)	5506(8)	94(9)
C6B	-58(11)	6606(9)	8299(7)	68(6)	C28B	1250(13)	3253(9)	5524(7)	71(6)
C7B	1895(12)	2361(8)	8783(7)	65(6)	C29B	1366(12)	3765(9)	5259(7)	64(6)
C8B	2005(11)	2450(10)	9300(7)	70(6)	C30B	896(11)	3893(10)	4854(7)	77(7)
C9B	2374(12)	1897(10)	8633(8)	79(7)	Cl1	9411(4)	4767(3)	9379(2)	97(2)
C10B	1139(11)	2200(10)	8638(9)	78(7)	Cl2	10466(5)	5516(4)	9153(3)	136(3)
C11B	688(14)	2695(11)	8655(7)	78(7)	C31	10003(14)	4933(13)	8955(8)	109(9)
C12B	-84(13)	2631(14)	8597(12)	130(13)	Cl3	9700(6)	4205(4)	5860(3)	139(3)
C13B	4133(10)	3819(9)	9365(7)	60(5)	Cl4	10481(4)	5139(3)	5628(2)	97(2)
C14B	4166(14)	3229(10)	9504(9)	92(8)	C32	9949(14)	4845(8)	6034(9)	84(8)
C15B	3797(15)	4166(14)	9714(9)	116(11)	Cl5	5707(9)	7930(6)	9656(7)	181(9)
C16B	4886(11)	4034(10)	9329(7)	69(6)	Cl6	6238(10)	8462(8)	10422(7)	200(9)
C17B	5212(11)	3960(9)	8874(6)	61(6)	C33	6390(20)	8220(17)	9908(10)	109(9)
C18B	5937(11)	4047(10)	8842(7)	70(6)	Cl7	6694(15)	3645(12)	10075(7)	232(18)
C19B	5036(11)	3597(8)	6142(8)	65(6)	Cl8	7178(12)	4484(9)	10572(6)	149(10)
C20B	5190(12)	4081(9)	5833(8)	75(7)	C34	7050(30)	4210(18)	10074(11)	78(15)
C21B	4921(11)	3087(9)	5860(7)	68(6)	Cl9	7050(13)	4032(11)	5091(8)	225(15)
C22B	5615(10)	3506(9)	6506(6)	61(6)	Cl10	8080(20)	4386(8)	5609(7)	250(19)
C23B	5452(12)	3173(9)	6931(7)	64(6)	C35	7280(20)	4360(30)	5546(19)	180(40)
C24B	6002(10)	2952(9)	7230(7)	64(6)					

Table S3. Selected bond lengths in **1** [Å].

Sn1A–Se1A	2.646(3)	Sn5A–C13A	2.15(2)	Sn1B–Se8B	2.688(2)	Sn6B–Se10B	2.647(3)
Sn1A–Se5A	2.687(2)	Sn6A–Se11A	2.541(3)	Sn1B–Se9B	2.654(3)	Sn6B–Se9B	2.512(3)
Sn1A–Se9A	2.661(3)	Sn6A–Se9A	2.514(3)	Sn1B–Cu1B	2.651(3)	Sn6B–Se11B	2.541(3)
Sn1A–Cu1A	2.649(3)	Sn6A–Se10A	2.655(3)	Sn1B–Cu2B	2.715(3)	Sn6B–N7B	2.484(18)
Sn1A–Cu2A	2.726(3)	Sn6A–N7A	2.442(18)	Sn1B–Cu3B	3.093(3)	Sn6B–C19B	2.19(2)
Sn1A–Cu3A	3.085(3)	Sn6A–C19A	2.20(2)	Sn2B–Se1B	2.733(3)	Sn7B–Se3B	2.543(3)
Sn2A–Se1A	2.739(3)	Sn7A–Se11A	2.707(3)	Sn2B–Se2B	2.661(3)	Sn7B–Se10B	2.512(3)
Sn2A–Se2A	2.663(3)	Sn7A–Se3A	2.538(3)	Sn2B–Se3B	2.722(3)	Sn7B–Se11B	2.712(2)
Sn2A–Se3A	2.733(3)	Sn7A–Se10A	2.517(3)	Sn3B–Se1B	2.793(3)	Sn7B–N9B	2.427(18)
Sn3A–Se1A	2.779(3)	Sn7A–N9A	2.395(18)	Sn3B–Se2B	2.509(3)	Sn7B–C25B	2.188(17)
Sn3A–Se2A	2.522(3)	Sn7A–C25A	2.16(2)	Sn3B–Se4B	2.509(3)	Se3B–Cu2B	2.457(3)
Sn3A–Se4A	2.517(3)	Se11–Cu1A	2.408(3)	Sn3B–N1B	2.334(18)	Se4B–Cu2B	2.400(4)
Sn3A–N1A	2.348(17)	Se3A–Cu2A	2.454(3)	Sn3B–C1B	2.163(16)	Se4B–Cu3B	2.316(4)
Sn3A–C1A	2.17(2)	Se4A–Cu2A	2.402(4)	Sn4B–Se5B	2.510(2)	Se5B–Cu1B	2.442(4)
Sn4A–Se6A	2.540(3)	Se4A–Cu3A	2.307(4)	Sn4B–Se7B	2.538(3)	Se5B–Cu2B	2.393(4)
Sn4A–Se7A	2.758(3)	Se5A–Cu3A	2.444(4)	Sn4B–Se6B	2.757(3)	Se7B–Cu3B	2.453(4)
Sn4A–Se8A	2.506(2)	Se6A–Cu3A	2.464(4)	Sn4B–N3B	2.356(19)	Se6B–Cu1B	2.486(3)
Sn4A–N3A	2.375(19)	Se7A–Cu1A	2.504(3)	Sn4B–C7B	2.152(19)	Se8B–Cu3B	2.435(4)
Sn4A–C7A	2.18(2)	Se8A–Cu1A	2.448(4)	Sn5B–Se7B	2.737(3)	Se11B–Cu1B	2.406(3)
Sn5A–Se5A	2.538(3)	Se8A–Cu2A	2.394(4)	Sn5B–Se6B	2.527(3)	Cu1B–Cu2B	2.599(4)
Sn5A–Se6A	2.737(3)	Cu1A–Cu2A	2.604(4)	Sn5B–Se8B	2.541(3)	Cu2B–Cu3B	3.000(4)
Sn5A–Se7A	2.530(3)	Cu2A–Cu3A	2.983(4)	Sn5B–N5B	2.395(18)		
Sn5A–N5A	2.383(17)	Sn1B–Se1B	2.647(3)	Sn5B–C13B	2.18(2)		

Table S4. Selected bond angles in **1** [°].

Se1A–Sn1A–Se5A	90.97(8)	Se9A–Sn6A–Se11A	115.02(8)	Se11A–Cu1A–Cu2A	115.47(13)
Se1A–Sn1A–Se9A	94.58(8)	Se9A–Sn6A–Se10A	102.64(9)	Se7A–Cu1A–Sn1A	104.35(12)
Se1A–Sn1A–Cu1A	148.93(10)	N7A–Sn6A–Se11A	83.7(4)	Se7A–Cu1A–Cu2A	124.89(13)
Se1A–Sn1A–Cu2A	94.79(9)	N7A–Sn6A–Se9A	91.1(4)	Se8A–Cu1A–Sn1A	117.95(13)
Se1A–Sn1A–Cu3A	91.28(9)	N7A–Sn6A–Se10A	166.2(4)	Se8A–Cu1A–Se7A	101.00(12)
Se5A–Sn1A–Cu2A	110.76(9)	C19A–Sn6A–Se11A	125.4(7)	Se8A–Cu1A–Cu2A	56.46(11)
Se5A–Sn1A–Cu3A	49.51(8)	C19A–Sn6A–Se9A	113.2(6)	Cu2A–Cu1A–Sn1A	62.52(10)
Se9A–Sn1A–Se5A	94.64(8)	C19A–Sn6A–Se10A	102.0(5)	Sn1A–Cu2A–Cu3A	65.24(9)
Se9A–Sn1A–Cu2A	152.71(9)	C19A–Sn6A–N7A	71.3(7)	Se3A–Cu2A–Sn1A	96.23(11)
Se9A–Sn1A–Cu3A	143.81(9)	Se3A–Sn7A–Se11A	108.63(8)	Se3A–Cu2A–Cu1A	104.54(13)
Cu1A–Sn1A–Se5A	111.54(9)	Se10A–Sn7A–Se11A	90.33(9)	Se3A–Cu2A–Cu3A	145.57(15)
Cu1A–Sn1A–Se9A	104.20(10)	Se10A–Sn7A–Se3A	110.75(10)	Se4A–Cu2A–Sn1A	101.59(12)
Cu1A–Sn1A–Cu2A	57.95(10)	N9A–Sn7A–Se11A	158.2(5)	Se4A–Cu2A–Se3A	113.48(14)
Cu1A–Sn1A–Cu3A	87.96(9)	N9A–Sn7A–Se3A	92.7(5)	Se4A–Cu2A–Cu1A	139.46(14)
Cu2A–Sn1A–Cu3A	61.40(9)	N9A–Sn7A–Se10A	85.8(5)	Se4A–Cu2A–Cu3A	49.29(10)
Se2A–Sn2A–Se1A	86.71(8)	C25A–Sn7A–Se11A	94.5(6)	Se8A–Cu2A–Sn1A	117.01(13)
Se2A–Sn2A–Se3A	91.05(9)	C25A–Sn7A–Se3A	111.2(6)	Se8A–Cu2A–Se3A	108.58(13)
Se3A–Sn2A–Se1A	97.62(8)	C25A–Sn7A–Se10A	133.5(6)	Se8A–Cu2A–Se4A	117.94(14)
Se2A–Sn3A–Se1A	88.67(9)	C25A–Sn7A–N9A	73.3(8)	Se8A–Cu2A–Cu1A	58.48(11)
Se4A–Sn3A–Se1A	102.45(9)	Sn1A–Se1A–Sn2A	100.42(9)	Se8A–Cu2A–Cu3A	105.74(12)
Se4A–Sn3A–Se2A	117.13(10)	Sn1A–Se1A–Sn3A	104.32(9)	Cu1A–Cu2A–Sn1A	59.54(10)
N1A–Sn3A–Se1A	167.8(5)	Sn2A–Se1A–Sn3A	85.45(8)	Cu1A–Cu2A–Cu3A	91.00(12)
N1A–Sn3A–Se2A	86.4(4)	Sn3A–Se2A–Sn2A	92.42(9)	Se4A–Cu3A–Sn1A	93.99(11)
N1A–Sn3A–Se4A	89.7(5)	Sn7A–Se3A–Sn2A	95.55(9)	Se4A–Cu3A–Se5A	139.46(16)
C1A–Sn3A–Se1A	97.0(6)	Cu2A–Se3A–Sn2A	109.55(11)	Se4A–Cu3A–Se6A	118.29(16)
C1A–Sn3A–Se2A	123.5(6)	Cu2A–Se3A–Sn7A	109.73(11)	Se4A–Cu3A–Cu2A	52.11(10)
C1A–Sn3A–Se4A	116.2(6)	Cu2A–Se4A–Sn3A	102.78(11)	Se5A–Cu3A–Sn1A	56.73(8)
C1A–Sn3A–N1A	76.6(7)	Cu3A–Se4A–Sn3A	101.64(12)	Se5A–Cu3A–Se6A	101.78(14)
Se6A–Sn4A–Se7A	89.88(9)	Cu3A–Se4A–Cu2A	78.59(13)	Se5A–Cu3A–Cu2A	109.94(13)
Se8A–Sn4A–Se6A	125.62(9)	Sn5A–Se5A–Sn1A	96.84(9)	Se6A–Cu3A–Sn1A	122.36(13)
Se8A–Sn4A–Se7A	92.96(8)	Cu3A–Se5A–Sn1A	73.76(10)	Se6A–Cu3A–Cu2A	110.31(14)
N3A–Sn4A–Se6A	87.3(4)	Cu3A–Se5A–Sn5A	81.63(11)	Cu2A–Cu3A–Sn1A	53.36(8)
N3A–Sn4A–Se7A	177.1(4)	Sn4A–Se6A–Sn5A	89.81(8)	Se1B–Sn1B–Se8B	90.42(8)
N3A–Sn4A–Se8A	88.3(4)	Cu3A–Se6A–Sn4A	95.81(10)	Se1B–Sn1B–Se9B	94.99(9)
C7A–Sn4A–Se6A	114.0(5)	Cu3A–Se6A–Sn5A	77.34(10)	Se1B–Sn1B–Cu1B	149.45(10)
C7A–Sn4A–Se7A	107.1(7)	Sn5A–Se7A–Sn4A	89.56(8)	Se1B–Sn1B–Cu2B	94.94(10)
C7A–Sn4A–Se8A	116.8(6)	Cu1A–Se7A–Sn4A	77.28(10)	Se1B–Sn1B–Cu3B	91.01(9)
C7A–Sn4A–N3A	74.6(8)	Cu1A–Se7A–Sn5A	105.07(11)	Se8B–Sn1B–Cu2B	110.88(9)
Se5A–Sn5A–Se6A	92.35(9)	Cu1A–Se8A–Sn4A	83.26(10)	Se8B–Sn1B–Cu3B	49.22(8)
Se7A–Sn5A–Se5A	118.05(8)	Cu2A–Se8A–Sn4A	101.11(11)	Se9B–Sn1B–Se8B	95.12(8)
Se7A–Sn5A–Se6A	90.58(9)	Cu2A–Se8A–Cu1A	65.06(12)	Se9B–Sn1B–Cu2B	152.03(10)
N5A–Sn5A–Se5A	91.3(4)	Sn6A–Se9A–Sn1A	94.52(9)	Se9B–Sn1B–Cu3B	143.93(9)
N5A–Sn5A–Se6A	174.8(4)	Sn7A–Se10A–Sn6A	89.83(9)	Cu1B–Sn1B–Se8B	111.26(9)
N5A–Sn5A–Se7A	91.1(4)	Sn6A–Se11A–Sn7A	88.16(8)	Cu1B–Sn1B–Se9B	103.82(10)
C13A–Sn5A–Se5A	117.1(7)	Cu1A–Se11A–Sn6A	104.01(11)	Cu1B–Sn1B–Cu2B	57.92(10)
C13A–Sn5A–Se6A	97.2(7)	Cu1A–Se11A–Sn7A	101.56(11)	Cu1B–Sn1B–Cu3B	87.77(10)
C13A–Sn5A–Se7A	123.8(7)	Se11A–Cu1A–Sn1A	102.42(12)	Cu2B–Sn1B–Cu3B	61.81(9)
C13A–Sn5A–N5A	77.8(8)	Se11A–Cu1A–Se7A	119.64(14)	Se2B–Sn2B–Se1B	87.00(8)
Se11–Sn6A–Se10A	91.02(9)	Se11A–Cu1A–Se8A	112.12(13)	Se2B–Sn2B–Se3B	90.68(9)

Se3B–Sn2B–Se1B	97.58(8)	C19B–Sn6B–Se9B	111.9(6)	Cu1B–Se11B–Sn6B	104.52(11)
Se2B–Sn3B–Se1B	88.75(9)	C19B–Sn6B–Se2	128.1(6)	Cu1B–Se11B–Sn7B	102.35(11)
Se2B–Sn3B–Se4B	117.23(10)	C19B–Sn6B–N7B	72.2(7)	Se11B–Cu1B–Sn1B	102.05(12)
Se4B–Sn3B–Se1B	101.92(9)	Se10A–Sn7B–Se3B	113.22(10)	Se6B–Cu1B–Sn1B	104.75(12)
N1B–Sn3B–Se1B	168.3(5)	Se10A–Sn7B–Se2	90.17(8)	Se6B–Cu1B–Cu2B	125.35(14)
N1B–Sn3B–Se2B	86.6(5)	Se3B–Sn7B–Se2	108.27(8)	Se5B–Cu1B–Sn1B	117.81(13)
N1B–Sn3B–Se4B	89.8(5)	N9B–Sn7B–Se10B	85.1(5)	Se5B–Cu1B–Se6B	101.08(13)
C1B–Sn3B–Se1B	96.8(6)	N9B–Sn7B–Se3B	91.5(5)	Se5B–Cu1B–Cu2B	56.57(11)
C1B–Sn3B–Se2B	120.2(6)	N9B–Sn7B–Se2	159.9(5)	Se11B–Cu1B–Se5B	111.74(13)
C1B–Sn3B–Se4B	119.5(6)	C25B–Sn7B–Se10B	129.6(6)	Se11B–Cu1B–Se6B	120.12(14)
C1B–Sn3B–N1B	76.4(7)	C25B–Sn7B–Se3B	112.9(6)	Se11B–Cu1B–Cu2B	114.53(13)
Se5B–Sn4B–Se7B	125.49(9)	C25B–Sn7B–Se2	94.1(6)	Cu2B–Cu1B–Sn1B	62.27(10)
Se5B–Sn4B–Se6B	92.41(8)	C25B–Sn7B–N9B	74.3(8)	Sn1B–Cu2B–Cu3B	65.30(9)
Se7B–Sn4B–Se6B	90.33(8)	Sn1B–Se1B–Sn2B	100.39(9)	Se5B–Cu2B–Se3B	109.68(13)
N3B–Sn4B–Se5B	88.0(4)	Sn1B–Se1B–Sn3B	104.34(9)	Se5B–Cu2B–Se4B	117.34(14)
N3B–Sn4B–Se7B	87.8(4)	Sn2B–Se1B–Sn3B	85.14(8)	Se5B–Cu2B–Cu1B	58.42(11)
N3B–Sn4B–Se6B	178.0(5)	Sn3B–Se2B–Sn2B	92.58(9)	Se3B–Cu2B–Sn1B	96.04(12)
C7B–Sn4B–Se5B	117.3(6)	Sn7B–Se3B–Sn2B	96.10(9)	Se3B–Cu2B–Cu1B	105.50(13)
C7B–Sn4B–Se7B	113.7(6)	Cu2B–Se3B–Sn2B	109.83(11)	Se3B–Cu2B–Cu3B	144.98(15)
C7B–Sn4B–Se6B	107.0(6)	Cu2B–Se3B–Sn7B	109.26(11)	Se4B–Cu2B–Sn1B	101.61(12)
C7B–Sn4B–N3B	74.5(8)	Cu2B–Se4B–Sn3B	103.24(11)	Se4B–Cu2B–Se3B	112.94(14)
Se6B–Sn5B–Se7B	91.02(9)	Cu3B–Se4B–Sn3B	101.96(13)	Se4B–Cu2B–Cu1B	139.08(14)
Se6B–Sn5B–Se8B	118.22(8)	Cu3B–Se4B–Cu2B	79.00(13)	Se4B–Cu2B–Cu3B	49.26(10)
Se8B–Sn5B–Se7B	92.45(9)	Cu1B–Se5B–Sn4B	83.32(10)	Se5B–Cu2B–Sn1B	117.21(13)
N5B–Sn5B–Se7B	174.4(4)	Cu2B–Se5B–Sn4B	101.38(11)	Se5B–Cu2B–Cu3B	105.28(12)
N5B–Sn5B–Se6B	90.8(4)	Cu2B–Se5B–Cu1B	65.01(12)	Cu1B–Cu2B–Sn1B	59.82(10)
N5B–Sn5B–Se8B	91.4(4)	Sn5B–Se6B–Sn4B	89.15(8)	Cu1B–Cu2B–Cu3B	90.74(12)
C13B–Sn5B–Se7B	97.3(5)	Cu1B–Se6B–Sn4B	77.61(10)	Se4B–Cu3B–Sn1B	93.31(11)
C13B–Sn5B–Se6B	120.3(6)	Cu1B–Se6B–Sn5B	104.93(11)	Se4B–Cu3B–Se7B	117.98(16)
C13B–Sn5B–Se8B	120.3(6)	Sn4B–Se7B–Sn5B	89.37(8)	Se4B–Cu3B–Se8B	138.95(17)
C13B–Sn5B–N5B	77.2(6)	Cu3B–Se7B–Sn4B	95.98(11)	Se4B–Cu3B–Cu2B	51.74(10)
Se9B–Sn6B–Se10B	103.92(9)	Cu3B–Se7B–Sn5B	76.93(10)	Se7B–Cu3B–Sn1B	122.83(14)
Se9B–Sn6B–Se11B	114.17(9)	Sn5B–Se8B–Sn1B	96.63(9)	Se7B–Cu3B–Cu2B	110.41(15)
Se11B–Sn6B–Se10B	91.02(8)	Cu3B–Se8B–Sn1B	74.09(10)	Se8B–Cu3B–Sn1B	56.70(9)
N7B–Sn6B–Se10B	163.8(4)	Cu3B–Se8B–Sn5B	81.11(11)	Se8B–Cu3B–Se7B	102.53(14)
N7B–Sn6B–Se9B	92.2(4)	Sn6B–Se9B–Sn1B	95.31(9)	Se8B–Cu3B–Cu2B	109.45(13)
N7B–Sn6B–Se2	83.4(4)	Sn7B–Se10B–Sn6B	89.87(8)	Cu2B–Cu3B–Sn1B	52.89(8)
C19B–Sn6B–Se10B	100.0(6)	Sn6B–Se11B–Sn7B	87.84(8)		

Crystal Structure of 2

Crystals suitable for X-ray diffraction analyses were investigated with a STOE IPDS-2T (**2**) diffractometer at 100 K using Mo-K_α radiation and a graphite monochromator (λ = 0.71073 Å). Upon numerical absorption correction (STOE X-AREA), the structure solution was performed by direct methods, followed by full-matrix-least-squares refinement against F^2, using SHELXT15, SHELXL15, and OLEX2 software.[4–6]

The highest peak of residual electron density on the difference Fourier map (4.727 $e^-/Å^3$) is found 0.938 Å away from Sn4. A photograph of a single crystal of **2** is shown in Figure S7, and a cut-out of the crystal structure is shown in Figure S8.

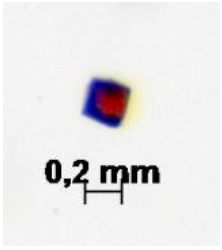

Figure S7. Photograph of the single crystal of **2** picked for X-ray diffraction.

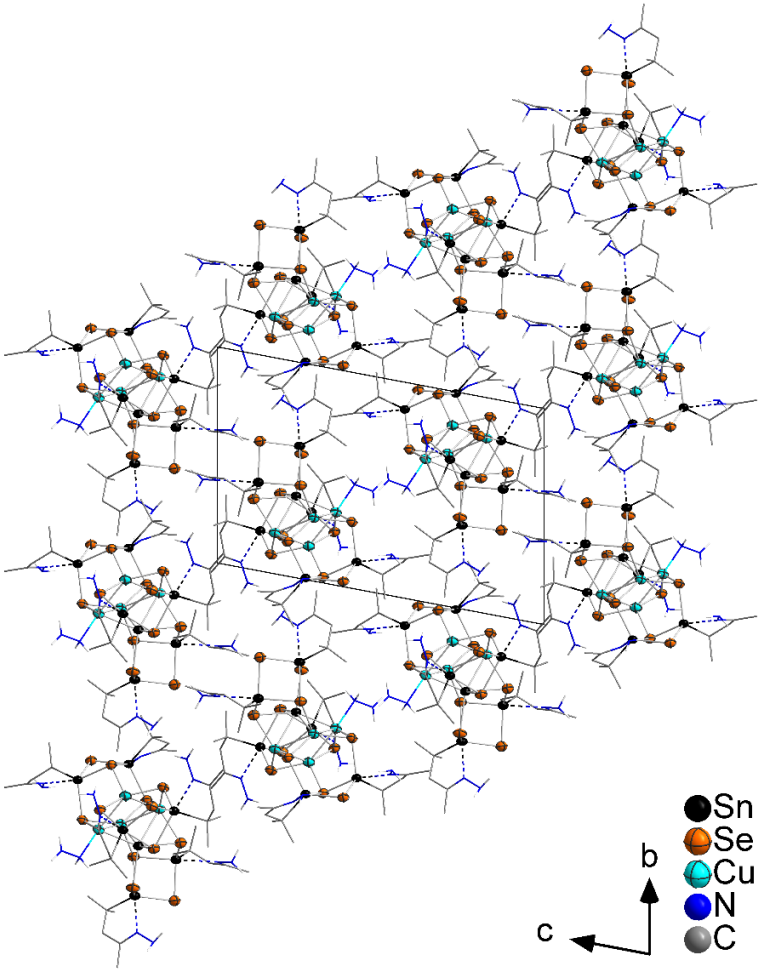

Figure S8. Excerpt of the crystal structure of **2** viewed along the *a* axis.

Table S5. Crystallographic data and refinement results of **2**.

Compound	**2**
Empirical Formula	$C_{36}H_{82}Cu_4N_{14}Se_{12}Sn_7$
Formula weight /g·mol^{-1}	2743.66
Crystal color and shape	dark orange block
Crystal size /mm^3	0.059 x 0.068 x 0.079
Crystal system	triclinic
Space group	$P\bar{1}$
a /Å	13.445(3)
b / Å	14.236(3)
c / Å	20.667(4)
α /°	78.374(15)
β /°	85.303(15)
γ /°	69.962(15)
V / Å^3	3639.7(12)
Z	2
Measurement Temperature /K	100
ρ_{calcd} / g·cm^{-3}	2.503
$\mu_{(Mo\ K\alpha)}$ / mm^{-1}	9.536
Absorption correction type	numerical
Min./max. transmission	0.2326 / 0.6769
2*θ* range / deg	3.18 – 53.93
No. of measured reflections	34386
R(int)	0.1762
Independent Reflections	15319
Independent Reflections ($I>2\sigma(I)$)	7916
No. of parameters	681
R_1 ($I>2\sigma(I)$) / wR_2 (all data)	0.0969 / 0.2309
S (all data)	0.883
Max. peak / hole / e$^-$ Å^3	4.727 / –2.900

Table S6. Fractional Atomic Coordinates (×10^4) and Equivalent Isotropic Displacement Parameters (Å^2×10^3) for **2**. U(eq) is defined as 1/3 of of the trace of the orthogonalised U_{IJ} tensor.

Atom	*x*	*y*	*z*	U(eq)	Atom	*x*	*y*	*z*	U(eq)
Sn1	3484.9(10)	1858.2(10)	8682.9(6)	40.4(3)	C1	3020(16)	2032(16)	9708(9)	45(5)
Sn2	2405.5(10)	3183.1(10)	7117.0(6)	39.2(3)	C2	2360(20)	3199(18)	9722(12)	64(6)
Sn3	5066.5(10)	3781.5(10)	7588.7(6)	39.7(3)	C3	4000(20)	1712(18)	10098(12)	64(6)
Sn4	5939.0(11)	6126.9(10)	7483.0(7)	44.9(3)	C4	2289(17)	1423(18)	9902(10)	57(6)
Sn5	7109.3(10)	4090.3(10)	8740.7(7)	42.9(3)	C5	2714(16)	357(15)	9769(10)	44(4)
Sn6	8579.0(10)	77.7(9)	7294.7(6)	38.2(3)	C6	2380(20)	-483(17)	10181(12)	57(6)
Sn7	7571.1(10)	1259.3(9)	5736.1(6)	38.6(3)	C7	1122(14)	4611(14)	6749(9)	40(4)
Se1	5325.7(15)	861.6(14)	8354.5(10)	41.8(4)	C8	818(15)	5349(14)	7233(10)	44(4)
Se2	3159.2(14)	3784.2(14)	8067.9(10)	40.7(4)	C9	1523(17)	5108(16)	6111(10)	51(5)
Se3	1998.8(15)	1826.6(15)	8008.2(10)	42.3(4)	C10	199(18)	4294(17)	6663(10)	52(5)
Se4	4000.4(14)	2449.4(14)	6416.0(9)	39.8(4)	C11	431(15)	3363(16)	6367(9)	44(4)
Se5	6966.0(14)	3070.4(14)	5882.4(9)	39.3(4)	C12	-449(15)	3172(17)	6011(12)	55(5)
Se6	9464.9(15)	245.1(14)	6144.2(9)	41.5(4)	C13	6507(17)	7033(16)	6627(11)	48(5)
Se7	6808.1(14)	271.3(14)	6762.7(9)	39.0(4)	C14	6680(20)	6550(20)	6053(12)	70(7)
Se8	8173.4(14)	1596.6(14)	7837.7(9)	39.6(4)	C15	7570(20)	7050(20)	6854(13)	69(7)
Se9	5678.7(15)	3277.8(15)	8881.9(10)	42.6(4)	C16	5672(19)	8127(14)	6497(11)	58(6)
Se10	7392.4(15)	4317.3(14)	7445.8(10)	41.4(4)	C17	4929(19)	8461(15)	7038(12)	57(6)
Se11	6378.5(17)	6005.6(16)	8693.8(10)	49.6(5)	C18	4239(17)	9584(13)	6951(13)	58(6)
Se12	4246.1(16)	5777.4(15)	7423.7(11)	49.0(5)	C19	8688(16)	3547(17)	9163(10)	50(5)
Cu1	6420.1(18)	1888.3(18)	8232.4(12)	42.8(5)	C20	9422(16)	3852(17)	8668(11)	53(5)
Cu2	5386.0(18)	1579.9(19)	7199.1(12)	46.1(6)	C21	9059(17)	2367(15)	9352(11)	50(5)
Cu3	5228.3(18)	3379.2(18)	6371.7(11)	40.8(5)	C22	8623(18)	3959(19)	9780(11)	58(6)
Cu4	6998.3(18)	2926.9(17)	7053.0(11)	41.5(5)	C23	7740(18)	3902(16)	10244(11)	51(5)
N1	4430(15)	4831(13)	5798(9)	55(4)	C24	7780(20)	4022(17)	10958(11)	66(7)
N2	3992(15)	4679(15)	5241(9)	61(5)	C25	8945(16)	-1359(15)	8022(10)	51(5)
N3	3368(13)	228(12)	9275(8)	47(4)	C26	7898(15)	-1469(14)	8304(10)	47(5)
N4	3787(16)	-657(14)	9066(9)	62(5)	C27	9560(16)	-2265(13)	7671(10)	48(5)
N5	1378(12)	2738(12)	6425(8)	43(4)	C28	9573(15)	-1230(14)	8523(10)	43(4)
N6	1642(13)	1798(11)	6219(8)	44(4)	C29	10491(16)	-851(17)	8267(11)	51(5)
N7	4881(17)	7801(14)	7549(10)	66(6)	C30	11310(20)	-950(20)	8745(13)	73(7)
N8	4170(20)	8123(19)	8048(13)	110(11)	C31	6828(16)	905(15)	4944(9)	44(4)
N9	6909(15)	3831(13)	10021(9)	52(4)	C32	5718(16)	997(17)	5144(10)	53(5)
N10	6076(17)	3737(19)	10440(9)	71(6)	C33	7491(18)	-196(17)	4871(11)	54(5)
N11	10427(13)	-383(12)	7668(7)	41(4)	C34	6889(14)	1663(17)	4319(10)	47(5)
N12	11206(14)	-9(12)	7401(9)	49(4)	C35	7937(14)	1867(14)	4201(10)	44(4)
N13	8476(12)	1717(11)	4704(7)	39(4)	C36	8242(16)	2235(15)	3514(10)	48(5)
N14	9433(13)	1920(12)	4652(9)	46(4)					

Table S7. Selected bond lengths [Å] in **2**.

Sn1–Se1	2.511(2)	Sn4–Se12	2.508(3)	Se1–Cu2	2.407(3)
Sn1–Se2	2.681(2)	Sn4–N7	2.345(17)	Se4–Cu2	2.393(3)
Sn1–Se3	2.546(2)	Sn4–C13	2.22(2)	Se4–Cu3	2.431(3)
Sn1–N3	2.446(16)	Sn5–Se9	2.534(2)	Se5–Cu3	2.401(3)
Sn1–C1	2.198(18)	Sn5–Se10	2.642(2)	Se5–Cu4	2.389(3)
Sn2–Se2	2.687(2)	Sn5–Se11	2.546(2)	Se7–Cu2	2.428(3)
Sn2–Se3	2.558(2)	Sn5–C19	2.18(2)	Se8–Cu1	2.355(3)
Sn2–Se4	2.521(2)	Sn6–Se6	2.575(2)	Se8–Cu4	2.417(3)
Sn2–N5	2.376(17)	Sn6–Se7	2.610(2)	Se9–Cu1	2.492(3)
Sn2–C7	2.208(18)	Sn6–Se8	2.510(2)	Se10–Cu4	2.509(3)
Sn3–Se2	2.671(2)	Sn6–N11	2.489(16)	Cu1–Cu2	2.823(4)
Sn3–Se9	2.742(2)	Sn6–C25	2.21(2)	Cu1–Cu4	2.785(3)
Sn3–Se12	2.632(2)	Sn7–Se5	2.497(2)	Cu2–Cu3	2.730(3)
Sn3–Cu1	2.817(3)	Sn7–Se6	2.573(2)	Cu3–Cu4	2.682(3)
Sn3–Cu3	2.666(3)	Sn7–Se7	2.638(2)	Cu3–N1	2.128(19)
Sn3–Cu4	2.713(3)	Sn7–N13	2.453(14)	N1–N2	1.42(3)
Sn4–Se10	2.658(2)	Sn7–C31	2.208(19)		
Sn4–Se11	2.577(3)	Se1–Cu1	2.373(3)		

Table S8. Selected bond angles [°] in **2**.

Se1–Sn1–Se2	105.67(8)	Se12–Sn3–Se2	85.49(7)	Se9–Sn5–Se10	100.13(8)
Se1–Sn1–Se3	115.66(8)	Se12–Sn3–Se9	101.74(8)	Se9–Sn5–Se11	113.04(8)
Se3–Sn1–Se2	88.72(8)	Se12–Sn3–Cu1	152.08(9)	Se11–Sn5–Se10	92.14(8)
N3–Sn1–Se1	86.2(4)	Se12–Sn3–Cu3	104.53(9)	Se6–Sn6–Se7	90.56(7)
N3–Sn1–Se2	167.6(4)	Se12–Sn3–Cu4	119.15(8)	Se8–Sn6–Se6	114.99(8)
N3–Sn1–Se3	83.0(4)	Cu3–Sn3–Se2	107.30(8)	Se8–Sn6–Se7	105.42(7)
C1–Sn1–Se1	122.9(6)	Cu3–Sn3–Se9	151.35(8)	N11–Sn6–Se6	82.4(3)
C1–Sn1–Se2	102.4(6)	Cu3–Sn3–Cu1	98.45(8)	N11–Sn6–Se7	168.4(3)
C1–Sn1–Se3	113.6(6)	Cu3–Sn3–Cu4	59.82(8)	N11–Sn6–Se8	86.0(4)
C1–Sn1–N3	72.9(7)	Cu4–Sn3–Se9	97.19(8)	C25–Sn6–Se6	123.8(4)
Se3–Sn2–Se2	88.33(8)	Cu4–Sn3–Cu1	60.45(7)	C25–Sn6–Se7	104.8(6)
Se4–Sn2–Se2	104.89(8)	Se11–Sn4–Se10	91.08(8)	C25–Sn6–Se8	112.1(5)
Se4–Sn2–Se3	112.64(8)	Se12–Sn4–Se10	102.25(8)	C25–Sn6–N11	72.1(7)
N5–Sn2–Se2	166.9(4)	Se12–Sn4–Se11	110.39(9)	Se5–Sn7–Se6	113.19(8)
N5–Sn2–Se3	84.8(4)	N7–Sn4–Se10	170.9(6)	Se5–Sn7–Se7	105.99(7)
N5–Sn2–Se4	88.1(4)	N7–Sn4–Se11	84.6(5)	Se6–Sn7–Se7	89.97(7)
C7–Sn2–Se2	99.4(5)	N7–Sn4–Se12	86.7(6)	N13–Sn7–Se5	89.6(3)
C7–Sn2–Se3	119.7(5)	C13–Sn4–Se10	98.7(5)	N13–Sn7–Se6	83.7(4)
C7–Sn2–Se4	122.3(5)	C13–Sn4–Se11	124.1(6)	N13–Sn7–Se7	164.4(3)
C7–Sn2–N5	74.6(6)	C13–Sn4–Se12	120.6(6)	C31–Sn7–Se5	117.2(6)
Se2–Sn3–Se9	85.86(7)	C13–Sn4–N7	77.3(7)	C31–Sn7–Se6	123.8(6)
Se2–Sn3–Cu1	102.73(8)	C19–Sn5–Se9	130.6(6)	C31–Sn7–Se7	98.6(5)
Se2–Sn3–Cu4	153.59(8)	C19–Sn5–Se10	106.2(6)	C31–Sn7–N13	73.6(6)
Se9–Sn3–Cu1	53.24(7)	C19–Sn5–Se11	107.0(6)	Cu1–Se1–Sn1	109.64(9)

Cu1–Se1–Cu2	72.39(10)	Se1–Cu1–Sn3	102.03(10)	Se4–Cu3–Cu4	130.36(12)
Cu2–Se1–Sn1	101.96(10)	Se1–Cu1–Se9	110.40(11)	Se5–Cu3–Sn3	114.49(11)
Sn1–Se2–Sn2	82.67(7)	Se1–Cu1–Cu2	54.37(9)	Se5–Cu3–Se4	130.15(11)
Sn3–Se2–Sn1	104.20(7)	Se1–Cu1–Cu4	126.73(12)	Se5–Cu3–Cu2	103.32(10)
Sn3–Se2–Sn2	102.53(7)	Se8–Cu1–Sn3	110.80(10)	Se5–Cu3–Cu4	55.75(8)
Sn1–Se3–Sn2	87.99(8)	Se8–Cu1–Se1	131.10(12)	Cu4–Cu3–Cu2	75.48(10)
Cu2–Se4–Sn2	103.92(9)	Se8–Cu1–Se9	116.72(12)	N1–Cu3–Sn3	102.4(5)
Cu2–Se4–Cu3	68.91(10)	Se8–Cu1–Cu2	103.74(10)	N1–Cu3–Se4	104.0(5)
Cu3–Se4–Sn2	109.97(9)	Se8–Cu1–Cu4	55.35(8)	N1–Cu3–Se5	99.6(5)
Cu3–Se5–Sn7	105.28(10)	Se9–Cu1–Sn3	61.84(7)	N1–Cu3–Cu2	155.9(5)
Cu4–Se5–Sn7	103.07(9)	Se9–Cu1–Cu2	125.56(11)	N1–Cu3–Cu4	124.6(5)
Cu4–Se5–Cu3	68.10(9)	Se9–Cu1–Cu4	101.53(10)	Sn3–Cu4–Cu1	61.63(7)
Sn7–Se6–Sn6	84.62(7)	Cu4–Cu1–Sn3	57.92(7)	Se5–Cu4–Sn3	113.20(11)
Sn6–Se7–Sn7	82.65(7)	Cu4–Cu1–Cu2	72.42(9)	Se5–Cu4–Se8	128.16(11)
Cu2–Se7–Sn6	108.47(10)	Se1–Cu2–Se7	103.38(11)	Se5–Cu4–Se10	115.86(11)
Cu2–Se7–Sn7	104.97(9)	Se1–Cu2–Cu1	53.24(9)	Se5–Cu4–Cu1	141.82(12)
Cu1–Se8–Sn6	104.40(10)	Se1–Cu2–Cu3	141.28(12)	Se5–Cu4–Cu3	56.15(8)
Cu1–Se8–Cu4	71.39(10)	Se4–Cu2–Se1	131.07(12)	Se8–Cu4–Sn3	112.36(10)
Cu4–Se8–Sn6	101.99(9)	Se4–Cu2–Se7	111.63(11)	Se8–Cu4–Se10	93.35(10)
Sn5–Se9–Sn3	97.39(8)	Se4–Cu2–Cu1	141.86(12)	Se8–Cu4–Cu1	53.26(8)
Cu1–Se9–Sn3	64.92(8)	Se4–Cu2–Cu3	56.20(9)	Se8–Cu4–Cu3	142.16(12)
Cu1–Se9–Sn5	102.06(9)	Se7–Cu2–Cu1	101.23(10)	Se10–Cu4–Sn3	82.35(8)
Sn5–Se10–Sn4	82.22(7)	Se7–Cu2–Cu3	106.64(11)	Se10–Cu4–Cu1	101.32(10)
Cu4–Se10–Sn4	122.61(10)	Cu3–Cu2–Cu1	96.81(11)	Se10–Cu4–Cu3	119.39(11)
Cu4–Se10–Sn5	108.65(9)	Sn3–Cu3–Cu2	74.60(8)	Cu3–Cu4–Sn3	59.22(7)
Sn5–Se11–Sn4	85.73(8)	Sn3–Cu3–Cu4	60.96(8)	Cu3–Cu4–Cu1	98.85(10)
Sn4–Se12–Sn3	97.40(8)	Se4–Cu3–Sn3	102.44(9)		
Sn3–Cu1–Cu2	70.87(8)	Se4–Cu3–Cu2	54.89(9)		

6 References for the Supporting Information

(1) Rinn, N.; Eußner, J. P.; Kaschuba, W.; Xie, X.; Dehnen, S. Formation and Reactivity of Organo-Functionalized Tin Selenide Clusters. *Chem. Eur. J.* **2016**, *22*, 3094–3104.

(2) Detty, M. R.; Seidler, M. D. Bis(trialkylsilyl) chalcogenides. 1. Preparation and reduction of group VIA oxides. *J. Org. Chem.* **1982**, *47*, 1354–1356.

(3) Hanna, J. V.; Boyd, S. E.; Healy, P. C.; Bowmaker, G. A.; Skelton, B. W.; White, A. H. Structural and solid state ^{31}P NMR studies of the four-coordinate copper(I) complexes $[Cu(PPh_3)_3X]$ and $[Cu(PPh_3)_3(CH_3CN)]X$. *Dalton Trans.* **2005**, 2547–2556.

(4) Sheldrick, G. M. Crystal structure refinement with SHELXL. *Acta Cryst., Sect. C: Struct. Chem.* **2015**, *71*, 3–8.

(5) Sheldrick, G. M. SHELXT - integrated space-group and crystal-structure determination. *Acta Cryst., Sect. A: Found. Adv.* **2015**, *71*, 3–8.

(6) Dolomanov, O. V.; Bourhis, L. J.; Gildea, R. J.; Howard, J. A. K.; Puschmann, H. OLEX2: A complete structure solution, refinement and analysis program. *J. Appl. Crystallogr.* **2009**, *42*, 339–341.

(7) Spek, A. L. PLATON SQUEEZE: a tool for the calculation of the disordered solvent contribution to the calculated structure factors. *Acta Crystallogr., Sect. C: Struct. Chem.* **2015**, *71*, 9-18.

4.3 Towards Understanding the Reactivity and Optical Properties of Organosilicon Sulfide Clusters

Katharina Hanau, Sebastian Schwan, Moritz R. Schäfer, Marius J. Müller, Christof Dues, Niklas Rinn, Simone Sanna, Sangam Chatterjee, Doreen Mollenhauer, Stefanie Dehnen, *Angew. Chem.* **2021**, *133*, 1196–1206; *Angew. Chem. Int. Ed.* **2021**, *60*, 1176–1186.

Abstract

We report about the successful extension of the class of organotetrel sulfide clusters by further examples of the still rare silicon-based species, synthesized from $RSiCl_3$ with R = phenyl (Ph, **I**), naphthyl (Np, **II**), and styryl (Sty, **III**) with Na_2S. Besides known $[(PhSi)_4S_6]$ (**IV**), new compounds $[(NpSi)_4S_6]$ (**1**) and $[(StySi)_4S_6]$ (**2**) were obtained, the first two of which underwent follow-up reactions with $[AuCl(PPh_3)]$ to form ternary complexes. Density functional theory (DFT) studies of cluster dimers helped to understand fundamental differences between the habitus of $\{Si_4S_6\}$-based vs. $\{Sn_4S_6\}$-based compounds. Investigations of the optical properties of crystalline compound **1** and intrinsically amorphous **2** indicated the former to show a pronounced nonlinear optical response, i.e. , second-harmonic generation, while for the latter, the chemical damage threshold seems to inhibit a corresponding observation that can be clearly put down to nonlinear optical effects. Calculations within the independent particle approximation (IPA) served to rationalize and compare electronic and optical excitations of $[(RSi)_4S_6]$ clusters (R = Ph, Np). The calculations reproduced the measured data and allowed for the interpretation of the main spectroscopic features.

Eigener Anteil

Die Synthese von Verbindung **3** wurde erstmals von Shen Chen im Rahmen seines Vertiefungspraktikums unter der Anleitung von Dr. Niklas Rinn und mir durchgeführt und von mir reproduziert. Zur Einkristallstrukturanalyse geeignete Kristalle

von **3** wurden von mir synthetisiert. Alle weiteren Synthesen wurden von mir geplant und durchgeführt. Die Einkristallstrukturanalysen wurden von Bertram Peters (**II**, **1**) und mir (**3**, **4**) durchgeführt und von mir ausgewertet. Die NMR-Experimente wurden von der zentralen NMR-Abteilung des Fachbereichs Chemie der Philipps-Universität Marburg unter der Leitung von Dr. Xiulan Xie durchgeführt und von mir ausgewertet. Die massenspektrometrischen und elementaranalytischen Untersuchungen wurden von der zentralen Serviceabteilung für Massenspektrometrie und Elementaranalytik des Fachbereichs Chemie der Philipps-Universität unter der Leitung von Dr. Uwe Linne durchgeführt und ausgewertet. Alle photophysikalischen Untersuchungen wurden von Marius Müller in der Arbeitsgruppe von Prof. Dr. Sangam Chatterjee an der Justus-Liebig-Universität Gießen durchgeführt und ausgewertet. Die quantenchemischen Berechnungen der strukturellen Eigenschaften der Verbindungen wurden von Sebastian Schwan und Moritz Schäfer in der Arbeitsgruppe von Prof. Dr. Doreen Mollenhauer an der Justus-Liebig-Universität Gießen durchgeführt. Die Berechnungen der optischen Eigenschaften wurden von Christof Dues in der Arbeitsgruppe von Prof. Dr. Simone Sanna an der Justus-Liebig-Universität Gießen durchgeführt. Das Manuskript wurde von allen Autor_innen gemeinsam verfasst.

How to cite: *Angew. Chem. Int. Ed.* **2021**, *60*, 1176–1186
International Edition: doi.org/10.1002/anie.202011370
German Edition: doi.org/10.1002/ange.202011370

Cluster Compounds | Hot Paper

Towards Understanding the Reactivity and Optical Properties of Organosilicon Sulfide Clusters

Katharina Hanau, Sebastian Schwan, Moritz R. Schäfer, Marius J. Müller, Christof Dues, Niklas Rinn, Simone Sanna, Sangam Chatterjee,* Doreen Mollenhauer,* and Stefanie Dehnen**

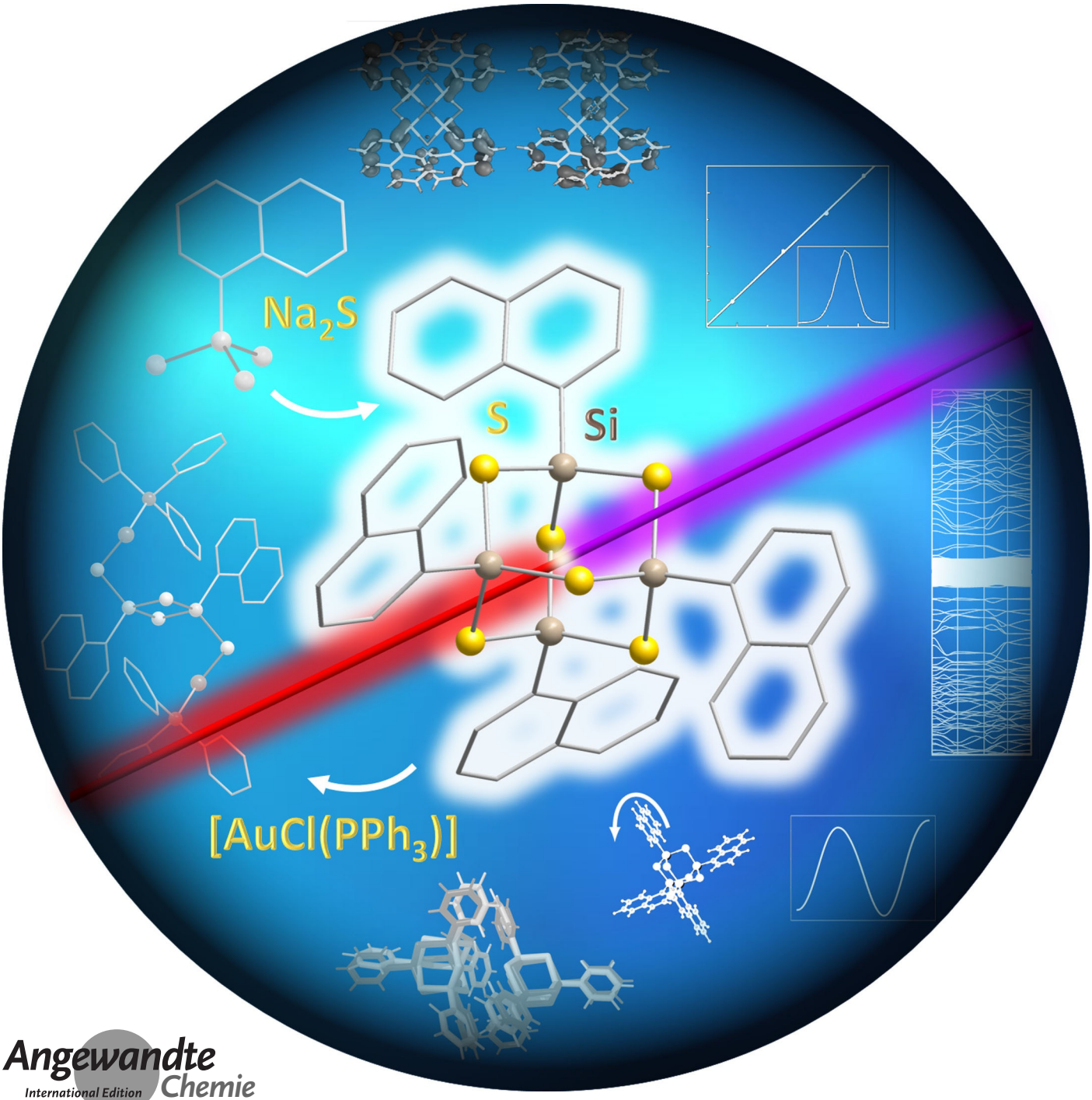

Abstract: *We report the extension of the class of organotetrel sulfide clusters with further examples of the still rare silicon-based species, synthesized from $RSiCl_3$ with R = phenyl (Ph, **I**), naphthyl (Np, **II**), and styryl (Sty, **III**) with Na_2S. Besides known $[(PhSi)_4S_6]$ (**IV**), new compounds $[(NpSi)_4S_6]$ (**1**) and $[(StySi)_4S_6]$ (**2**) were obtained, the first two of which underwent reactions with $[AuCl(PPh_3)]$ to form ternary complexes. DFT studies of cluster dimers helped us understand the differences between the habit of $\{Si_4S_6\}$- and $\{Sn_4S_6\}$-based compounds. Crystalline **1** showed a pronounced nonlinear optical response, while for intrinsically amorphous **2**, the chemical damage threshold seems to inhibit a corresponding observation. Calculations within the independent particle approximation served to rationalize and compare electronic and optical excitations of $[(RSi)_4S_6]$ clusters (R = Ph, Np). The calculations reproduced the measured data and allowed for the interpretation of the main spectroscopic features.*

Introduction

The chemical and structural properties of tetrel chalcogenide clusters with organic substituents have been extensively studied in the past.[1] In particular, a large variety of compounds has been reported for the element combinations Sn/E[1a,2] (E = S, Se, Te) and Ge/E,[1c,3] whereas significantly fewer compounds with Si/E-based cluster cores have been known so far.[1b,4] Several studies investigating the reactivity and properties of tin chalcogenide clusters were undertaken, showing the possible derivatization of the organic substituents[5,2f] as well as the formation of ternary inorganic cluster cores by introducing transition metal complexes.[6]

In addition to the chemical features of such clusters, the styryl-substituted cluster $[(StySn)_4S_6]$ (Sty = 4-vinylphenyl), which was determined via DFT calculations to have a heteroadamantane-type molecular structure, was recently shown to possess an extreme nonlinear optical behavior.[7] These findings led to the investigation of further compounds of the type $[(RSn)_4S_6]$ with cyclic and/or aromatic substituents R to understand how the substituents influence the compounds' properties. Generally, it was shown that distinct order within the solid material (crystallinity or pronounced π-stacking interactions) leads to second-harmonic generation (SHG), while a high degree of amorphousness results in white-light generation (WLG).[8]

In this context, we intended to find out, whether the principles of Sn/E chemistry can also be applied to the Si/E elemental combination, and whether a replacement of Sn atoms with Si atoms leads to changes in the cluster's reactivity and properties. Herein, we present the first results of these studies.

The preparation of corresponding silicon analogs from $RSiCl_3$ (R = organic substituent) and a corresponding chalcogen source is much more challenging than the corresponding tin or germanium chemistry, as the use of the most appropriate reactant, $E(SiMe_3)_2$ (E = S, Se, Te), logically lacks the driving force of Si–Cl bond formation. Here, a Si–Cl bond needs to be cleaved at the same time in the other reactant. So, the use of binary chalcogen salts such as A_2E (A = alkali metal) is required, which leads to a more complicated work-up. However, besides the reproduction of known $[(PhSi)_4S_6]$ (**IV**) we herein report on the successful synthesis of two new organosilicon sulfide compounds, $[(NpSi)_4S_6]$ (**1**) and $[(StySi)_4S_6]$ (**2**), their characterization and follow-up chemistry with gold complexes to form ternary complexes $[\{RSi(\mu\text{-}S)\}_2\{AuPPh_3(\mu\text{-}S)\}_2]$ (**3**: R = Ph, **4**: R = Np). We used density functional theory (DFT) methods to gain insight in structural features of the adamantane-based compounds, in particular regarding inter-cluster interactions that contribute to the macroscopic habitus of the solid. All new compounds were investigated regarding their linear and nonlinear optical properties, which were additionally studied by means of quantum chemistry. The calculations explain the preferred habitus of the compounds, and reveal the deep impact of the ligands in the optical response

Results and Discussion

Syntheses, Crystal Structures and Spectroscopic Data

The reactions of $RSiCl_3$ with R = phenyl (Ph, **I**), naphthyl (Np, **II**), and styryl (Sty, **III**) with Na_2S discussed herein are summarized in Scheme 1.

While synthesizing $NpSiCl_3$ (**II**) as a precursor for $[(NpSi)_4S_6]$ (**1**), single crystals were obtained upon distillation, and the molecular structure (Figure 1, left) was determined via single crystal X-ray diffraction. As expected, the Si atom

[*] K. Hanau, Dr. N. Rinn, Prof. Dr. S. Dehnen
Fachbereich Chemie und Wissenschaftliches Zentrum für Materialwissenschaften (WZMW), Philipps-Universität Marburg
Hans-Meerwein-Str. 4, 35043 Marburg (Germany)
E-mail: dehnen@chemie-uni-marburg.de
S. Schwan, M. R. Schäfer, Prof. Dr. D. Mollenhauer
Institute of Physical Chemistry, Justus Liebig University Giessen
Heinrich-Buff-Ring 17, 35392 Giessen (Germany)
and
Center for Materials Research (LaMa), Justus Liebig University Giessen
Heinrich-Buff-Ring 16, 35392 Giessen (Germany)
E-mail: Doreen.Mollenhauer@phys.Chemie.uni-giessen.de
M. J. Müller, Prof. Dr. S. Chatterjee
Institute of Experimental Physics I and Center for Materials Research (LaMa), Justus Liebig University Giessen
Heinrich-Buff-Ring 17, 35392 Giessen (Germany)
E-mail: Sangam.Chatterjee@exp1.physik.uni-giessen.de
C. Dues, Prof. Dr. S. Sanna
Institute of Theoretical Physics and Center for Materials Research (LaMa), Justus Liebig University Giessen
Heinrich-Buff-Ring 16, 35392 Giessen (Germany)
E-mail: simone.sanna@theo.physik.uni-giessen.de
Supporting information and the ORCID identification number(s) for the author(s) of this article can be found under: https://doi.org/10.1002/anie.202011370.

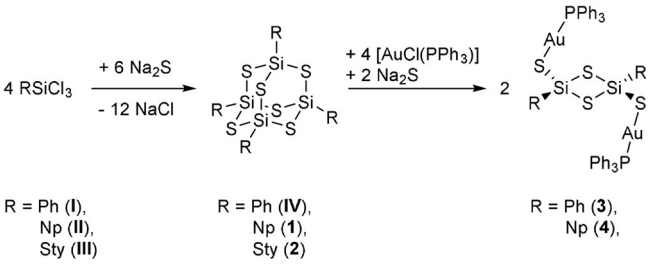

Scheme 1. Summary of reactions done to produce compounds **IV** and **1**–**5**.

exhibits a trigonal pyramidal coordination environment. Furthermore, π-interactions between the naphthyl substituents are observed in the unit cell, alternating between parallel-displaced π-stacking and T-shaped CH/π-interactions (Figure 1, right). The distance between the adjacent naphthyl rings with π-stacking is slightly larger (3.4397(18) Å) than the distance between the layers in graphene (3.35 Å),[9] whereas the distance between the center of one of the naphthyl rings to the closest H atom of the next perpendicular naphthyl ring (2.9371(1) Å) is in the typical range of strong CH/π-interactions.[10]

The reaction of **II** with 1.5 equivalents of Na_2S affords a crystalline, colorless solid. Upon dissolution in toluene and cooling to −25 °C, single crystals of $[(NpSi)_4S_6]\cdot 0.5\,C_7H_8$ (**1**·0.5 C_7H_8) suitable for X-ray diffraction were obtained. The molecular structure of **1** is shown in Figure 2. **1** crystallizes in the triclinic space group $P\bar{1}$ with two molecules per asymmetric unit. Like $[(PhSi)_4S_6]$, **1** is an adamantane-type Si/S cluster with four organic substituents, each bound to one Si atom. The molecule shows minor deviations from T_d symmetry, due to slightly different angles in the inorganic core and different orientations of the organic substituents. Furthermore, the two individuals differ greatly in the orientation of the organic substituents (see Figure 2, bottom), indicating a very low energy barrier for rotation of the organic substituents about the Sn–C bond, which in most cases leads to intrinsic amorphousness. Notably, while both $[(PhSn)_4S_6]$ and $[(NpSn)_4S_6]$ are amorphous (with the Np compound

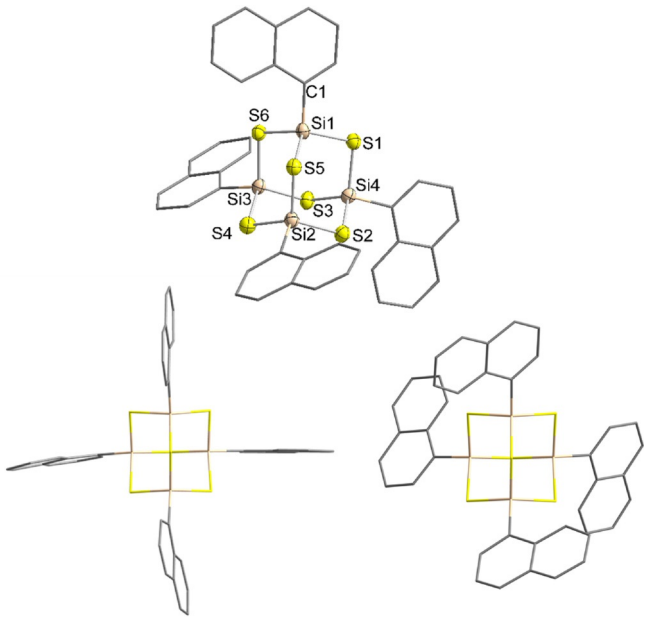

Figure 2. Molecular structure of **1** (top) and visualization of the two different orientations of the organic substituents in the two individuals within the asymmetric unit (bottom); the structure at the top refers to the bottom right individual. Ellipsoids drawn at 50% probability level. H atoms omitted for clarity. Selected distances and angles [Å, °]: Si–S 2.111(3)–2.153(3), Si–C 1.837(8)–1.876(8); Si–S–Si 103.42(11)–105.64(13), S–Si–S 110.31(12)–113.28(12), S–Si–C 104.1(3)–110.1-(2).[15]

comprising a considerable amount of order according to its optical response, see also below),[7b] the two Si analogs are crystalline. Initially, this was ascribed to the smaller radius of the Si/S core with respect to the Sn/S core only, as the corresponding smaller volume per given number of cluster molecules causes the aromatic rings of neighboring clusters to approach more closely overall, and thus form more efficient π-stacking interactions. In this work, we present a refined version of this interpretation (see below).

The reaction of $StySiCl_3$ (**III**) with 1.5 equivalents of Na_2S should proceed similarly and lead to the formation of

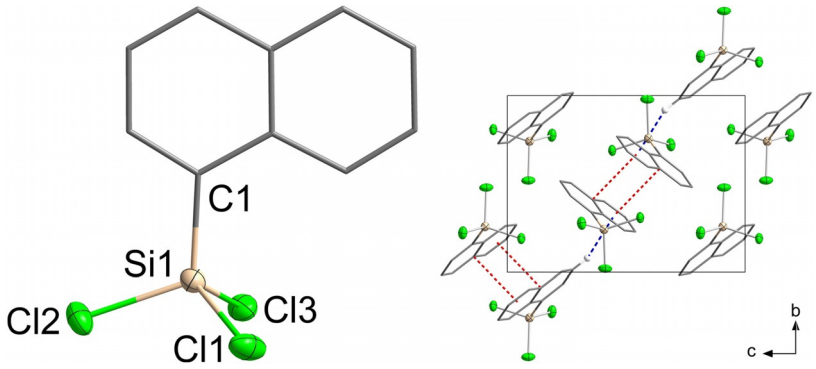

Figure 1. Molecular structure (left) and crystal structure (right) of **II**. Ellipsoids drawn at 50% probability level. H atoms omitted for clarity; π-stacking and CH/π-interactions are indicated as dashed lines. Selected distances and angles [Å, °]: Si–Cl 2.0313(7)–2.0385(7)), Si–C 1.8426(18); Cl–Si–Cl 106.42(3)–107.58(3), Cl–Si–C 111.42(6)–112.56(6), $C_{Np}\cdots\pi$ (red) 3.4397(18), C_{Np}-H$\cdots\pi$ (blue) 2.9371(1).[15]

$[(StySi)_4S_6]$ (**2**). However, only the crude product could be isolated upon evaporation of the solvent in form of a colorless "solid" with the consistency of cotton candy or honey—depending on the duration of the reaction and drying process. We attribute this to the high polymerization tendency of the styryl substituents, and the corresponding oligomerization/polymerization that proceeds visibly as time goes by. Notably, this was not the case for the Sn analogs, which we take as a further hint for the correlation of the nature of the T/E cluster core with the properties of the organic substituents: in the Sn/S clusters, the styryl substituents of neighboring cluster units are obviously not close enough to allow for a chemical reaction of neighboring vinyl groups. As a consequence of the different situation with an underlying Si/S cluster core, **2** could neither be obtained as single crystals, nor could individual clusters be detected by means of liquid injection field desorption/ionization (LIFDI) or electrospray ionization (ESI) mass spectrometry. However, we were able to collect ^{29}Si NMR data of a freshly prepared sample of **2** that turned out to be sufficiently soluble. A downfield shift of ≈9 ppm of the observed singlet with respect to the precursor signal is in accordance with the NMR data of other Si/S adamantane-type clusters and their corresponding organosilicon trichloride precursors reported previously, such as $[(EtSi)_4S_6]$/$EtSiCl_3$, $[(PhSi)_4S_6]$/$PhSiCl_3$, or $[(CH_2{=}CHSi)_4S_6]$/$CH_2{=}CHSiCl_3$.[11] Another indication is given by the ^{1}H and ^{13}C NMR spectra, which clearly show the signals of the styryl substituent at a significant downfield-shift compared to the starting compound **III**, with the *ipso*- and *meta*-atoms being the most affected, which indicates a reaction at the Si atom to have taken place. Hence, the NMR data indicate the formation of a compound comprising individual adamantane-type clusters $[(StySi)_4S_6]$. Yet we assume that they start to unstoppably form oligo-/polymers shortly upon synthesis.

Further studies on the reactivity of the adamantane-like organosiliconsulfide clusters were undertaken. The addition of Na_2S and $[AuCl(PPh_3)]$ leads to the fragmentation of the clusters and the formation of the four-membered rings $[\{RSi(\mu\text{-}S)\}_2\{AuPPh_3(\mu\text{-}S)\}_2]$ (**3**: R = Ph, **4**: R = Np). Colorless single crystals of **3**·CH_2Cl_2 and **4** were obtained by layering the respective reaction solutions with *n*-hexane. Their molecular structures are shown in Figure 3. **3**·CH_2Cl_2 crystallizes in the monoclinic space group *C*2/*c*, and **4** crystallizes in the triclinic space group $P\bar{1}$, both with half a molecule per asymmetric unit. The molecules in these compounds have an inversion center in the center of an $\{RSi(\mu\text{-}S)\}_2$ ring, with nearly linear $\{Au(PPh_3)(\mu\text{-}S)\}$ substituents attached to the Si atoms. Although the structural parameters of the central unit in both compounds are quite similar, they differ significantly in the orientation of the $\{Au(PPh_3)(\mu\text{-}S)\}$ units: whereas they point away from the central $\{Si_2S_2\}$ ring in **3** with a C1–Si1–S2–Au1 *cis* arrangement, the corresponding atoms in **4** show a *trans* arrangement. Thus, while the interatomic distances in these compounds are similar, the Si1–S2–Au1 and S2–Au1–P1 bond angles are different. Homologous Sn/S compounds exhibiting this structural motif as well as a *cis* or *trans* arrangement depending on the organic moiety at the tetrel atom were described previously, showing the same trends in the T–S–Au and S–Au–P bond angles.[12]

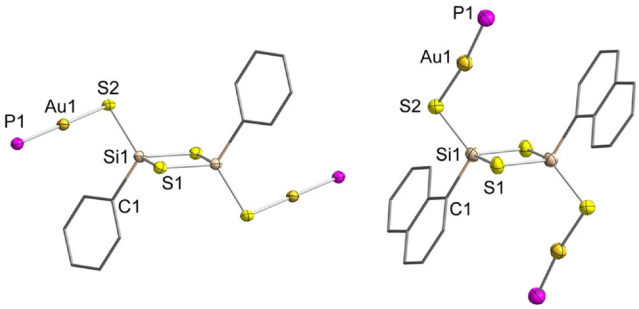

Figure 3. Molecular structure of **3** (left) and **4** (right) Ellipsoids drawn at 50% probability level. H atoms and P-bound phenyl groups omitted for clarity. Selected distances and angles [Å, °]: **3**: Si–S 2.091(2)–2.144(2), S–Au 2.3136(16), Au–P 2.2534(16), Si–C 1.870(7); Si–S–Si 82.40(9), S–Si–S 97.60(9)–115.54(10), Si–S–Au 90.97(7), S–Au–P 178.03(6). **4**: Si–S 2.095(2)–2.1589(3), S–Au 2.297(2), Au–P 2.256(2), Si–C 1.865(8), Si–S–Si 82.58(10), S–Si–S 97.42(10)–115.64(10), Si–S–Au 103.57(9), S–Au–P 173.35(7).[15]

Upon fragmentation of the adamantane-type cluster and formation of **4**, a further downfield shift by 5.6 ppm was observed in the ^{29}Si NMR spectrum. Table 1 summarizes the respective NMR data for compounds **I**–**IV**, **1**, **2**, and **4**. Note that NMR data of compound **3** were not obtained owing to very poor solubility of the crystals.

Table 1: ^{29}Si NMR shifts of compounds **I**–**IV**, **1**, **2**, and **4** reported in this work.

Compound	I	II	III	IV	1	2	4
δ (^{29}Si)/ppm	−0.9	−0.4	−0.9	10.9	6.8	8.7	12.4

Quantum Chemical Investigation of Structural Features

It was experimentally shown, that $[(PhSi)_4S_6]$ (**IV**) and $[(NpSi)_4S_6]$ (**1**) are observed in a crystalline phase, while $[(PhSn)_4S_6]$ and $[(NpSn)_4S_6]$ are intrinsically amorphous. Nevertheless, it was suggested that $[(NpSn)_4S_6]$ features a structure with a higher amount of order compared to $[(PhSn)_4S_6]$, owing to more efficient π-stacking interactions between the Np substituents as compared to the Ph substituents.[7] This assumption was based on the different nonlinear optical responses of the two compounds, which showed SHG (requiring phase matching) for the Np compound but not for the Ph analog, for which WLG was reported.

To explain the general difference observed in the $[(RSn)_4S_6]$ and $[(RSi)_4S_6]$ cluster compounds with R = Ph, Np, one may consider the smaller radius of the $\{Si_4S_6\}$ core with respect to the $\{Sn_4S_6\}$ core to enable a stronger interaction of the neighboring clusters through more efficient π-stacking interactions. To investigate this hypothesis, quantum chemical calculations of the interaction in cluster dimers as a minimal model were carried out, which already provide valuable insights into the cluster interaction that can be transferred to the extended crystalline or amorphous material.

In order to classify the flexibility of the substituents, we initially calculated the rotation barriers of the substituents for both cluster cores. Rotation barriers of the substituent at the single cluster are hardly present (< 1 kJ mol^{-1}) for the clusters with phenyl substituents, while for the clusters with naphthyl substituents, a barrier height of 17 kJ mol^{-1} is obtained for the $[(NpSi)_4S_6]$ cluster and 9 kJ mol^{-1} for the $[(NpSn)_4S_6]$ cluster (see Figure 4 and Figure S12). The larger rotation barrier for the cluster with an $\{Si_4S_6\}$ core as compared to the cluster with an $\{Sn_4S_6\}$ core can indeed be explained by the smaller core radius. The smaller Si–C distance in this cluster (1.889 Å) in comparison with the corresponding Sn–C distance (2.088 Å) increases the barrier by a stronger interaction between the hydrogen atom of the substituent and the sulfur atoms of the cluster. The relative positions of S and H atoms at the rotation barrier are visualized in Figure 5.

Furthermore, the substituent–substituent interaction can increase the rotation barrier, but this is of minor importance for the considered conformers. In summary, the calculations indicate a high orientational flexibility for phenyl substituents on both Si/S and Sn/S clusters, as opposed to a comparatively lower freedom of orientation for naphthyl substituents. The latter show a higher orientational flexibility for the cluster with larger core radius (Sn/S) than for those with smaller core radius (Si/S), which is in agreement with the tendency for (a) higher order in compounds with R = Np than in compounds with R = Ph, and (b) higher order in $\{Si_4S_6\}$-based clusters than in $\{Sn_4S_6\}$-based clusters.

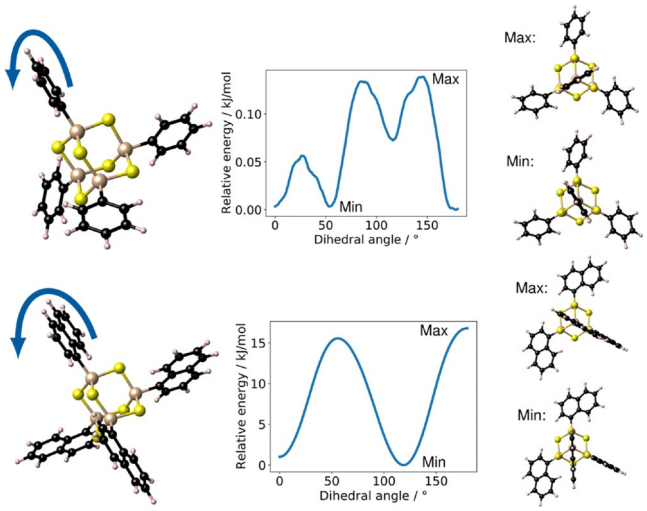

Figure 4. Scan of the phenyl group (top) and naphthyl group (bottom) rotations by variation of the dihedral angle for corresponding clusters $[(PhSi)_4S_6]$ and $[(NpSi)_4S_6]$ calculated at the BP86-D3/cc-pVDZ(-PP) level of theory. Structures at the minimum and maximum positions of the scan are shown on the right hand side. The corresponding scans for the Sn/S core cluster analoges are given in Figure S12.

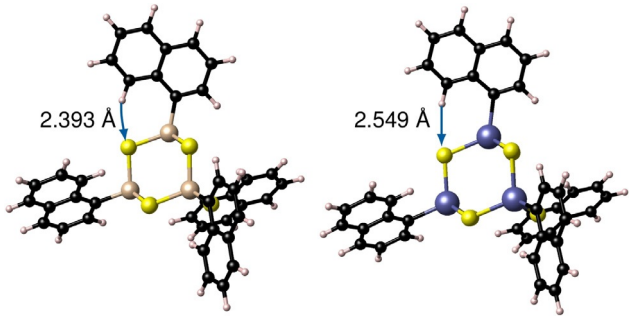

Figure 5. Comparison of the S–H distances at the energetic maximum of the rotational scan for $[(NpSi)_4S_6]$ (left) and $[(NpSn)_4S_6]$ (right), calculated at the BP86-D3/cc-pVDZ(-PP) level of theory.

The investigation of the cluster dimer structures was performed to analyze the interaction between the molecules with different cluster cores and substituents. The cluster dimer structures were determined by two computational approaches and their results were combined to obtain a larger number of possible conformers. The dissociation energies of all cluster dimers are plotted against their core–core distance in Figure 6, and selected cluster dimer structures are plotted in Figure 7.

First, we discuss the obtained cluster dimers in regard of their core–core distances and geometric structures. Most of the cluster dimers have a distance of the two adamantane cores between 5.9 and 6.5 Å (orange region in Figure 6). The $[(PhSi)_4S_6]$ cluster dimers show a core–core distance range that is shifted to slightly smaller values than the range calculated for $[(NpSi)_4S_6]$. The same trend, but even more pronounced, is observed for the $\{Sn_4S_6\}$-based cluster dimers. Cluster dimers in this region of inter-cluster distances yielded stacked or alternating substituents and different orientations of the cluster cores (Figure 7). In all of them, a minimum of two substituents of one cluster interact with at least two substituents of the other cluster. In the "stacked dimer" conformers, the substituents are arranged directly towards each other. In the "alternating dimer" conformers, the substituents of one cluster are located in a void between the substituents of the other cluster. Interestingly, the "alternating dimer" structure is slightly preferred on average for clusters with phenyl substituents, while for naphthyl substituents the "stacked dimer" structure is slightly preferred. The

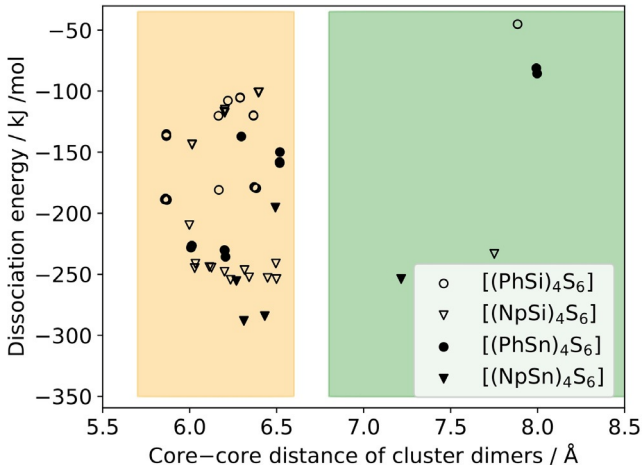

Figure 6. Dissociation energy of cluster dimers, plotted against the corresponding core–core distance calculated at the BP86-D3/cc-pVDZ-(-PP) level of theory. Medium core–core distances are indicated by an orange background, large core–core distances by a green background. The region of small core–core distances is plotted in Figure S13.

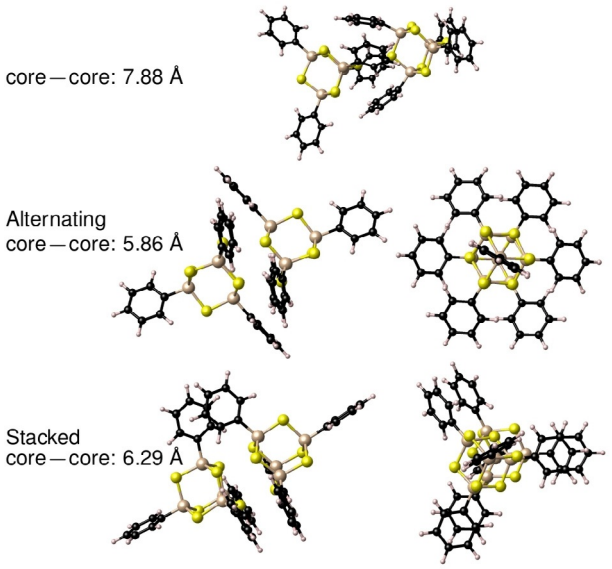

Figure 7. Examples for cluster dimers emerging from the calculations, shown for dimers of $[(PhSi)_4S_6]$ calculated at the BP86-D3/cc-pVDZ(-PP) level of theory. Top: cluster dimer with a large core–core distance. Centre: cluster dimer with medium core–core distance and alternating substituents (two views). Bottom: cluster dimer with medium core–core distance and stacked substituents (two views).

core–core distances between Si/S and Sn/S clusters, respectively, differ only slightly for analogous cluster dimers (by ≈ 0.15 Å on average). The "alternating dimers" show a high similarity to the arrangement of the cluster in the crystal structures, as demonstrated for $[(PhSi)_4S_6]$ in Figure 8. Although similar structural units are present, the core–core distance in the crystal structure (closest core–core distances: 7.05–7.46 Å in **IV**, 7.44–7.58 Å in **1**) is much larger (by 0.5 to 1.0 Å) as compared to the calculated cluster dimers, as in the crystal, the interaction is shared between more than two clusters. Besides the majority of cluster dimers with a core–core distance between 6.0 and 6.5 Å, there are a few cluster dimers with core–core distances between 7.2 and 8.0 Å, with a poor relative orientation of the clusters to each other (green region in Figure 6; example of a structure shown in Figure 7, top). The Si/S cluster dimers with phenyl and naphthyl

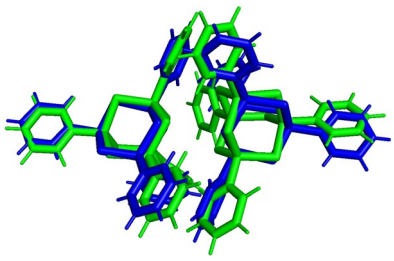

Figure 8. Comparison of the relative orientation of $[(PhSi)_4S_6]$, as an example of the generated dimer structures (green, core–core distance 6.37 Å) calculated at the BP86-D3/cc-pVDZ(-PP) level of theory, and a dimer extracted from the crystal structure of $[(PhSi)_4S_6]$[7a] (blue, core–core distance 7.05 Å), indicating the good agreement of the model with the experimental data.

substituents listed in this green region show larger core–core distances than the corresponding crystal structures. On the other hand, for some of the Sn/S-based cluster dimers, we found a fusion of cluster structures (purple region in Figure S13). Since we do not consider them to be relevant for the solid-state structures of this study, we have not considered the fused clusters further.

Second, we discuss the obtained cluster dimers depending on their dissociation energy. Considering each individual cluster composition, the majority of dimer clusters with core–core distances between 5.9 and 6.5 Å yield higher absolute dissociation energies as compared to the absolute dissociation energies of the cluster dimers with core–core distances between 7.2 and 8.0 Å. The difference in dissociation energies between the medium and large core–core cluster dimers is smaller for clusters with Np ligands than for those with Ph ligands.

Considering the cluster dimers with core–core distances between 5.9 and 6.5 Å, there are 2–3 regions of dissociation energies for the individual cluster compositions in Figure 6, each of which correlates with a certain number of substituents interacting with each other. Thus, the highest dissociation energies were obtained for cluster dimers in which three substituents of one cluster interact with three substituents of the other one. The "stacked dimer" and "alternating dimer" conformers for individual cluster compositions yield similar dissociation energies. Among the cluster dimers with highest dissociation energies, $[(NpSi)_4S_6]$ exhibits a dissociation energy that is by about 65 kJ mol^{-1} higher than that of $[(PhSi)_4S_6]$. A similar, but slightly smaller, difference in dissociation energies is calculated for the corresponding $\{Sn_4S_6\}$-based cluster dimers (≈ 53 kJ mol^{-1}). Obviously, the larger Np substituents lead to a stronger interaction between cluster dimers than Ph substituents. Other than originally anticipated, the investigation of the cluster dimers did not indicate larger dispersive interaction for clusters comprising a smaller radius of the cluster core. The $\{Sn_4S_6\}$-based clusters have a higher absolute dissociation energy than the $\{Si_4S_6\}$-based cluster dimers, which illustrates a stronger interaction overall. To understand this result, we performed a decomposition analysis of the cluster dimer binding energy contributions into the substituent–substituent interaction, the substituent–core and core–core interaction (see Figure 9).

The decomposition of the binding energy reveals similar substituent–substituent binding energies for cluster dimers with the same substituent. The larger naphthyl substituents show a higher binding energy than the smaller phenyl substituents due to larger dispersive interactions. In contrast, the core–core binding energy is larger for the Sn/S-based cluster dimers than for the Si/S based cluster dimers due to the larger adamantane core. This stronger core–core interaction for the larger Sn/S-based cluster dimers leads to higher absolute values of the dissociation energies than observed for the Si/S-based analogs. For the cluster dimers with larger core–core distances (green region in Figure 6), the same trend in dissociation energies is observed, although larger core–core distances are found here than for crystalline $[(PhSi)_4S_6]$ and $[(NpSi)_4S_6]$. We therefore believe that these insights can be transferred to crystalline and amorphous cluster materials

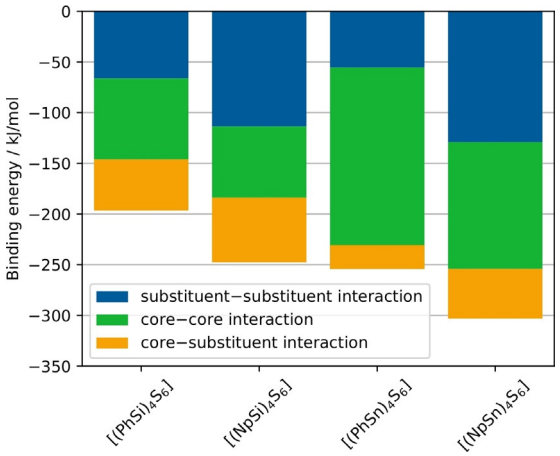

Figure 9. Decomposition of the binding energy contributions of cluster dimers into substituent–substituent interaction, the substituent–core and core–core interaction calculated at the BP86-D3/cc-pVDZ(-PP) level of theory.

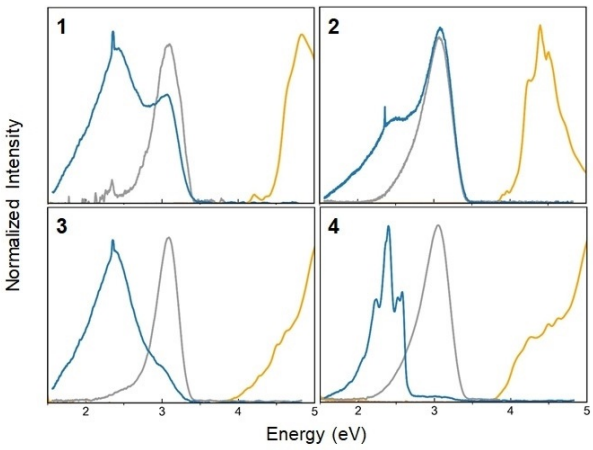

Figure 10. Linear absorption spectra in solution (yellow line) and photoluminescence spectra (solid = blue line, solution = gray line) of compounds (**1**–**4**).

with core–core distances between the medium and large core–core distance regions of Figure 6.

In conclusion, we propose that the predominance of the relatively isotropic core–core interactions in $[(PhSn)_4S_6]$ outplay the rather directional interactions involving the substituents, which explains why this compound shows a distinctly lower tendency for order in the solid than the crystalline $\{Si_4S_6\}$-based homologue. This trend is also visible for the clusters with Np substituents, yet for $[(NpSn)_4S_6]$ the relatively similar strengths of core–core and substituent–substituent interactions allow for a higher degree of intermolecular order, which is in agreement with the (virtually contradicting) experimental findings: the powder produces SHG (as a sign of phase matching) in spite of an apparently amorphous nature according to X-ray diffraction. The results of this study thus contribute significantly to the overall understanding of the origin of (dis)order in compounds of the type $[(RT)_4E_6]$ (T = Si, Ge, Sn; E = S, Se, Te).

Optical Properties

We explored the optical response of compounds **1**–**4** by optical spectroscopy. The absorption and emission spectra are summarized in Figure 10.

Clearly, the emission and absorption data are mirror-image-like for the solution data. The emission spectra of the solid phase show an additional resonance about 500 meV below the emission maximum in solution. Such features are commonly attributed to excitons or an ensemble thereof. Notably, the higher-energy emission maximum persists in the condensed matter phase for all samples. However, it is significantly quenched by the existence of Au/S moieties in compounds **3** and **4** in contrast to **1** and **2**. This apparently enhances the lower-energy emission channels. In particular, for compound **4**, several distinct emission channels are observed which are tentatively attributed to transitions involving atomic orbitals of the Au^I atom.

The crystalline compound **1** shows a clear nonlinear optical response. In agreement with the observation made for **IV**,[7b] we observe SHG here in spite of the centrosymmetric space group, which therefore is attributed to surface effects or defects of the crystal (see Figure 11). The other compounds, in general, do not show a nonlinear response that is clearly distinguishable from luminescence effects owing to chemical transformations. Hence, we can neither confirm nor exclude that the adamantane-based compound **2** exhibits WLG, but its significantly higher chemical sensitivity to oxygen and humidity as compared to the heavier homologue hampers a clear statement to date (note that it is technically not possible to prevent that the samples are exposed to air for a very short moment prior to the measurement).

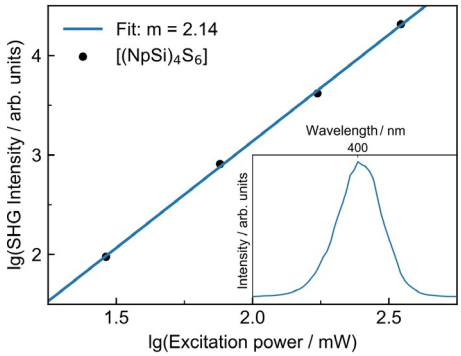

Figure 11. Nonlinear optical response of compound **1**. Excitation power dependency of SHG. SHG spectrum from excitation at 800 nm (inset).

Calculation of Optical Properties

We investigated the role of the substituents (phenyl vs. naphthyl) on the optical response of the molecular clusters. Thereby, we modeled two of the synthesized clusters with the same core but different substituents, $[(PhSi)_4S_6]$ and $[(NpSi)_4S_6]$. The structural relaxation of single clusters and molecular crystals performed by the plane-wave implemen-

tation of the DFT within the periodic supercell method leads to geometries of the same symmetry and in overall close agreement with the structures calculated with a localized basis. The optimized geometries were employed for the calculation of the electronic and optical excitations.

Figure 12 shows the relaxed geometry as well as the HOMO and LUMO states for the $[(PhSi)_4S_6]$ and $[(NpSi)_4S_6]$ clusters. The structural differences between the cluster cores of the two molecules are limited. The Si–S distance amounts to 2.15 Å in both clusters, while the S–C bond length is 1.87 Å in $[(PhSi)_4S_6]$ and 1.88 Å in $[(NpSi)_4S_6]$. However, the different substituents have a deeper impact on the molecular electronic structure. The (degenerate) HOMO of the $[(PhSi)_4S_6]$ molecule is localized at the S atoms in the cluster core, while the HOMO of the $[(NpSi)_4S_6]$ cluster is localized on the naphthyl rings. The LUMO of both systems is similar and localized on the substituents (see Figure 12). Thus, the DFT-calculated HOMO–LUMO gap of the two systems is rather different and amounts to 3.76 eV for $[(PhSi)_4S_6]$ and 2.96 eV for the $[(NpSi)_4S_6]$ cluster. Quasiparticle effects, calculated in an approximate manner by the ΔSCF method as described in Ref. [13], open up the fundamental independent-particle-approximation (IPA) gap to a value of 6.54 eV for $[(PhSi)_4S_6]$ and 5.09 eV for the $[(NpSi)_4S_6]$ cluster (see Figure S15 in the Supporting Information). The energy of the lowest excitonic excitation, describing the transition of one electron to the LUMO leaving a hole behind in the HOMO, is calculated following the procedure described in Ref. [13]. Excitonic excitations of 3.92 eV for $[(PhSi)_4S_6]$ and 2.89 eV for the $[(NpSi)_4S_6]$ cluster, respectively, are predicted. These energies are rather close to the HOMO–LUMO gap, suggesting that the quasiparticle shifts are nearly canceled out by the electron-hole attraction. Thus, as many-body effects due to the electron-electron and the electron-hole interaction counterbalance, the IPA-calculated optical excitation spectra are expected to yield a reasonable description of the measured optical response, at least for the low-energy excitations.

The extinction coefficient of $[(PhSi)_4S_6]$ (blue line) and $[(NpSi)_4S_6]$ (black line) single clusters is shown in Figure 13. The components of the dielectric tensor are averaged to allow for a direct comparison with experimental data later in the manuscript. The general shapes of the dielectric functions are rather different, although the structures of the two clusters are similar. In order to rationalize these differences and understand their origin, we analyzed the electronic transitions of the two clusters. Indeed, spectral resonances can be directly related to electronic transitions between occupied and empty states at the IPA level.

The onset of the optical absorption corresponds exactly to the DFT-calculated HOMO–LUMO transition in the case of the $[(NpSi)_4S_6]$ cluster (black line). Structures in the first peak match quite well the energy of the HOMO–LUMO + 1,2 (degenerate) and HOMO–LUMO + 3. The main peak at about 4 eV is mainly due to transitions from the HOMO to a group of energetically close states localized at the C atoms of the naphthyl rings. Instead, in the case of the $[(PhSi)_4S_6]$ cluster (blue line), the onset of the optical absorption is located at much higher energies than the DFT-calculated HOMO–LUMO difference. Indeed, the HOMO–LUMO transition probability is small, due to the different spatial localization and orbital character of the two states. We assign the first spectral peak to transitions from the HOMO to three molecular orbitals about 4.4 eV above the HOMO and with a spatial extension partially overlapping the HOMO. Summarizing, the absorption spectra of $[(PhSi)_4S_6]$ and $[(NpSi)_4S_6]$ clusters are rather different concerning the positions and line shapes of the spectral features. The deviations in the optical response originate from the qualitatively different and differently localized electronic states involved in the transitions resulting in the main spectral peaks of the two compounds.

The optical answer of the isolated clusters represents the basis for understanding the absorption spectra of the solid material comprising the molecules. According to the calculations, which started from the experimental crystal data, the

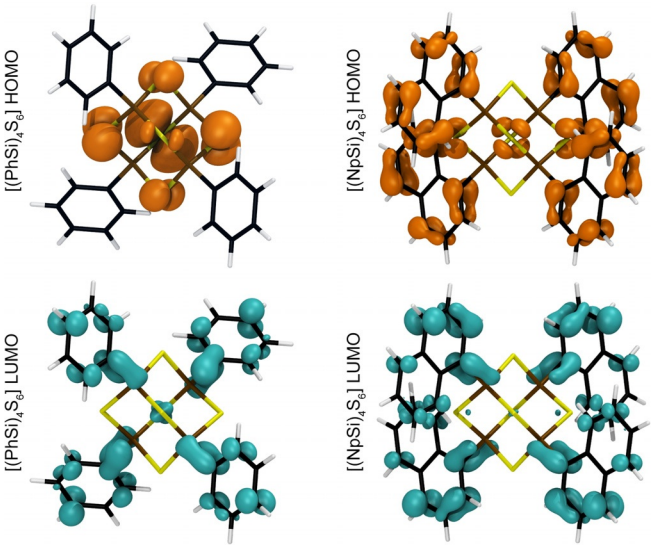

Figure 12. Optimized molecular structures and orbital characters of the HOMO and LUMO states of $[(PhSi)_4S_6]$ (left) and $[(NpSi)_4S_6]$ (right) single clusters.

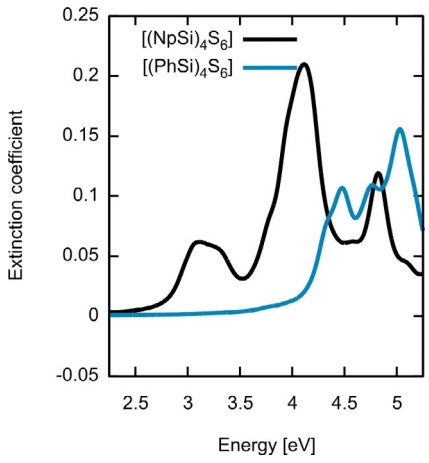

Figure 13. Extinction coefficients calculated in the independent-particle approximation for isolated $[(PhSi)_4S_6]$ (blue line) and $[(NpSi)_4S_6]$ (black line) clusters.

optimized geometries show only small modifications of the geometrical parameters determined for the isolated molecules. The largest bond length deviation is 1.4 pm, while the bond angles of the substituents are rotated by 13.2° with respect to the single molecules due to the presence of toluene. When the single clusters aggregate to form the crystalline material, the discrete energy levels broaden to become energy bands. These have been calculated in the IPA approximation along the directions in reciprocal space shown in Figure S16, and are illustrated in Figure 14. The electronic band gap of the crystals is slightly smaller than the HOMO–LUMO energy differences of the corresponding molecules; however, the orbital characters of valence and conduction band edges closely resembles those of the HOMO and LUMO of the parent molecules (see Figure 12). As the band dispersion is rather flat and no major rearrangement is expected upon inclusion of quasiparticle effects, self-energy correction mainly serves to widen the band gap, and may be replaced by a numerically less costly scissors-shift for the calculation of the optical response.

We then proceeded with the optical characterization of the synthesized crystalline compounds. Owing to the synthesis method, the experimental crystal structure of $[(NpSi)_4S_6]$ (**1**) comprises toluene molecules (0.5 C_7H_8 per formula unit of **1**, see Table S1). As illustrated in Figure S17, the extinction coefficient calculated with and without toluene does not substantially differ, demonstrating that the optical response of the molecular cluster is not affected by the presence of solvent. The extinction coefficient calculated within the IPA for the $[(PhSi)_4S_6]$ (**IV**) derived and $[(NpSi)_4S_6]$ (**1**) derived molecular crystals is shown in Figure 15.

For both compounds, the spectral signatures of the isolated clusters are clearly recognizable in the optical answer of the corresponding molecular crystals. They barely shift in energy, and the relative intensity compares well with that predicted for the single clusters. It can thus be concluded that the transitions leading to the absorption peaks of the single clusters are chiefly responsible for the major peaks in the dielectric function of the semiconducting crystals. The main difference between molecules and crystals comprising these molecules is that the crystal absorption features are broadened with respect to the molecular peaks due to the energy dispersion of the molecular states upon aggregation. As the onset of the molecular and crystalline absorption coincides, we can exclude new intermolecular low-energy electronic transitions to occur when the clusters aggregate to form crystals. Thus, for the investigated compounds, the molecules seem to individually interact with light rather than jointly. However, the relative orientation of the molecules in the solids (ordered vs. non-ordered) controls the nature of the nonlinear optical response (with or without phase matching).

In order to compare the calculated spectra of the crystalline material comprising $[(NpSi)_4S_6]$ cluster (**1**) with the measured data, we accounted for many-body effects in an approximated manner by means of a scissors-shift.[14] We chose a scissor-shift of 0.7 eV, correcting the DFT underestimation of the experimentally measured band gap of the molecular crystals. The corresponding results are shown by the blue line Figure 16 together with experimental results (yellow line) from Figure 10. The comparison with the experimental data shows that calculations at the IPA level with scissors-shifts already agree with the measurements.

The calculations fairly describe the main absorption peak, originating from transitions between the valence band edge

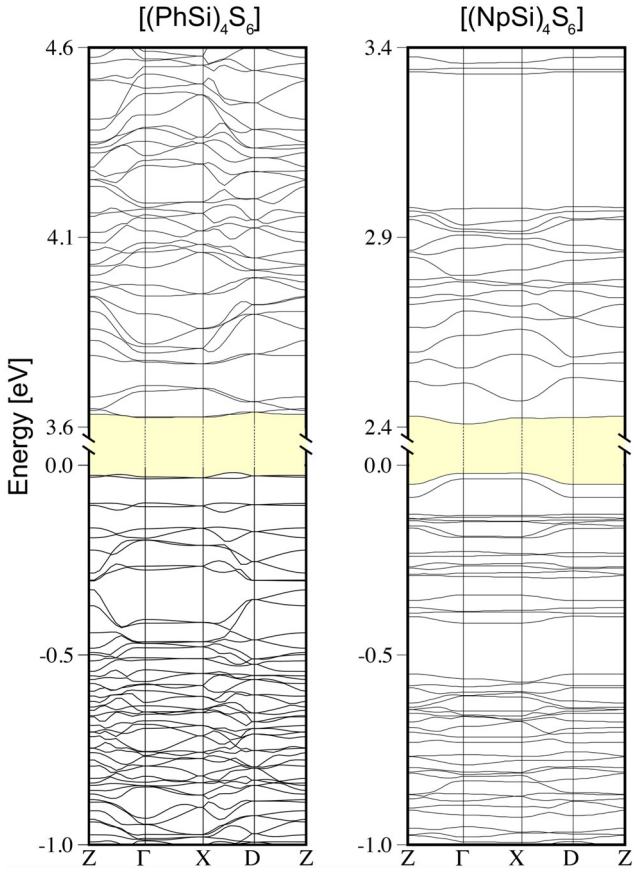

Figure 14. Electronic structure of the crystals comprising $[(PhSi)_4S_6]$ and $[(NpSi)_4S_6]$ molecules calculated within the IPA. The fundamental band gap is indicated in yellow.

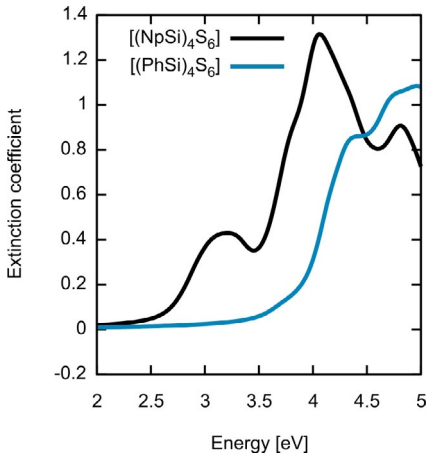

Figure 15. Extinction coefficient of the $[(PhSi)_4S_6]$ derived (blue line) and $[(NpSi)_4S_6]$ derived (black line) molecular crystals calculated within the IPA at the DFT equilibrium geometry.

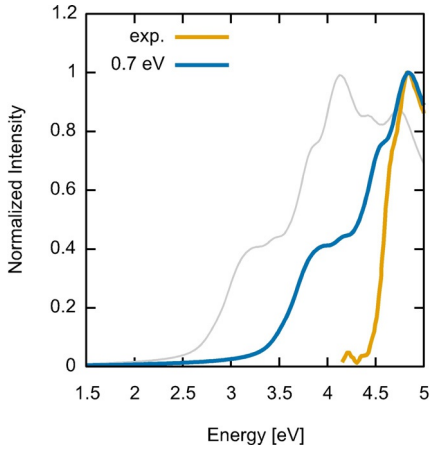

Figure 16. Extinction coefficient of the crystals comprising $[(NpSi)_4S_6]$ molecules, calculated within the IPA with scissor-shifts of 0.7 eV (blue line). The measured curve (yellow line) as well as the IPA calculation without scissors-shift (gray line) are shown for comparison.

and bands localized at the C atoms of the naphthyl rings, including the shoulder observed at about 4.6 eV. However, the intensity of the peak at about 3.5 eV corresponding to the transition from the valence band maximum to the conduction band minimum is overestimated in the calculations in comparison with the measured spectra. More refined and computationally demanding approaches accounting for quasiparticle effects in a perturbative manner and accounting for the electron-hole attraction by means of the Bethe-Salpeter equation might further improve the agreement with the experiment.

The calculation of the second-order polarizability tensor for the crystalline phases of $[(PhSi)_4S_6]$ (**IV**) and $[(NpSi)_4S_6]$ (**1**) shows vanishing optical nonlinearities for all tensor components, as expected for a centrosymmetric crystal structure. Deviations from this behavior in experiments thus arise from structural defects and amorphous regions in the samples, as well as from surface-related contributions. At least for centrosymmetric crystals, they are not inherent bulk properties.

Conclusion

We presented the synthesis of new members of the rare class of organosilicon sulfide clusters of the general formula $[(RSi)_4S_6]$. We added new members with R = naphthyl (Np, **1**) and styryl (Sty, **2**), which were investigated with respect to their reactivity towards $[AuCl(PPh_3)]$, their structures, and their optical properties by a combination of comprehensive experimental and theoretical studies. The investigations contributed to characterize and further understand the chemical behavior of such clusters, which showed to behave differently from the much better known germanium and tin homologues. Our studies indicate a much more pronounced tendency to polymerization in case of **2** than observed for its Sn homologue, and confirm the expected, much higher air and water sensitivity of the Si compounds. Second, the observation that clusters with the combination Ph/Si/S (reported previously) and Np/Si/S (**1**) are crystalline, while the Sn homologues are amorphous was studied on the bases of cluster dimer models calculated with DFT methods. Different types of intra-cluster interactions were found, that led to different dissociation energies as a function of the nature of the substituents, their relative orientation, and the core compositions $\{Si_4S_6\}$ versus $\{Sn_4S_6\}$. The detailed study ultimately helped to explain the experimental findings on the basis of much stronger isotropic interactions in the $\{Sn_4S_6\}$-based cases in comparison with directional interactions that play a much more notable role in the $\{Si_4S_6\}$-based materials. Regarding the optical properties of the new compounds and the products of their reaction with the gold complex, we could show that the emission is quenched upon fragmentation and formation of the gold compounds. Moreover, the crystalline compound **1** was proved to exhibit SHG as a consequence of high order that allows for phase matching; however, the SHG signal does not stem from the crystalline bulk but should be attributed to surface phenomena or structural defects. The behavior of **2** is clearly different, but its chemical nature inhibited a statement regarding the compound's nonlinear response. The experimental findings were corroborated by static and time-dependent DFT calculations of both the molecules and the crystalline material, which are in full agreement with the measurements and therefore indicate the applicability of the used methods and models.

Acknowledgements

This work was supported by the Deutsche Forschungsgemeinschaft within the framework of GRK 1782 and FOR 2824. S.C. acknowledges personal support through the Heisenberg Programme under contracts (CH660/02 and CH660/08). The Höchstleistungrechenzentrum Stuttgart (HLRS) is gratefully acknowledged for grants of high-performance computer time. The authors acknowledge the computational resources provided by the HPC Core Facility and the HRZ of the Justus Liebig University Giessen. Open access funding enabled and organized by Projekt DEAL.

Conflict of interest

The authors declare no conflict of interest.

Keywords: DFT calculations · gold · nonlinear optics · organosilicon chalcogenide clusters · X-ray diffraction

[1] a) P. Pfeiffer, R. Lehnardt, *Ber. Dtsch. Chem. Ges.* **1903**, *36*, 3027–3030; b) J. A. Forstner, E. L. Muetterties, *Inorg. Chem.* **1966**, *5*, 552–554; c) K. Moedritzer, *Inorg. Chem.* **1967**, *6*, 1248–1249.

[2] a) C. Dorfelt, A. Janeck, D. Kobelt, E. F. Paulus, H. Scherer, *J. Organomet. Chem.* **1968**, *14*, P22–P24; b) R. A. Varga, C. Silvestru, *Acta Crystallogr. Sect. E* **2007**, *63*, m2789–m2789; c) Z. Hassanzadeh Fard, C. Müller, T. Harmening, R. Pöttgen, S.

Dehnen, *Angew. Chem. Int. Ed.* **2009**, *48*, 4441 – 4444; *Angew. Chem.* **2009**, *121*, 4507 – 4511; d) N. Rinn, J. P. Eußner, W. Kaschuba, X. Xie, S. Dehnen, *Chem. Eur. J.* **2016**, *22*, 3094 – 3104; e) J. P. Eußner, R. O. Kusche, S. Dehnen, *Chem. Eur. J.* **2015**, *21*, 12376 – 12388; f) B. Peters, N. Lichtenberger, E. Dornsiepen, S. Dehnen, *Chem. Sci.* **2020**, *11*, 16 – 26.

[3] a) M. N. Bochkarev, L. P. Maiorova, N. S. Vyazankin, G. A. Razuvaev, *J. Organomet. Chem.* **1974**, *82*, 65 – 71; b) S. Heimann, M. Hołyńska, S. Dehnen, *Chem. Commun.* **2011**, *47*, 1881 – 1883; c) E. Dornsiepen, S. Dehnen, *Dalton Trans.* **2019**, *48*, 3671 – 3675.

[4] a) J. C. J. Bart, J. J. Daly, *Chem. Commun.* **1968**, 1207; b) F. Fehér, R. Lüpschen, *Z. Naturforsch. B* **1971**, *26*, 1191 – 1192; c) M. Unno, D. Ishii, H. Matusmoto, *Bull. Chem. Soc. Jpn.* **1999**, *72*, 2469 – 2473; d) U. Herzog, G. Rheinwald, *J. Organomet. Chem.* **2001**, *628*, 133 – 143; e) V. Y. Lee, S. Miyazaki, H. Yasuda, A. Sekiguchi, *J. Am. Chem. Soc.* **2008**, *130*, 2758 – 2759; f) P. Zark, A. Schäfer, A. Mitra, D. Haase, W. Saak, R. West, T. Müller, *J. Organomet. Chem.* **2010**, *695*, 398 – 408; g) K. Schwedtmann, A. Hepp, K. Schwedtmann, J. J. Weigand, F. Lips, *Eur. J. Inorg. Chem.* **2019**, 4719 – 4726; h) D. Reiter, P. Frisch, D. Wendel, F. M. Hörmann, S. Inoue, *Dalton Trans.* **2020**, *49*, 7060 – 7068.

[5] a) K. Hanau, N. Rinn, M. Argentari, S. Dehnen, *Chem. Eur. J.* **2018**, *24*, 11711 – 11716; b) J.-P. Berndt, A. Engel, R. Hrdina, S. Dehnen, P. R. Schreiner, *Organometallics* **2019**, *38*, 329 – 335.

[6] a) E. Dornsiepen, E. Geringer, N. Rinn, S. Dehnen, *Coord. Chem. Rev.* **2019**, *380*, 136 – 169; b) E. Dornsiepen, F. Pieck, R. Tonner, S. Dehnen, *J. Am. Chem. Soc.* **2019**, *141*, 16494 – 16500; c) E. Dornsiepen, F. Weigend, S. Dehnen, *Chem. Eur. J.* **2019**, *25*, 2486 – 2490; d) K. Hanau, N. Rinn, S. Dehnen, *Inorg. Chem.* **2020**, *59*, 198 – 202.

[7] a) N. W. Rosemann, J. P. Eußner, A. Beyer, S. W. Koch, K. Volz, S. Dehnen, S. Chatterjee, *Science* **2016**, *352*, 1301 – 1304; b) N. W. Rosemann, J. P. Eußner, E. Dornsiepen, S. Chatterjee, S. Dehnen, *J. Am. Chem. Soc.* **2016**, *138*, 16224 – 16227.

[8] a) E. Dornsiepen, F. Dobener, S. Chatterjee, S. Dehnen, *Angew. Chem. Int. Ed.* **2019**, *58*, 17041 – 17046; *Angew. Chem.* **2019**, *131*, 17197 – 17202; b) E. Dornsiepen, F. Dobener, N. Mengel, O. Lenchuk, C. Dues, S. Sanna, D. Mollenhauer, S. Chatterjee, S. Dehnen, *Adv. Opt. Mater.* **2019**, *7*, 1801793.

[9] D. D. L. Chung, *J. Mater. Sci.* **2002**, *37*, 1475 – 1489.

[10] M. Nishio, *Phys. Chem. Chem. Phys.* **2011**, *13*, 13873 – 13900.

[11] H.-G. Horn, M. Hemeke, *Chem. Ztg.* **1982**, *106*, 263 – 266.

[12] a) K. Jurkschat, S. van Dreumel, G. Dyson, D. Dakternieks, T. J. Bastow, M. E. Smith, M. Dräger, *Polyhedron* **1992**, *11*, 2747 – 2755; b) J. P. Eußner, S. Dehnen, *Chem. Commun.* **2014**, *50*, 11385 – 11388.

[13] A. Riefer, S. Sanna, A. Schindlmayr, W. G. Schmidt, *Phys. Rev. B* **2013**, *87*, 53.

[14] F. Schmidt, A. Riefer, W. G. Schmidt, A. Schindlmayr, M. Imlau, F. Dobener, N. Mengel, S. Chatterjee, S. Sanna, *Phys. Rev. Mater.* **2019**, *3*, 239.

[15] Deposition Number(s) 2015922 (for **II**), 2015925 (for **1**), 2015923 (for **3**), and 2015924 (for **4**) contain(s) the supplementary crystallographic data for this paper. These data are provided free of charge by the joint Cambridge Crystallographic Data Centre and Fachinformationszentrum Karlsruhe Access Structures service www.ccdc.cam.ac.uk/structures.

Manuscript received: August 21, 2020
Revised manuscript received: October 1, 2020
Accepted manuscript online: October 2, 2020
Version of record online: December 15, 2020

Towards Understanding the Reactivity and Optical Properties of Organosilicon Sulfide Clusters

Katharina Hanau,[a] Sebastian Schwan,[b,c] Moritz R. Schäfer,[b,c] Marius J. Müller,[d] Christof Dues,[e] Niklas Rinn,[a] Simone Sanna,*[e] Sangam Chatterjee,*[d] Doreen Mollenhauer,*[b,c] and Stefanie Dehnen*[a]

[a] Prof. Dr. S. Dehnen, K. Hanau
Fachbereich Chemie und Wissenschaftliches Zentrum für Materialwissenschaften (WZMW)
Philipps-Universität Marburg
Hans-Meerwein-Str. 4, 35043 Marburg, Germany
E-mail: dehnen@chemie-uni-marburg.de.

[b] Prof. Dr. Doreen, Mollenhauer, Sebastian Schwan, Moritz R. Schäfer
Institute of Physical Chemistry
Justus Liebig University Giessen
Heinrich-Buff-Ring 17, 35392 Giessen, Germany
E-mail: Doreen.Mollenhauer@phys.Chemie.uni-giessen.de

[c] Prof. Dr. Doreen, Mollenhauer, Sebastian Schwan, Moritz R. Schäfer,
Center for Materials Research (LaMa)
Justus-Liebig University Giessen
Heinrich-Buff-Ring 16, 35392 Giessen, Germany

[d] Prof. Dr. S. Chatterjee, M. J. Müller
Institute of Experimental Physics I and Center for Materials Research (LaMa)
Justus Liebig University Giessen
Heinrich-Buff-Ring 17, 35392 Giessen, Germany
E-mail: Sangam.Chatterjee@exp1.physik.uni-giessen.de

[e] Prof. Dr. S. Sanna, C. Dues
Institut für Theoretische Physik and Center for Materials Research (LaMa)
Justus-Liebig-Universität Gießen,
Heinrich-Buff-Ring 16, 35392 Gießen, Germany
E-mail: simone.sanna@theo.physik.uni-giessen.de

Supporting Information

1 Methods

General synthetic methods: All syntheses were performed under exclusion of air and moisture using standard Schlenk techniques. All solvents were dried and freshly distilled prior to use. $NpSiCl_3$,[1] $StySiCl_3$,[2] $[(PhSi)_4S_6]$,[3] Na_2S,[4] and $[AuCl(PPh_3)]$[5] were prepared according to literature procedures. Further chemicals were purchased from Sigma Aldrich.

Spectroscopy and spectrometry: ^1H, ^{13}C, ^{29}Si, and ^{31}P NMR spectra were recorded with a Bruker AV 500 (**2**, **3**, **4**) or a Bruker AV III HD 300 (**1**) spectrometer. The chemical shifts are given in ppm relative to the residual protons of deuterated solvents for ^1H spectra and relative to the solvent signal for ^{13}C spectra. ^{13}C, ^{29}Si, and ^{31}P spectra were measured with ^1H decoupling. LIFDI mass spectra were recorded with an AccuTOF GCv mass spectrometer (JEOL). Micro X-ray fluorescence spectroscopy (μ-XRF) was carried out using a Bruker M4 Tornado spectrometer with an Rh target X-ray tube, poly-capillary optics and a Si drift detector. Elemental analysis was performed on an Elementar vario MICRO CUBE apparatus.

Single-crystal X-ray diffraction: Crystals suitable for X-ray diffraction were investigated with a STOE STADIVARI (**II**, **1**) or a STOE IPDS2 (**3**, **4**) diffractometer at 100 K. The STADIVARI uses Cu-K_α radiation (λ = 1.54186) from an X-ray micro source with X-ray optics and a Pilatus 300K Si hybrid pixel array detector. The IPDS2 uses Mo-K_α radiation and a graphite monochromator (λ = 0.71073). Upon spherical (STADIVARI) or numerical (IPDS2) absorption correction and scaling (STOE LANA), the structure solution was performed by direct methods followed by full-matrix-least-squares refinement against F^2, using SHELXT15, SHELXL15, and OLEX2 software.[6]

Single crystals of $NpSiCl_3$ (II) suitable for X-ray diffraction were isolated after distillation of the product.

Synthesis of $[(NpSi)_4S_6]$ (1): $NpSiCl_3$ (2.277 g, 8.7 mmol) was dissolved in 5 mL THF and Na_2S (1.019 g, 13.1 mmol) was suspended in 17 mL THF. Both flasks were cooled to 0 °C and the $NpSiCl_3$-solution was added slowly to the Na_2S-suspension. The reaction mixture was stirred for 18 h and allowed to warm to room temperature. After removal of the solvent *in vacuo*, the resulting white solid was extracted with 36 mL toluene and NaCl was filtered off. The volume of the filtrate was reduced *in vacuo* until the first crystals formed and the filtrate was stored at -25 °C for 2 d to obtain **1** as a colorless, crystalline solid. Some solid was redissolved in toluene to yield single crystals of **1** suitable for single crystal x-ray diffractometry. Yield: 22.1%. ^1H NMR (300 MHz, C_6D_6, 25 °C): δ = 2.11 (s, 1.5H, C*H*$_3$ (Tol)), 7.02 (m, 1H, *o*-/*p*-Tol), 7.13 (m, 1H, *m*-Tol), 7.30-7.35 (m, 2H, Np), 7.54-7.62 (m, 3H, Np), 8.32-8.34 (m, 1H, Np), 9.34-9.40 (m, 1H, Np) ppm. ^{13}C NMR (75.5 MHz, C_6D_6, 25 °C): δ = 21.4 (s, Tol), 125.2 (s, Np), 125.7 (*p*-Tol), 126.1 (s, Np), 127.3 (s, Np), 128.6 (s, *m*-Tol), 129.3 (s, *o*-Tol), 129.6 (s, Np), 131.5 (s, Np), 133.4 (s, Np), 134.4 (s, Np), 135.8 (s, Np), 137.9 (s, *i*-Tol) ppm. **^{29}Si NMR** (59.65 MHz, C_6D_6, 25 °C): δ = 6.8 (s) ppm. **HR-LIFDI-MS:** $C_{40}H_{28}S_6Si_4$ (**1**): calc. 811.95923, found: 811.95619. 0 **Elemental analysis:** Calculated for $C_{40}H_{28}S_6Si_4{\cdot}0.5(C_7H_8)$: C 60.79, H 3.75, S 22.38; found: C 60.70, H 3.934, S 19.351. The relatively large deviation of S is a systematic error found for our sulfide clusters.

Synthesis of $[(StySi)_4S_6]$ (2): Na_2S (0.4984 g, 6.39 mmol) was suspended in 10 mL THF and $StySiCl_3$ (1.012 g, 4.26 mmol) was added slowly at 0 °C. The reaction mixture was stirred for 18 h and allowed to warm to room temperature. After removal of the solvent *in vacuo*, the resulting colorless “oil” was extracted with 20 mL toluene and NaCl was filtered off. The solvent was removed under reduced pressure to yield **2** as crude product. Yield: 85.9%. **^{1}H NMR** (500.2 MHz, C_6D_6, 25 °C): δ = 5.07 (d, J_{HH} = 10.9 Hz, 1H, $C_6H_4CHCH_2$), 5.54 (d, J_{HH} = 17.7 Hz, 1H, $C_6H_4CHCH_2$), 6.43 (dd, J_{HH} = 10.9 Hz, J_{HH} = 17.6 Hz, 1H, $C_6H_4CHCH_2$), 7.19 (d, $^3J_{HH}$ = 8.1 Hz, 2H, *m*-Ph), 7.97 (d, $^3J_{HH}$ = 8.1 Hz, 2H, *o*-Ph) ppm. **^{13}C NMR** (125.8 MHz, C_6D_6, 25 °C): δ = 116.5 (s, vinyl *C*H_2), 127.0 (s, *m*-Ph), 133.4 (s, *o*-Ph), 134.5 (s, *p*-Ph), 136.4 (s, vinyl *C*H), 141.6 (s, *ipso*-Ph) ppm. **^{29}Si NMR** (99.4 MHz, C_6D_6, 25 °C): δ

= 8.7 ppm. **Elemental analysis:** Calculated for $C_{32}H_{28}S_6Si_4$: C 53.58, H 3.93, S 26.82; found: C 51.95, H 4.104, S 21.933. Elemental analyses did not provide satisfactory result, as it has so far not been possible to isolate the product in a pure (or defined) form owing to its immediate oligomerization/polymerization tendency, and its very different to handle macroscopic consistency (see main text).

Synthesis of [{PhSi(μ-S)}$_2${AuPPh$_3$(μ-S)}$_2$] (3): [(PhSi)$_4$S$_6$] (100 mg, 0.163 mmol), Na_2S (51 mg, 0.652 mmol), and [AuCl(PPh$_3$)] (184 mg, 0.372 mmol) were dissolved in 20 mL dichloromethane at −40 °C. The mixture was stirred and allowed to warm to room temperature for 18 h. After filtration, the colorless solution was layered with *n*pentane to give colorless blocks of **3** (82.5 mg, 20%). Due to the low solubility of the crystals, NMR spectra of **3** could not be recorded. **Elemental analysis:** Calculated for $C_{48}H_{40}Au_2P_2S_4Si_2{\cdot}CH_2Cl_2$: C 43.85, H 3.15, S 9.56; found: C 43.88, H 3.141, S 8.973.

Synthesis of [{NpSi(μ-S)}$_2${AuPPh$_3$(μ-S)}$_2$] (4): [(NpSi)$_4$S$_6$] (114 mg, 0.140 mmol), Na_2S (44 mg, 0.561 mmol), and [AuCl(PPh$_3$)] (139 mg, 0.390 mmol) were dissolved in 20 mL dichloromethane at −40 °C. The mixture was stirred and allowed to warm to room temperature for 18 h. After filtration, the colorless solution was layered with 10 mL *n*pentane to give colorless blocks of **4** (60 mg, 15.8%). **^{29}Si-NMR** (99.4 MHz, CD_2Cl_2, 25 °C): δ = 12.4 ppm. **Elemental analysis:** Calculated for $C_{56}H_{44}Au_2P_2S_4Si_2{\cdot}CH_2Cl_2$: C 47.47, H 3.22, S 8.89; found: C 46.88, H 3.12, S 5.514.

Computational details for the structural studies: Density functional theory (DFT) calculations were performed using the Gaussian09 software package.[7] All structure optimizations and frequency calculations were carried out by applying the generalized gradient approximation density functional BP86 combined with the Grimme dispersion correction with Becke-Johnson damping.[8] All elements with the exception of Sn were described with an all-electron correlation consistent valence double-zeta Dunning-type basis set (cc-pVDZ).[9] For Sn, the effective core potential ECP28MDF in combination with the related cc-pVDZ-PP was applied.[10] Furthermore, density fitting was employed for all calculations. Frequency calculations have been performed for all optimized structures to confirm these as minimum structures. Imaginary frequencies (below 22 cm^{-1}) were obtained for several monomer and dimer cluster structures, however. These were identified as rotational contributions of non-interactive phenyl or naphthyl rings. The clusters with phenyl substituents exhibit smaller imaginary frequencies than naphthyl-substituted clusters, which correlates with the rotation barriers of these substituents.

Rotational scans of the phenyl- and naphthyl groups for optimized single cluster [(PhSi)$_4$S$_6$], [(NpSi)$_4$S$_6$], [(PhSn)$_4$S$_6$], and [(NpSn)$_4$S$_6$] were performed using the built-in scan tool from Gaussian09. The conformers with lowest energy serve for this study. The conformers of the monomers [(PhSi)$_4$S$_6$], [(NpSi)$_4$S$_6$], [(PhSn)$_4$S$_6$], and [(NpSn)$_4$S$_6$] are structurally very similar. One of the four substituents was rotated while the dihedral angles of the other three substituents with respect to the adamantane core were fixed.

Cluster interactions of dimers consisting of two [(PhSi)$_4$S$_6$], [(NpSi)$_4$S$_6$], [(PhSn)$_4$S$_6$], or [(NpSn)$_4$S$_6$] clusters, respectively, were investigated. The starting structures of the cluster dimers were generated for AdPh$_4$ and AdNp$_4$ dimers, with a small adamantane core in order to obtain a variety of conformers (rotation barrier is the largest). The elements, the structure and the core−core distances were adjusted to the desired compound. This way, a large number of starting structures were specified for all compounds.

Two different approaches were used to generate the cluster dimers. First, a conformer analysis was performed with the program CREST[11] with the xTB-GFN2 method,[12] which was developed by Grimme *et al*. With CREST, 70 to 120 conformers of AdPh$_4$ and AdNp$_4$ were obtained due to the flat energy potential curves. The dimer structures with a root-mean-square deviation (RMSD) of atomic positions smaller than 1.1 Å were considered as similar

structures and assigned to a group. From each group, the structure with the lowest energy was chosen for the DFT calculation conducted thereupon. This left 7 conformers for cluster dimers with phenyl substituents and 10 conformers for cluster dimers with naphthyl substituents, for which the core was modified to a larger Si/S or Sn/S adamantane-type cores. The core−core distances were adjusted accordingly. To test this approach, the same calculations were repeated with CREST for $[(NpSi)_4S_6]$, and very similar results were obtained.

In order to find additional conformers, cluster dimers were created by using dimer starting structures extracted from the crystal structure of $AdPh_4$.[13] Before optimization, the adamantane core was adjusted to the larger Si/S or Sn/S adamantane-type cores, and the core-core distances were increased to prevent steric hindrance between the phenyl substituents. In addition, the phenyl and naphthyl groups of these cluster dimers were systematically rotated. From the 2178 cluster dimers obtained, 13 dimers of each stoichiometry were randomly chosen for the DFT optimization.

For further characterization of the cluster dimer structures, we calculated the core−core distances as difference between the centers of mass of the monomers. The dissociation energy E_{Diss} was calculated by subtracting the energy of the monomer $E_{Mono,opt}$ from the total energy of the dimer structure $E_{Dim,opt}$:

$$E_{\mathrm{Diss}} = E_{\mathrm{Dim,opt}} - 2 \cdot E_{\mathrm{Mono,opt}}$$

Thus, 23 different conformers were determined for the $[(PhSi)_4S_6]$ and $[(PhSn)_4S_6]$ dimers and 20 different conformers for the $[(NpSi)_4S_6]$ and $[(NpSn)_4S_6]$ dimers.

The binding energy of the most favorable cluster dimers were calculated by subtracting the energies of the singly calculated monomers in the frozen structure of the dimer from the cluster dimer energy. To gain a deeper insight into the individual binding energy contributions, we calculated the binding energy of the core−core interaction and the substituent−core interaction. Starting from the optimized structure of the most favorable cluster dimer, we removed the substituents and added hydrogen atoms at the right distance and direction to the cluster cores. The binding energy of the frozen-core structures were calculated as descripted above. This procedure was repeated under consideration of the substituents. The outermost substituent was removed, because it does not contribute to the interaction. In order to calculate the binding energy between the substituents of the first cluster and the core of the second cluster, we subtracted the core−core binding energy and the substituent−core binding energy from the total binding energy. With this procedure, we assume to obtain a realistic estimate of the different binding energy contributions for cluster dimers.

Optical spectroscopy: The linear absorption data were acquired in a Cary 3 Bio UV vis spectrometer; compounds (**1**) and (**2**) were dissolved in THF, compounds (**3**) and (**4**) were dissolved in DCM. For the corresponding photoluminescence data, the solutions were excited using 0.9 mW of a frequency-quadrupled Nd:Yag laser emitting ns pulses at 4.66 eV (266 nm). The photoluminescence was imaged onto a 32 cm Cerny-Turner-type Spectrograph equipped with an open-electrode CCD camera. The same setup was used for measuring the solid state compounds, where the samples were encapsulated in fused silica slides.

The nonlinear optical response was measured using a Ti:sapphire laser oscillator emitting 80-fs pulses at a repetition rate of 78 MHz. Powers up to 350 mW impinged on the sample in a confocal microscope using a 0.6 NA long working distance objective lens. The second harmonic was spectrally separated using a 328 mm Cerny-Turner-type spectrograph and detected using a back-illuminated UV-VIS optimized CCD TE deep-cooled camera.

Computational details for the optical response: The optical response of $[(PhSi)_4S_6]$ (**IV**) and $[(NpSi)_4S_6]$ (**1**) was calculated with the Vienna Ab initio Simulation Package (VASP 5.4.4),[14] a plane-wave implementation of the DFT.

The electron-ion interaction is described within the projector-augmented-wave formalism (PAW).[15] The exchange-correlation (XC) functional is parametrized in the popular version proposed by Perdew-Burke-Ernzerhof (PBE) of the generalized gradient approximation (GGA),[16] which represents a well-tempered balance between computational efficiency, numerical accuracy, and reliability. The number of valence electrons that were employed for the simulation of the H, C, S, and Si atoms amounted to 1 ($1s^1$), 4 ($2s^2\ 2p^2$), 6 ($3s^2\ 3p^4$) and 4 ($3s^2\ 3p^2$), respectively. Structural optimization was performed with an energy cutoff of 400 eV for the plane wave expansion of the wave functions and a mesh of 4×4×2 k points to sample the Brillouin zone. The ionic relaxation was performed starting from the positions as determined by X-ray diffraction until the forces are smaller than 1 meV/Å. As (semi)local XC functionals failed to correctly describe the long-range vdW interactions, we applied a semi-empirical DFT-D3 correction scheme with zero damping,[8a] which has been found to be sufficiently accurate. These parameters are thus on the same footing as in our previous study[17] and ensure well converged structures. We used the formalism proposed by Gajdoš et al. to calculate the imaginary part of the frequency dependent dielectric function by a summation over empty states.[18] The real part is derived by means of the Kramers-Kronig relations. The number of electronic states considered in the calculations was increased to n >2000 for both [$(PhSi)_4S_6$] and [$(NpSi)_4S_6$] for the calculation of the linear optical properties. Thus, all electronic states within a distance of at least 25 eV from the Fermi energy were included. As standard DFT calculations typically yield significantly too small band gaps, quasiparticle or scissors shifts deduced from the experimental HOMO-LUMO gap were applied to widen the [$(NpSi)_4S_6$] band gap. For the comparison with measured optical spectra we used real and imaginary parts of the dielectric function, $\varepsilon_r(\omega)$ and $\varepsilon_i(\omega)$, respectively. We obtained the extinction coefficient κ using the approximation

$$\kappa = \sqrt{\sqrt{\varepsilon_r^2 + \varepsilon_i^2} - \varepsilon_r(\omega)}$$

Our calculations were compared with optical absorption measurements in powder samples. In order to allow for comparison with the experimental data we averaged over the three Cartesian directions to

$$\varepsilon(\omega) = \frac{1}{3} \sum_{i=x,y,z} \varepsilon_{ii}(\omega).$$

The nonlinear optical coefficients were calculated at the IPA level both postprocessing the wave functions and eigenvalues from the electronic structure calculations as the sum of two-band and three-band contributions following the approach described in ref. [19] and from the Berry-phase formulation of the dynamical polarization within the real-time approach described in ref. [20].

2 NMR Spectroscopy

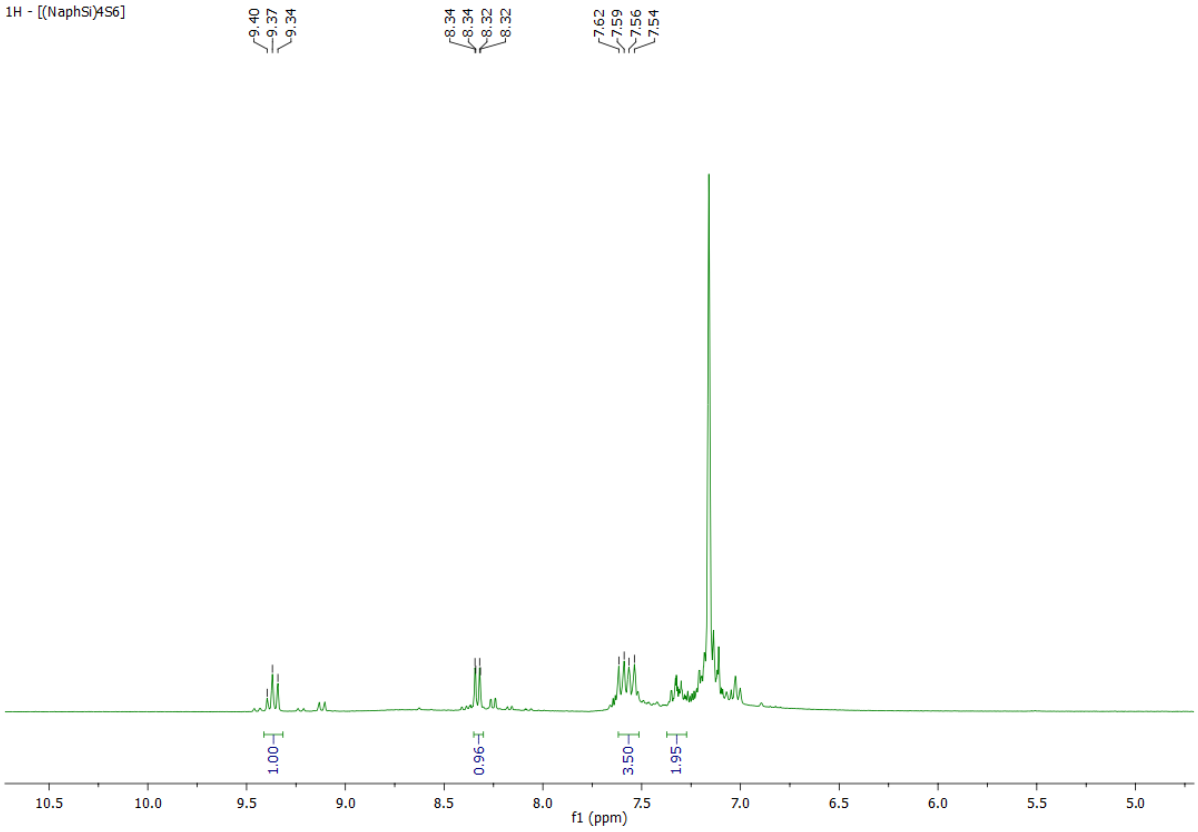

Figure S1. ^{1}H NMR spectrum of **1**.

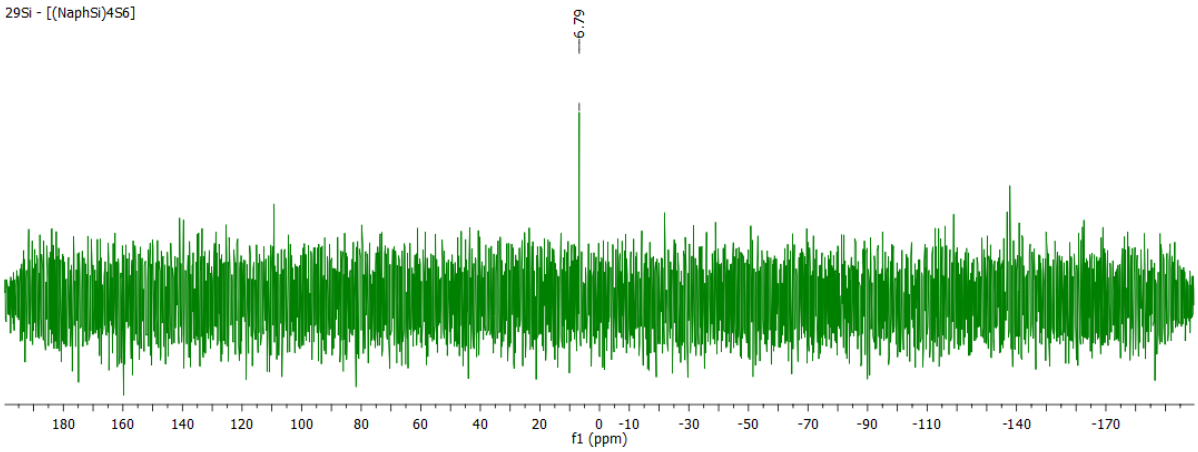

Figure S2. ^{29}Si NMR spectrum of **1**.

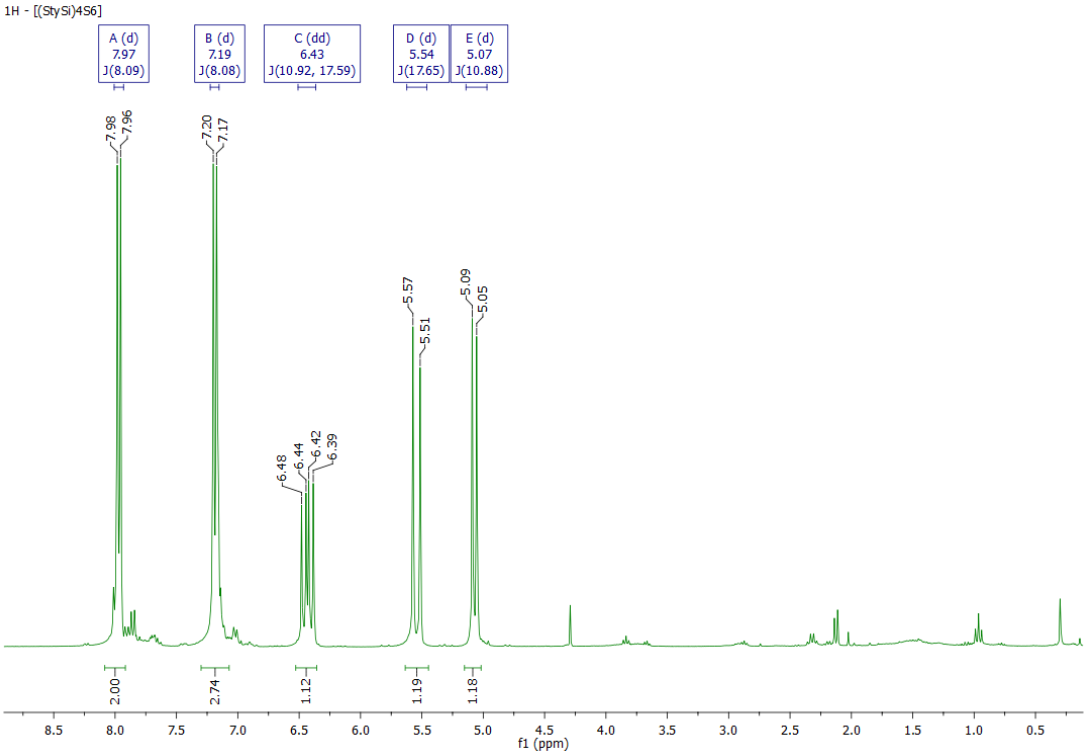

Figure S3. ^{1}H NMR spectrum of **2**.

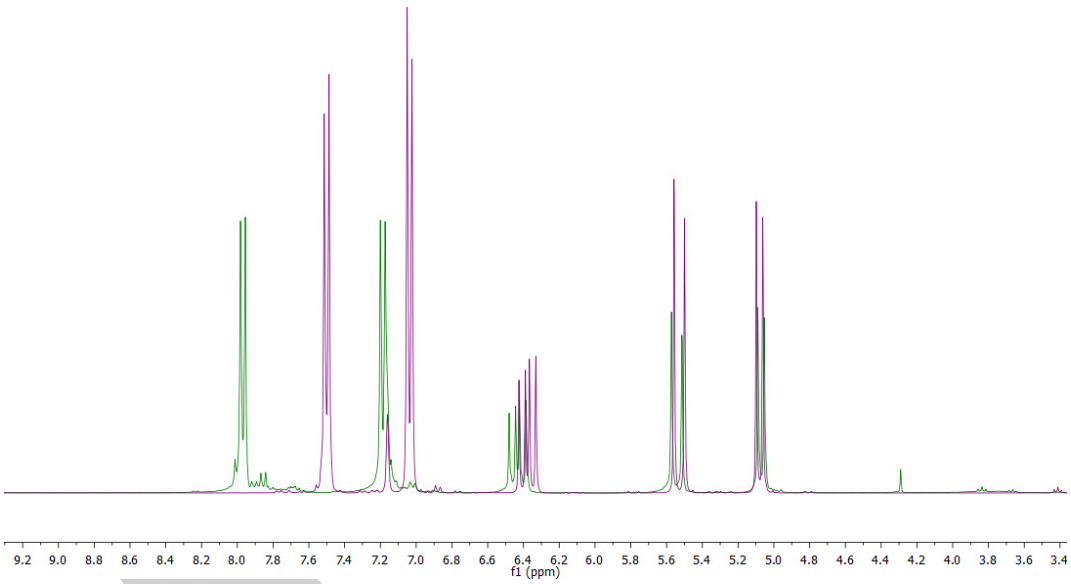

Figure S4. Comparison of the ^{1}H NMR spectra of **III** (purple) and **2** (green).

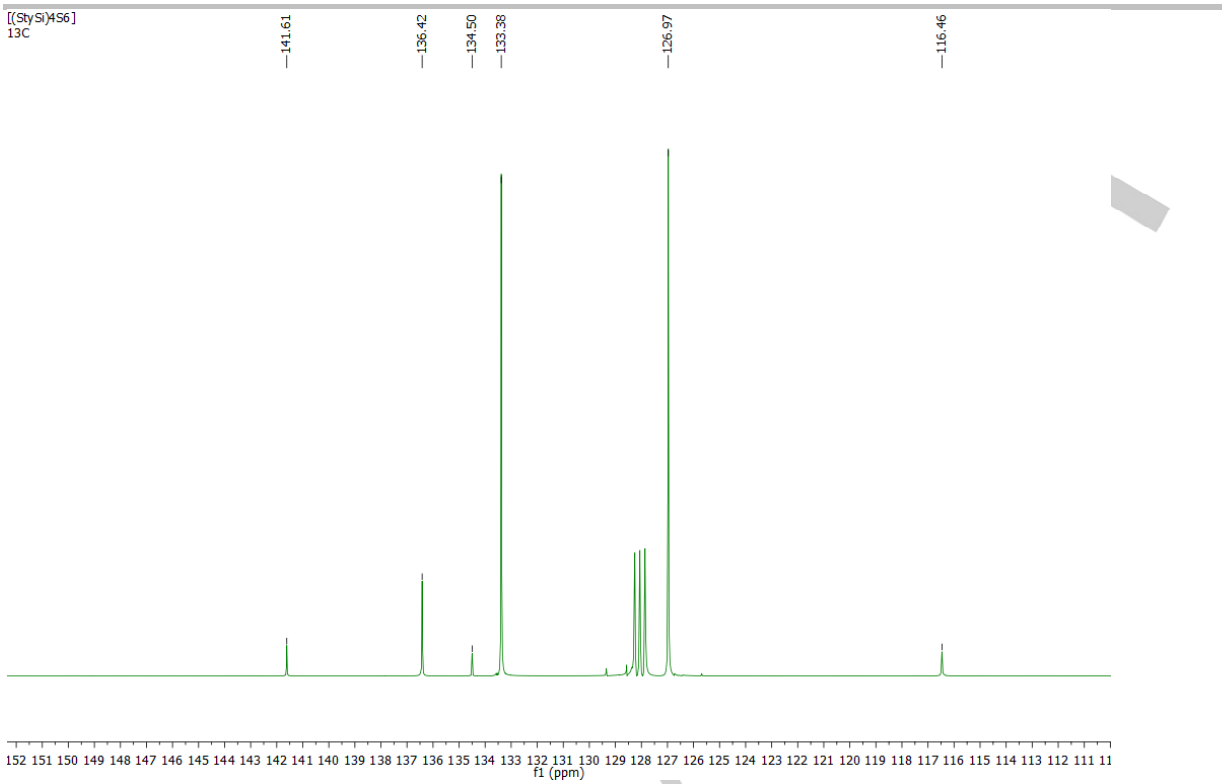

Figure S5. ^{13}C NMR spectrum of **2**.

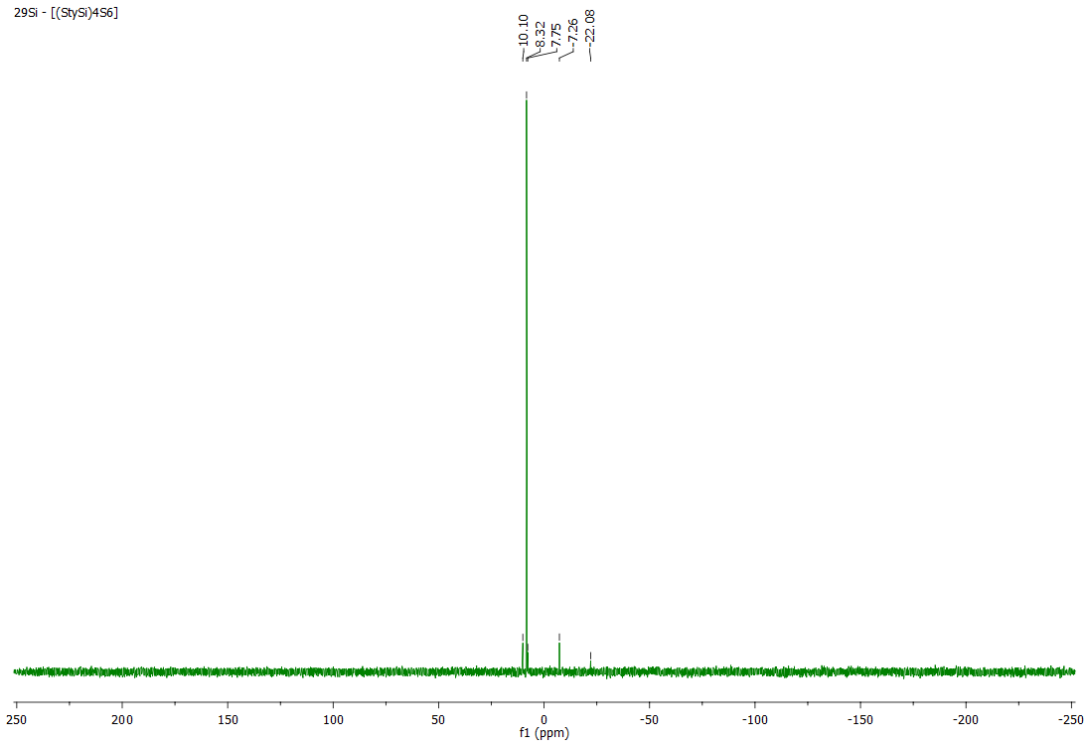

Figure S6. ^{29}Si NMR spectrum of **2**.

3 Mass Spectrometry

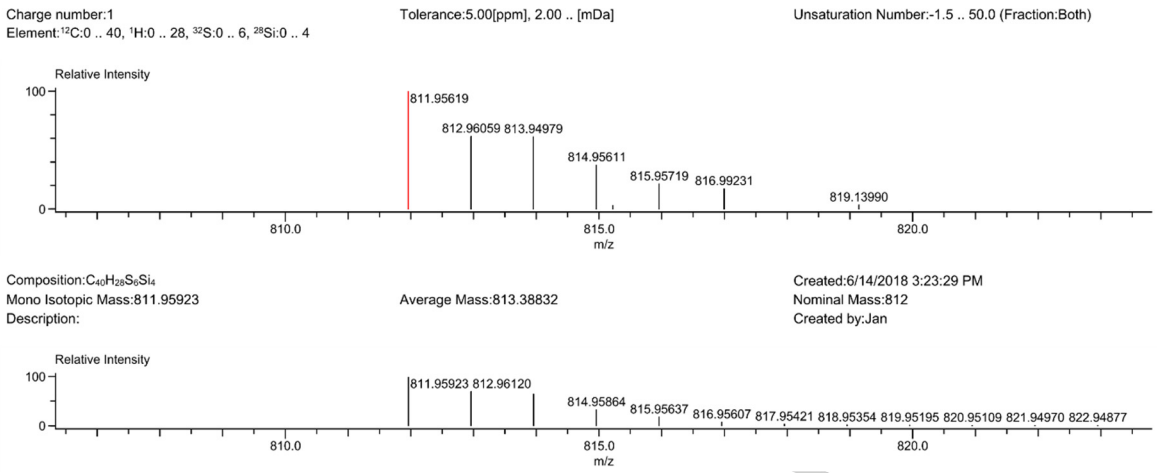

Figure S7. LIFDI mass spectrum of **1**.

4 Details of the X-ray Diffraction Measurements, Structure Solution, and Refinements

Table S1. Crystallographic data and refinement results of **II** and **1**.

Compound	**II**	**1**·0.5C_7H_8
Empirical Formula	$C_{10}H_7Cl_3Si$	$C_{40}H_{28}S_6Si_4$, 0.5(C_7H_8)
Formula weight /g·mol^{-1}	261.60	859.41
Crystal color and shape	colorless block	colorless block
Crystal size /mm³	0.106 x 0.103 x 0.102	0.1 x 0.1 x 0.01
Crystal system	monoclinic	triclinic
Space group [Flack parameter]	$P2_1/c$	$P\bar{1}$
a /Å	9.9459(3)	13.4738(3)
b / Å	9.0919(2)	13.9032(4)
c / Å	12.3406(4)	24.0970(5)
α /°	90	99.824(2)
β /°	93.103(2)	104.702(2)
γ /°	90	95.208(2)
V / Å³	1114.29(6)	4259.46(18)
Z	4	4
ρ_{calcd} / g·cm^{-3}	1.559	1.340
$\mu_{(Cu\ K\alpha)}$ / mm^{-1}	8.110	4.285
Absorption correction type	sphere	sphere
Min./max. transmission	0.0319 / 0.1521	0.1544 / 0.6874
2*θ* range / deg	8.904 – 142.904	6.516 – 129.992
No. of measured reflections	10819	100192
R(int)	0.0300	0.0668
Independent Reflections	2138	100192
Independent Reflections ($I>2\sigma(I)$)	1688	36510
No. of parameters	1271	966
R_1 ($I>2\sigma(I)$) / wR_2 (all data)	0.0228 / 0.0509	0.0464 / 0.1136
S (all data)	0.859	0.504
Max. peak / hole / e$^-$ Å³	0.44 / –0.23	0.55 / −0.35
CCDC number	2015922	2015925

Crystal Structure of II

The highest peak of residual electron density on the difference Fourier map (0.44 e^-/ $Å^3$) is found 1.01 Å from Si1. Excerpts of the crystal structure of **II** are shown in Figure S8.

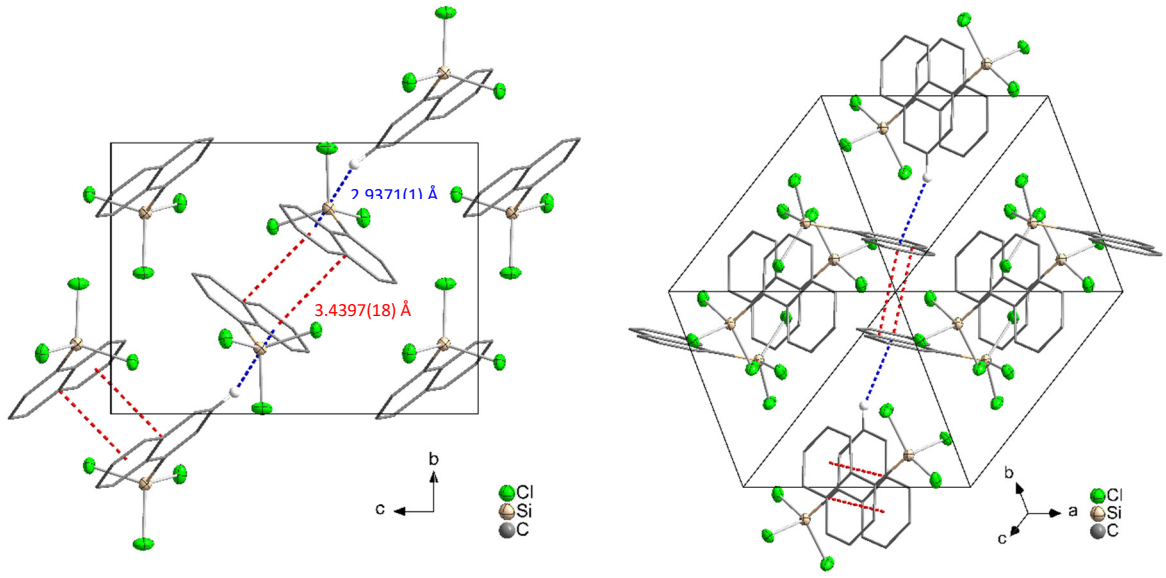

Figure S8. Excerpt of the crystal structure of **II** viewed along the *a* axis (left) and along [1,1,1] (right); π-stacking and CH/π-interactions are indicated as red and blue dashed lines, respectively.

Table S2. Fractional atomic coordinates (×10^4) and equivalent isotropic displacement parameters (Å^2×10^3) for **II**. U(eq) is defined as 1/3 of the trace of the orthogonalised U_{IJ} tensor.

Atom	*X*	*y*	*z*	U(eq)	Atom	*x*	*y*	*z*	U(eq)
Cl1	1528.9(5)	9799.2(5)	4115.1(4)	32.63(13)	C4	4775(2)	4943(2)	2687.4(15)	27.0(4)
Cl2	-468.3(4)	7229.6(6)	3124.8(4)	29.33(12)	C5	5077.7(18)	5879.2(19)	3588.3(15)	21.6(4)
Cl3	848.8(4)	6906.9(5)	5588.4(3)	25.61(12)	C6	6398.5(19)	5977(2)	4071.3(16)	25.9(4)
Si1	1242.8(5)	7579.7(5)	4063.6(4)	19.42(11)	C7	6682.1(19)	6857(2)	4947.6(16)	26.0(4)
C1	2685.0(18)	6591.5(18)	3533.0(14)	19.6(4)	C8	5648.7(18)	7694(2)	5381.5(15)	24.1(4)
C2	2456(2)	5661(2)	2659.4(15)	24.0(4)	C9	4361.6(18)	7630.0(19)	4932.4(14)	21.3(4)
C3	3503(2)	4836(2)	2234.2(15)	27.9(4)	C10	4026.3(18)	6723.0(18)	4023.4(14)	19.0(4)

Table S3. Bond lengths for **II** [Å].

Cl3−Si1	2.0367(6)	C10−C5	1.425(2)	C9−C8	1.368(3)
Cl2−Si1	2.0313(7)	C10−C9	1.417(3)	C2−C3	1.407(3)
Cl1−Si1	2.0385(7)	C1−C2	1.379(3)	C4−C3	1.359(3)
Si1−C1	1.8426(18)	C5−C4	1.419(3)	C7−C6	1.362(3)
C10−C1	1.440(3)	C5−C6	1.416(3)	C7−C8	1.408(3)

Table S4. Bond angles for **II** [°].

Cl3−Si1−Cl1	107.58(3)	C9−C10−C5	117.73(16)	C8−C9−C10	121.35(17)
Cl2−Si1−Cl3	106.42(3)	C10−C1−Si1	122.11(13)	C1−C2−C3	121.61(18)
Cl2−Si1−Cl1	106.51(3)	C2−C1−Si1	118.55(14)	C3−C4−C5	121.21(17)
C1−Si1−Cl3	111.98(6)	C2−C1−C10	119.30(16)	C6−C7−C8	119.69(17)
C1−Si1−Cl2	111.42(6)	C4−C5−C10	119.29(17)	C7−C6−C5	121.25(17)
C1−Si1−Cl1	112.56(6)	C6−C5−C10	119.38(17)	C9−C8−C7	120.61(17)
C5−C10−C1	118.62(16)	C6−C5−C4	121.33(16)	C4−C3−C2	119.97(18)
C9−C10−C1	123.64(15)				

Crystal Structure of 1

The studied crystal was twinned. Therefore, the twin data refinement was carried out with a batch scale factor of 0.4770(6). Some of the co-crystallized solvent molecules could not be found/refined due to their disorder. They were thus detracted from the data by the back-Fourier-transform method.[21] The void is located at (0.000, 0.500, 0.000), has a volume of 357 Å^3 and contains 93 electrons, which amounts to a bit less than 2 molecules of toluene. The highest peak of residual electron density on the difference Fourier map (0.55 e$^-$/ Å^3) is found 3.991 Å from C44. Excerpts of the crystal structure of **1** are shown in Figure S9.

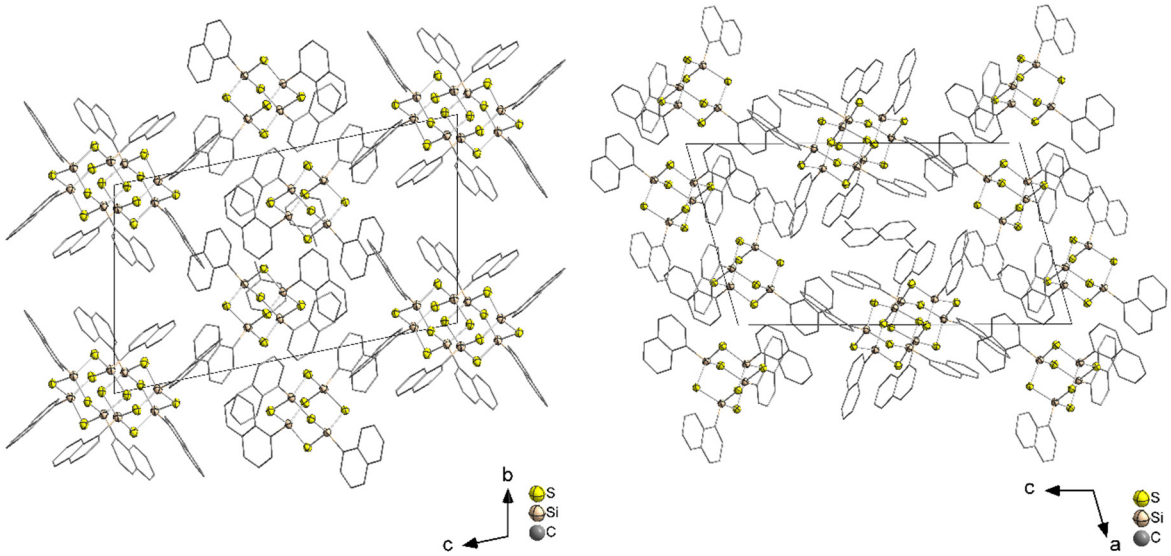

Figure S9. Excerpt of the crystal structure of **1** viewed along the *a* axis (left) and along the *b* axis (right).

Table S5. Fractional atomic coordinates (×10^4) and equivalent isotropic displacement parameters (Å^2×10^3) for **1**. U(eq) is defined as 1/3 of the trace of the orthogonalized U_{IJ} tensor.

Atom	*x*	*y*	*z*	U_{eq}	Atom	*x*	*y*	*z*	U_{eq}
S1	1077.2(14)	4504.1(15)	5633.8(8)	35.5(5)	S7	7773.1(15)	11174.4(16)	9120.9(9)	42.4(5)
S2	2244.3(14)	2321.6(16)	5555.6(8)	38.6(5)	S8	8845.8(14)	8993.5(16)	9348.0(8)	40.5(5)
S3	-170.6(14)	2384.2(16)	4552.8(8)	37.3(5)	S9	6567.7(14)	8921.7(15)	8200.0(8)	35.3(5)
S4	-58.2(14)	982.0(16)	5638.7(9)	40.4(5)	S10	6416.7(14)	7950.1(16)	9431.5(8)	41.1(5)
S5	1205.7(13)	3089.3(15)	6727.0(8)	34.1(5)	S11	7642.6(14)	10202.2(16)	10366.2(8)	38.3(5)
S6	-1206.0(13)	3171.8(15)	5738.6(8)	34.4(5)	S12	5375.1(13)	10142.2(15)	9226.3(8)	36.3(5)
Si1	290.4(15)	3962.9(16)	6204.2(9)	32.3(5)	Si5	6874.2(15)	10917.4(17)	9698.0(9)	34.4(5)
Si2	1383.4(15)	1850.5(17)	6106.6(9)	33.6(5)	Si6	7855.2(15)	8828.8(17)	9900.4(9)	34.6(5)
Si3	-913.8(15)	1953.8(17)	5169.8(9)	32.2(5)	Si7	5692.1(15)	8762.6(17)	8817.1(9)	33.9(5)
Si4	1276.5(14)	3199.8(16)	5079.4(9)	32.1(5)	Si8	8014.8(15)	9765.2(17)	8730.0(9)	33.7(5)
C1	36(5)	5065(6)	6684(3)	35.0(18)	C41	6699(6)	12148(6)	10047(3)	37.5(19)
C2	348(5)	5988(6)	6595(3)	40(2)	C42	5717(6)	12428(7)	9937(4)	48(2)
C3	111(6)	6869(6)	6908(4)	48(2)	C43	5529(6)	13378(6)	10170(4)	49(2)
C4	-476(6)	6798(7)	7285(4)	52(2)	C44	6337(7)	14048(7)	10528(4)	56(2)
C5	-840(5)	5888(7)	7390(3)	45(2)	C45	7360(6)	13822(6)	10665(4)	46(2)
C6	-1488(6)	5833(8)	7763(4)	54(2)	C46	8184(7)	14503(7)	11036(4)	57(2)
C7	-1858(6)	4941(8)	7852(4)	58(3)	C47	9172(7)	14291(7)	11170(4)	59(3)
C8	-1577(6)	4092(7)	7581(3)	50(2)	C48	9378(6)	13373(7)	10935(4)	49(2)
C9	-943(5)	4125(7)	7215(3)	45(2)	C49	8587(6)	12668(6)	10563(3)	46(2)
C10	-562(5)	5016(6)	7095(3)	38.2(19)	C50	7552(6)	12872(7)	10426(3)	43(2)
C11	2102(6)	1012(6)	6545(3)	39.1(19)	C51	8499(5)	8138(6)	10447(3)	37.5(19)
C12	1606(6)	82(6)	6519(4)	48(2)	C52	9485(6)	7865(6)	10443(4)	52(2)
C13	2065(7)	-584(6)	6861(4)	47(2)	C53	10013(6)	7350(7)	10844(4)	57(3)
C14	3034(7)	-312(7)	7215(4)	57(3)	C54	9596(6)	7087(6)	11262(4)	56(2)
C15	3611(7)	601(7)	7264(4)	49(2)	C55	8620(6)	7344(6)	11304(3)	45(2)
C16	4623(7)	877(8)	7622(4)	58(3)	C56	8177(7)	7086(7)	11733(4)	57(2)
C17	5193(7)	1748(8)	7666(4)	66(3)	C57	7256(7)	7339(7)	11785(4)	61(3)
C18	4749(6)	2409(8)	7322(4)	61(3)	C58	6727(7)	7866(7)	11391(4)	59(3)
C19	3762(6)	2178(6)	6953(3)	45(2)	C59	7107(6)	8136(6)	10959(3)	45(2)
C20	3163(6)	1281(7)	6917(3)	46(2)	C60	8074(5)	7877(6)	10895(3)	40(2)
C21	-2214(5)	1259(6)	4777(3)	35.7(19)	C61	4422(5)	8008(6)	8427(3)	38(2)
C22	-2495(6)	378(6)	4942(4)	45(2)	C62	3535(5)	8388(6)	8516(3)	39.2(19)
C23	-3482(6)	-208(6)	4661(4)	50(2)	C63	2531(5)	7806(6)	8268(3)	42(2)
C24	-4153(6)	86(6)	4213(4)	45(2)	C64	2427(6)	6908(7)	7959(3)	48(2)
C25	-3918(5)	957(7)	4029(3)	44(2)	C65	3283(6)	6475(6)	7833(3)	41(2)
C26	-4609(6)	1251(7)	3572(4)	54(2)	C66	3175(6)	5536(7)	7503(4)	51(2)
C27	-4379(6)	2119(8)	3396(4)	59(3)	C67	3993(7)	5128(7)	7383(4)	58(3)
C28	-3449(6)	2735(6)	3685(3)	47(2)	C68	4999(7)	5674(6)	7613(4)	53(2)
C29	-2740(5)	2476(6)	4149(3)	39.7(19)	C69	5151(6)	6581(6)	7949(4)	48(2)
C30	-2945(6)	1574(6)	4326(3)	38.5(19)	C70	4295(6)	7039(6)	8075(3)	39(2)
C31	1961(5)	3615(6)	4563(3)	31.8(18)	C71	8874(5)	10000(6)	8260(3)	38(2)
C32	2209(5)	4612(6)	4597(3)	37.5(19)	C72	9856(6)	9724(6)	8392(3)	45(2)
C33	2715(5)	4976(6)	4220(3)	42(2)	C73	10581(6)	9976(6)	8089(4)	48(2)
C34	2954(5)	4331(6)	3789(3)	38.6(19)	C74	10341(6)	10484(6)	7662(4)	50(2)
C35	2716(5)	3319(7)	3733(3)	40(2)	C75	9343(6)	10785(6)	7492(3)	42(2)
C36	2961(5)	2666(7)	3287(3)	44(2)	C76	9060(7)	11288(7)	7033(4)	54(2)
C37	2713(6)	1663(7)	3224(3)	52(2)	C77	8106(7)	11555(7)	6864(4)	60(3)
C38	2228(5)	1277(7)	3605(3)	46(2)	C78	7355(7)	11295(7)	7150(4)	58(3)
C39	1984(5)	1904(6)	4043(3)	41(2)	C79	7605(6)	10829(6)	7601(3)	47(2)
C40	2216(5)	2942(6)	4116(3)	35.2(18)	C80	8599(6)	10532(6)	7797(3)	40(2)
C81	5248(5)	5982(6)	4275(3)	37.0(19)					
C82	5338(5)	6376(6)	4854(3)	38.0(19)					
C83	4917(5)	7212(6)	5014(3)	46(2)					
C84	4397(6)	7661(6)	4586(4)	50(2)					
C85	4285(6)	7285(7)	4001(4)	56(2)					
C86	4722(6)	6445(6)	3851(3)	47(2)					
C87	5711(5)	5052(6)	4099(3)	43(2)					

Table S6. Selected bond lengths in **1** [Å].

S1−Si1	2.128(3)	S6−Si3	2.122(3)	S10−Si6	2.125(3)
S1−Si4	2.142(3)	Si1−C1	1.869(8)	S10−Si7	2.111(3)
S2−Si2	2.116(3)	Si2−C11	1.876(8)	S11−Si5	2.131(3)
S2−Si4	2.125(3)	Si3−C21	1.854(7)	S11−Si6	2.126(3)
S3−Si3	2.126(3)	Si4−C31	1.861(7)	S12−Si5	2.134(3)
S3−Si4	2.133(3)	S7−Si5	2.115(3)	S12−Si7	2.133(3)
S4−Si2	2.121(3)	S7−Si8	2.115(3)	Si5−C41	1.837(8)
S4−Si3	2.139(3)	S8−Si6	2.135(3)	Si6−C51	1.847(8)
S5−Si1	2.142(3)	S8−Si8	2.131(3)	Si7−C61	1.853(7)
S5−Si2	2.153(3)	S9−Si7	2.146(3)	Si8−C71	1.858(7)
S6−Si1	2.136(3)	S9−Si8	2.149(3)		

Table S7. Selected bond angles in **1** [°].

Si1−S1−Si4	104.12(12)	S6−Si3−S4	112.23(12)	C41−Si5−S11	108.2(3)
Si2−S2−Si4	103.67(11)	C21−Si3−S3	109.4(3)	C41−Si5−S12	107.6(3)
Si3−S3−Si4	104.13(11)	C21−Si3−S4	106.9(3)	S10−Si6−S8	111.74(12)
Si2−S4−Si3	104.47(13)	C21−Si3−S6	104.6(3)	S10−Si6−S11	111.70(12)
Si1−S5−Si2	104.76(11)	S2−Si4−S1	112.15(12)	S11−Si6−S8	112.71(13)
Si3−S6−Si1	104.90(11)	S2−Si4−S3	112.72(13)	C51−Si6−S8	106.8(3)
S1−Si1−S5	111.37(11)	S3−Si4−S1	111.96(12)	C51−Si6−S10	106.0(3)
S1−Si1−S6	111.90(12)	C31−Si4−S1	106.7(3)	C51−Si6−S11	107.4(3)
S6−Si1−S5	111.32(13)	C31−Si4−S2	106.5(2)	S10−Si7−S9	110.89(12)
C1−Si1−S1	106.7(3)	C31−Si4−S3	106.3(2)	S10−Si7−S12	112.39(12)
C1−Si1−S5	110.1(2)	Si8−S7−Si5	105.64(13)	S12−Si7−S9	112.47(12)
C1−Si1−S6	105.1(2)	Si8−S8−Si6	103.42(11)	C61−Si7−S9	109.1(2)
S2−Si2−S4	113.28(12)	Si7−S9−Si8	103.78(11)	C61−Si7−S10	104.8(3)
S2−Si2−S5	110.55(13)	Si7−S10−Si6	105.20(13)	C61−Si7−S12	106.8(3)
S4−Si2−S5	112.06(12)	Si6−S11−Si5	104.12(12)	S7−Si8−S8	113.05(12)
C11−Si2−S2	109.8(2)	Si7−S12−Si5	103.72(12)	S7−Si8−S9	110.31(12)
C11−Si2−S4	104.1(3)	S7−Si5−S11	112.55(12)	S8−Si8−S9	112.25(13)
C11−Si2−S5	106.6(3)	S7−Si5−S12	110.98(12)	C71−Si8−S7	105.4(3)
S3−Si3−S4	110.38(12)	S11−Si5−S12	112.00(13)	C71−Si8−S8	105.6(3)
S6−Si3−S3	112.93(13)	C41−Si5−S7	105.1(3)	C71−Si8−S9	109.8(2)

Table S8. Crystallographic data and refinement results of **3** and **4**.

Compound	**3**·CH_2Cl_2	**4**
Empirical Formula	$C_{48}H_{40}Au_2P_2S_4Si_2$, CH_2Cl_2	$C_{56}H_{44}Au_2P_2S_4Si_2$
Formula weight /g·mol^{-1}	1342.02	1357.20
Crystal color and shape	colorless plate	colorless plate
Crystal size /mm³	0.279 x 0.258 x 0.0.168	0.594 x 0.204 x 0.102
Crystal system	monoclinic	triclinic
Space group [Flack parameter]	*C*2/*c*	$P\bar{1}$
a /Å	17.0944(6)	9.1114(7)
b / Å	14.7258(6)	9.2410(8)
c / Å	19.7490(7)	15.7564(13)
α /°	90	106.597(7)
β /°	108.047(3)	91.667(7)
γ /°	90	101.759(7)
V / Å³	4726.8(3)	1239.31(18)
Z	4	1
ρ_{calcd} / g·cm^{-3}	1.886	1.819
$\mu_{(Mo\ K\alpha)}$ / mm^{-1}	6.644	6.232
Absorption correction type	numerical	numerical
Min./max. transmission	0.2660 / 0.8204	0.0548 / 0.4320
2*θ* range / deg	3.732 – 58.500	4.586 – 51.998
No. of measured reflections	26951	13736
R(int)	0.0525	0.0791
Independent Reflections	6411	4883
Independent Reflections ($I>2\sigma(I)$)	4872	3950
No. of parameters	285	334
R_1 ($I>2\sigma(I)$) / wR_2 (all data)	0.0223 / 0.0486	0.0473 / 0.1125
S (all data)	0.867	0.963
Max. peak / hole / e$^-$/Å³	1.51 / −1.48	3.01 / −2.26
CCDC number	2015923	2015924

Crystal Structure of 3

The highest peak of residual electron density on the difference Fourier map (1.51 $e^{-}/Å^3$) is found 0.900 Å from Au1. Excerpts of the crystal structure of **3** are shown in Figure S10.

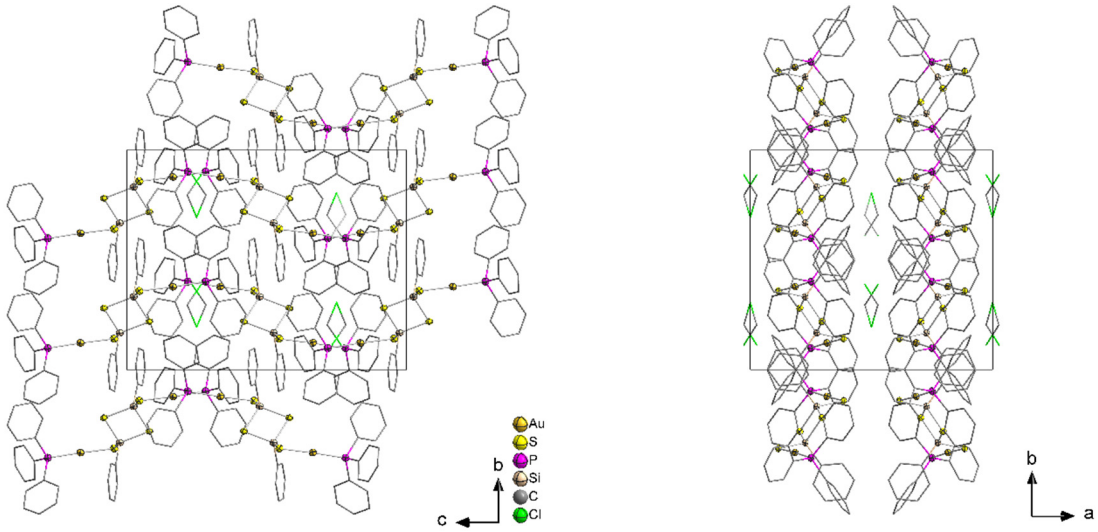

Figure S10. Excerpt of the crystal structure of **3** viewed along the *a* axis (left) and along the *c* axis (right).

Table S9. Fractional atomic coordinates (×10^4) and equivalent isotropic displacement parameters (Å^2×10^3) for **3**. U(eq) is defined as 1/3 of the trace of the orthogonalized U_{IJ} tensor.

Atom	*x*	*y*	*z*	U(eq)	Atom	*x*	*y*	*z*	U(eq)
Au1	8155.1(2)	6221.3(2)	3347.9(2)	19.92(4)	C12	6556(2)	4685(2)	2581.2(19)	33.4(8)
S1	7044.9(5)	7807.7(5)	4189.5(4)	20.65(15)	C13	6829(2)	6903(2)	1730.7(17)	24.3(6)
S2	8844.4(4)	6410.9(5)	4547.0(4)	21.18(15)	C14	6190(2)	6756(2)	1107(2)	31.2(7)
P1	7493.3(5)	5985.3(5)	2184.7(4)	21.23(16)	C15	5731(2)	7470(2)	739.6(19)	30.8(7)
Si1	7737.1(5)	6676.0(5)	4752.4(5)	18.57(16)	C16	5906(2)	8343(3)	986(2)	34.2(8)
C1	7062.0(19)	5648(2)	4602.1(17)	21.7(6)	C17	6526(3)	8498(3)	1608(2)	49.5(11)
C2	6207(2)	5732(2)	4441.3(19)	27.6(7)	C18	6985(2)	7785(2)	1987(2)	39.4(9)
C3	5707(2)	4977(2)	4340(2)	34.4(8)	C19	8222.2(19)	5835(2)	1690.8(17)	22.4(6)
C4	6054(2)	4124(2)	4402(2)	33.2(8)	C20	8437(2)	6552(2)	1334.0(19)	29.6(7)
C5	6891(2)	4022(2)	4566(2)	33.7(8)	C21	9036(2)	6446(2)	1006(2)	34.7(8)
C6	7393(2)	4777(2)	4658.8(18)	27.3(7)	C22	9424(2)	5627(2)	1025(2)	32.4(8)
C7	6864.6(19)	4967(2)	2040.6(18)	23.9(6)	C23	9213(2)	4907(2)	1372(2)	34.9(8)
C8	6688.1(19)	4467(2)	1416.7(18)	24.2(6)	C24	8625(2)	5006(2)	1718(2)	31.5(7)
C9	6201.8(19)	3692(2)	1330.7(18)	27.8(7)	Cl2	5000	8058.6(11)	2500	89.3(8)
C10	5893(2)	3420(2)	1863(2)	31.3(7)	Cl1	5263.7(13)	6134.1(13)	2660.5(18)	67.6(8)
C11	6063(2)	3916(3)	2486(2)	37.8(9)	C25	4725(6)	7033(5)	2168(5)	45(2)

Table S10. Selected bond lengths [Å] and angles [°] in **3**.

Au1−S2	2.3120(8)	P1−Au1−S2	178.03(3)	S1−Si1−Si1^1	48.77(3)
Au1−P1	2.2510(8)	Si1−S1−Si1^1	82.48(4)	S1^1−Si1−Si1^1	48.75(3)
S1−Si1^1	2.1449(11)	Si1−S2−Au1	90.95(4)	S2−Si1−S1^1	111.13(5)
S1−Si1	2.1444(11)	C7−P1−Au1	111.93(11)	S2−Si1−S1	115.57(5)
S2−Si1	2.0918(11)	C7−P1−C19	106.61(14)	S2−Si1−Si1^1	126.93(5)
P1−C7	1.815(3)	C13−P1−Au1	115.43(11)	C1−Si1−S1	109.41(10)
P1−C13	1.813(3)	C13−P1−C7	106.76(15)	C1−Si1−S1^1	110.72(11)
P1−C19	1.818(3)	C13−P1−C19	104.70(14)	C1−Si1−S2	111.67(10)
Si1−S1^1	2.1449(11)	C19−P1−Au1	110.79(10)	C1−Si1−Si1^1	121.36(11)
Si1−Si1^1	2.8274(16)	S1−Si1−S1^1	97.52(4)		
Si1−C1	1.870(3)				

^{1}: 3/2-X, 3/2-Y, 1-Z

Crystal Structure of 4

The highest peak of residual electron density on the difference Fourier map (3.01 $e^{-}/Å^3$) is found 0.89 Å from Au1. Excerpts of the crystal structure of **4** are shown in Figure S11.

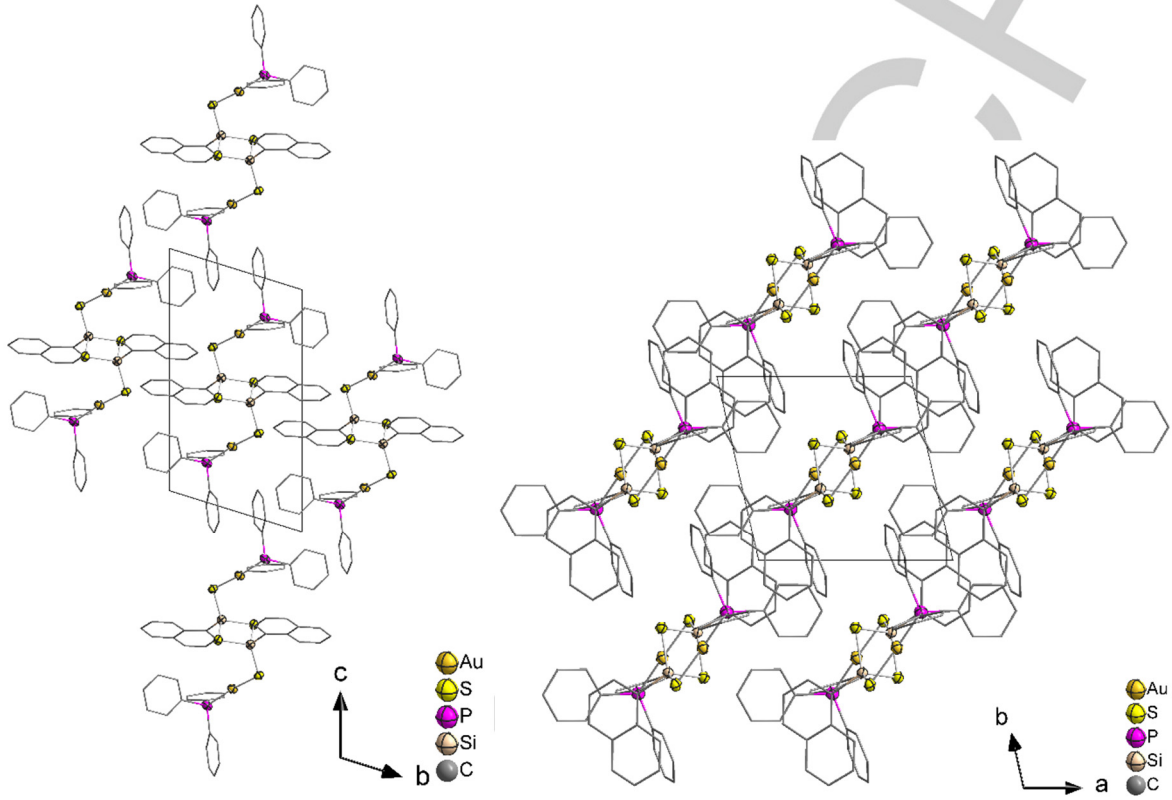

Figure S11. Excerpt of the crystal structure of **4** viewed along the *a* axis (left) and along the *c* axis (right).

Table S11. Fractional atomic coordinates (×10^4) and equivalent isotropic displacement parameters (Å^2×10^3) for **4**. U(eq) is defined as 1/3 of the trace of the orthogonalized U_{IJ} tensor.

Atom	*x*	*y*	*z*	U(eq)	Atom	*x*	*y*	*z*	U(eq)
Au1	6103.2(3)	5277.9(3)	7370.2(2)	34.67(12)	C15	7340(20)	11687(17)	9323(9)	117(6)
S2	4281(2)	3274(2)	6481.9(12)	32.3(4)	C16	7569(18)	10204(15)	9283(7)	91(5)
S1	4202(2)	6343(2)	5547.3(12)	31.5(4)	C17	9696(9)	7274(9)	8178(5)	34.9(16)
P1	7755(2)	7194(2)	8377.7(13)	37.5(4)	C18	10765(10)	8668(10)	8388(5)	42.3(18)
Si1	4022(2)	3918(2)	5324.2(13)	27.8(4)	C19	12235(10)	8656(13)	8240(6)	53(2)
C1	2201(8)	2767(8)	4681(4)	28.5(14)	C20	12675(10)	7270(13)	7877(6)	52(2)
C2	1154(8)	3534(9)	4468(5)	32.4(15)	C21	11620(12)	5904(12)	7661(6)	53(2)
C3	-268(9)	2730(10)	4030(5)	38.9(18)	C22	10151(10)	5896(10)	7819(6)	43.2(19)
C4	-647(9)	1164(10)	3790(5)	38.7(17)	C23	7656(10)	6976(10)	9472(5)	46.1(19)
C5	395(9)	300(10)	3970(5)	36.4(16)	C24A	8930(30)	7226(18)	10098(12)	41(4)
C6	8(9)	-1330(10)	3743(5)	40.6(18)	C24B	8540(20)	6380(20)	9843(14)	61(5)
C7	997(10)	-2138(9)	3941(5)	40.9(18)	C25A	8810(40)	7030(20)	10914(15)	53(6)
C8	2433(10)	-1347(9)	4344(5)	41.2(18)	C25B	8430(30)	6240(30)	10692(17)	69(6)
C9	2830(9)	215(9)	4584(5)	33.1(15)	C26	7378(15)	6636(13)	11169(7)	69(3)
C10	1828(8)	1114(8)	4414(5)	30.8(15)	C27A	6160(30)	6260(30)	10602(16)	80(6)
C11	7418(9)	9095(10)	8475(5)	42.1(19)	C27B	6390(30)	7390(30)	10817(14)	66(5)
C12	6977(11)	9402(10)	7702(5)	47(2)	C28A	6250(30)	6410(30)	9737(13)	61(5)
C13	6732(13)	10840(12)	7748(7)	61(3)	C28B	6500(20)	7570(30)	9987(13)	58(5)
C14	6939(17)	11963(15)	8532(8)	83(4)					

Table S12. Selected bond lengths [Å] and angles [°] in **4**.

Au1−S2	2.297(2)	P1−Au1−S2	173.35(7)	S2−Si1−S1^1	115.64(10)
Au1−P1	2.256(2)	Si1−S2−Au1	103.57(9)	S2−Si1−Si1^1	130.00(13)
S2−Si1	2.095(2)	Si1−S1−Si1^1	82.58(10)	S1−Si1−S1^1	97.42(10)
S1−Si1^1	2.159(3)	C11−P1−Au1	113.0(3)	S1^1−Si1−Si1^1	48.39(7)
S1−Si1	2.137(3)	C17−P1−Au1	114.7(3)	S1−Si1−Si1^1	49.04(7)
P1−C11	1.810(8)	C17−P1−C11	106.9(4)	C1−Si1−S2	109.1(2)
P1−C17	1.796(8)	C23−P1−Au1	111.6(3)	C1−Si1−S1	111.2(2)
P1−C23	1.795(8)	C23−P1−C11	105.8(4)	C1−Si1−S1^1	108.4(2)
Si1−S1^1	2.159(3)	C23−P1−C17	104.2(4)	C1−Si1−Si1^1	120.9(2)
Si1−Si1^1	2.835(4)	S2−Si1−S1	114.55(12)		
Si1−C1	1.865(8)				

^{1}: 1-X, 1-Y, 1-Z

5 Cartesian Coordinates of the Calculated Structures in the Gas Phase

Minimum structures of the cluster monomers calculated at BP86-D3/cc-pVDZ level of theory are given in Tables S13−S16

Table S13. Cartesian coordinates of $[(PhSi)_4S_6]$.

S	2.55433628	-0.29872054	0.13015851
Si	1.02848834	-1.39222039	1.20513182
C	1.87458073	-2.65566202	2.30503137
C	3.27748826	-2.81000704	2.32652876
C	1.07614135	-3.47934861	3.13288149
S	0.29122564	2.51271157	0.13463471
Si	-1.10546566	1.24428128	1.22078195
C	-2.13349127	2.42413065	2.25716302
C	-2.13627669	2.37836850	3.66795738
C	-2.92308803	3.39439018	1.59648709
S	-2.51615927	0.25838467	-0.10973734
Si	-1.24154206	-1.04235823	-1.29524466
C	-2.38107572	-1.90987744	-2.50854879
C	-3.28402783	-1.13320898	-3.27165921
C	-2.34730087	-3.30879851	-2.69558833
S	0.14743511	0.08221688	-2.54310261
Si	1.39172284	1.09308344	-1.08466000
C	2.67791997	2.08560100	-2.02518957
C	2.99088960	1.79274407	-3.37099486
C	3.37637344	3.12256116	-1.36443164
S	-0.25947539	-2.56424631	-0.10375019
S	-0.11837439	-0.13865969	2.56808873
C	4.36600521	3.85355270	-2.03985055
C	3.98100647	2.52586463	-4.04483800
C	4.66849923	3.55591772	-3.38026029
C	-3.20238452	-3.92086712	-3.62653604
C	-4.13707931	-1.74676725	-4.20174611
C	-4.09688242	-3.14106809	-4.37932633
C	-3.70012600	4.29949355	2.33538858
C	-2.91496787	3.28509964	4.40564425
C	-3.69652328	4.24508353	3.74053617
C	1.67272043	-4.43831119	3.96564398
C	3.87240781	-3.77043827	3.16103478
C	3.07129790	-4.58419108	3.98004485
H	3.14217208	3.35996926	-0.31465352
H	2.45757374	0.98503689	-3.89632087
H	4.90301293	4.66020852	-1.51813905
H	4.21631881	2.29176566	-5.09415098
H	5.44389755	4.13046477	-3.90967448
H	-1.64747628	-3.92564486	-2.11049316
H	-3.31981027	-0.04080870	-3.13448455
H	-3.16987430	-5.01228177	-3.76425559
H	-4.83730914	-1.13468986	-4.79021089
H	-4.76690434	-3.62207168	-5.10823562
H	-2.92886621	3.44025915	0.49587195
H	-1.52548137	1.62946273	4.19580273
H	-4.31157748	5.05082841	1.81301509
H	-2.91101281	3.24139316	5.50531801
H	-4.30640601	4.95506041	4.31982510
H	-0.01978720	-3.36806390	3.12456304
H	3.91096408	-2.17602896	1.68677769
H	1.04403653	-5.07491240	4.60653699
H	4.96706875	-3.88353793	3.17129792
H	3.53885591	-5.33649932	4.63351629

Table S14. Cartesian coordinates of [(NpSi)$_4$S$_6$].

S	2.56657572	-0.34762781	0.37368617
Si	0.90766135	-1.55677507	1.08867223
C	1.66448839	-2.97585560	2.07120157
C	2.57664550	-3.91401085	1.46163269
C	1.33199053	-3.11680137	3.42028426
S	0.35194313	2.50220679	0.54340046
Si	-1.18854865	1.14043693	1.24851806
C	-2.31661478	2.14674098	2.37400511
C	-2.45688481	1.76220520	3.70924811
C	-3.03430157	3.30062954	1.88689282
S	-2.43571355	0.38959040	-0.36577696
Si	-1.04754822	-0.74976473	-1.59030510
C	-2.04711781	-1.44157724	-3.03054235
C	-1.68928807	-1.08750305	-4.33324155
C	-3.16880880	-2.32454235	-2.81607371
S	0.50068757	0.50631836	-2.46113120
Si	1.59012843	1.24979626	-0.73077626
C	2.96196071	2.35585050	-1.39899609
C	3.07798798	2.52935135	-2.77989667
C	3.88979449	3.02380644	-0.51769739
S	-0.22018625	-2.46057182	-0.53486161
S	-0.37154730	-0.46483116	2.46889043
C	4.91976296	3.85928321	-1.09601576
C	4.09135530	3.35079344	-3.34121687
C	4.99267544	4.00143444	-2.51359576
C	-3.89421808	-2.81946069	-3.96591947
C	-2.40536070	-1.57703840	-5.45768652
C	-3.48566747	-2.42563984	-5.27474799
C	-3.88428112	4.02908768	2.80353164
C	-3.29261575	2.48181667	4.60397871
C	-3.99113822	3.59234280	4.15736683
C	1.87213224	-4.16533910	4.21123791
C	3.12357784	-4.97971877	2.27309650
C	2.75009940	-5.07685529	3.64646049
H	2.37400269	2.02323921	-3.45814597
H	4.15359545	3.46502170	-4.43362863
H	5.78239784	4.64083978	-2.93880907
C	-3.60319110	-2.73800965	-1.51952521
H	-0.83506300	-0.41462914	-4.50449525
C	-5.00584389	-3.69302552	-3.77080449
H	-2.09588210	-1.27756738	-6.47002233
H	-4.04787983	-2.81082386	-6.14011456
C	-2.94876919	3.76419708	0.53837771
H	-1.91246389	0.88353835	4.08785058
C	-4.60085739	5.17196547	2.33744146
H	-3.37971352	2.15084994	5.64952112
H	-4.64210233	4.15737526	4.84314701
H	0.63696814	-2.40525920	3.89189843
H	1.58848215	-4.24642844	5.27107335
H	3.17489282	-5.89363966	4.25121118
C	-4.49288250	5.59222900	1.02012832
C	-3.65891134	4.87991793	0.11636900
H	-5.24339314	5.71482480	3.04840622
H	-5.05035410	6.47494404	0.67256231
H	-3.57347779	5.21385354	-0.92839199
H	-2.31045949	3.23044170	-0.17985644
C	2.97039026	-3.84484880	0.09018479
C	4.02714974	-5.91519834	1.68546635
C	3.85160089	-4.77087051	-0.45126285
C	4.38659100	-5.81591574	0.34959392
H	2.57037707	-3.04582604	-0.54996319
H	4.13696687	-4.69273156	-1.51088139
H	5.08417389	-6.54326817	-0.09210480
H	4.43418120	-6.72017282	2.31741794
C	-4.68880013	-3.58912268	-1.36365055
C	-5.39853770	-4.07268379	-2.49595013
H	-3.07074498	-2.37768251	-0.62798426
H	-5.00067107	-3.89067473	-0.35263995
H	-6.25729424	-4.74673812	-2.35829112
H	-5.54688426	-4.06042720	-4.65698220
C	5.84484029	4.52659418	-0.23823134
C	3.84404161	2.90237518	0.90493103
C	5.76912315	4.38465526	1.13935160
C	4.75906900	3.56497367	1.71173325
H	6.62260834	5.15865487	-0.69496128
H	6.48814047	4.90427810	1.79032401
H	3.07223744	2.27408627	1.37170989
H	4.69955088	3.45275066	2.8045247978

Table S15. Cartesian coordinates of $[(PhSn)_4S_6]$.

S	2.79824933	-0.29409155	0.13516696
Sn	1.10707370	-1.54810426	1.36916664
C	2.17773885	-2.93736690	2.60666886
C	3.39026460	-3.48989652	2.14848393
C	1.66397589	-3.29677850	3.86817186
S	0.26781264	2.84855182	0.16691975
Sn	-1.29446256	1.39831154	1.36793585
C	-2.45515095	2.71245045	2.60649048
C	-2.93040293	2.26465885	3.85478732
C	-2.74022120	4.01940298	2.16385233
S	-2.83116286	0.27532662	-0.16369989
Sn	-1.39383416	-1.18299831	-1.50216660
C	-2.66276385	-2.23881557	-2.87459478
C	-2.97294770	-1.66577462	-4.12384074
C	-3.18620635	-3.49780797	-2.51974929
S	0.13955657	0.11608107	-2.90026263
Sn	1.50069047	1.26992620	-1.23309215
C	2.91733929	2.44582955	-2.33630528
C	3.31528244	2.03786257	-3.62473672
C	3.44946706	3.61872324	-1.76501826
S	-0.29440905	-2.87913123	-0.13609149
S	-0.20071645	-0.16201510	2.90072209
C	4.38239220	4.38294090	-2.48711586
C	4.24874470	2.80707693	-4.34092133
C	4.78165503	3.97691500	-3.77230132
C	-4.02233043	-4.18240400	-3.41874428
C	-3.80973116	-2.35606620	-5.01774820
C	-4.33397520	-3.61169873	-4.66494056
C	-3.50345465	4.87763566	2.97420776
C	-3.69302814	3.12842840	4.65993456
C	-3.97948712	4.43218521	4.21955208
C	2.36644325	-4.21234317	4.67084831
C	4.08735119	-4.40471266	2.95650561
C	3.57542051	-4.76573067	4.21488849
H	3.13631193	3.94340794	-0.76008846
H	2.89701211	1.12419925	-4.07615794
H	4.79794173	5.30035321	-2.04299591
H	4.55957727	2.49058498	-5.34829583
H	5.51221386	4.57738646	-4.33541310
H	-2.94100400	-3.95122972	-1.54623598
H	-2.56088022	-0.68416692	-4.40683795
H	-4.43066046	-5.16687619	-3.14368254
H	-4.05185727	-1.91037152	-5.99464646
H	-4.98879010	-4.15007450	-5.36690186
H	-2.36498330	4.37497586	1.19116494
H	-2.70442534	1.24540653	4.20627822
H	-3.72556540	5.89948759	2.63060695
H	-4.06352127	2.78061270	5.63632470
H	-4.57649265	5.10653454	4.85216624
H	0.71933031	-2.86208078	4.23179055
H	3.79849772	-3.20616134	1.16556607
H	1.96714816	-4.49287879	5.65748700
H	5.03566728	-4.83575510	2.60089718
H	4.12362077	-5.48200883	4.84559413

Table S16. Cartesian coordinates of [(NpSn)$_4$S$_6$].

S	2.87258975	-0.31448999	0.33272804
Sn	1.07560590	-1.67923117	1.27168866
C	1.99008730	-3.22904974	2.45146145
C	2.89410352	-4.16547207	1.85025781
C	1.68208439	-3.29797447	3.80645240
S	0.34073313	2.81368655	0.50349220
Sn	-1.31717895	1.27755456	1.43393202
C	-2.57452609	2.41291848	2.76064547
C	-2.63602830	2.03552410	4.09834249
C	-3.32779938	3.53094547	2.27255797
S	-2.74384535	0.36220830	-0.32671008
Sn	-1.20881286	-0.91267766	-1.73802748
C	-2.36244690	-1.75570727	-3.34708679
C	-2.02711124	-1.41106930	-4.65261676
C	-3.44986947	-2.64949529	-3.07457823
S	0.45610905	0.49324727	-2.84704549
Sn	1.70671025	1.40560484	-0.95423280
C	3.20535755	2.66287422	-1.85077201
C	3.23924890	2.76609596	-3.23779744
C	4.14591458	3.37211714	-1.03348844
S	-0.21386574	-2.76801287	-0.49627427
S	-0.32679788	-0.44978587	2.85303484
C	5.13546272	4.20036572	-1.68909315
C	4.21516805	3.58318272	-3.87437140
C	5.14036225	4.28239091	-3.11394631
C	-4.19275493	-3.18630683	-4.19482196
C	-2.76267887	-1.94350812	-5.74837523
C	-3.82046910	-2.81083684	-5.52047897
C	-4.15667279	4.25985199	3.20885500
C	-3.45357968	2.75768765	5.01230934
C	-4.19526843	3.84426011	4.57368304
C	2.26313896	-4.30632439	4.62551167
C	3.48054947	-5.18775583	2.69049292
C	3.14168917	-5.22810179	4.07630986
H	2.51177377	2.21651285	-3.85641005
H	4.22897769	3.65446608	-4.97227402
H	5.89799414	4.91574102	-3.60172060
C	-3.83503812	-3.03503029	-1.75543582
H	-1.18963907	-0.72308216	-4.85075034
C	-5.27866850	-4.07745815	-3.94317905
H	-2.48515831	-1.66134328	-6.77503401
H	-4.39299114	-3.22561426	-6.36501555
C	-3.30036859	3.95957669	0.91141512
H	-2.05288983	1.17469564	4.46286114
C	-4.91366636	5.37571849	2.74142222
H	-3.49154069	2.44684354	6.06710571
H	-4.82948327	4.40657639	5.27698693
H	0.98594516	-2.57322479	4.25819913
H	2.00955600	-4.34765222	5.69539414
H	3.59409232	-6.01046669	4.70583383
C	-4.86262280	5.76424747	1.41045865
C	-4.04865890	5.04909592	0.48922598
H	-5.54148453	5.92429749	3.46109268
H	-5.45147976	6.62663649	1.06371348
H	-4.01104309	5.36055447	-0.56504416
H	-2.67534594	3.41765334	0.18389914
C	3.24330242	-4.13906694	0.46660916
C	4.38268114	-6.12879142	2.10971654
C	4.12400035	-5.06910258	-0.06688331
C	4.69942667	-6.07295946	0.76005788
H	2.80708255	-3.36860208	-0.18892137
H	4.37778626	-5.02850031	-1.13639029
H	5.39653153	-6.80499761	0.32547461
H	4.82399375	-6.90310652	2.75678769
C	-4.89623710	-3.90384258	-1.54509041
C	-5.62523071	-4.43037586	-2.64689317
H	-3.28158811	-2.63712047	-0.89002498
H	-5.17429639	-4.18628663	-0.51902213
H	-6.46485801	-5.11849049	-2.46738683
H	-5.83814909	-4.48085772	-4.80182520
C	6.08059031	4.91324152	-0.89208818
C	4.15443814	3.30141004	0.39203061
C	6.05940723	4.82046932	0.49209888
C	5.08745845	4.00743677	1.13781910
H	6.82991418	5.54079685	-1.39974029
H	6.79421643	5.37552997	1.09431258
H	3.40888580	2.67674293	0.90925672
H	5.07407505	3.93688279	2.23542947

Minimum structures of the alternating (first) and stacking (second) cluster dimers calculated at BP86-D3/cc-pVDZ level of theory are given in Tables S17−S24.

Table S17. Cartesian coordinates of $[(PhSi)_4S_6]_2$ (alternating).

S	1.49970598	-2.07688909	0.08535839
Si	2.26418564	-1.00314978	-1.63830185
C	1.63277414	-1.94950293	-3.13507285
C	1.40656894	-3.34155544	-3.05529689
C	0.89245194	-4.04142830	-4.15851800
C	0.60005603	-3.35894122	-5.35219123
C	0.83331764	-1.97575921	-5.44400077
C	1.34793653	-1.27391858	-4.34234762
H	1.51246350	-0.18794718	-4.41854201
H	0.60864577	-1.43867502	-6.37828795
H	0.19006329	-3.90722957	-6.21427894
H	0.71459912	-5.12529871	-4.08443773
H	1.61713559	-3.88091195	-2.11874729
S	4.43514276	-1.03527933	-1.72548037
Si	5.00950386	0.08441428	0.05278908
C	6.89114776	0.08678208	0.03556018
C	7.60403350	1.12598530	-0.60394917
C	9.00670776	1.09541608	-0.66104341
C	9.71098043	0.02539194	-0.08212653
C	9.01153706	-1.01589306	0.55261124
C	7.60901718	-0.98664959	0.61054921
H	7.06563183	-1.80684575	1.10633869
H	9.56106305	-1.85529532	1.00562972
H	10.81084592	0.00233185	-0.12661156
H	9.55241881	1.91117603	-1.15956685
H	7.05718703	1.96500578	-1.06293059
S	4.40547773	-0.90173536	1.89553275
Si	2.23311171	-0.88635932	1.73953736
C	1.58188837	-1.71754223	3.29446132
C	1.31923402	-3.10520799	3.30837109
C	0.79086315	-3.71584230	4.45686713
C	0.52187040	-2.94765711	5.60303257
C	0.79226834	-1.56814844	5.60199182
C	1.32009570	-0.95518599	4.45437978
H	1.51385874	0.12870991	4.45612456
H	0.58660069	-0.96455031	6.49934940
H	0.10129675	-3.42604496	6.50091778
H	0.58366254	-4.79701337	4.45554193
H	1.51235365	-3.71157713	2.40986254
S	1.43168735	1.12815418	1.78237006
Si	2.20358366	1.98272357	-0.05402215
C	1.52791447	3.73543497	-0.12158288
C	1.27948372	4.35698517	-1.36541425
C	0.73417065	5.64976828	-1.41630456
C	0.43313893	6.33493452	-0.22627782
C	0.68862498	5.72839905	1.01587417
C	1.23417321	4.43585130	1.06925537
H	1.41674396	3.96243537	2.04637405
H	0.45756533	6.26358191	1.94968077
H	-0.00091330	7.34580999	-0.26711541
H	0.53899611	6.12348333	-2.39069013
H	1.49743026	3.82100721	-2.30219916
S	1.46766105	1.00438996	-1.84125819
S	4.37452113	2.16319738	-0.02252926
S	-4.40554116	0.90170798	-1.89556582
Si	-5.00956174	-0.08442104	-0.05281234
C	-6.89120513	-0.08683807	-0.03553761
C	-7.60399851	-1.12579346	0.60448207
C	-9.00666915	-1.09526265	0.66166568
C	-9.71103286	-0.02552624	0.08232681
C	-9.01168269	1.01551015	-0.55292003
C	-7.60916472	0.98630680	-0.61094462
H	-7.06585285	1.80631298	-1.10712830
H	-9.56127971	1.85468708	-1.00626969
H	-10.81089619	-0.00249691	0.12688119
H	-9.55230681	-1.91082712	1.16058922
H	-7.05707955	-1.96458560	1.06379507
S	-4.37456777	-2.16320223	0.02252200
Si	-2.20363334	-1.98272883	0.05402892
C	-1.52796025	-3.73543741	0.12161194
C	-1.23417693	-4.43585651	-1.06921435
C	-0.68863281	-5.72840493	-1.01581137
C	-0.43319832	-6.33494038	0.22635137
C	-0.73427358	-5.64977173	1.41636561
C	-1.27957717	-4.35698551	1.36545359
H	-1.49755379	-3.82100497	2.30222993
H	-0.53914086	-6.12348642	2.39075953
H	0.00084788	-7.34581778	0.26720690
H	-0.45753731	-6.26358922	-1.94960834
H	-1.41671285	-3.96244250	-2.04634037
S	-1.46771466	-1.00437122	1.84125298
Si	-2.26424596	1.00316392	1.63827759
C	-1.63284159	1.94952821	3.13504513
C	-1.40663494	3.34158015	3.05526698
C	-0.89252634	4.04145564	4.15849078
C	-0.60013871	3.35897197	5.35216784
C	-0.83340199	1.97579024	5.44397971
C	-1.34801443	1.27394767	4.34232490
H	-1.51254453	0.18797686	4.41852099
H	-0.60873706	1.43870880	6.37827036
H	-0.19015152	3.90726251	6.21425680
H	-0.71467288	5.12532583	4.08440926
H	-1.61719452	3.88093440	2.11871444
S	-4.43520171	1.03529092	1.72544689
S	-1.49977165	2.07689673	-0.08539192
Si	-2.23317179	0.88634222	-1.73955438
C	-1.58195418	1.71748252	-3.29450374
C	-1.31917245	3.10512384	-3.30843254
C	-0.79079758	3.71570413	-4.45695549
C	-0.52193819	2.94749025	-5.60313311
C	-0.79246839	1.56800763	-5.60207497
C	-1.32028966	0.95509709	-4.45443239
H	-1.51414729	-0.12878209	-4.45616177
H	-0.58690864	0.96438739	-6.49944229
H	-0.10136533	3.42583549	-6.50104136
H	-0.58348957	4.79685478	-4.45564380
H	-1.51219503	3.71151526	-2.40991827
S	-1.43173782	-1.12816776	-1.78236655

Table S18. Cartesian coordinates of [(PhSi)$_4$S$_6$] (stacking).

S	1.01715024	0.59843551	1.73410988
Si	2.62731818	-0.86493810	1.69681824
C	2.19502463	-2.16992271	2.98040083
C	1.31942625	-3.23316444	2.66172771
C	1.01213525	-4.21267611	3.61702285
C	1.58122167	-4.14620676	4.89975759
C	2.44786690	-3.09139859	5.23113689
C	2.74903023	-2.10479287	4.27874409
H	3.42751817	-1.27920432	4.54597763
H	2.89060968	-3.03374200	6.23734378
H	1.34023521	-4.91664250	5.64809071
H	0.31967764	-5.02753812	3.35939816
H	0.87336392	-3.29818327	1.65770450
S	4.51803325	-0.00584080	2.32417885
Si	4.89789958	1.49919507	0.79278237
C	6.53062639	2.28075614	1.30388835
C	6.56626586	3.50643568	2.00539615
C	7.79161429	4.05167233	2.42198020
C	8.99261543	3.37625343	2.14402665
C	8.96840899	2.15361919	1.45009529
C	7.74427342	1.60764955	1.03274375
H	7.73016187	0.64838711	0.49079865
H	9.90790122	1.62287490	1.23222758
H	9.95298146	3.80448402	2.47045130
H	7.80863154	5.00843089	2.96614313
H	5.62775571	4.03784063	2.23005006
S	3.41456858	3.07098061	0.69908866
Si	1.58268271	1.99236829	0.18453560
C	0.32370077	3.38077218	0.15927662
C	0.19123771	4.19736901	-0.98631444
C	-0.57898242	5.36865770	-0.93381533
C	-1.22041095	5.73668814	0.26112333
C	-1.11502899	4.91783955	1.39632470
C	-0.34484044	3.74510918	1.34862317
H	-0.25062916	3.11501767	2.24640195
H	-1.63519382	5.19359132	2.32556932
H	-1.82343251	6.65513507	0.30120702
H	-0.67798030	6.00024227	-1.82968799
H	0.70657263	3.92022241	-1.91951427
S	1.67346733	1.09618593	-1.79737621
Si	3.28841382	-0.33656000	-1.58098286
C	3.63365262	-1.09004070	-3.26528530
C	4.20313969	-2.37887555	-3.36501127
C	4.62702514	-2.87393361	-4.60815095
C	4.49073182	-2.08292770	-5.76284924
C	3.92416578	-0.80005131	-5.67365058
C	3.49675654	-0.30562489	-4.43080698
H	3.06072512	0.70345946	-4.36417002
H	3.81351256	-0.18052025	-6.57673973
H	4.82933895	-2.46848310	-6.73697716
H	5.06972632	-3.87951340	-4.67590971
H	4.32401535	-2.99568548	-2.46035363
S	2.75318497	-1.92787711	-0.20556473
S	5.21702393	0.57695778	-1.14371098
S	-3.42722681	-2.04316142	-2.33726542
Si	-4.86081446	-1.50095034	-0.81044898
C	-6.49016802	-2.34136073	-1.23069460
C	-6.52345266	-3.51418852	-2.01767075
C	-7.74281434	-4.15931957	-2.28066642
C	-8.94003018	-3.64040326	-1.75783566
C	-8.91790666	-2.47610340	-0.96994419
C	-7.69969734	-1.83002550	-0.70645182
H	-7.68707940	-0.91921274	-0.08651221
H	-9.85438051	-2.06878603	-0.55895759
H	-9.89573985	-4.14638904	-1.96480422
H	-7.75819740	-5.07143731	-2.89678384
H	-5.58764032	-3.92785900	-2.42614070
S	-4.37445275	-2.23875664	1.18297531
Si	-2.48881711	-1.25637715	1.61352720
C	-1.96558029	-1.85015189	3.31966236
C	-2.46729745	-3.06505071	3.83833479
C	-2.09791996	-3.49698634	5.12216206
C	-1.21527225	-2.72520073	5.89595236
C	-0.69771927	-1.52346899	5.38434123
C	-1.07242753	-1.08641785	4.10568341
H	-0.66596551	-0.14051953	3.71662689
H	0.00704771	-0.92527548	5.98041942
H	-0.92133659	-3.06619885	6.90043810
H	-2.50030183	-4.44195144	5.51830103
H	-3.15852142	-3.67597312	3.23641115
S	-2.66589118	0.91341950	1.77586557
Si	-3.30332154	1.46897579	-0.22257139
C	-3.69917641	3.30389672	-0.23870737
C	-3.63605485	4.02880040	-1.44828815
C	-4.10351636	5.35157312	-1.50838195
C	-4.63642203	5.96185099	-0.36021704
C	-4.69903210	5.24959923	0.85071254
C	-4.23534977	3.92615884	0.91050973
H	-4.29907925	3.36635638	1.85711192
H	-5.11530475	5.72606238	1.75152520
H	-5.00640799	6.99769082	-0.40900655
H	-4.05046000	5.90843786	-2.45638742
H	-3.22647027	3.55174913	-2.35244232
S	-5.23638040	0.63445180	-0.78183560
S	-1.73831234	1.09960170	-1.67901772
Si	-1.58922093	-1.07213935	-1.65726749
C	-0.37010553	-1.60461504	-2.97770553
C	-0.30668112	-0.91030491	-4.20680756
C	0.43437011	-1.43382823	-5.27670811
C	1.11530540	-2.65440551	-5.13117471
C	1.07822341	-3.33793985	-3.90574203
C	0.33717934	-2.81832725	-2.83261446
H	0.29650253	-3.36689405	-1.87905775
H	1.62913665	-4.28229388	-3.78391335
H	1.69591342	-3.06353194	-5.97039102
H	0.47966118	-0.88782088	-6.23121698
H	-0.85283854	0.03834924	-4.32917597
S	-0.92057651	-1.86941888	0.23511494

Table S19. Cartesian coordinates of $[(NpSi)_4S_6]_2$ (alternating).

S	-1.32424564	-1.07316990	-2.00078151
Si	-2.22050522	-2.25698887	-0.41807486
C	-1.42963569	-3.96133947	-0.56329180
C	-0.76164447	-4.48047463	0.54804986
C	-0.02830332	-5.69315576	0.47171388
C	0.05674420	-6.37319255	-0.73267454
C	-0.62438772	-5.89908544	-1.89379900
C	-0.56387070	-6.60701636	-3.13210008
C	-1.26330845	-6.16165164	-4.24501570
C	-2.05378108	-4.98254974	-4.15938314
C	-2.11826249	-4.25990735	-2.97519380
C	-1.40418927	-4.68278048	-1.81165979
H	-2.73427776	-3.35019701	-2.93087217
H	-2.61729676	-4.63489934	-5.03831367
H	-1.21275671	-6.72131329	-5.19138813
H	0.04288747	-7.52505692	-3.18295897
H	0.64794604	-7.29967880	-0.80946886
H	0.48392584	-6.07147344	1.36669649
H	-0.77773108	-3.94032349	1.50729100
S	-4.37249084	-2.51918649	-0.66795970
Si	-5.12907965	-0.48549303	-0.50216299
C	-7.00390483	-0.57650953	-0.71319091
C	-7.59554762	-1.82201770	-0.93453733
C	-8.99965515	-1.95696192	-1.10229902
C	-9.81386806	-0.83674510	-1.04825109
C	-9.26196667	0.46002880	-0.82539670
C	-10.09501350	1.61772482	-0.76920906
C	-9.55336795	2.87605243	-0.55234498
C	-8.14982997	3.02211043	-0.38257808
C	-7.31215878	1.91617330	-0.43180350
C	-7.83256607	0.60403682	-0.65327249
H	-6.22968391	2.05313353	-0.29673403
H	-7.72087998	4.02069857	-0.20984269
H	-10.20623447	3.76110509	-0.51098290
H	-11.18116040	1.49016553	-0.90213334
H	-10.90413235	-0.92992078	-1.17711960
H	-9.43198155	-2.95401266	-1.27477140
H	-6.96882281	-2.72612741	-0.98259943
S	-4.77789260	0.35085369	1.47895798
Si	-2.60638676	0.44089651	1.59925324
C	-2.15222007	1.15588336	3.28277684
C	-1.47512809	2.37659169	3.32700377
C	-0.99262580	2.91223691	4.54948730
C	-1.16614465	2.20524134	5.72860060
C	-1.86892120	0.96314630	5.74373416
C	-2.07531424	0.24040166	6.95748270
C	-2.79783747	-0.94449279	6.96983750
C	-3.34360508	-1.45373531	5.75938090
C	-3.14378026	-0.78551168	4.55843935
C	-2.39677977	0.43167600	4.50557064
H	-3.57354898	-1.19772830	3.63404461
H	-3.92683785	-2.38679601	5.77043167
H	-2.95510420	-1.48738881	7.91425981
H	-1.65783777	0.65103325	7.89057381
H	-0.76932908	2.59835689	6.67823133
H	-0.46612332	3.87618578	4.54578383
H	-1.28606354	2.94014546	2.40030824
S	-1.69887538	-1.53248412	1.54575116
S	-1.75437272	1.78817593	0.14225245
Si	-2.25546621	0.85904983	-1.75581830
C	-1.48949176	1.96844539	-3.07279571
C	-0.58803072	1.40344344	-3.97763810
C	0.12098508	2.20127166	-4.91310657
C	-0.05607321	3.57562925	-4.92182162
C	-0.98095899	4.20275209	-4.03399241
C	-1.18974951	5.61493626	-4.05342428
C	-2.12248871	6.21134751	-3.21647954
C	-2.88523778	5.41092652	-2.32205988
C	-2.69213771	4.03694665	-2.26445424
C	-1.73386054	3.38923097	-3.10375994
H	-3.29042459	3.43626581	-1.56429443
H	-3.63254648	5.88219826	-1.66603451
H	-2.27768686	7.30054216	-3.24722784
H	-0.60108721	6.22309515	-4.75852997
H	0.51119908	4.20672792	-5.62448340
H	0.82089871	1.72155096	-5.61059431
H	-0.39752292	0.31911163	-3.96705579
S	-4.40025059	0.78525689	-2.11518378
S	1.18221247	0.58578907	2.17822675
Si	2.06504308	1.86915830	0.66184443
C	1.29130775	3.56567404	0.93950570
C	0.54315386	4.13738601	-0.09155670
C	-0.13860087	5.37077334	0.08228664
C	-0.07239245	6.02958551	1.29979509
C	0.69744896	5.50191752	2.38000685
C	0.78837869	6.18602760	3.63021957
C	1.55591822	5.67727432	4.66928339
C	2.25570084	4.45187528	4.49757212
C	2.17538235	3.75435426	3.29971999
C	1.40191493	4.25014487	2.20498004
H	2.71739140	2.80403422	3.19297772
H	2.86111342	4.04619187	5.32175472
H	1.62135634	6.21812013	5.62555243
H	0.24060957	7.13415313	3.75094056
H	-0.60952337	6.97953246	1.45177017
H	-0.72660921	5.77871252	-0.75159785
H	0.45611503	3.62676210	-1.06275513
S	4.21510493	2.12646838	0.90226311
Si	4.99291133	0.11338979	0.62793795
C	6.86796082	0.23222892	0.82033926
C	7.48798551	-0.50795885	1.82929126
C	8.89470783	-0.46569296	2.02244275
C	9.68305702	0.32182611	1.19833898
C	9.10165073	1.09783024	0.15156326
C	9.90785745	1.91048451	-0.70107790
C	9.33725338	2.66322992	-1.71677469
C	7.93045881	2.63015018	-1.91675049
C	7.11853886	1.84972116	-1.10504978
C	7.66926189	1.06027536	-0.04907854
H	6.03277430	1.84007961	-1.27754912
H	7.47844133	3.22873049	-2.72198372
H	9.96960062	3.28599335	-2.36759659
H	10.99674882	1.92737301	-0.53469352
H	10.77516666	0.36127230	1.33873117
H	9.34986523	-1.06172945	2.82764626
H	6.88235078	-1.14289358	2.49463094
S	4.63798892	-0.67463345	-1.36833501
Si	2.46554206	-0.70372076	-1.51580303
C	2.05626943	-1.28523557	-3.26188466
C	1.30610957	-2.45193806	-3.42213005
C	0.88513543	-2.89295251	-4.70455452
C	1.21495413	-2.15511438	-5.83035974
C	2.00097126	-0.96799578	-5.72652585
C	2.36260684	-0.21364517	-6.88390513
C	3.14351307	0.92929394	-6.77718789
C	3.58509558	1.36717613	-5.49887470
C	3.23826606	0.66431037	-4.35284113
C	2.44086054	-0.51964033	-4.42304889

H	3.58208751	1.02667091	-3.37379596
H	4.20091339	2.27488780	-5.41329711
H	3.41869211	1.49805487	-7.67829887
H	2.01346984	-0.56319587	-7.86850299
H	0.88001762	-2.47835365	-6.82898861
H	0.28466286	-3.80979138	-4.78374028
H	1.01237365	-3.04758008	-2.54430609
S	1.55675581	1.26435447	-1.35245468
S	1.61045654	-2.14517876	-0.14716820
Si	2.12789214	-1.32082424	1.79446794
C	1.43281824	-2.54694468	3.04665181
C	0.47339381	-2.10054604	3.95768478
C	-0.16208605	-2.99181060	4.86215437
C	0.16402998	-4.33865913	4.84661675
C	1.15494097	-4.84459790	3.95216274
C	1.51044544	-6.22768323	3.94457885
C	2.48804680	-6.70979477	3.08468643
C	3.14263252	-5.82108979	2.18884142
C	2.81000247	-4.47329251	2.16151943
C	1.81311994	-3.93896301	3.03531855
H	3.32338111	-3.80629431	1.45458627
H	3.91503760	-6.20279311	1.50461577
H	2.75517826	-7.77742066	3.09285975
H	0.99527775	-6.90585079	4.64331957
H	-0.33397589	-5.04276085	5.53232427
H	-0.92145347	-2.60026122	5.55318717
H	0.17900552	-1.04010174	3.97820163
S	4.27825481	-1.23979334	2.17011095

Table S20. Cartesian coordinates of $[(NpSi)_4S_6]_2$ (stacking).

S	1.69516822	-2.00385067	0.62028539
Si	1.92343103	-1.51099154	-1.48529132
C	0.63714124	-2.44990473	-2.49204532
C	-0.00630630	-1.75829277	-3.52050695
C	-1.05479207	-2.35139055	-4.26815552
C	-1.50821940	-3.61911388	-3.94176390
C	-0.86373296	-4.38107067	-2.92325961
C	-1.29489685	-5.70346740	-2.60415214
C	-0.60959642	-6.47385489	-1.67544165
C	0.54679932	-5.94830085	-1.03675402
C	0.96916308	-4.65062383	-1.29623524
C	0.26786602	-3.81630272	-2.21939807
H	1.86472019	-4.26359612	-0.78964954
H	1.11649411	-6.57239945	-0.33177786
H	-0.94698360	-7.49604618	-1.44598313
H	-2.17606087	-6.10625321	-3.12807225
H	-2.36752162	-4.05759740	-4.47293672
H	-1.52810687	-1.78193066	-5.07902146
H	0.27596585	-0.71843526	-3.74628770
S	3.82387247	-2.14352039	-2.31414866
Si	5.26677883	-0.94094242	-1.21264565
C	6.97520018	-1.37998066	-1.88795886
C	7.93143338	-1.89587108	-1.01036289
C	9.23444824	-2.24549079	-1.45504072
C	9.57975209	-2.07606211	-2.78653118
C	8.64224562	-1.55168017	-3.72568291
C	8.99242903	-1.37344367	-5.09787591
C	8.07760802	-0.86204627	-6.00641644
C	6.77144640	-0.50821873	-5.57192845
C	6.39927522	-0.66948791	-4.24419642
C	7.31329907	-1.19354222	-3.27905430
H	5.38351511	-0.38750203	-3.93163592
H	6.04625200	-0.10187889	-6.29295782
H	8.35958717	-0.72910133	-7.06193158
H	10.00829873	-1.65142127	-5.42103589
H	10.58749323	-2.34413202	-3.14234913
H	9.96266320	-2.64990244	-0.73605724
H	7.68066302	-2.03805867	0.05241534
S	5.00898336	1.19022343	-1.56652610
Si	3.03178907	1.64836999	-0.76601110
C	2.95413725	3.53740996	-0.90656125
C	4.02911024	4.15203511	-0.24894777
C	4.20316611	5.55926822	-0.25744806
C	3.29842985	6.36066451	-0.93630751
C	2.18394671	5.79053579	-1.61703883
C	1.24160992	6.61697263	-2.29814828
C	0.13655054	6.07060497	-2.93144834
C	-0.06499146	4.66651066	-2.90293285
C	0.83962490	3.83538981	-2.25811674
C	1.99102519	4.35503742	-1.59780466
H	0.64795075	2.75639053	-2.24121026
H	-0.95596540	4.22960942	-3.37755172
H	-0.59375183	6.72146243	-3.43355026
H	1.40243173	7.70631947	-2.29440000
H	3.42434089	7.45506066	-0.95768711
H	5.05930628	6.00363642	0.27192946
H	4.76730097	3.53362794	0.28687240
S	1.44854237	0.58999575	-1.79695049
S	2.98062582	1.28911516	1.37954488
Si	3.28023699	-0.85363527	1.55679026
C	3.19546555	-1.24138899	3.39734769
C	2.24128078	-2.15812966	3.84291491
C	2.10600223	-2.47189824	5.22034413
C	2.92349110	-1.85739689	6.15422406
C	3.91845451	-0.91653824	5.75391629
C	4.76827420	-0.28508384	6.71106681
C	5.74065767	0.62114965	6.31433729
C	5.90093932	0.92681808	4.93566565
C	5.08861845	0.33143065	3.97978396
C	4.07126576	-0.60106823	4.35031219
H	5.23513244	0.58001765	2.91876428
H	6.67699673	1.64047420	4.61997768
H	6.39010897	1.10094694	7.06227029
H	4.63630988	-0.53561098	7.77578981
H	2.81673254	-2.08763323	7.22652716
H	1.33969054	-3.19237211	5.53475877
H	1.56947101	-2.65379766	3.12553826
S	5.26515513	-1.47119831	0.89509329
S	-1.92961840	1.87325587	-1.54011709
Si	-1.70441512	2.20426570	0.60469810
C	-0.68332443	3.76984207	0.83187788
C	0.49385617	3.67591412	1.57555512
C	1.29506151	4.81498928	1.84699221
C	0.89473912	6.06122116	1.39539080
C	-0.31221557	6.21828384	0.65075147
C	-0.73842381	7.50346113	0.20149130
C	-1.91074338	7.65488245	-0.52441931
C	-2.69447025	6.51394913	-0.84289905
C	-2.30549261	5.24849201	-0.42236330
C	-1.11592310	5.05697445	0.34290088
H	-2.92471565	4.37848480	-0.68430957
H	-3.61922251	6.63045274	-1.42812335
H	-2.22976693	8.65268996	-0.86186931
H	-0.11296721	8.37685303	0.44549860
H	1.50422496	6.95427767	1.60381147
H	2.22882781	4.69513095	2.41489068

H	0.82377573	2.70115608	1.96266978
S	-3.60893032	2.65876431	1.56968280
Si	-4.78019347	0.85850831	1.26064009
C	-6.47334468	1.15750206	2.04187562
C	-6.72819740	2.39427836	2.63848163
C	-7.98203819	2.68316231	3.24042472
C	-8.98525207	1.72693087	3.24269645
C	-8.77887288	0.44700075	2.64674832
C	-9.80809358	-0.54197938	2.64534213
C	-9.60195367	-1.78480158	2.06503031
C	-8.35041037	-2.08481745	1.46193707
C	-7.32899156	-1.14478181	1.44629432
C	-7.50344536	0.14623429	2.03326486
H	-6.36865070	-1.39971735	0.97549792
H	-8.18716889	-3.07152716	1.00282684
H	-10.40343165	-2.53904616	2.07047370
H	-10.77305594	-0.29645327	3.11676193
H	-9.96167246	1.94055725	3.70632580
H	-8.14809440	3.66817982	3.70186025
H	-5.94702528	3.17038320	2.64712936
S	-3.90402243	-0.84285034	2.27797374
Si	-1.96541254	-1.09939022	1.31491783
C	-1.31361837	-2.62608049	2.21503252
C	-1.08821447	-3.79149603	1.47969123
C	-0.80317341	-5.02572573	2.12035471
C	-0.79079487	-5.10385432	3.50416432
C	-1.02052785	-3.94478228	4.30401518
C	-1.03124333	-4.01539427	5.73051552
C	-1.21812223	-2.87476583	6.49909940
C	-1.37630285	-1.61266553	5.86525518
C	-1.38915512	-1.51361302	4.48062035
C	-1.24006007	-2.67034064	3.65556211
H	-1.50453664	-0.52686049	4.00890813
H	-1.48993352	-0.70428193	6.47522088
H	-1.22403242	-2.94176651	7.59751636
H	-0.88065404	-4.99634854	6.20900145
H	-0.60553810	-6.06493211	4.00998081
H	-0.61805613	-5.91637297	1.50340790
H	-1.13713533	-3.77478060	0.38036364
S	-0.61708642	0.58807511	1.56281714
S	-2.14658668	-1.63871702	-0.77848924
Si	-3.15627073	0.08932283	-1.63026685
C	-3.43542757	-0.28575932	-3.46001639
C	-2.92657737	0.59871577	-4.41273344
C	-3.08851828	0.36334782	-5.80457629
C	-3.74946476	-0.77494091	-6.24168849
C	-4.28427095	-1.71418905	-5.30918112
C	-4.92637248	-2.91031288	-5.75071772
C	-5.42270972	-3.83078965	-4.83851809
C	-5.30473510	-3.57952727	-3.44419813
C	-4.68813279	-2.42425883	-2.98363349
C	-4.14482232	-1.46486930	-3.89135699
H	-4.60161890	-2.25397885	-1.90127563
H	-5.70329090	-4.30691307	-2.72121759
H	-5.91024455	-4.75228109	-5.19114871
H	-5.01607457	-3.09005036	-6.83376634
H	-3.86443011	-0.97706857	-7.31848947
H	-2.67471719	1.08107759	-6.52857919
H	-2.37664276	1.49570487	-4.08831351
S	-5.14824442	0.45759789	-0.84779364

Table S21. Cartesian coordinates of $[(PhSn)_4S_6]_2$ (alternating).

S	1.41948178	1.66184291	-1.69918952
Sn	2.17873153	-0.62232735	-2.10927277
Sn	2.20633594	2.11792205	0.56467971
S	1.40539653	0.63463288	2.32882700
S	1.37924909	-2.33953776	-0.57478044
Sn	2.19179771	-1.55480432	1.59110019
S	4.63389212	-1.66153583	1.65544443
S	4.62404436	-0.66075269	-2.27281268
S	4.65360203	2.24963873	0.59990310
Sn	5.31956268	-0.01644569	-0.02196207
C	1.39041306	-1.15495553	-4.03019053
C	1.22386355	-0.16691543	-5.01882707
C	0.95829755	-2.47483507	-4.26105338
C	0.61015880	-0.50149526	-6.23886238
H	1.55352664	0.86791387	-4.83664534
C	0.34609600	-2.80190281	-5.48281509
H	1.07725126	-3.24680626	-3.48458217
C	0.16728929	-1.81567835	-6.46872435
H	0.47416292	0.26949992	-7.01303882
H	0.00236793	-3.83208338	-5.66364292
H	-0.31927032	-2.07273027	-7.42172405
C	1.41380267	-2.94513086	3.02599502
C	1.22405909	-4.29290008	2.66659300
C	1.01219725	-2.48225186	4.29345081
C	0.61711777	-5.17616782	3.57679413
H	1.53122613	-4.65523762	1.67302240
C	0.40683706	-3.37074890	5.19832026
H	1.15043973	-1.42594612	4.57283317
C	0.20435212	-4.71473122	4.83887383
H	0.46299086	-6.22998692	3.29751838
H	0.08731096	-3.00993167	6.18819853
H	-0.27668645	-5.40670281	5.54654891
C	1.44433349	4.06178837	1.05078713
C	1.24227630	4.41908251	2.39726995
C	1.06336966	4.93704010	0.01600656
C	0.64395859	5.65327386	2.70648600
H	1.53204082	3.73201675	3.20768887
C	0.46609822	6.16903799	0.33256935
H	1.21071679	4.65485252	-1.03828822
C	0.25150068	6.52476585	1.67567158
H	0.47998590	5.93418139	3.75838051
H	0.16241988	6.85309566	-0.47490570
H	-0.22330352	7.48686271	1.92052931
C	7.46754938	-0.00941562	-0.05276231
C	8.17888481	0.85916890	0.79853430
C	8.15976823	-0.87570616	-0.92196367
C	9.58444430	0.85814481	0.77898046
H	7.64122699	1.54274686	1.47467231
C	9.56539446	-0.87175727	-0.93656110
H	7.60707564	-1.55144335	-1.59385950
C	10.27623508	-0.00677009	-0.08661603
H	10.14088709	1.53782326	1.44242238
H	10.10690730	-1.54696917	-1.61671110
H	11.37683048	-0.00526934	-0.10035412
S	-1.41244445	-1.67265939	1.73929705
Sn	-2.20734606	-2.12760316	-0.51979238
Sn	-2.19358960	0.60801129	2.13568709
S	-1.37942102	2.33291408	0.61235277
S	-1.41443935	-0.64042519	-2.28677498
Sn	-2.17774931	1.55914538	-1.55916008
S	-4.62270270	1.69058785	-1.66897699
S	-4.65436736	-2.25091655	-0.58415076
S	-4.63613443	0.64831717	2.24802364
Sn	-5.32007440	0.03017820	-0.01900941

C	-1.44854684	-4.06967677	-1.01804252
C	-1.02611550	-4.93365932	0.01013470
C	-1.29245330	-4.43787326	-2.36768354
C	-0.43379978	-6.16530842	-0.31641360
H	-1.13744110	-4.64270575	1.06652902
C	-0.69849133	-5.67174932	-2.68701006
H	-1.61551567	-3.76008255	-3.17329828
C	-0.26504904	-6.53193595	-1.66316174
H	-0.09772253	-6.84029088	0.48582389
H	-0.57067364	-5.96142577	-3.74153820
H	0.20595531	-7.49376182	-1.91629975
C	-1.38688343	2.93857093	-2.99670503
C	-0.99801581	2.47045577	-4.26620081
C	-1.17528772	4.28289777	-2.63684657
C	-0.38381712	3.35076172	-5.17312872
H	-1.15245482	1.41643827	-4.54562310
C	-0.55963043	5.15774523	-3.54922950
H	-1.47119823	4.64867993	-1.64115706
C	-0.15986960	4.69132710	-4.81366376
H	-0.07416055	2.98597420	-6.16467292
H	-0.38806658	6.20878869	-3.26965948
H	0.32823002	5.37661815	-5.52299534
C	-1.41506687	1.14421411	4.06017441
C	-1.01194015	2.47130582	4.30163739
C	-1.22432829	0.15197430	5.04028276
C	-0.40407726	2.80149988	5.52485315
H	-1.15059608	3.24695837	3.53217801
C	-0.61536384	0.48952462	6.26178749
H	-1.53165059	-0.88829379	4.84992765
C	-0.20099414	1.81117492	6.50186590
H	-0.08314855	3.83754281	5.71407379
H	-0.46059172	-0.28481031	7.02907650
H	0.28191490	2.07089299	7.45599999
C	-7.46810058	0.03702734	-0.04600896
C	-8.16279878	1.21599035	-0.38142633
C	-8.17691426	-1.13673047	0.27811806
C	-9.56848001	1.21817433	-0.39059838
H	-7.61209649	2.13385593	-0.64174173
C	-9.58254246	-1.12778787	0.26700751
H	-7.63716952	-2.06217199	0.53456714
C	-10.27681800	0.04825904	-0.06585085
H	-10.11202829	2.13839490	-0.65422028
H	-10.13707056	-2.04487089	0.51842195
H	-11.37746249	0.05255116	-0.07407589

Table S22. Cartesian coordinates of $[(PhSn)_4S_6]_2$ (stacking).

Sn	-1.75512245	0.97561227	1.59394100
Sn	1.68205188	-1.95181646	0.32488213
Sn	5.23577559	-0.67428222	-0.41096217
Sn	-2.01508399	0.41048226	-2.21300618
Sn	3.09554611	1.10799072	2.22903987
Sn	-5.18461427	0.93994740	-0.15120413
Sn	-3.19021808	-2.32485541	0.16037067
Sn	2.22010977	1.42212431	-1.46797692
S	-1.67985014	-1.45289507	1.87569818
S	1.06682346	-0.73766345	-1.69827044
S	-4.28254193	1.35773664	-2.37988527
S	5.39282161	0.45185780	1.76104193
S	-4.03125462	1.87778562	1.78344718
S	1.50096650	-0.73464832	2.43907613
S	2.23467369	2.71628004	0.61547330
S	-5.46717324	-1.46500582	0.23029566
S	3.96846033	-2.73670371	-0.10874226
S	-0.94261023	1.85120112	-0.53171720
S	-2.15485568	-2.03134519	-2.02484517
S	4.53091849	0.89518848	-2.14033196
C	-0.73662784	1.93131943	3.21846326
C	0.57226277	-3.78116264	0.43025610
C	7.22573522	-1.27929465	-0.94955469
C	-1.16017270	0.77919140	-4.14957074
C	3.23940512	2.05700170	4.14571466
C	-7.14768615	1.81307392	-0.14817230
C	-3.45247753	-4.41851999	0.53840618
C	1.56766077	2.79347278	-2.98883502
C	-0.63645504	1.28248272	4.46411666
C	0.20099995	-4.42661885	-0.76473566
C	8.02556759	-0.43724767	-1.74724715
C	-1.52245303	1.95492801	-4.83452167
C	3.12422495	1.28464868	5.31654299
C	-7.72948531	2.22591785	1.06696949
C	-3.45422131	-4.89183615	1.86376451
C	0.76010981	3.90118756	-2.66691459
C	-0.11640033	1.97961989	5.56765348
C	-0.38468971	-5.70315187	-0.70844285
C	9.32992834	-0.83376852	-2.09001097
C	-1.06484801	2.16279283	-6.14612519
C	3.31963462	1.88704154	6.57154232
C	-9.01728062	2.78939446	1.06772276
C	-3.73047127	-6.24610464	2.12029610
C	0.44296124	4.84356592	-3.66030141
C	0.30060015	3.31339063	5.42689868
C	-0.58786682	-6.33216563	0.53013931
C	9.83320304	-2.06599106	-1.63802292
C	-0.24610258	1.20557014	-6.76869087
C	3.62853004	3.25552755	6.65490768
C	-9.72112299	2.93961185	-0.13977486
C	-4.00307263	-7.12272443	1.05629188
C	0.93877550	4.68503201	-4.96512481
C	0.21815521	3.94969412	4.17813461
C	-0.23054093	-5.67770514	1.72041708
C	3.74060782	4.02620925	5.48431308
C	-9.13922310	2.52880462	-1.35162891
C	9.03380985	-2.90618161	-0.84360459
C	0.12378869	0.03912479	-6.07881012
C	-3.99828171	-6.64871066	-0.26741782
C	1.74076727	3.57634934	-5.28399750
C	-0.30556411	3.26333198	3.06897500
C	0.35063618	-4.39927158	1.67588633
C	3.54744090	3.42835628	4.22719991
C	-7.85165410	1.96477077	-1.35920307
C	7.72873533	-2.51539610	-0.49723969
C	-0.33640197	-0.18023496	-4.76897185
C	-3.72438510	-5.29539833	-0.52902421
C	2.05606289	2.62604024	-4.29883723
H	-0.96223951	0.23672973	4.57669624
H	0.36277860	-3.93915807	-1.73782768
H	7.63338870	0.52720909	-2.10733489
H	-2.16605323	2.70803148	-4.35437770
H	2.87860884	0.21283367	5.25543814
H	-7.17986134	2.11482538	2.01519518
H	-3.23714607	-4.20893896	2.70002649
H	0.37752109	4.03639943	-1.64401967
H	-0.03347168	1.47635459	6.54263216
H	-0.68459323	-6.20707535	-1.63946636
H	9.95492817	-0.17673175	-2.71410625
H	-1.34782700	3.08135375	-6.68157682

H	3.23030545	1.28360652	7.48786303
H	-9.47164741	3.11360147	2.01652842
H	-3.73261277	-6.61709870	3.15669068
H	-0.18859448	5.70899596	-3.40793826
H	0.71565014	3.85180208	6.29066572
H	-1.05074708	-7.32836430	0.57014138
H	10.85473244	-2.37440763	-1.90806703
H	0.10965997	1.37241966	-7.79686605
H	3.78516363	3.72453683	7.63833624
H	-10.72929552	3.38136004	-0.13651079
H	-4.22300349	-8.18193851	1.25957999
H	0.69519115	5.42788612	-5.73997819
H	0.56479712	4.98764752	4.06327150
H	-0.40805139	-6.16411662	2.69132864
H	3.98170848	5.09832419	5.54916531
H	-9.68928276	2.64849378	-2.29763155
H	9.42674339	-3.87245133	-0.49186085
H	0.76833299	-0.71080290	-6.56220286
H	-4.21114780	-7.33509781	-1.10127570
H	2.12242573	3.44541397	-6.30762545
H	-0.37275760	3.76721034	2.09315387
H	0.62991954	-3.88819082	2.61039160
H	3.63585295	4.03582836	3.31276565
H	-7.39752096	1.64834695	-2.31170834
H	7.10428310	-3.17945100	0.12135173
H	-0.05170040	-1.10051599	-4.23696127
H	-3.72229490	-4.92834986	-1.56744404
H	2.68832164	1.76209307	-4.55529368

Table S23. Cartesian coordinates of $[(NpSn)_4S_6]_2$ (alternating).

Sn	2.0873546	2.3834615	0.0284209
Sn	-1.7363065	-2.1643846	0.8306481
Sn	-5.3414291	-0.8077556	0.7806772
S	2.1702178	1.6516887	2.3640015
S	-4.0348280	-2.7280220	1.4977455
S	0.9074288	0.8700451	-1.4657284
S	-0.7953537	-0.2055957	1.9416956
S	-5.3611679	-0.5700953	-1.6592870
C	1.0142393	4.2463541	-0.0472426
C	-0.7175330	-3.9709368	1.4203640
C	-7.3783734	-1.2253856	1.3506519
C	1.3539133	5.3335265	0.8230411
C	0.1733994	-3.9407265	2.4890258
C	-8.4292039	-0.2959702	1.0540431
C	0.6133860	6.5685047	0.6885998
C	0.9162685	-5.1024634	2.8371192
C	-9.7799994	-0.6399324	1.4444811
C	-0.4275173	6.6597644	-0.2828123
C	0.7651082	-6.2696567	2.1043612
C	-10.0175521	-1.8801085	2.1101412
C	-0.7292350	5.5877995	-1.1075941
C	-0.1672131	-6.3487815	1.0270317
C	-8.9774381	-2.7551695	2.3853528
C	0.0088832	4.3773297	-0.9993854
C	-0.9480519	-5.1786863	0.6817708
C	-7.6470326	-2.4258550	2.0010316
H	0.3314773	-3.0154698	3.0646939
H	1.6200769	-5.0624467	3.6789951
H	-0.9960078	7.5988771	-0.3572869
H	1.3577794	-7.1634593	2.3563161
H	-11.0496158	-2.1303930	2.4032962
H	-1.5404283	5.6590851	-1.8466033
H	-9.1727100	-3.7082897	2.8997891
H	-0.2395619	3.5399568	-1.6670852
H	-6.8319948	-3.1336044	2.2233767
S	4.4064554	2.8889003	-0.6028255
S	-1.5267473	-1.9074316	-1.5957920
S	-4.6632176	1.2133020	1.9770290
Sn	3.1330571	-0.5777591	2.2019243
Sn	2.2712796	-1.1640031	-1.5035080
Sn	-2.3444983	1.5689806	1.2739985
Sn	-3.0196302	-0.0698827	-2.1611817
Sn	5.4853528	0.7013997	-0.5133385
S	2.1223818	-2.1967774	0.6933493
S	5.5162380	-0.3685949	1.7035815
C	2.5978985	-1.4899941	4.0801979
C	1.3722620	-2.7106831	-2.7005968
S	4.5722085	-0.7835808	-2.2311622
S	-2.4303998	2.0567831	-1.1230178
C	-1.6846317	3.3663049	2.2606559
C	-3.0007656	0.1679658	-4.3102921
C	7.5494185	1.0644431	-1.0186640
C	3.1049231	-2.7794340	4.4459346
C	1.5700984	-0.8938807	4.8051476
C	0.7697103	-2.4253585	-3.9663716
C	1.2398104	-3.9600087	-2.1021476
C	-0.6777375	3.2632067	3.2141254
C	-2.3049636	4.6282072	1.9777533
C	-2.1002194	1.0527749	-4.9892257
C	-3.9560055	-0.5546271	-5.0201032
C	7.9453491	2.3758191	-1.2635069
C	8.4866131	-0.0178583	-1.1018086
C	2.5294886	-3.4419793	5.5972805
H	1.1643999	0.0816381	4.4942548
C	1.0087315	-1.5519268	5.9353794
C	-0.0376829	-3.4552380	-4.5843853
C	0.4793752	-4.9807351	-2.7364463
H	1.6902505	-4.1660785	-1.1178800
H	-0.2175396	2.2887984	3.4328007
C	-0.2173083	4.4162762	3.9071758
C	-1.8464430	5.7907597	2.7058352
C	-2.2382896	1.2122929	-6.4209834
C	-4.0690262	-0.4128169	-6.4313914
H	-4.6456246	-1.2348976	-4.4945660
H	7.2171597	3.2001986	-1.1964986
C	9.2958584	2.6688162	-1.6039761
C	9.8583655	0.2891560	-1.4477979
C	1.4795184	-2.7984738	6.3193969
H	0.1879579	-1.0709228	6.4880744
C	-0.1609224	-4.7224203	-3.9387376
H	0.3791289	-5.9592070	-2.2458228
H	0.6006897	4.3171221	4.6355805
C	-0.7954310	5.6510094	3.6599738
C	-3.2363093	0.4625726	-7.1120947
H	-4.8286975	-0.9949927	-6.9745897
H	9.5923534	3.7111988	-1.7953726
C	10.2280082	1.6459694	-1.6926325
H	1.0388475	-3.3197277	7.1837726
H	-0.7831229	-5.4969233	-4.4145099
H	-0.4435355	6.5488460	4.1896997
H	-3.3277762	0.5863158	-8.2029984
H	11.2749489	1.8666808	-1.9551001
C	0.9343872	7.6637447	1.5438654
C	1.9453047	7.5609879	2.4891266

C	2.3895407	5.2643155	1.8029391
C	2.6800904	6.3502623	2.6164433
H	2.9675356	4.3336428	1.9171501
H	3.4825757	6.2716033	3.3650266
H	2.1816456	8.4155530	3.1412837
H	0.3572564	8.5958432	1.4388845
C	-0.3660071	-7.5568398	0.2920553
C	-1.3173482	-7.6323243	-0.7162670
C	-1.9180461	-5.2955026	-0.3606162
C	-2.1052904	-6.4923423	-1.0365419
H	-2.5302861	-4.4229363	-0.6349333
H	-2.8625499	-6.5539259	-1.8321085
H	-1.4664949	-8.5737517	-1.2665536
H	0.2423002	-8.4370156	0.5546286
C	-10.8393891	0.2710956	1.1528566
C	-10.5888761	1.4724090	0.5054035
C	-8.2092370	0.9501068	0.3927193
C	-9.2618268	1.8133616	0.1236604
H	-7.1874833	1.2303871	0.0897008
H	-9.0673507	2.7676583	-0.3882684
H	-11.4155436	2.1651876	0.2865103
H	-11.8640735	0.0003112	1.4535646
C	3.0032838	-4.7401095	5.9567611
C	3.9935286	-5.3689361	5.2140352
C	4.1239431	-3.4544554	3.7091357
C	4.5564734	-4.7199637	4.0800369
H	4.5685401	-2.9638482	2.8279126
H	5.3369301	-5.2245151	3.4915146
H	4.3428183	-6.3730245	5.4981787
H	2.5581075	-5.2395271	6.8317221
C	-0.6939238	-3.1668931	-5.8181100
C	-0.5451561	-1.9322768	-6.4336346
C	0.9042239	-1.1718729	-4.6298737
C	0.2706075	-0.9311443	-5.8400438
H	1.5172498	-0.3794213	-4.1694600
H	0.3869724	0.0432684	-6.3345933
H	-1.0634018	-1.7188797	-7.3799218
H	-1.3226759	-3.9478033	-6.2746890
C	-2.4494283	7.0559199	2.4408322
C	-3.4680371	7.1813370	1.5067416
C	-3.3581085	4.7934456	1.0284505
C	-3.9272024	6.0376465	0.7976518
H	-3.7232355	3.9201576	0.4660308
H	-4.7367652	6.1382815	0.0593913
H	-3.9238322	8.1645461	1.3141928
H	-2.0846208	7.9352606	2.9947889
C	-1.3457672	2.0883766	-7.1105887
C	-0.3448593	2.7704182	-6.4310728
C	-1.0528134	1.7607801	-4.3300307
C	-0.1922683	2.5954790	-5.0273703
H	-0.9013195	1.6165367	-3.2511176
H	0.6189413	3.1087969	-4.4895387
H	0.3402925	3.4354514	-6.9782415
H	-1.4593398	2.2028191	-8.2003774
C	10.8064050	-0.7741306	-1.5353663
C	10.4293503	-2.0874250	-1.2942742
C	8.1351410	-1.3807901	-0.8623144
C	9.0819169	-2.3910628	-0.9553438
H	7.0953755	-1.6357028	-0.6011207
H	8.7864866	-3.4340410	-0.7668847
H	11.1708338	-2.8975190	-1.3657097
H	11.8476819	-0.5299906	-1.7995379

Table S24. Cartesian coordinates of $[(NpSn)_4S_6]_2$ (stacking).

Sn	1.7489252	1.8659662	-1.2974236
Sn	-2.6582011	-2.1907994	1.6035694
Sn	-5.5788950	-0.1583348	0.2383670
S	1.2090544	1.7754018	1.0870941
S	-5.0959065	-2.0495622	1.7209726
S	1.3344736	-0.0470740	-2.7521256
S	-1.4903391	-0.2178178	2.4447276
S	-4.9528476	-0.6153720	-2.0900454
C	0.8586779	3.6360277	-2.1426962
C	-2.2187253	-3.6560676	3.1357370
C	-7.7302214	-0.0123447	0.2148432
C	0.0953216	3.5121641	-3.2987634
C	-3.0282682	-3.5763433	4.2669859
C	-8.4696722	-0.9529320	0.9247474
C	-0.4434994	4.6676360	-3.9283532
C	-2.7691040	-4.3969606	5.4005750
C	-9.8923235	-0.9090257	0.9131077
C	-0.1982178	5.9272443	-3.4019951
C	-1.6938489	-5.2739273	5.3952897
C	-10.5519419	0.0722343	0.1883408
C	0.5925326	6.0917170	-2.2253055
C	-0.8380138	-5.3781133	4.2576094
C	-9.8266891	1.0526662	-0.5534344
C	1.1273622	4.9202829	-1.5634676
C	-1.1080443	-4.5597068	3.0937118
C	-8.3796903	1.0171838	-0.5435013
H	-0.1083760	2.5240140	-3.7395218
H	-3.8752321	-2.8719653	4.2980757
H	-7.9607317	-1.7427454	1.5006154
H	-1.0475439	4.5489860	-4.8396477
H	-3.4213389	-4.3206452	6.2835821
H	-10.4624029	-1.6603232	1.4803371
H	-0.6064062	6.8260602	-3.8912594
H	-1.4794674	-5.9007508	6.2753438
H	-11.6528610	0.1095425	0.1732296
S	4.1486362	2.4579994	-1.4337886
S	-1.8939387	-2.7704130	-0.6380259
S	-4.6532396	1.9176888	1.0974273
Sn	2.3160139	-0.2622331	1.8556373
Sn	2.5589573	-1.8546001	-1.6543306
Sn	-2.2102288	1.6111629	1.0009479
Sn	-2.5234891	-0.8270300	-1.9824478
Sn	5.2821648	0.5602987	-0.4405269
S	1.7031584	-2.2623183	0.5965687
S	4.7294941	0.1183343	1.9051229
C	1.6490288	-0.6485294	3.8647802
C	2.3873596	-3.5386085	-3.0053538
S	4.9777768	-1.5129873	-1.7105498
S	-1.5911010	1.3385539	-1.3415763
C	-1.5272951	3.6030433	1.4461433
C	-1.6316140	-1.2286227	-3.8976298
C	7.3830238	1.0437335	-0.4880718
C	0.8953366	-1.7937962	4.0980084
C	1.9016766	0.2982345	4.9096330
C	3.2035934	-3.4478909	-4.1315577
C	1.4901420	-4.6427391	-2.8418046
C	-1.7299196	4.5335549	0.4302074
C	-0.9177015	3.9755839	2.6855313
C	-1.5536872	-0.1775750	-4.8688725
C	-0.9232818	-2.4132399	-4.0631329

C	7.7558935	2.2844286	-0.9963372
C	8.3667849	0.1191496	-0.0039777
H	0.7184019	-2.5220699	3.2919655
C	0.3275436	-2.0340480	5.3790346
C	1.3323246	0.0398225	6.2159121
C	3.1599147	-4.4502622	-5.1401493
H	3.8936429	-2.5974999	-4.2534769
C	1.4439962	-5.6559372	-3.8761207
H	-2.1845754	4.2315901	-0.5270145
C	-1.3374903	5.8872909	0.6133093
C	-0.4849098	5.3465332	2.8457046
C	-0.6578966	-0.3490637	-5.9917593
C	-0.0822018	-2.5935284	-5.1963307
H	-0.9728361	-3.2112073	-3.3055777
H	6.9908372	2.9867647	-1.3650405
C	9.1276310	2.6606826	-1.0462163
C	9.7598563	0.5091502	-0.0591381
H	-0.2832961	-2.9342966	5.5371506
C	0.5361992	-1.1292861	6.4095234
H	3.8126615	-4.3591895	-6.0214108
C	2.2952695	-5.5280281	-5.0148805
H	-1.5020858	6.6131497	-0.1952199
C	-0.7204787	6.2782135	1.7911665
C	0.0670799	-1.5717930	-6.1211150
H	0.4709167	-3.5356863	-5.3139092
H	9.4050149	3.6457774	-1.4510708
C	10.1043995	1.7897879	-0.5872849
H	0.0932463	-1.3051823	7.4027459
H	2.2501382	-6.3027407	-5.7966444
H	-0.3930435	7.3208842	1.9251201
H	0.7513275	-1.6916566	-6.9757964
H	11.1679742	2.0749490	-0.6230958
C	0.8701398	7.3830261	-1.6831116
C	1.6420451	7.5251861	-0.5390241
C	1.8985488	5.1052847	-0.3759360
C	2.1529170	6.3744208	0.1216292
H	2.2893880	4.2287420	0.1629295
H	2.7464742	6.4874749	1.0407606
H	1.8520553	8.5272577	-0.1350310
H	0.4608483	8.2677888	-2.1964841
C	0.2916970	-6.2503349	4.2429747
C	1.1240567	-6.3239850	3.1349400
C	-0.2397070	-4.6766920	1.9692467
C	0.8537462	-5.5310408	1.9865289
H	-0.4357346	-4.0582360	1.0810132
H	1.5140170	-5.5859049	1.1090386
H	1.9970346	-6.9936366	3.1426443
H	0.4950267	-6.8613406	5.1366549

C	-10.4903398	2.0674016	-1.3065643
C	-9.7682699	3.0114375	-2.0224244
C	-7.6704403	2.0063143	-1.2897577
C	-8.3464111	2.9794075	-2.0119435
H	-6.5685128	1.9997485	-1.2887529
H	-7.7775108	3.7315085	-2.5787844
H	-10.2932039	3.7879888	-2.5991723
H	-11.5918412	2.0858120	-1.3083996
C	1.5927350	0.9597472	7.2769768
C	2.3907263	2.0777765	7.0737438
C	2.6962245	1.4710730	4.7325260
C	2.9445429	2.3348056	5.7892506
H	3.1298099	1.6877110	3.7432139
H	3.5640586	3.2290585	5.6280060
H	2.5898492	2.7718963	7.9043085
H	1.1550188	0.7575537	8.2675057
C	0.5333857	-6.7466809	-3.7385832
C	-0.3001752	-6.8469437	-2.6337306
C	0.6236070	-4.7859114	-1.7189260
C	-0.2536125	-5.8564224	-1.6148861
H	0.6376900	-4.0156677	-0.9343990
H	-0.9188494	-5.9313706	-0.7424716
H	-1.0017407	-7.6897874	-2.5442456
H	0.5020590	-7.5075873	-4.5344782
C	0.1614409	5.7270663	4.0605410
C	0.3583364	4.8091339	5.0827670
C	-0.7112650	3.0645679	3.7633172
C	-0.0922011	3.4685196	4.9356260
H	-1.0516508	2.0219540	3.6663461
H	0.0587092	2.7463712	5.7502175
H	0.8610500	5.1143072	6.0130235
H	0.4974103	6.7705888	4.1715426
C	-0.5280573	0.7092704	-6.9401256
C	-1.2666334	1.8777068	-6.8132224
C	-2.3097328	1.0296867	-4.7784583
C	-2.1760746	2.0313370	-5.7306213
H	-3.0204860	1.1630503	-3.9471744
H	-2.7815842	2.9460019	-5.6458770
H	-1.1570779	2.6837413	-7.5543736
H	0.1680412	0.5773618	-7.7835029
C	10.7535962	-0.3982228	0.4164118
C	10.4002081	-1.6388785	0.9273638
C	8.0408267	-1.1648617	0.5287603
C	9.0320232	-2.0232632	0.9833027
H	6.9861170	-1.4796194	0.5799053
H	8.7560479	-3.0077948	1.3896570
H	11.1769712	-2.3286844	1.2908246
H	11.8109526	-0.0923749	0.3697228

Minimum structures of the cluster monomers calculated at DFT-PBE level of theory with a plane waves basis set and employed for the calculation of the optical response are given in Tables S25 and S26.

Table S25. Cartesian coordinates of $[(PhSi)_4S_6]$.

Si	4.237155	4.292046	4.329780
Si	6.680245	6.625975	4.329780
Si	6.625546	4.237533	6.697234
Si	4.291854	6.680509	6.697234
S	5.458710	5.459021	2.997820
S	5.458710	5.459021	8.029275
S	2.922998	5.502447	5.518219
S	7.994401	5.415595	5.518219
S	5.415265	2.923295	5.508795

S	5.502135	7.994726	5.508795
C	3.186557	3.204852	3.230171
C	7.730842	7.713169	3.230171
C	7.712393	3.186862	7.797124
C	3.205006	7.731159	7.797124
C	3.824078	2.261930	2.402154
C	7.093321	8.656091	2.402154
C	8.652191	3.824611	8.628517
C	2.265208	7.093410	8.628517

C	3.077222	1.436860	1.560313
C	7.840177	9.481161	1.560313
C	9.476922	3.077670	9.470619
C	1.440477	7.840372	9.470619
C	1.683663	1.543186	1.533670
C	9.233737	9.374856	1.533670
C	9.373465	1.683818	9.494047
C	1.543934	9.234203	9.494047
C	1.039449	2.475879	2.349873
C	9.877951	8.442163	2.349873
C	8.443874	1.039396	8.674469
C	2.473546	9.878625	8.674469
C	1.785970	3.302246	3.193120
C	9.131450	7.615775	3.193120
C	7.617763	1.786003	7.831041
C	3.299637	9.132039	7.831041
H	4.912661	2.171522	2.415736
H	6.004738	8.746499	2.415736
H	8.740358	4.913395	8.617366
H	2.177041	6.004626	8.617366
H	3.583528	0.709770	0.923698
H	7.333872	10.208272	0.923698
H	10.201501	3.584138	10.109926
H	0.715898	7.333904	10.109926
H	1.099586	0.898095	0.875496
H	9.817813	10.019926	0.875496
H	10.018306	1.099682	10.152402
H	0.899093	9.818339	10.152402
H	-0.048047	2.561371	2.330986
H	10.965447	8.356671	2.330986
H	8.360498	-0.048300	8.690925
H	2.556902	10.966321	8.690925
H	1.270000	4.027495	3.825395
H	9.647399	6.890546	3.825395
H	6.894899	1.269892	7.196154
H	4.022500	9.648129	7.196154

Table S26. Cartesian coordinates of $[(NpSi)_4S_6]$.

Si	5.996220	7.557732	14.051818
Si	8.185820	6.971769	11.512204
Si	7.768060	4.676868	13.963092
Si	5.289380	5.233095	11.697180
S	7.403720	8.549331	12.755314
S	9.266260	5.509014	12.661946
S	6.657820	6.094095	10.277432
S	6.216100	3.670422	12.857042
S	6.961600	6.125259	15.335078
S	4.353460	6.711222	12.949684
C	5.270120	8.883882	15.167834
C	8.624700	3.364389	14.999930
C	3.917860	4.419828	10.703066
C	9.426340	7.771407	10.349284
C	10.153640	7.017108	9.363420
C	9.643260	9.140208	10.447822
C	11.084040	7.706874	8.507884
C	10.003940	5.614917	9.184252
C	9.830380	1.284213	16.497998
C	10.333280	2.604945	16.626896
C	8.772580	1.011339	15.659952
C	10.558160	9.811158	9.605992
C	11.262940	9.106860	8.655768
C	11.424400	2.891364	17.489538
C	9.727980	3.670695	15.871152
C	11.808260	6.975927	7.529148
C	11.634120	5.616114	7.386280
C	10.723100	4.933320	8.223424
C	8.175200	2.052456	14.914878
C	11.912300	4.174401	17.614520
C	11.321820	5.224842	16.876376
C	10.260060	4.979352	16.029376
C	3.713380	3.053064	10.846594
C	3.076440	5.162199	9.802672
C	2.701780	2.372937	10.132452
C	1.886660	3.065916	9.265784
C	2.047660	4.463172	9.077244
C	1.209720	5.182359	8.184308
C	1.366520	6.539547	8.001884
C	2.373940	7.231392	8.711362
C	3.204600	6.561324	9.586544
C	5.707780	10.193631	15.014802
C	4.277600	8.590302	16.167184
C	5.203880	11.244765	15.813006
C	4.252280	10.984113	16.773372
C	3.766960	9.666153	16.976586
C	2.785580	9.392250	17.965816
C	2.314880	8.111817	18.162848
C	2.812880	7.051506	17.372476
C	3.767040	7.284753	16.402848
H	10.299980	0.486570	17.077852
H	10.699520	10.887093	9.715772
H	9.099840	9.727326	11.190278
H	11.972400	9.615858	7.999596
H	12.509080	7.516341	6.889190
H	12.196060	5.065914	6.630404
H	10.585580	3.857133	8.110498
H	9.308180	5.062848	9.816180
H	7.339320	1.802913	14.258882
H	8.389700	-0.005502	15.564494
H	11.870880	2.070075	18.054234
H	12.751320	4.381629	18.280108
H	11.707820	6.240276	16.975508
H	9.823820	5.808684	15.472512
H	4.342600	2.474913	11.525602
H	2.573740	1.299039	10.273956
H	1.101580	2.549799	8.708766
H	0.434980	4.635078	7.643020
H	0.716580	7.080822	7.313086
H	2.497680	8.305563	8.567350
H	3.972940	7.120260	10.120814
H	6.460380	10.433535	14.261566
H	5.573800	12.259548	15.661008
H	3.855280	11.789526	17.395246
H	2.410100	10.220973	18.569914
H	1.560800	7.914165	18.925874
H	2.440740	6.038130	17.528918
H	4.133700	6.448008	15.808166

7 Calculation of Rotation Profiles

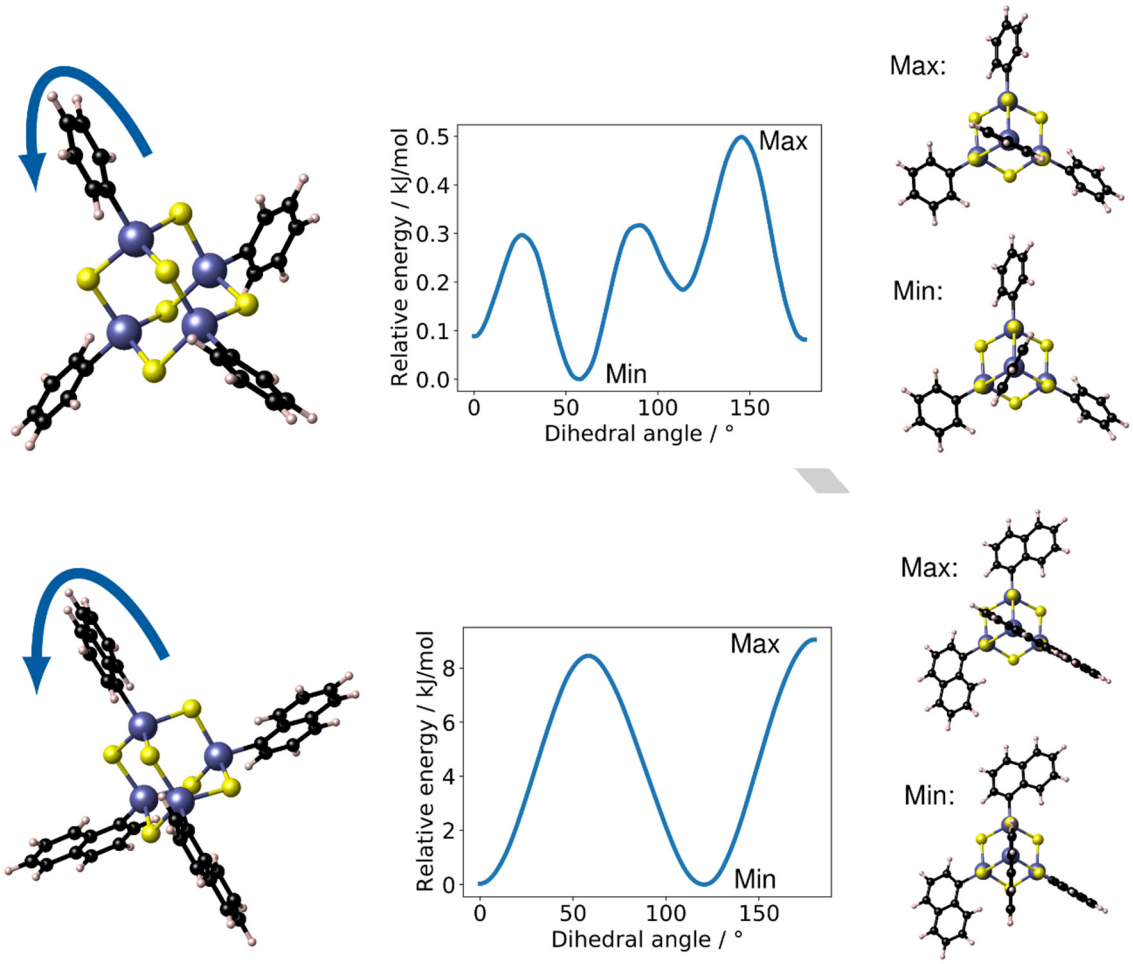

Figure S12. Scan of the phenyl and naphtyl rotation for $[(PhSn)_4S_6]$ and $[(NpSn)_4S_6]$ clusters. The corresponding scans for Si/S core clusters are given in Figure 4 in the main document.

8 Analysis of the Structures

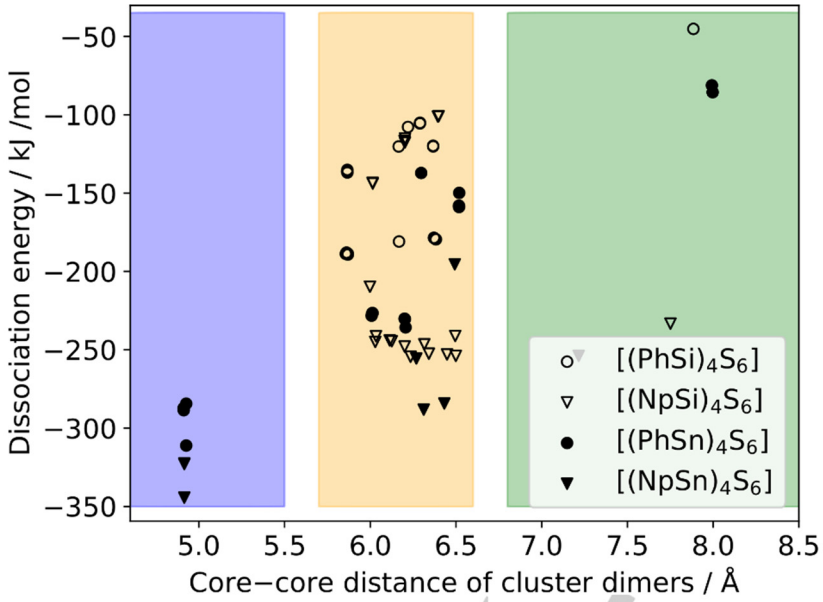

Figure S13. Dissociation energy of cluster dimers, plotted against the corresponding core−core distance calculated at the BP86-D3/cc-pVDZ(-PP) level of theory. Small core−core distances are marked by a purple background, medium core−core distances are marked by an orange background and large core−core distances by a green background.

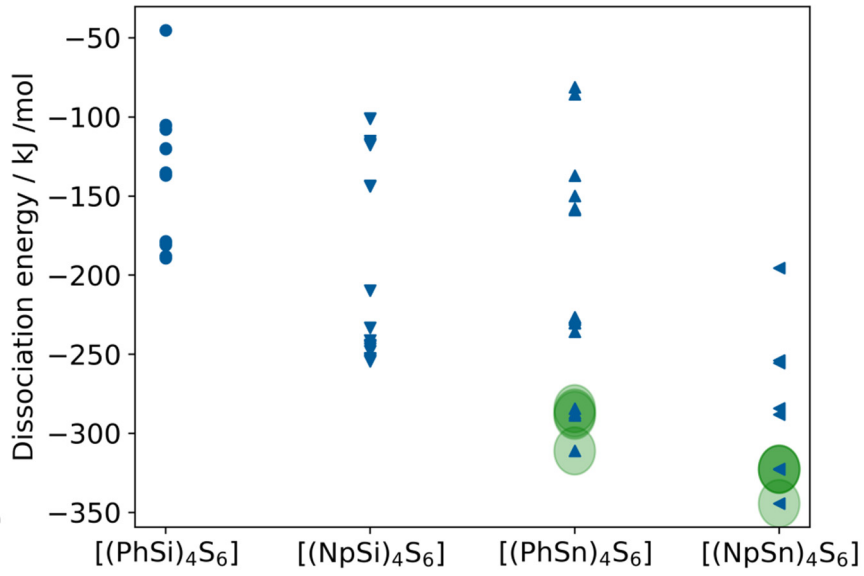

Figure S14. Dissociation energies of the calculated cluster dimers. The fused cluster dimers are marked with a green circle.

9 Calculation of Quasiparticle Gaps

The calculation of the quasiparticle gaps is performed by total energy calculations of charged molecules. Due to the interactions with the periodic images, the total energy of charged systems depends on the cell size. In order to correct the calculated excitation energies, the gaps were determined for cubic cells with edge L = 20, 25, 30, 35, 40 Å (Figure S15). The quasiparticle gap values depend linearly on $1/L$, and the extrapolation to $L \to \infty$ leads to the values of 6.5366 eV for [(PhSi)$_4$S$_6$] and 5.0909 eV for [(NpSi)$_4$S$_6$] clusters.

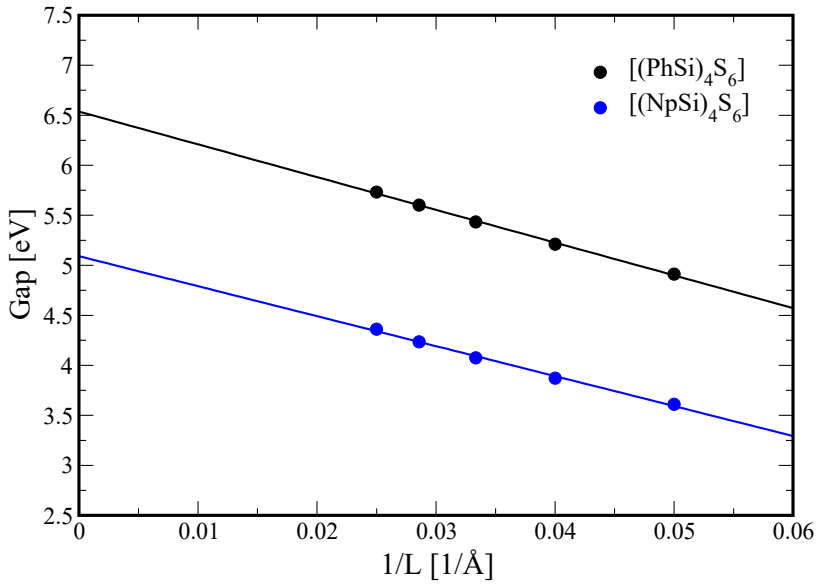

Figure S15. Dependence of the calculated quasiparticle gaps on the cell size.

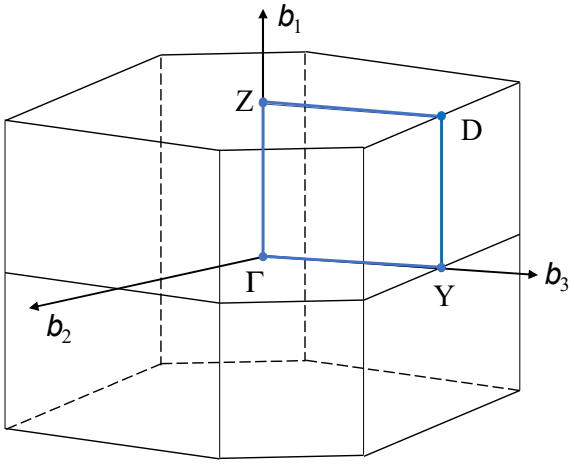

Figure S16. First Brillouin zone of crystals comprising [(PhSi)$_4$S$_6$] and [(NpSi)$_4$S$_6$] molecules. The path employed for the band structure calculations is highlighted.

10 Analysis of the Influence of Crystal Solvent

In order to clarify whether the solvent has any effect on the optical response of the clusters, we calculated the dielectric function of a supercell modelling toluene incorporated in the crystalline $[(NpSi)_4S_6]$ structure, and of a supercell modelling an ideal $[(NpSi)_4S_6]$ crystal without toluene. The corresponding absorption spectra are shown in Figure 17. The calculations are performed both with the atomic positions as determined by X-ray diffraction experiments (solid lines) and with the DFT equilibrium geometry (dashed lines). Although the structural optimization redistributes the spectral weight of the different features, the extinction coefficient calculated with and without toluene does not substantially differ. This demonstrates that the optical response of the molecular cluster is not affected by the presence of solvent.

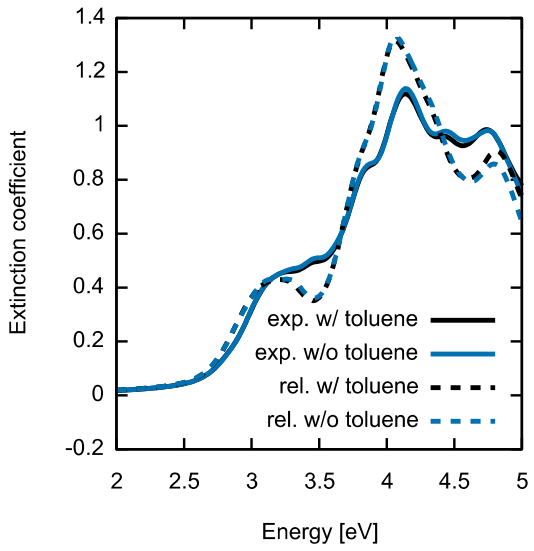

Figure S17. Extinction coefficient of the $[(NpSi)_4S_6]$ molecular crystals calculated within the IPA at the DFT equilibrium geometry (dotted line) and at the experimentally determined atomic positions (solid line). Black and blue curves refer to supercell with and without toluene solvent.

11 References for the Supporting Information

[1] B. M. Moore, S. M. Ramirez, G. R. Yandek, T. S. Haddad, J. M. Mabry, *J. Organomet. Chem.* **2011**, *696*, 2676–2680.

[2] T. S. Haddad, B. D. Viers, S. H. Phillips, *J. Inorg. Organomet. Polym.* **2001**, *11*, 155–164.

[3] N. W. Rosemann, J. P. Eußner, E. Dornsiepen, S. Chatterjee, S. Dehnen, *J. Am. Chem. Soc.* **2016**, *138*, 16224–16227

[4] P. Braunstein, H. Lehner, D. Matt, *Inorg. Synth.* **1990**, *27*, 218–221.

[5] G. Brauer, *Handbuch der Präparativen Anorganischen Chemie;* Ferdinand Enke Verlag, Stuttgart, **1975**.

[6] a) G. M. Sheldrick, *Acta Crystallogr, Sect. A* **2015**, *71*, 3–8; b) G. M. Sheldrick, *Acta Crystallogr, Sect. C* **2015**, *71*, 3–8; c) O. V. Dolomanov, L. J. Bourhis, R. J. Gildea, J. A. K. Howard, H. Puschmann, *J. Appl. Crystallogr.* **2009**, *42*, 339–341.

[7] M. J. Frisch, G. W. Trucks, Schlegel, M. H. H. B, G. E. Scuseria, M. A. Robb, J. R. Cheeseman, G. Scalmani, V. Barone, B. Mennucci, G. A. Petersson, H. Nakatsuji, M. Caricato, X. Li, H. P. Hratchian, A. F. Izmaylov, J. Bloino, G. Zheng, J. L. Sonnenberg, *Gaussian09;* Gaussian, Inc, Wallingford, CT, **2009**.

[8] a) S. Grimme, J. Antony, S. Ehrlich, H. Krieg, *The Journal of Chemical Physics* **2010**, *132*, 154104; b) S. Grimme, S. Ehrlich, L. Goerigk, *J. Comput. Chem.* **2011**, *32*, 1456–1465; c) A. D. Becke, *Phys. Rev. A* **1988**, *38*, 3098–3100; d) J. P. Perdew, W. Yue, *Phys. Rev. B* **1986**, *33*, 8800–8802.

[9] R. A. Kendall, T. H. Dunning, R. J. Harrison, *The Journal of Chemical Physics* **1992**, *96*, 6796–6806.

[10] B. Metz, H. Stoll, M. Dolg, *The Journal of Chemical Physics* **2000**, *113*, 2563–2569.

[11] P. Pracht, F. Bohle, S. Grimme, *Phys. Chem. Chem. Phys.* **2020**, *22*, 7169–7192.

[12] a) S. Grimme, C. Bannwarth, P. Shushkov, *Journal of chemical theory and computation* **2017**, *13*, 1989–2009; b) C. Bannwarth, S. Ehlert, S. Grimme, *Journal of chemical theory and computation* **2019**, *15*, 1652–1671.

[13] I. Boldog, A. B. Lysenko, E. B. Rusanov, A. N. Chernega, K. V. Domasevitch, *Acta crystallographica. Section C, Crystal structure communications* **2009**, *65*, o248-o252.

[14] a) G. Kresse, J. Furthmüller, *Computational Materials Science* **1996**, *6*, 15–50; b) G. Kresse, J. Furthmüller, *Phys. Rev. B* **1996**, *54*, 11169–11186.

[15] P. E. Blöchl, *Phys. Rev. B* **1994**, *50*, 17953–17979.

[16] J. P. Perdew, K. Burke, M. Ernzerhof, *Physical review letters* **1996**, *77*, 3865–3868.

[17] E. Dornsiepen, F. Dobener, S. Chatterjee, S. Dehnen, *Angew. Chem.* **2019**, *131*, 17197–17202; *Angew. Chem. Int. Ed.* **2019**, *58*, 17041–17046.

[18] M. Gajdoš, K. Hummer, G. Kresse, J. Furthmüller, F. Bechstedt, *Phys. Rev. B* **2006**, *73*, 045112.

[19] A. Riefer, S. Sanna, A. Schindlmayr, W. G. Schmidt, *Phys. Rev. B* **2013**, *87*, 195208.

[20] C. Attaccalite, M. Grüning, *Phys. Rev. B* **2013**, *88*, 235113.

[21] A.L. Spek, *Acta Crystallogr., Sect. C: Struct. Chem.* **2015**, *71*, 9-18.

5 Zusammenfassung

5.1 Zusammenfassung in deutscher Sprache

Diese Dissertation beschäftigt sich mit der Synthese und Reaktivität von Organozinnselenid- und Organosiliciumsulfid-Clustern und gliedert sich in drei Teile. Alle im Folgenden genannten Reaktionen und Verbindungen sind in Schema 5.1 zusammengefasst.

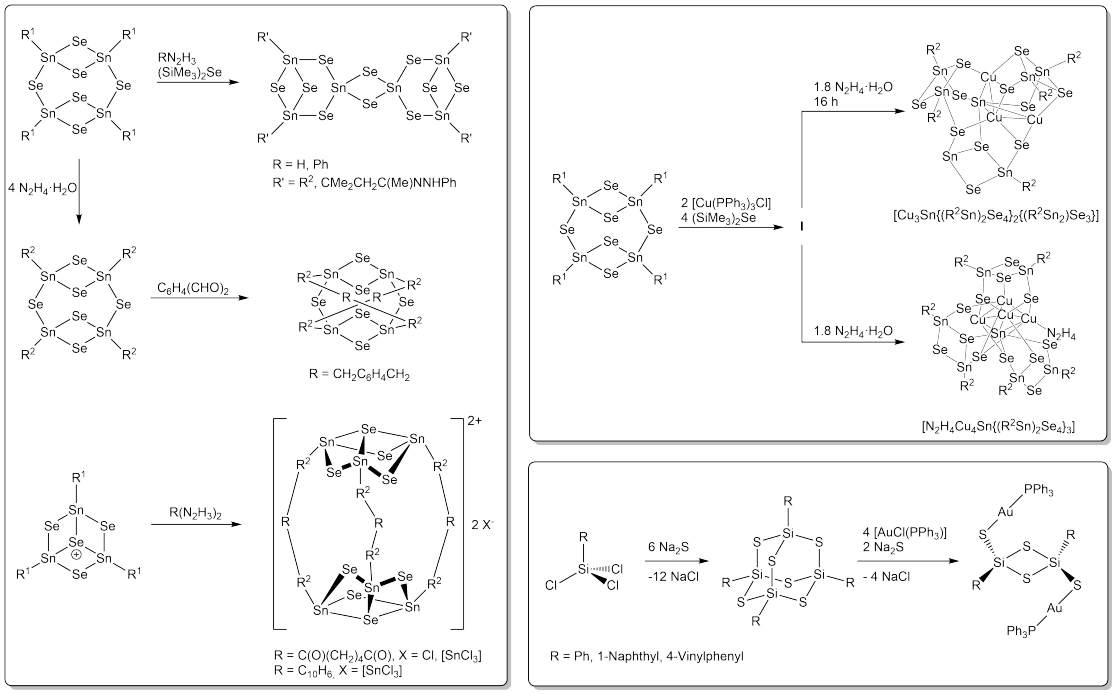

Schema 5.1: Übersicht über alle in dieser Dissertation vorgestellten Verbindungen und ihre Synthesen. Reaktionen, die zu demselben Paper gehören, sind zusammen eingerahmt.

Im ersten Teil dieser Dissertation wurde die Reaktivität von organisch funktionalisierten Organozinnselenid-Clustern der Zusammensetzung $[(R^fSn)_xSe_y]$ (R^f = Substituent mit funktioneller Gruppe; x, y ∈ ℕ) gegenüber bifunktionellen Verbindungen sowie gegenüber $[CuCl(PPh_3)_3]$ untersucht. Dabei konnte bei der Umsetzung des doppeldeckerartigen Clusters $[(R^2Sn)_4Se_6]$ (R^2 = $CMe_2CH_2CMeNNH_2$) mit *o*-Phthaldialdehyd ein intramolekular verknüpfter Doppeldecker-Cluster erhalten werden, dessen Substituenten kreuzweise miteinander verbunden sind. Bei der Verwendung von $[(R^1Sn)_3Se_4Cl]$ (R^1 = CMe_2CH_2CMeO) und den längerkettigen bifunktionellen Verbindungen Adipinsäuredihydrazid und 1,1'-(1,5-Naphthalindiyl)bishydrazin konnten größere, rugbyballartige Kapselmoleküle der allgemeinen Zusammensetzung $[(\mu\text{-}R)_3(Sn_3Se_4)_2]^{2+}$ in Form ihrer Salze mit $[SnCl_3]^-$- bzw. Cl^--Anionen synthetisiert werden. Diese kationischen Cluster schließen im Festkörper Lösungsmittelmoleküle und/oder Gegenionen ein. Massenspektrometrisch konnte gezeigt werden, dass die Kapseln auch nach Freisetzung der Lösungsmittelmoleküle intakt bleiben, wobei selbst unter ESI-MS-Bedingungen Moleküle mit eingeschlossenen Anionen detektiert wurden. Des Weiteren konnten bei den Umsetzungen des doppeldeckerartigen Clusters $[(R^1Sn)_4Se_6]$ mit $(SiMe_3)_2Se$ und Hydrazinhydrat oder Phenylhydrazin die entsprechend substituierten Bis-Defektheterokuban-Cluster $[R_4Sn_6Se_{10}]$ (R = R^2, $CMe_2CH_2CMeNNPhH$) erhalten werden. All diese Strukturmotive waren bereits für Organozinnsulfid-Cluster bekannt, konnten aber hier erstmals für Organozinnselenid-Cluster erhalten werden. Ein Vergleich der Innenvolumina der Kapselmoleküle untereinander und mit dem 1,1'-(1,5-Naphthalindiyl)bishydrazin-basierten Organozinnsulfid-Cluster zeigte, dass diese vor allem von den vorliegenden Substituenten abhängig sind und der Wechsel von Schwefel zu Selen als verwendetes Chalkogenid nahezu keinen Einfluss hat.

Bei der Umsetzung von $[(R^1Sn)_4Se_6]$ mit $[Cu(PPh_3)_3Cl]$ konnte nach einer Reaktionszeit von 16 h ein leuchtend orangefarbenes Pulver isoliert werden, dessen genaue Zusammensetzung bisher ungeklärt ist. Die Zugabe von Hydrazinhydrat zu einer Suspension dieses Pulvers führte, abhängig von der Reaktionszeit, zur Bildung der ternären Cluster $[(Cu_3Sn)\{(R^2Sn)_2Se_4\}_2\{(R^2Sn_2)Se_3\}]\cdot 1.87\,CH_2Cl_2\cdot 2solv$ (solv = CH_2Cl_2 und/oder C_6H_{14}) (Reaktionszeit: 16 h) und $[(N_2H_4)(Cu_4Sn)\{(R^2Sn)_2Se_4\}_3]$ (sofortige Aufarbeitung nach Hydrazinhydrat-Zugabe). Beide Cluster bestehen jeweils aus ei-

nem $\{Cu_xSn\}$-Kern (x = 3, 4), der hauptsächlich von $\{(RSn)_2Se_4\}$-Einheiten umgeben ist. Letztere stellen ein häufiges Strukturmotiv in ternären Organozinn-Münzmetallchalkogenid-Clustern dar. Der Vergleich mit den Synthesen bereits bekannter organisch funktionalisierter Cu/Sn/Se-Cluster deutet auf ein komplexes Gleichgewicht in den entsprechenden Reaktionslösungen hin, da schon kleine Änderungen der Reaktionsbedingungen zur Bildung verschiedener Cluster führen.

Im letzten Teil der Dissertation wurden neue Organosiliciumsulfid-Cluster der Zusammensetzung $[(RSi)_4S_6]$ (R = 1-Naphthyl (Np), 4-Vinylphenyl (Sty)) mit Adamantanstruktur synthetisiert. Photophysikalische Messungen in der Arbeitsgruppe *Chatterjee* zeigten für das kristalline $[(NpSi)_4S_6]$ Frequenzverdopplung (SHG), während aufgrund der geringen Stabilität für $[(StySi)_4S_6]$ bisher kein eindeutiger Beleg für Weißlichtemssion (WLG) existiert. Mit Hilfe quantenchemischer Rechnungen, die in der Arbeitsgruppe *Mollenhauer* durchgeführt wurden, konnte außerdem eine Erklärung für die größere Neigung zur Kristallisation der Organosiliciumsulfid-Cluster im Vergleich zu den analogen Organozinnsulfid-Clustern gefunden werden: In den Organozinnsulfid-Clustern haben die relativ isotropen Clusterkern-Clusterkern-Wechselwirkungen einen deutlich größeren Einfluss als die gerichteten Wechselwirkungen mit Substituentenbeteiligung. In den Organosiliciumsulfid-Clustern ist dieser Unterschied deutlich geringer, was zu einem höheren Grad an intermolekularer Ordnung und letztlich zur Kristallisation führt. In ersten Experimenten zur Reaktivität adamantanartiger Organosiliciumsulfid-Cluster konnte gezeigt werden, dass diese sich ähnlich wie Organozinnsulfid-Cluster verhalten. So führten die Umsetzungen von $[(PhSi)_4S_6]$ bzw. $[(NpSi)_4S_6]$ mit $[AuCl(PPh_3)]$ zur teilweisen Zersetzung der Cluster unter Bildung von Organosilicium-Goldsulfid-Komplexen der allgemeinen Zusammensetzung $[\{RSi(\mu\text{-}S)\}_2\{AuPPh_3(\mu\text{-}S)\}_2]$ mit zentralem $\{Si_2S_2\}$-Vierring.

5.2 English Summary

The topic of this dissertation is the synthesis and reactivity of organotin selenide and organisilicon sulfide clusters. The reactions and compounds mentioned below are summarized in Scheme 5.2.

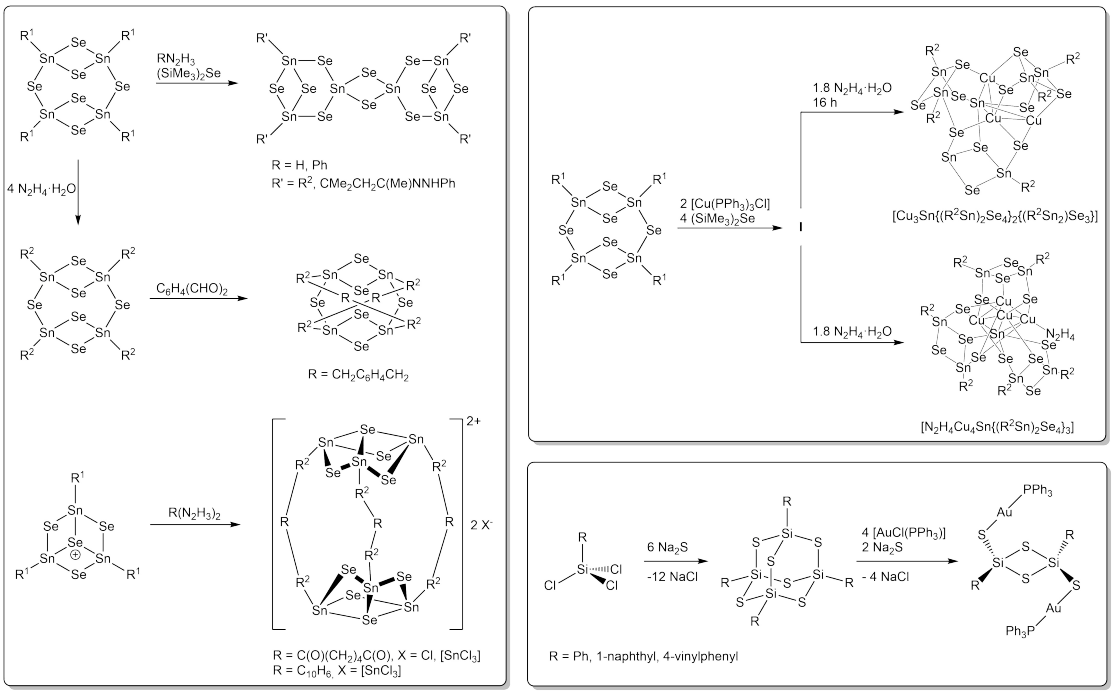

Scheme 5.2: Overview over all compounds presented in this dissertation, and their syntheses. Reactions belonging to one paper are framed.

In the first part of this dissertation, the reactivity of organo-functionalized organotin selenide clusters with the general formula $[(R^fSn)_xSe_y]$ (R^f = substituent with functional group; x, y $\in \mathbb{N}$) toward bifunctional compounds and toward $[CuCl(PPh_3)_3]$ was investigated. The reaction of the doubledecker-type cluster $[(R^2Sn)_4Se_6]$ ($R^2 = CMe_2CH_2CMeNNH_2$) with *o*-phthalaldehyde yielded a doubledecker-type cluster whose substituents are connected intramolecularly in a crosswise manner. When reacting $[(R^1Sn)_3Se_4Cl]$ ($R^1 = CMe_2CH_2CMeO$) with bifunctional compounds with longer chains, namely adipinic acid hydrazide or 1,1'-(1,5-naphthalenediyl)bishydrazine, bigger rugby ball-type capsule molecules with the general formula $[(\mu\text{-}R)_3(Sn_3Se_4)_2]^{2+}$ were obtained as their salts with $[SnCl_3]^-$

or Cl^- counterions. These cationic clusters contain solvent molecules and/or counter ions in their solid state. Mass spectrometric measurements showed that these capsules stay intact upon release of the solvent molecules and even under ESI-MS conditions it was possible to detect molecules with encapsulated anions. Furthermore, reactions of the doubledecker-type cluster $[(R^1Sn)_4Se_6]$ with $(SiMe_3)_2Se$ and hydrazine hydrate or phenylhydrazine yielded the correspondingly substituted bis-defect heterocubane-type clusters $[R_4Sn_6Se_{10}]$ (R = R^2, $CMe_2CH_2CMeNNPhH$). Although all of these structural motifs were already known for organotin sulfide clusters, they could be obtained for organotin selenide clusters for the first time in this work. The comparison of the inner volumes of the rugby ball-type molecules with each other and with that of the 1,1'-(1,5-naphthalenediyl)bishydrazine-based tinsulfide cluster showed that these are primarily dependant on the present substituents and the switch from sulfur to selenium as the chalcogenide barely affects the inner volume.

16 hours after the start of the reaction of $[(R^1Sn)_4Se_6]$ with $[Cu(PPh_3)_3Cl]$, a bright orange powder was isolated whose exact composition is yet unknown. Depending on the reaction time, the addition of hydrazine hydrate to a suspension of this powder led to the formation of the ternary clusters $[(Cu_3Sn)\{(R^2Sn)_2Se_4\}_2\{(R^2Sn_2)Se_3\}]\cdot 1.87\,CH_2Cl_2\cdot 2solv$ (solv = CH_2Cl_2 and/or C_6H_{14}) (reaction time: 16 h) and $[(N_2H_4)(Cu_4Sn)\{(R^2Sn)_2Se_4\}_3]$ (instant work-up after addition of hydrazine hydrate). Both clusters are based on a $\{Cu_xSn\}$ core (x = 3, 4), which is mainly surrounded by $\{(RSn)_2Se_4\}$ moieties. The latter are a common structural motif in ternary organotin coinage metal chalcogenide clusters. The comparison with the synthesis of the already known organo-functionalized Cu/Sn/Se clusters suggests a complex equilibrium in the respective reaction solutions, as even small changes to the reaction conditions lead to a variety of different clusters.

In the last part of this dissertation, new adamantane-type organosilicon sulfide clusters with the general formula $[(RSi)_4S_6]$ (R = 1-naphthyl (Np), 4-vinylphenyl (Sty)) were synthesized. Photophysical measurements were conducted in the *Chatterjee* group and showed second harmonic generation (SHG) for the crystalline $[(NpSi)_4S_6]$, whereas no definite proof for white light generation (WLG) of $[(StySi)_4S_6]$ exists yet, due to its lower stability. Quantumchemical calculations by

the *Mollenhauer* group found an explanation for the organosilicon sulfide clusters' higher tendency to crystallize as compared to the analog organotin sulfide clusters: In the organotin sulfide clusters, the relatively isotropic cluster core-cluster core interactions have a significantly higher influence than the directional interactions with substituent-contribution. In the organosilicon sulfide clusters, this difference is much lower which leads to a higher degree of intermolecular order and ultimately to crystallization. First experiments on the reactivity of adamantane-type organosilicon sulfide clusters showed a similar behavior to organotin sulfide clusters. The reactions of $[(PhSi)_4S_6]$ or $[(NpSi)_4S_6]$ with $[AuCl(PPh_3)]$ resulted in the partial decomposition of the clusters and the subsequent formation of organosilicon gold-sulfide complexes with the general formula $[\{RSi(\mu\text{-}S)\}_2\{AuPPh_3(\mu\text{-}S)\}_2]$ which exhibit a central $\{Si_2S_2\}$ four-membered ring.

A Literatur

[1] P. Pfeiffer, R. Lehnardt, *Ber. Dtsch. Chem. Ges.* **1903**, *36*, 3027–3030.

[2] Y. Étienne, *Comptes Rendus Académie des Sciences* **1952**, *235*, 966–968.

[3] K. Moedritzer, *Inorg. Chem.* **1967**, *6*, 1248–1249.

[4] C. Dorfelt, A. Janeck, D. Kobelt, P. E. F., H. Scherer, *J. Organomet. Chem.* **1968**, *14*, P22–P24.

[5] J. C. Bart, J. J. Daly, *Chem. Commun.* **1968**, 1207.

[6] D. Kobelt, E. Paulus, H. Scherer, *Acta Crystallogr. B* **1972**, *28*, 2323–2326.

[7] R. H. Benno, C. J. Fritchie, *J. Chem. Soc. Dalton Trans.* **1973**, 543–546.

[8] J. C. J. Bart, J. J. Daly, *J. Chem. Soc. Dalton Trans.* **1975**, 2063–2068.

[9] W. Ando, T. Kadowaki, Y. Kabe, M. Ishii, *Angew. Chem. Int. Ed.* **1992**, *31*, 59–61.

[10] M. Unno, Y. Kawai, H. Shioyama, H. Matsumoto, *Organometallics* **1997**, *16*, 4428–4434.

[11] R. A. Varga, C. Silvestru, *Acta Crystallogr. E* **2007**, *63*, m2789.

[12] M. Unno, D. Ishii, H. Matusmoto, *Bull. Chem. Soc. Jpn.* **1999**, *72*, 2469–2473.

[13] Z. Hassanzadeh Fard, L. Xiong, C. Müller, M. Hołyńska, S. Dehnen, *Chem. Eur. J.* **2009**, *15*, 6595–6604.

[14] Z. Hassanzadeh Fard, C. Müller, T. Harmening, R. Pöttgen, S. Dehnen, *Angew. Chem. Int. Ed.* **2009**, *48*, 4441–4444.

[15] Z. Hassanzadeh Fard, M. Hołyńska, S. Dehnen, *Inorg. Chem.* **2010**, *49*, 5748–5752.

[16] J. P. Eußner, B. E. K. Barth, E. Leusmann, Z. You, N. Rinn, S. Dehnen, *Chem. Eur. J.* **2013**, *19*, 13792–13802.

[17] A. Engel, S. Dehnen, *Eur. J. Inorg. Chem.* **2019**, *2019*, 4313–4320.

[18] N. Rinn, J.-P. Berndt, A. Kreher, R. Hrdina, M. Reinmuth, P. R. Schreiner, S. Dehnen, *Organometallics* **2016**, *35*, 3215–3220.

[19] J.-P. Berndt, A. Engel, R. Hrdina, S. Dehnen, P. R. Schreiner, *Organometallics* **2019**, *38*, 329–335.

[20] C. Pöhlker, I. Schellenberg, R. Pöttgen, S. Dehnen, *Chem. Commun.* **2010**, *46*, 2605–2607.

[21] Z. You, D. Fenske, S. Dehnen, *Dalton Trans.* **2013**, *42*, 8179–8182.

[22] Z. You, S. Dehnen, *Inorg. Chem.* **2013**, *52*, 12332–12334.

[23] E. Leusmann, M. Wagner, N. W. Rosemann, S. Chatterjee, S. Dehnen, *Inorg. Chem.* **2014**, *53*, 4228–4233.

[24] M. R. Halvagar, Z. Hassanzadeh Fard, S. Dehnen, *Chem. Eur. J.* **2011**, *17*, 4371–4374.

[25] N. Rinn, J. P. Eußner, W. Kaschuba, X. Xie, S. Dehnen, *Chem. Eur. J.* **2016**, *22*, 3094–3104.

[26] B. Peters, N. Lichtenberger, E. Dornsiepen, S. Dehnen, *Chem. Sci.* **2020**, *11*, 6–26.

[27] M. R. Halvagar, Z. Hassanzadeh Fard, S. Dehnen, *Chem. Commun.* **2010**, *46*, 4716–4718.

[28] B. E. K. Barth, E. Leusmann, K. Harms, S. Dehnen, *Chem. Commun.* **2013**, *49*, 6590–6592.

[29] J. P. Eußner, S. Dehnen, *Chem. Commun.* **2014**, *50*, 11385–11388.

[30] E. Leusmann, E. Geringer, B. Weinert, S. Dehnen, *Dalton Trans.* **2016**, *45*, 15298–15302.

[31] N. Rinn, L. Guggolz, K. Gries, K. Volz, J. Senker, S. Dehnen, *Chem. Eur. J.* **2017**, *23*, 15607–15611.

[32] N. Rinn, K. Hanau, L. Guggolz, A. Rinn, S. Chatterjee, S. Dehnen, *Z. Anorg. Allg. Chem.* **2017**, *643*, 1508–1512.

[33] N. Rinn, L. Guggolz, J. Lange, S. Chatterjee, T. Block, R. Pöttgen, S. Dehnen, *Chem. Eur. J.* **2018**, *24*, 5840–5848.

[34] E. Dornsiepen, F. Weigend, S. Dehnen, *Chem. Eur. J.* **2019**, *25*, 2486–2490.

[35] E. Dornsiepen, F. Pieck, R. Tonner, S. Dehnen, *J. Am. Chem. Soc.* **2019**, *141*, 16494–16500.

[36] E. Dornsiepen, E. Geringer, N. Rinn, S. Dehnen, *Coord. Chem. Rev.* **2019**, *380*, 136–169.

[37] J. P. Eußner, R. O. Kusche, S. Dehnen, *Chem. Eur. J.* **2015**, *21*, 12376–12388.

[38] N. W. Rosemann, J. P. Eußner, A. Beyer, S. W. Koch, K. Volz, S. Dehnen, S. Chatterjee, *Science* **2016**, *352*, 1301–1304.

[39] E. Dornsiepen, F. Dobener, S. Chatterjee, S. Dehnen, *Angew. Chem. Int. Ed.* **2019**, *58*, 2–8.

[40] B. E. K. Barth, B. A. Tkachenko, J. P. Eußner, P. R. Schreiner, S. Dehnen, *Organometallics* **2014**, *33*, 1678–1688.

[41] E. Leusmann, F. Schneck, S. Dehnen, *Organometallics* **2015**, *34*, 3264–3271.

[42] E. Geringer, E. Leusmann, F. Tambornino, M. Gerhard, M. Koch, S. Dehnen, *Chem. Commun.* **2020**, *56*, 4769–4772.

[43] Z. Hassanzadeh Fard, M. R. Halvagar, S. Dehnen, *J. Am. Chem. Soc.* **2010**, *132*, 2848–2849.

[44] R. Hauser, K. Merzweiler, *Z. Anorg. Allg. Chem.* **2002**, *628*, 905–906.

[45] E. Dornsiepen, J. P. Eußner, N. W. Rosemann, S. Chatterjee, S. Dehnen, *Inorg. Chem.* **2017**, *56*, 11326–11335.

[46] E. Geringer, S. Dehnen, *Z. Anorg. Allg. Chem.* **2018**, *644*, 920–924.

[47] Y.-P. Étienne, *Angew. Chem.* **1955**, *67*, 753.

[48] J. A. Forstner, E. L. Muetterties, *Inorg. Chem.* **1965**, *5*, 552–554.

[49] K. Schwedtmann, A. Hepp, K. Schwedtmann, J. J. Weigand, F. Lips, *Eur. J. Inorg. Chem.* **2019**, 4719–4726.

[50] W. Ando, T. Kadowaki, A. Watanabe, N. Choi, Y. Kabi, T. Erata, M. Ishii, *Nippon Kagaku Kaishi* **1994**, *3*, 214–223.

[51] U. Herzog, G. Rheinwald, *J. Organomet. Chem.* **2001**, *628*, 133–143.

[52] A. Haas, R. Hitze, *Z. Naturforsch.* **1984**, *39b*, 890–896.

[53] H.-G. Horn, M. Hemeke, *Chem.-Ztg.* **1982**, *106*, 263–266.

[54] M. Unno, H. Shioyama, H. Matsumoto, *Phosphorus Sulfur and Silicon* **1997**, *120*, 377–378.

[55] F. Fehér, R. Lüpschen, *Z. Naturforsch.* **1971**, *26b*, 1191–1192.

[56] N. W. Rosemann, J. P. Eußner, E. Dornsiepen, S. Chatterjee, S. Dehnen, *J. Am. Chem. Soc.* **2016**, *138*, 16224–16227.

[57] H.-G. Horn, M. Probst, *Monatshefte für Chemie* **1995**, *126*, 1169–1178.

[58] H.-G. Horn, M. Hemeke, *Chem.-Ztg.* **1985**, *109*, 145–148.

[59] S. R. Bahr, P. Boudjouk, *Inorg. Chem.* **1992**, *31*, 712–713.

[60] E. Dornsiepen, F. Dobener, N. Mengel, O. Lenchuk, C. Dues, S. Sanna, D. Mollenhauer, S. Chatterjee, S. Dehnen, *Adv. Optical Mater.* **2019**, *7*, 1801793.

[61] W. Zinth, U. Zinth, *Optik*, 5. Aufl., De Gruyter, Berlin, **2018**.

[62] W. Demtröder, *Experimentalphysik 2 - Elektrizität und Optik*, 7. Aufl., Springer Spektrum, Berlin, **2017**.

[63] J. Heintze, *Lehrbuch zur Experimentalphysik - Band 4: Wellen und Optik*, 1. Aufl., (Hrsg.: P. Bock), Springer Spektrum, Berlin, **2017**.

[64] N. W. Rosemann, H. Locke, P. R. Schreiner, S. Chatterjee, *Adv. Opt. Mater.* **2018**, *6*, 1701162.

[65] E. Dornsiepen, Dissertation, Philipps-Universität Marburg, **2019**.

[66] P. M. Nikolić, Z. V. Popović, *J. Phys. C: Solid State Phys.* **1979**, *12*, 1151–1156.

[67] X. Hu, G. Song, W. Li, Y. Peng, L. Jiang, Y. Xue, Q. Liu, Z. Chen, J. Hu, *Mater. Res. Bull.* **2013**, *48*, 2325–2332.

[68] S. K. Panda, A. Antonakos, E. Liarokapis, S. Bhattacharya, S. Chaudhuri, *Mater. Res. Bull.* **2007**, *42*, 576–583.

[69] N. G. Deshpande, A. A. Sagade, G. Y. G., L. C. D., R. Sharma, *J. Alloys Compd.* **2007**, *436*, 421–426.

[70] M. A. Zwijnenburg, R. G. Bell, F. Corà, *J. Solid State Chem.* **2008**, *181*, 2480–2487.

[71] D. I. Bletskan, V. V. Vakulchak, K. E. Glukhov, *Appl. Phys. A* **2014**, *117*, 1499–1514.

[72] M. Argentari, Masterarbeit, Philipps-Universität Marburg, **2017**.

[73] K. Jurkschat, S. Van Druemel, G. Dyson, D. Dakternieks, B. T. J., M. E. Smith, M. Dräger, *Polyhedron* **1992**, *11*, 2747–2755.

B Wissenschaftlicher Lebenslauf

Zum Schutz personenbezogener Daten wurde der Lebenslauf aus der öffentlich zugänglichen Version dieser Dissertationsschrift entfernt.

C Publikationsliste

Publikationen

(6) *Towards Understanding the Reactivity and Optical Properties of Organosilicon Sulfide Clusters.*
K. Hanau, S. Schwan, M. R. Schäfer, M. J. Müller, C. Dues, N. Rinn, S. Sanna, S. Chatterjee, D. Mollenhauer, S. Dehnen, *Angew. Chem.* **2021**, *133*,1196–1206; *Angew. Chem. Int. Ed.* **2021**, *60*, 1176–1186.

(5) *Variations in the Interplay of Intermetallic and Metal Chalcogenide Units in Organotinn-Copper Selenide Clusters.*
K. Hanau, N. Rinn, S. Dehnen, *Inorg. Chem.* **2020**, *59*, 198–202.

(4) *Organotin Selenide Clusters and Hybrid Capsules.*
K. Hanau, N. Rinn, M. Argentari, S. Dehnen, Chem. Eur. J. **2018**, *24*, 11711–11716.

(3) *Trigonal Bipyramidal Metalselenide Clusters with Palladium and Tin Atoms in Various Positions.*
N. Rinn, K. Hanau, L. Guggolz, A. Rinn, S. Chatterjee, S. Dehnen, *Z. Anorg. Allg. Chem.* **2017**, *23*, 1508-–1512.

(2) *Metal-Ligand Cooperation in H_2 Activation with Iron Complexes Bearing Hemilabile Bis(phosphino)amine Ligands.*
N. Frank, K. Hanau, R. Langer, *Inorg. Chem.* **2014**, *53*, 113351-–1343.

(1) *Formation of an iron phosphine-borane complex by formal insertion of BH_3 into the Fe–P bond.*
N. Frank, K. Hanau, K. Flosdorf, R. Langer, *Dalton Trans.* **2013**, *42*, 11252-–11261.

Tagungsbeiträge

(6) *Synthesis and Reactivity of Organotetrel Chalcogenide Clusters.*
K. Hanau, N. Rinn, S. Schwan, M. R. Schäfer, M. J. Müller, C. Dues, S. Sanna, S. Chatterjee, D. Mollenhauer, S. Dehnen.
Posterbeitrag zur „Online Conference on Inorganic Chemistry“, September 2020.

(5) *Organosilicon Chalcogenide Clusters.*
K. Hanau, S. Dehnen.
Posterbeitrag zur „18. Vortragstagung der Wöhler-Vereinigung“ in Berlin, September 2016.

(4) *Functional Binary and Ternary Organotetrel Chalcogenide Clusters.*
K. Hanau, E. Dornsiepen, S. Dehnen.
Zwischenbegutachtung des Graduiertenkollegs „Funktionalisierung von Halbleitern (GRK 1782)“ in Marburg, September 2016.

(3) *Silicon Chalcogenide Clusters with Organic Functionality.*
K. Hanau, S. Dehnen.
Posterbeitrag zum „1st International Symposium on New Molecules and Clusters“ in Shanghai (China), Mai 2016.

(2) *Synthesis of Gallium Chalcogenide Clusters with Organic Functionality.*
K. Hanau, S. Dehnen.

Posterbeitrag zum „International Symposium on Inorganic Ring Systems (IRIS 14)“ in Regensburg, Juli 2015.

(1) *Synthesis of Gallium Chalcogenide Clusters with Organic Functionality.*
K. Hanau, S. Dehnen.
Posterbeitrag zur „17. Vortragstagung der Wöhler-Vereinigung“ in Saarbrücken, September 2014.

D Genehmigungen zum Abdruck der Publikationen

Die Veröffentlichung „*Towards Understanding the Reactivity and Optical Properties of Organosilicon Sulfide Clusters.* K. Hanau, S. Schwan, M. R. Schäfer, M. J. Müller, C. Dues, N. Rinn, S. Sanna, S. Chatterjee, D. Mollenhauer, S. Dehnen, *Angew. Chem.* **2021**, *133*,1196–1206; *Angew. Chem. Int. Ed.* **2021**, *60*, 1176–1186“ wurde als *open-access*-Artikel unter den Bedingungen der Creative Commons CC BY Lizenz publiziert:

Die Genehmigungen zur Verwendung der weiteren Publikationen in dieser Dissertationsschrift sind im Folgenden abgedruckt.

JOHN WILEY AND SONS LICENSE
TERMS AND CONDITIONS

Jan 12, 2021

This Agreement between Katharina Hanau ("You") and John Wiley and Sons ("John Wiley and Sons") consists of your license details and the terms and conditions provided by John Wiley and Sons and Copyright Clearance Center.

License Number	4986470981730
License date	Jan 12, 2021
Licensed Content Publisher	John Wiley and Sons
Licensed Content Publication	Chemistry - A European Journal
Licensed Content Title	Organotin Selenide Clusters and Hybrid Capsules
Licensed Content Author	Katharina Hanau, Niklas Rinn, Mario Argentari, et al
Licensed Content Date	Jul 15, 2018
Licensed Content Volume	24
Licensed Content Issue	45
Licensed Content Pages	6
Type of use	Dissertation/Thesis
Requestor type	Author of this Wiley article

Format	Print and electronic
Portion	Full article
Will you be translating?	No
Title	Synthese und Eigenschaften von Organozinnselenid- und Organosiliciumsulfid-Clustern
Institution name	Philipps-Universität Marburg
Expected presentation date	Jan 2021
Requestor Location	Katharina Hanau Hans-Meerwein-Straße 4 Marburg, 35043 Germany Attn: Katharina Hanau
Publisher Tax ID	EU826007151
Total	0.00 EUR
Terms and Conditions	

TERMS AND CONDITIONS

This copyrighted material is owned by or exclusively licensed to John Wiley & Sons, Inc. or one of its group companies (each a"Wiley Company") or handled on behalf of a society with which a Wiley Company has exclusive publishing rights in relation to a particular work (collectively "WILEY"). By clicking "accept" in connection with completing this licensing transaction, you agree that the following terms and conditions apply to this transaction (along with the billing and payment terms and conditions established by the Copyright Clearance Center Inc., ("CCC's Billing and Payment terms and conditions"), at the time that you opened your RightsLink account (these are available at any time at http://myaccount.copyright.com).

Variations in the Interplay of Intermetallic and Metal Chalcogenide Units in Organotin–Copper Selenide Clusters

Author: Katharina Hanau, Niklas Rinn, Stefanie Dehnen

Publication: Inorganic Chemistry

Publisher: American Chemical Society

Date: Jan 1, 2020

PERMISSION/LICENSE IS GRANTED FOR YOUR ORDER AT NO CHARGE

This type of permission/license, instead of the standard Terms & Conditions, is sent to you because no fee is being charged for your order. Please note the following:

- Permission is granted for your request in both print and electronic formats, and translations.
- If figures and/or tables were requested, they may be adapted or used in part.
- Please print this page for your records and send a copy of it to your publisher/graduate school.
- Appropriate credit for the requested material should be given as follows: "Reprinted (adapted) with permission from (COMPLETE REFERENCE CITATION). Copyright (YEAR) American Chemical Society." Insert appropriate information in place of the capitalized words.
- One-time permission is granted only for the use specified in your request. No additional uses are granted (such as derivative works or other editions). For any other uses, please submit a new request.

BACK CLOSE WINDOW

Danksagung

Diese Arbeit hätte ohne die Unterstützung vieler Menschen nicht das Licht der Welt erblickt. Ihnen allen gilt mein Dank dafür.

Meiner Doktormutter Prof. Dr. Stefanie Dehnen danke ich für das mir entgegengebrachte Vertrauen, die Freiheit bei der Bearbeitung meines Themas und viele hilfreiche Gespräche und Diskussionen. Danke, dass du auch dann noch an mich geglaubt hast als ich das zwischenzeitlich nicht mehr konnte.

Prof. Dr. Sangam Chatterjee danke ich herzlich für die Übernahme des Zweitgutachtens.

Prof. Dr. Wolf-Christian Pilgrim danke ich für die Mitwirkung an der Prüfungskommission.

Ich danke meinen Kooperationspartner_innen Marius Müller, Prof. Dr. Sangam Chatterjee, Sebastian Schwan, Moritz Schäfer, Prof. Dr. Doreen Mollenhauer, Christof Dues und Prof. Dr. Simone Sanna für die Messung meiner Proben bzw. die Rechnungen an meinen Verbindungen.

Besonderer Dank gebührt meinem „Disney-Labor“, namentlich Dr. Silke Santner, Dr. Isabell Nußbruch, Dr. Carsten Donsbach, Bertram Peters und Simon Nier, für die entspannte Arbeitsatmosphäre, die vielen (ernsten und lustigen) Gespräche und die kreativen Problemlösungen. Mit euch hat selbst der tristeste Arbeitstag noch Spaß gemacht! Carsten und Bertram danke ich insbesondere für die Unterstützung bei Kristallstrukturlösungen und -messungen und µ-RFA-Messungen, aber ausdrücklich nicht für die Musikauswahl.

Dr. Niklas Rinn danke ich für seine Unterstützung im Labor und die geduldige Beantwortung meiner Fragen.

Allen aktuellen und ehemaligen Mitarbeiter_innen im AK Dehnen danke ich herzlich für die tolle Forschungsumgebung sowie die spaßigen Aktionen außerhalb des Labors, sei es auf Tagungen, beim Grillen an der Uni oder beim Paddeln auf

der Lahn. Neben den bereits erwähnten Menschen möchte ich hier besonders Ursula Siepe, Andrea Tschirch, Uwe Justus, Bettina Wagner und Dr. Bastian Weinert hervorheben, die durch ihre Arbeit im Hintergrund für ein immer reibungsloses Funktionieren des Arbeitsalltags gesorgt haben. Dr. Eike Dornsiepen, Eugenie Geringer und Dr. Annikka Engel danke ich für fachliche Unterstützung und schöne Gespräche. Außerdem danke ich Dr. Johanna Heine, Dr. Bastian Weinert, Dr. Isabell Nußbruch, Bettina Wagner, Eugenie Geringer, Dr. Annikka Engel, Dr. Nathalie Dehnhardt, Dr. Frank Tambornino, Dr. Silke Santner und Dr. Lisa Vondung für die Kochgelegenheiten außerhalb des Labors und köstliche Nudeln mit Gedöns.

Den Mitarbeiter_innen der Serviceabteilungen für Kristallstrukturanalyse, Massenspektrometrie und Elementaranalytik und NMR-Spektroskopie danke ich für die schnelle und kompetente Bearbeitung meiner Messaufträge.

Natalie Brüll, Roman-Malte Richter, Zhong Zheng und Shen Chen danke ich für ihre Unterstützung bei meinen Experimenten.

Ich danke dem DFG-Graduiertenkolleg 1782 „Funktionalisierung von Halbleitern“, dessen Netzwerk ich nutzen durfte. Vielen Dank auch an Isabelle Kimmel für ihre immer netten und schnellen Antworten per E-Mail.

Für das Korrekturlesen dieser Arbeit danke ich Dr. Niklas Rinn, Dominik Keiper, Dr. Annikka Engel und Anna-Lisa Hanau.

Einige Herzensmenschen begleiten mich mittlerweile seit Jahr(zehnt)en: Sandra, Nina, Caro und Silke danke ich für wunderschöne Ablenkungen, lustige Spieleabende und immer offene Ohren. Schön, dass es euch gibt.

Meinen Eltern und meiner Schwester danke ich für die finanzielle und mentale Unterstützung während meiner gesamten Studienzeit und vor allem in den letzten zwei Jahren. Dieter Hanau danke ich für die finanzielle Unterstützung während meines Studiums.

Anja und Arthur danke ich für ihre Ruhe und Gelassenheit und die Unterhaltung in Home-Office-Phasen.

Ganz besonders möchte ich mich bei Dome bedanken. Mit dir ist selbst Alltägliches wunderschön.